NASA CR-112323
N73 24057

FEASIBILITY STUDY OF
MODIFICATIONS TO BQM-34E DRONE
FOR NASA RESEARCH APPLICATIONS

ASTM 72-40 27 DECEMBER 1972

PREPARED UNDER CONTRACT NO. NAS1-11758

for

NATIONAL AERONAUTICS AND SPACE ADMINISTRATION

TELEDYNE RYAN AERONAUTICAL

2701 HARBOR DRIVE, SAN DIEGO, CALIFORNIA 92112 AREA CODE 714/291-7311

Prepared by ______________________
H. A. James
Design Specialist

Approved by ______________________
P. E. DiBartola
Manager
Preliminary Design
Advanced Systems

Approved by ______________________
H. G. Timmons
Director
Advanced Systems

FOREWORD

Contributions for this report on various subjects were made by the following personnel for Advanced Systems: D. C. Harper and H. M. Allen, design; D. O. Nevinger, weights; R. W. Thompson, parametric, wing sizing; H. A. James, Project Leader, aerodynamics and performance; F. L. Miller, systems; J. Wilcox, reliability; and N. M. Bowers, structures and materials.

SUMMARY

The feasibility of modifying an existing supersonic drone, BQM-34E, into a NASA free-flight research vehicle is examined in this study. This remotely controlled vehicle would be capable of free-flight validation testing of wing configurations representative of a wide range of research applications for advanced transports and fighters as well as RPVs. This study is addressed to three main topics per Contract No. NAS 1-11758, i.e.: aerodynamics and performance, design and structures, and command and control system.

Appropriate structural and control system modifications, reliability and operational considerations, and ROM costs indicate that the BQM-34E drone is indeed suitable as a NASA research vehicle.

During the initial portion of the study, wing sizing to specified aerodynamic and performance criteria was accomplished. This resulted in the definition of six point designs matched to the modified BQM-34E with its basic propulsion system. From these results, NASA selected a representative research configuration for more in-depth structural design and control system studies.

The structural design studies identified several alternative engineering solutions for the testing of high and low-wing configurations. These were evaluated in terms of cost, complexity, and model similarity. Representative control and high-lift devices were configured for transonic flutter mode suppression research testing. Practical methods of achieving variations of wing bending and torsional rigidity were identified.

The results of a comprehensive analysis of command and control systems required for various types of research programs are summarized. The basic control and AFSC system is amenable to modifications with existing hardware to accommodate steady-state as well as dynamic loads, flutter, and variable-stability research programs.

CONTENTS

LIST OF FIGURES

LIST OF FIGURES (Continued)

LIST OF TABLES

LIST OF TABLES (Continued)

1.0 INTRODUCTION

NASA is conducting intensive laboratory and flight test programs to enhance the development of both advanced civilian and military aircraft. In support of these programs, a relatively low-cost, remotely controlled, research vehicle could provide critically needed test data in a most expeditious manner and without the risk of human life. It would be particularly valuable in the critical test and development phase, prior to the availability of full-scale, manned research aircraft and/or during the validation phase in support of corrections with wind tunnel test data. In support of these objectives, the purpose of this study is to determine the feasibility of adapting the supersonic BQM-34E drone to accommodate a proposed free-flight research program which would include wings having a broad range of applications.

At contract go-ahead, study guidelines and objectives were established at a joint NASA/Teledyne Ryan meeting, as summarized in Reference 1. The proposed NASA research drone would be capable of accepting research wings with a broad range of subsonic and supersonic application.

This study encompasses only the conceptual phase and defines, in general, the engineering approach and rough order of magnitude of resources required to modify an existing drone into a remotely controlled research vehicle. The particular vehicle is unique in that it offers continuously powered flight test performance capabilities throughout the subsonic and supersonic flight regimes, with reasonable endurance. From an aerodynamic standpoint, this configuration is representative of an ideal limit, in terms of aerodynamic cleanliness.

In terms of structural integrity, this vehicle has a rugged airframe designed to operate up to ultimate dynamic pressure of 2133 psf, which compares quite favorably with that of any of the known advanced fighters.

The current shoulder wing crossover structure is readily adaptible to interchangeable wings at low cost. Low-wing installations are also feasible at increased cost and complexity, depending upon emphasis in accordance with research priorities.

Preliminary design guidelines for sizing six possible research wings, based on a modified BQM-34E system, are summarized in Table 1-1.

TABLE 1-1

WINGS PLANNED FOR STUDY

Wing No.	Application	Aspect Ratio	t/cr	t/ct	Sweep Angle	$\Lambda_{c/4}$	Taper Ratio	Mc	C_L	W_b/b
1	Transport	7.0	.11	.07	38° at C/2	40.37	.35	.98	.36	.145
2	Transport	8.0	.12	.08	30° at C/2	32.34	.38	.90	.4	.145
3	Air-to-Air	4.0	.05	.04	40° at LE	36.01	.38	1.40	.6	.186
4	Endurance Turbojet	9.0	.12	.06	35° at C/4	35.0	.30	.90	.5	.068
5	Endurance Turbofan	9.0	.14	.12	25° at C/4	25.0	.30	.75	.6	.068
6	Delta	2.56	.03	.03	50.5° at LE	42.3	.127	1.4	.25	.090

(4) Ratio thickness/chord at root

(5) Ratio thickness/chord at tip

(6) Sweep Angle

(7) Taper Ratio

(8) Mach Number at Cruise

(9) Coefficient of Lift (Design)

(10) Body Width to Span Ratio

2.0 TECHNICAL APPROACH

The technical approach utilized in the initial portion of the study was to conduct preliminary design studies of wing configurations having a wide range of subsonic and supersonic applications. This was accomplished for six types of wings, in accordance with design and model similarity criteria summarized in Table 1-1. It will be noted that wings applicable to advanced subsonic transports incorporating supercritical wing technology, an advanced-maneuverability fighter, an SST, and RPV are included.

The initial study guidelines included the following considerations:

a. Revision to internal fuel system for a capacity of about 400 pounds fuel.

b. MARS or parachute recovery.

c. Conventional ailerons plus stabilizer tail.

d. Air launch primary, ground launch secondary.

e. High and low-wing test capability.

f. Remote or onboard command and guidance systems.

g. Unique, one-of-a-kind, research vehicle.

In this portion of the study, tail volume coefficients and wing-body geometric similarity constraints were kept close to those typical for each wing application. This portion of the study was then summarized into a summary document designated as ASTM 72-22. This was submitted to NASA, along with three-view layouts and area distributions of each point design. This portion of the study provided NASA with a basis for selection of a configuration (1-30) for Tasks II and III. Engineering design and structural studies were then carried out for a feasible, one-of-a-kind, research drone capable of testing a variety of high and low-wing configurations. The associated studies involving advanced structural materials, proportional control, and control law system capabilities were carried out on the basis of the low-wing sonic transport wing configuration identified in this study as wing 1-30-2. This study was concluded with ROM costs and recommendations for an immediate follow-on program.

3.0 RESULTS

The results of this feasibility study are presented in Paragraphs 3.1 through 3.4. These results are presented in a logical sequence, starting with the preliminary parametrics and wing sizing studies and followed by more in-depth engineering studies accomplished on a NASA-selected representative research drone configuration.

3.1 PRELIMINARY STUDIES

Preliminary vehicle sizing data was first explored by means of the Teledyne Ryan Advanced Systems vehicle-sizing program designated as AVSYN. The computerized program, AVSYN, can accept up to 145 design and mission variables to size remotely piloted vehicles quickly. The feasibility of accomplishing designated 20 to 31-minute missions with a NASA payload of 250 pounds with a reasonably sized vehicle based on the BQM-34E propulsion system was examined. Trends versus wing aspect ratio and wing area are shown in Figures 3-1, 3-2, and 3-3.

The significant results from this portion of the study indicated the feasibility of vehicle gross weights from 2500 to 3000 pounds and fuel loads of about 400 pounds, sufficient to accomplish the NASA mission requirements.

Wing-Sizing Study

The preliminary wing design criteria for wing aspect ratios, Mach numbers, and lift coefficients from Table 3-1 were utilized to determine wing area and Reynolds number versus altitude for an assumed fixed weight of 2500 pounds.

The results of this sizing study are illustrated for each of the wing applications in Figures 3-4 through 3-15. These data provided a range of wing areas to be considered for each of the applications. It was noted that small wings were bounded by geometric body width to span constraint Wb/b. At 1-g flight condition, results show that small wings achieved higher Reynolds numbers than did the larger wings. An additional constraint to provide longitudinal trim and stability involved horizontal applicable tail volume coefficients for each type of wing considered in this study. Coordination with NASA (Mr. Ferris) confirmed our views that

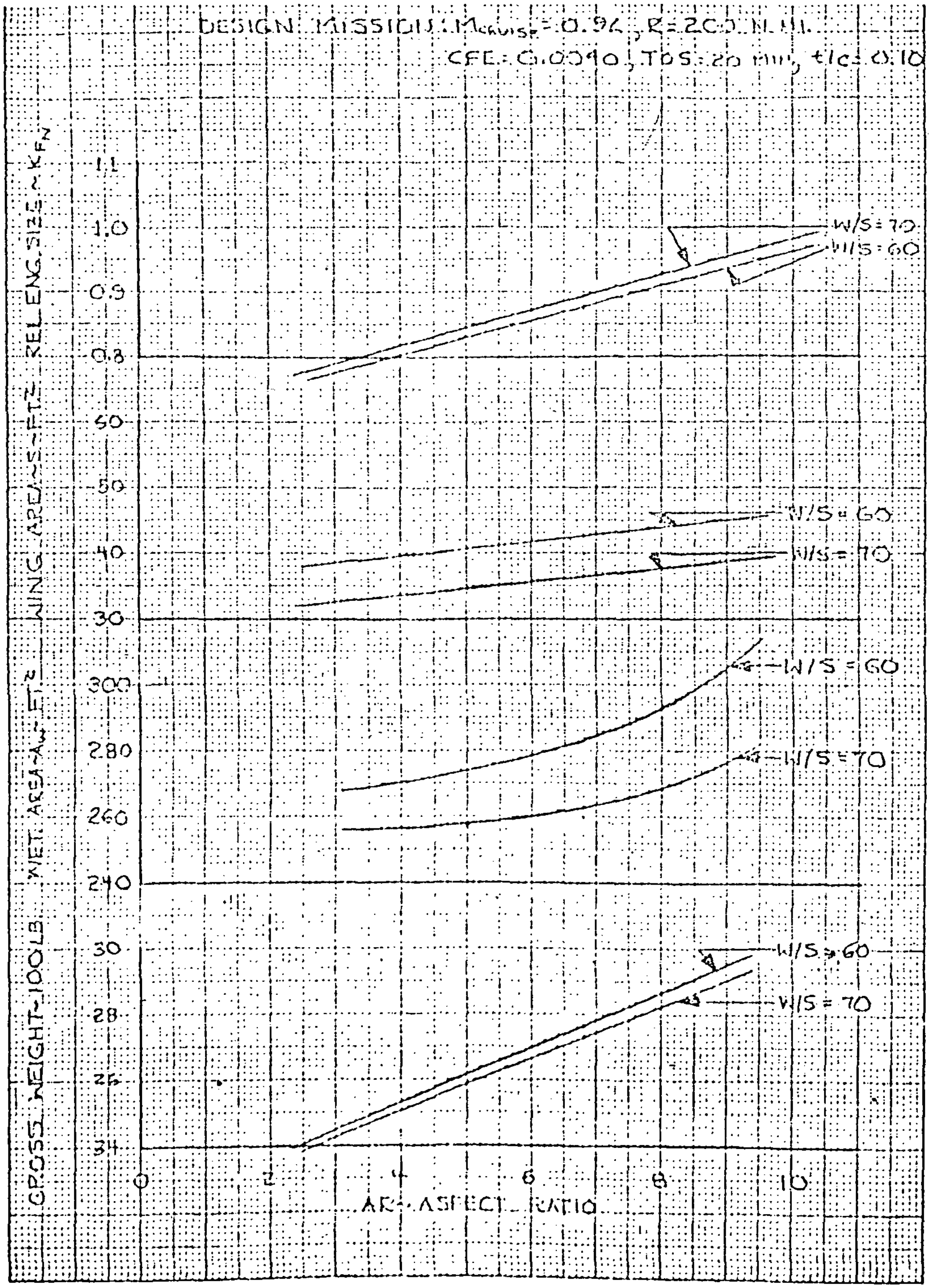

Figure 3-1. AVSYN Results

Figure 3-2. AVSYN Results, Sea Level Launch

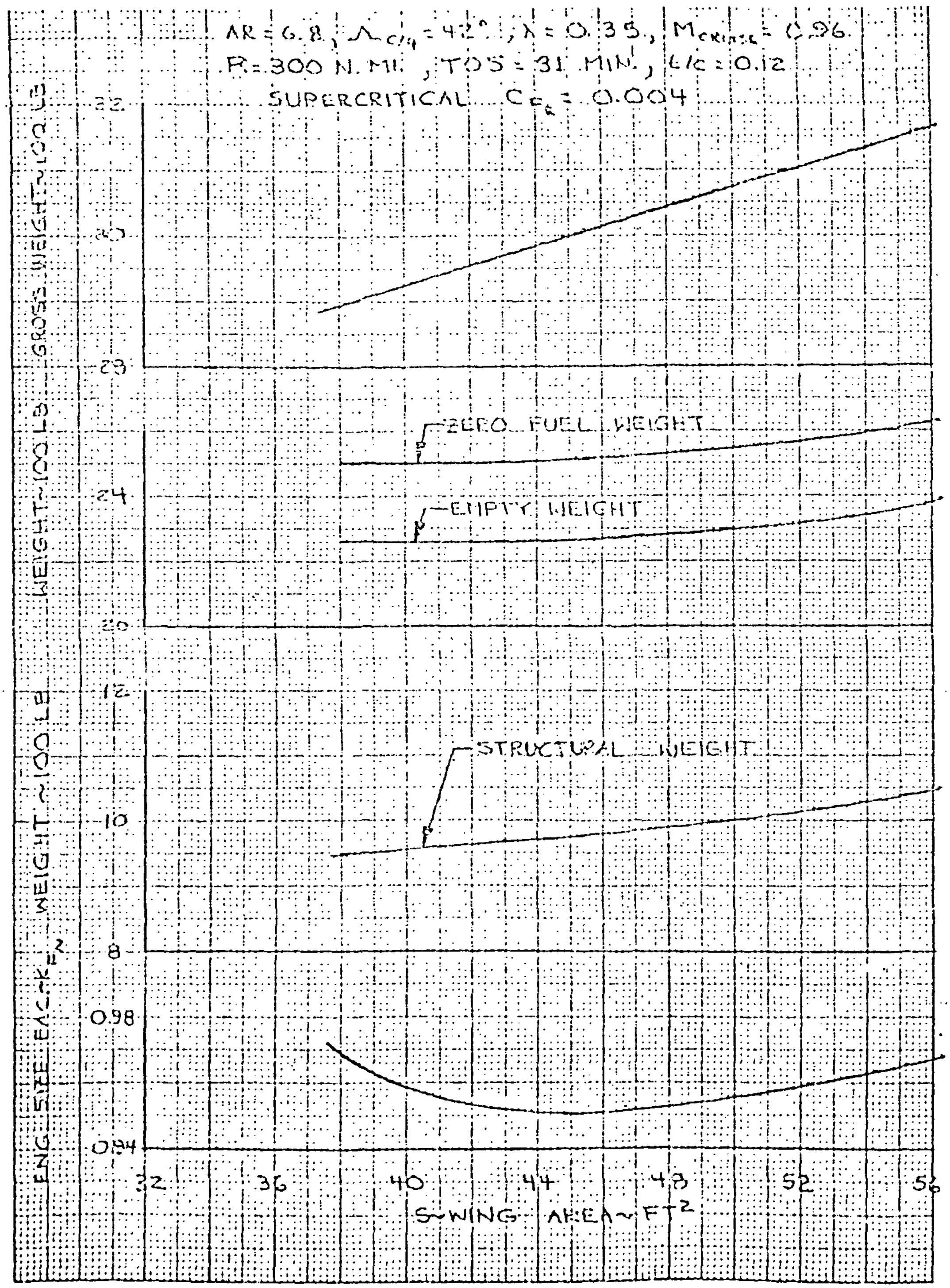

Figure 3-3. AVSYN Wing Parameter Study

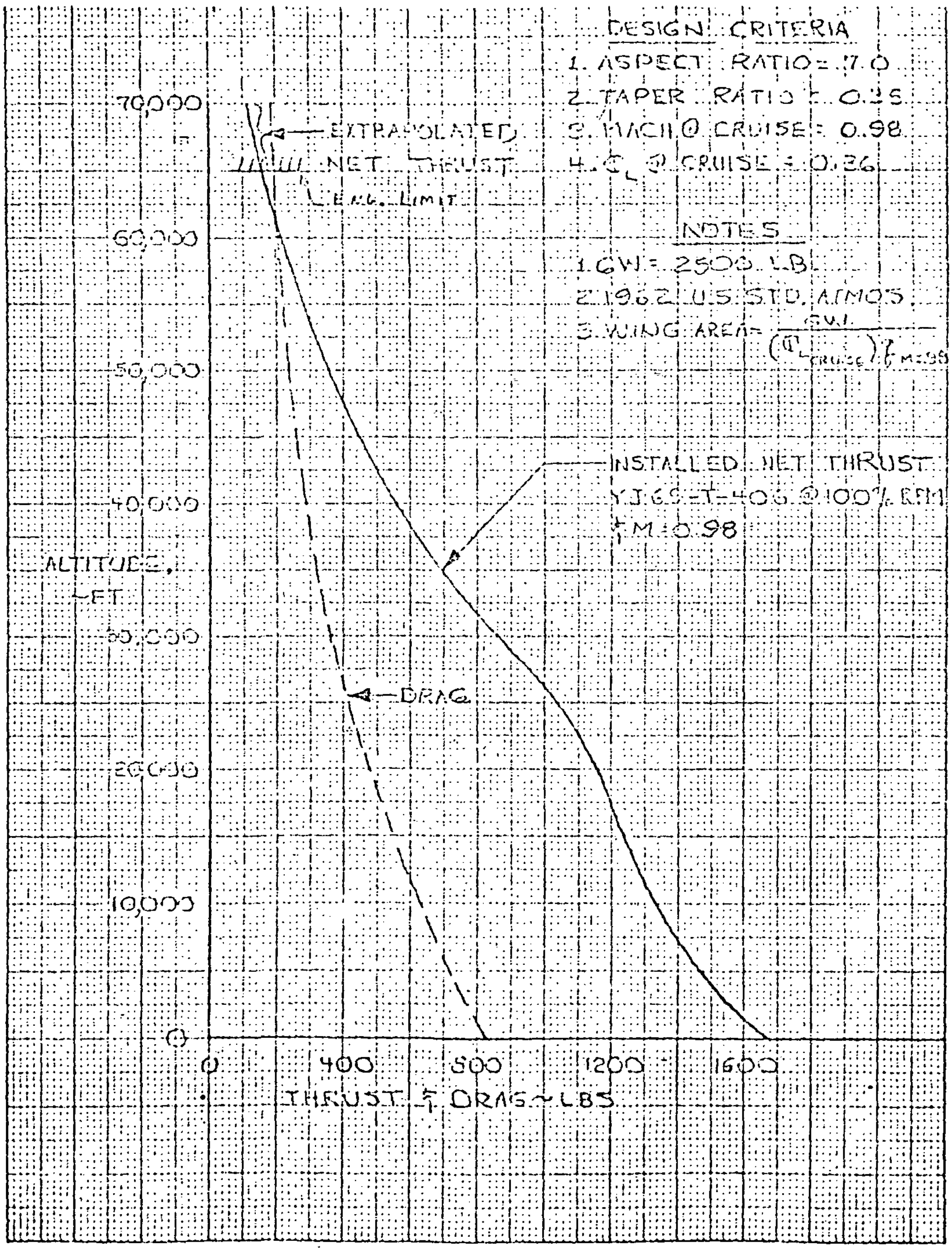

Figure 3-4. NASA Wing Study, Preliminary Estimate of the Thrust Required and Available for the No. 1 Wing Design

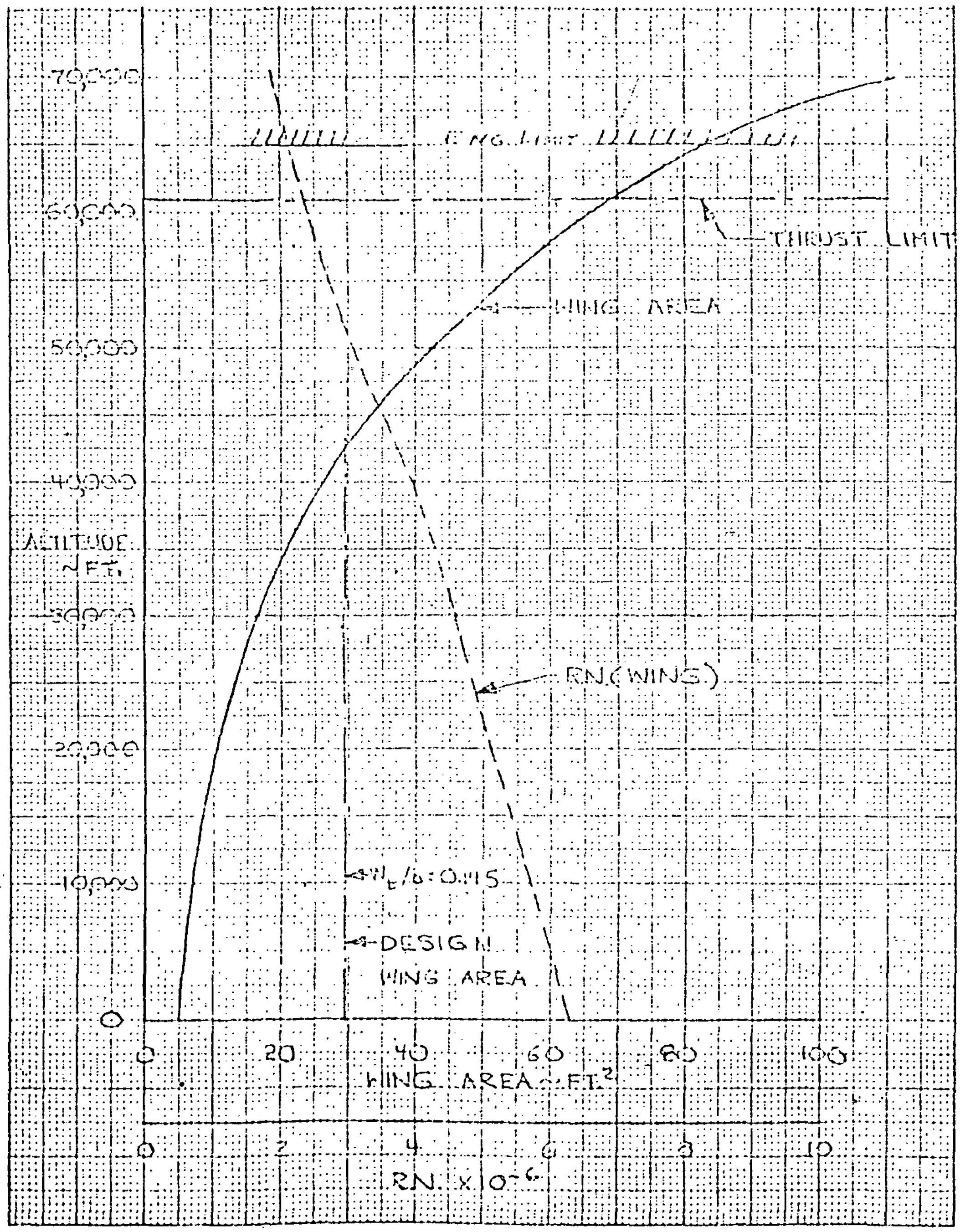

Figure 3-5. NASA Wing Study, Sizing Study for Wing No. 1

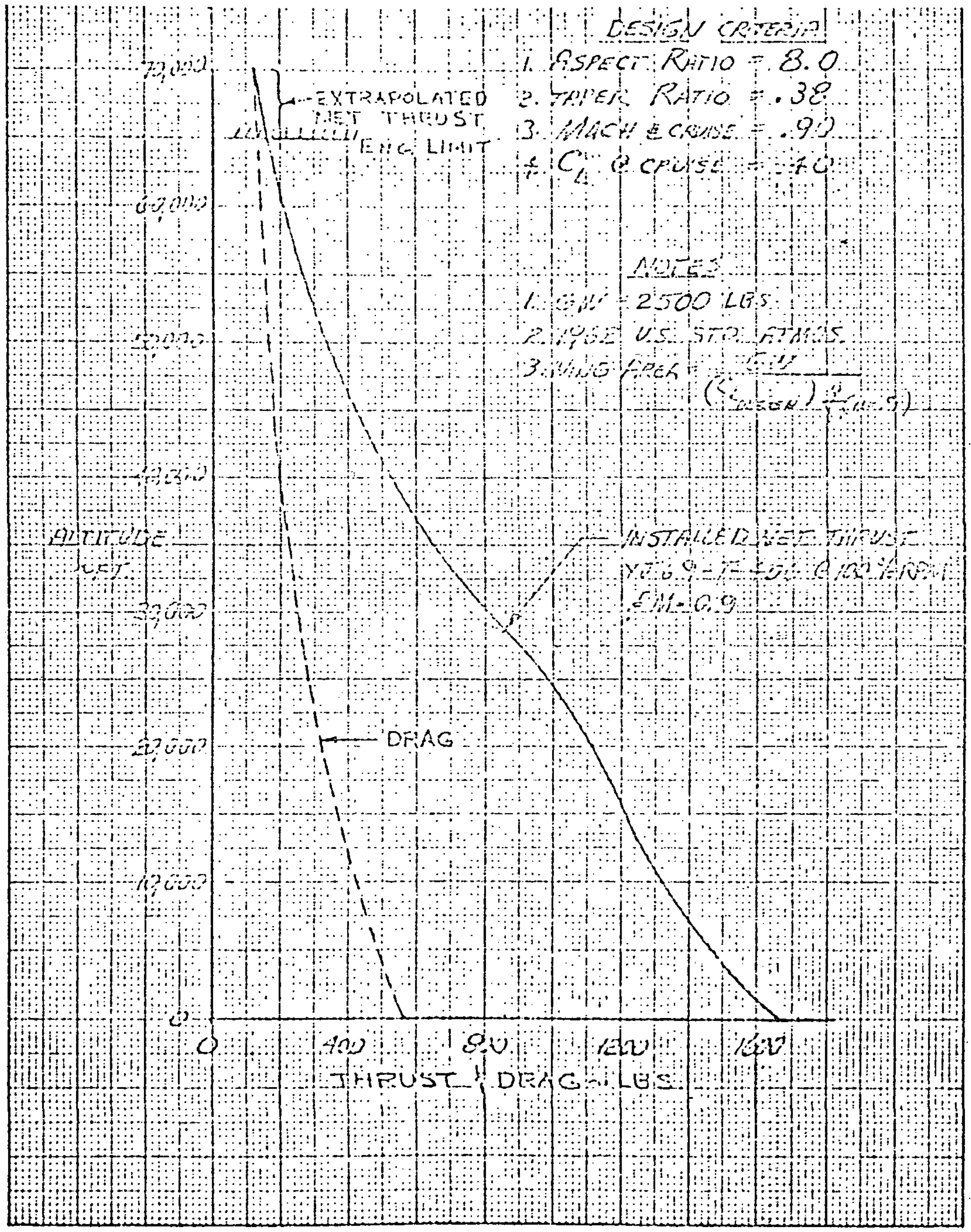

Figure 3-6. NASA Wing Study, Preliminary Estimate of the Thrust Required and Available for the No. 2 Wing Design

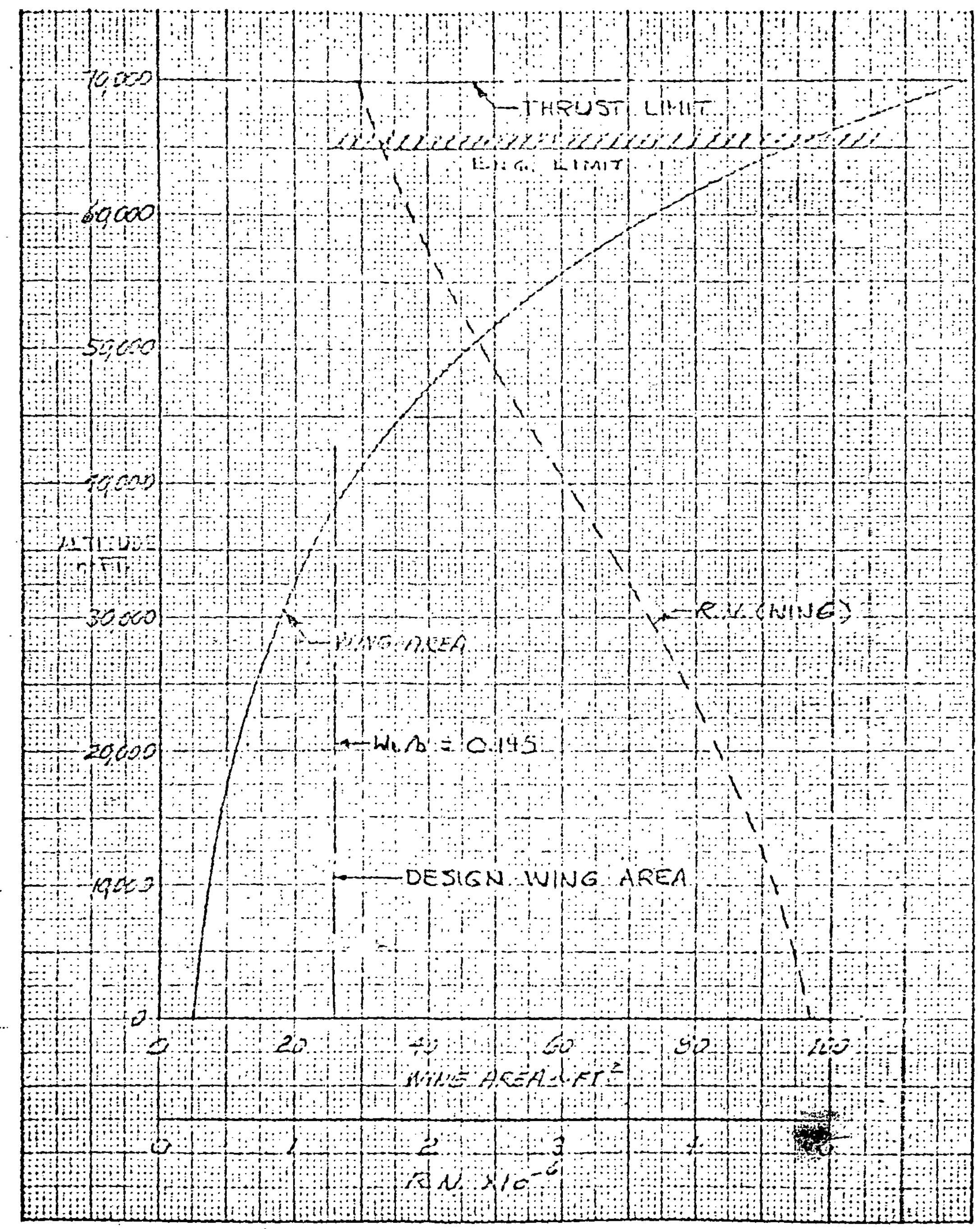

Figure 3-7. NASA Wing Study, Sizing Study for Wing No. 2

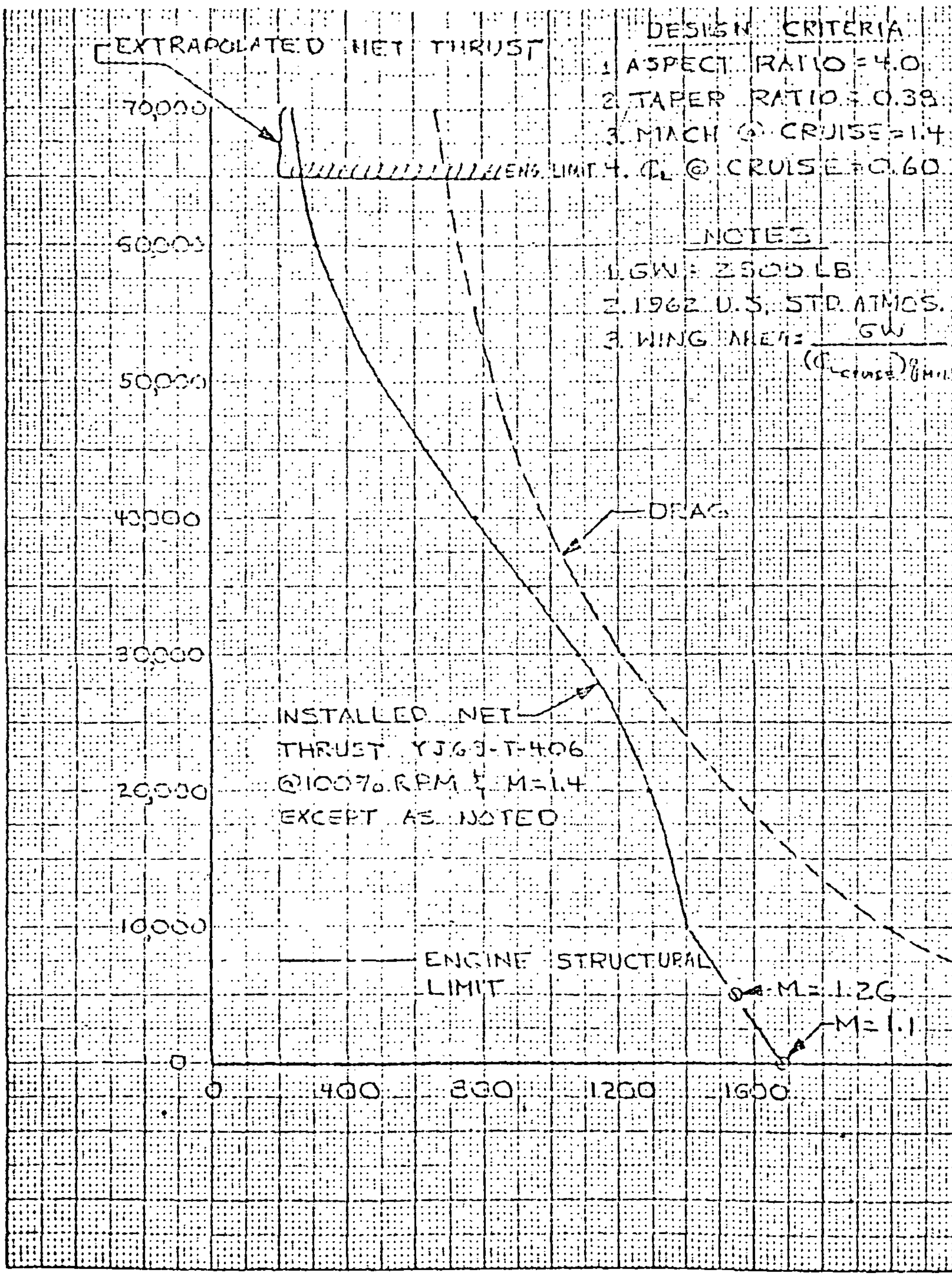

Figure 3-8. NASA Wing Study, Preliminary Estimate of Thrust Required and Available for the No. 3 Wing Design

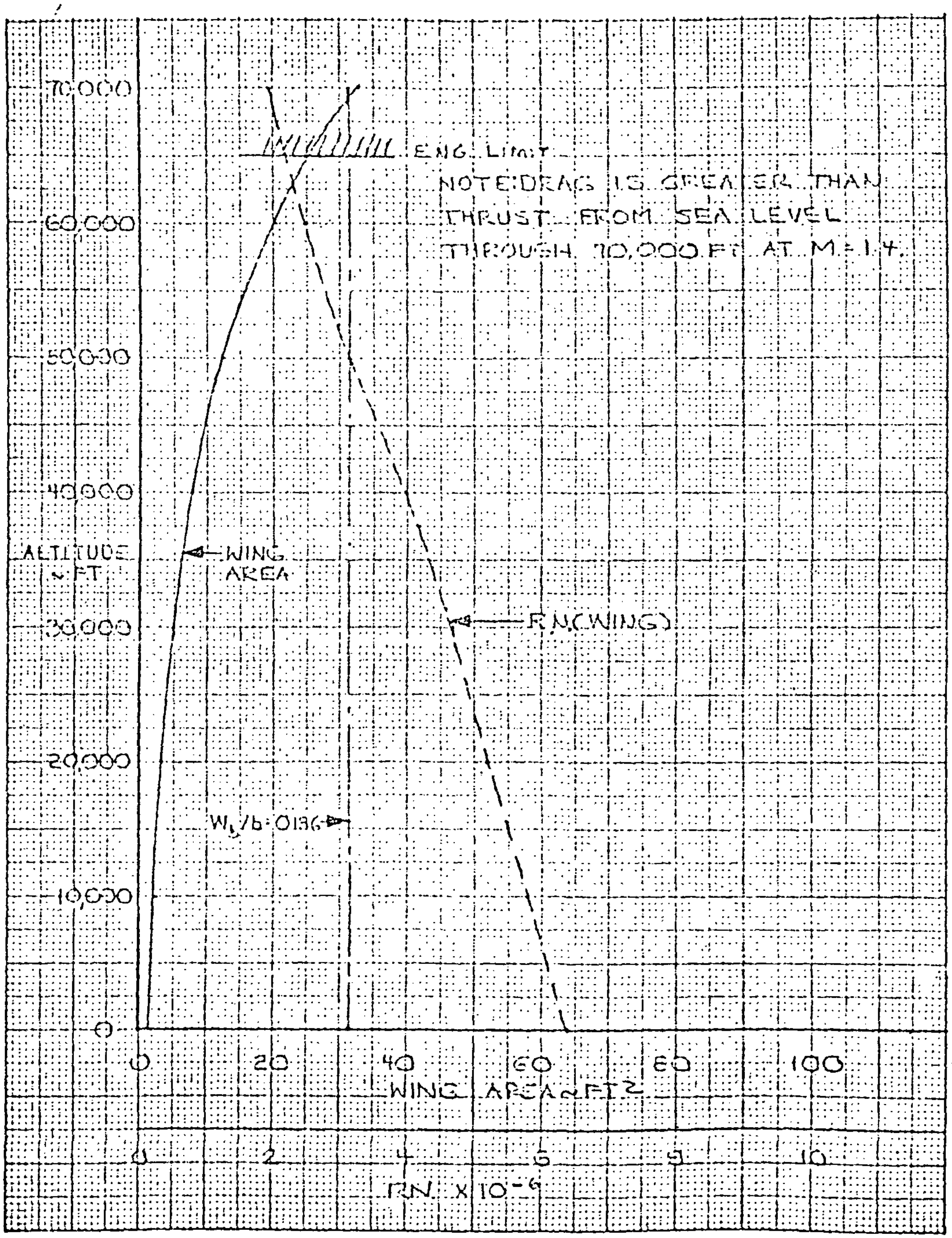

Figure 3-9. NASA Wing Study, Sizing Study for Wing No. 3

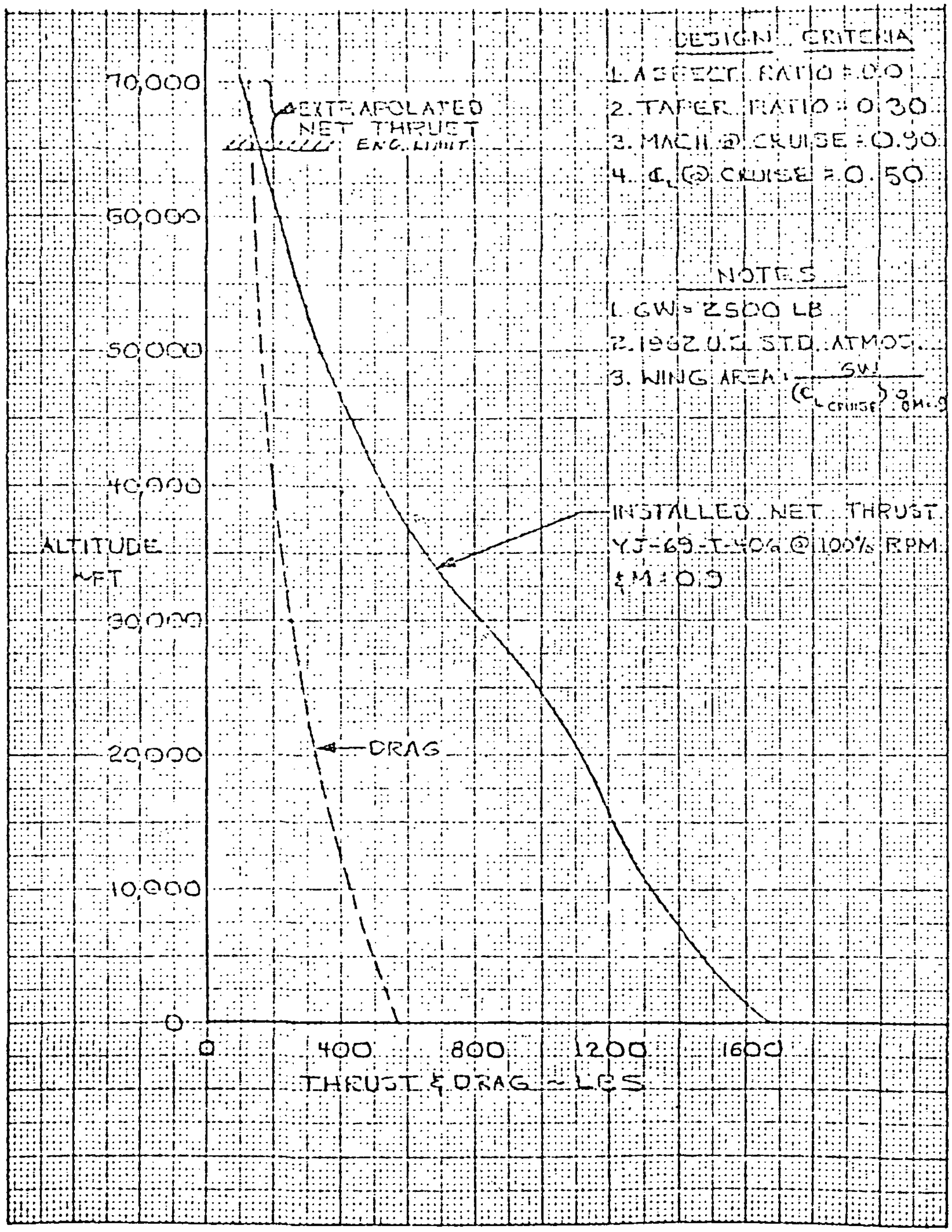

Figure 3-10. NASA Wing Study, Preliminary Estimate of Thrust Required and Available for the No. 4 Wing Design

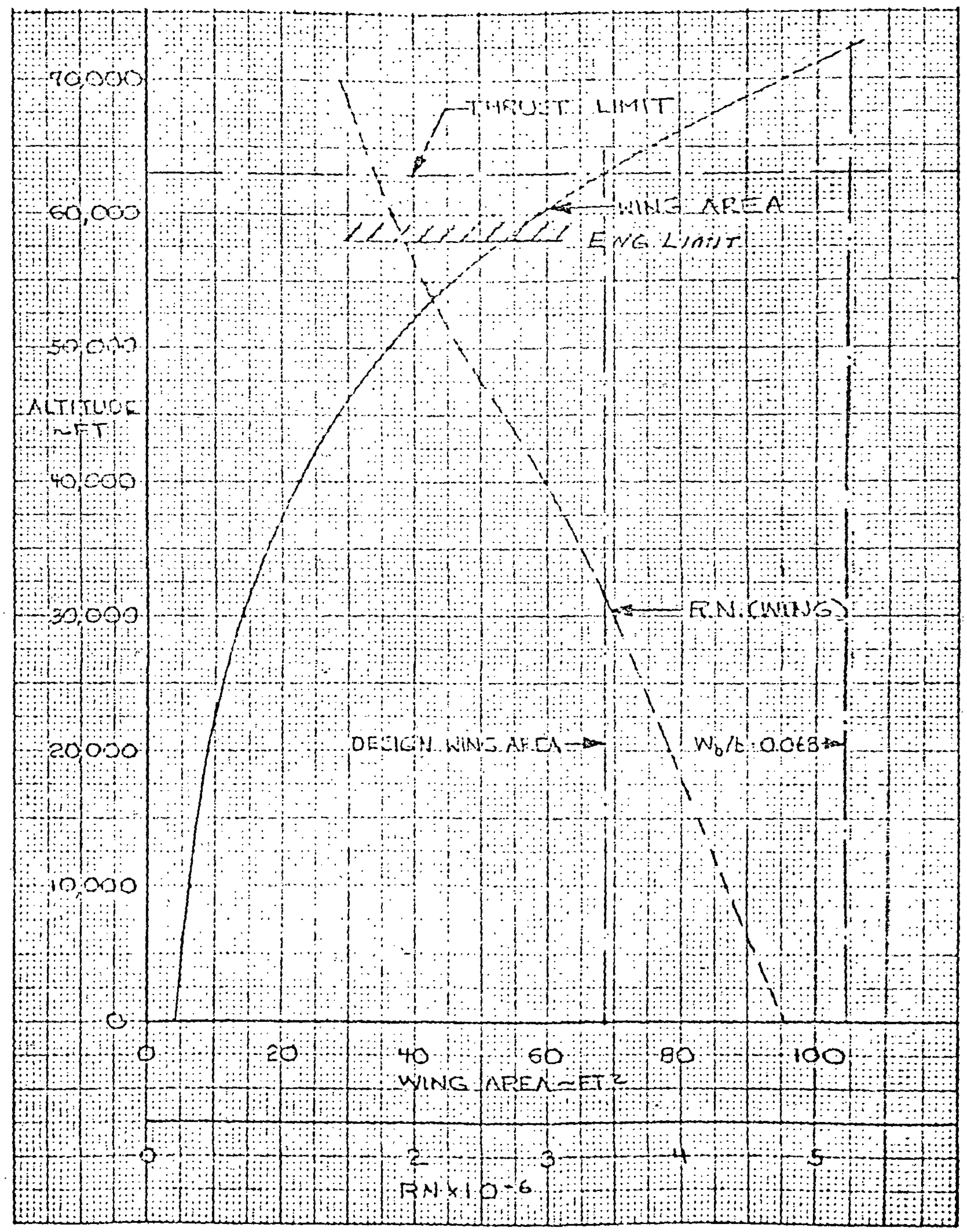

Figure 3-11. NASA Wing Study, Sizing Study for Wing No. 4

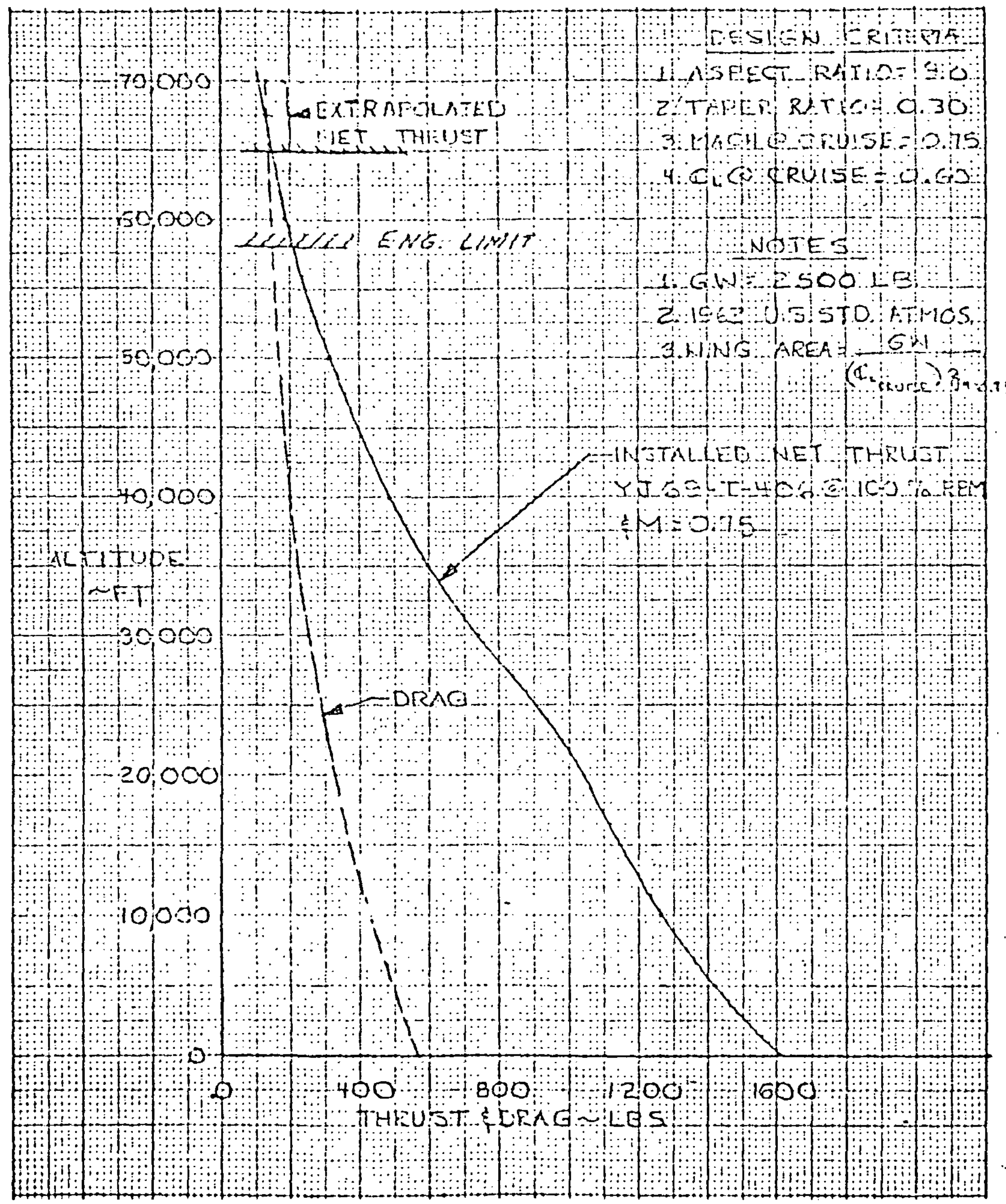

Figure 3-12. NASA Wing Study, Preliminary Estimate of Thrust Required and Available for No. 5 Wing Design

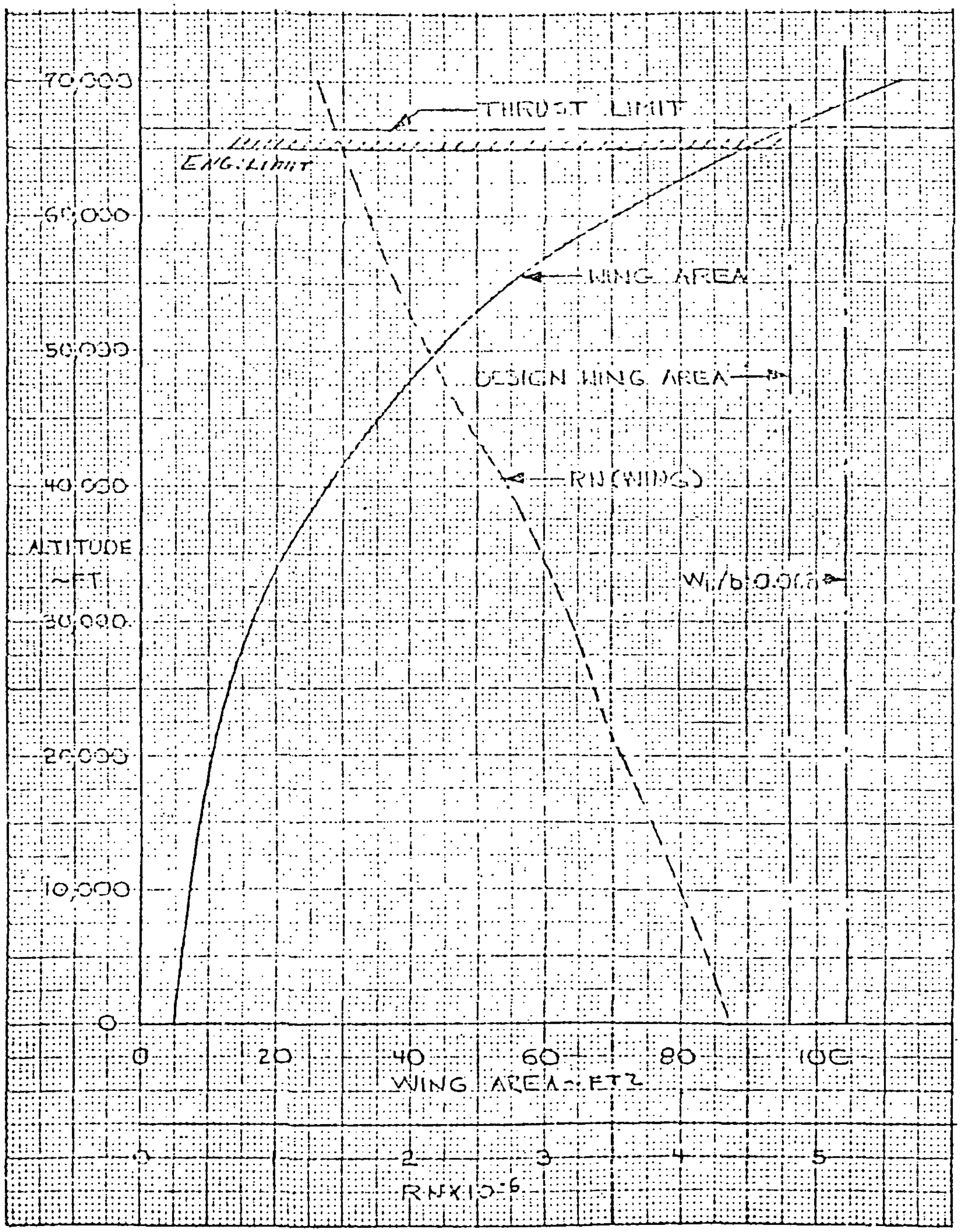

Figure 3-13. NASA Wing Study, Sizing Study for Wing No. 5

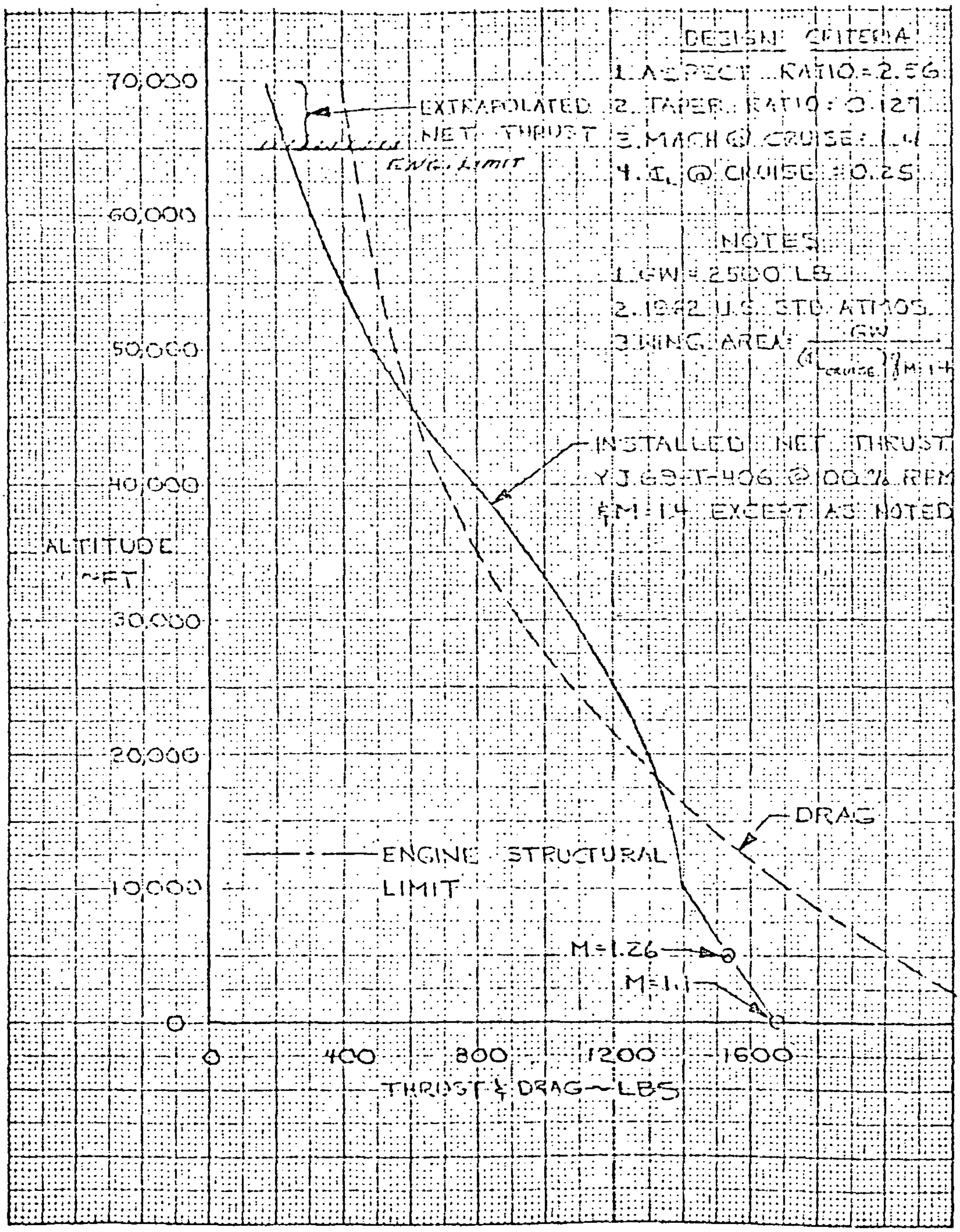

Figure 3-14. NASA Wing Study, Preliminary Estimate of Thrust Required and Available for the No. 6 Wing Design

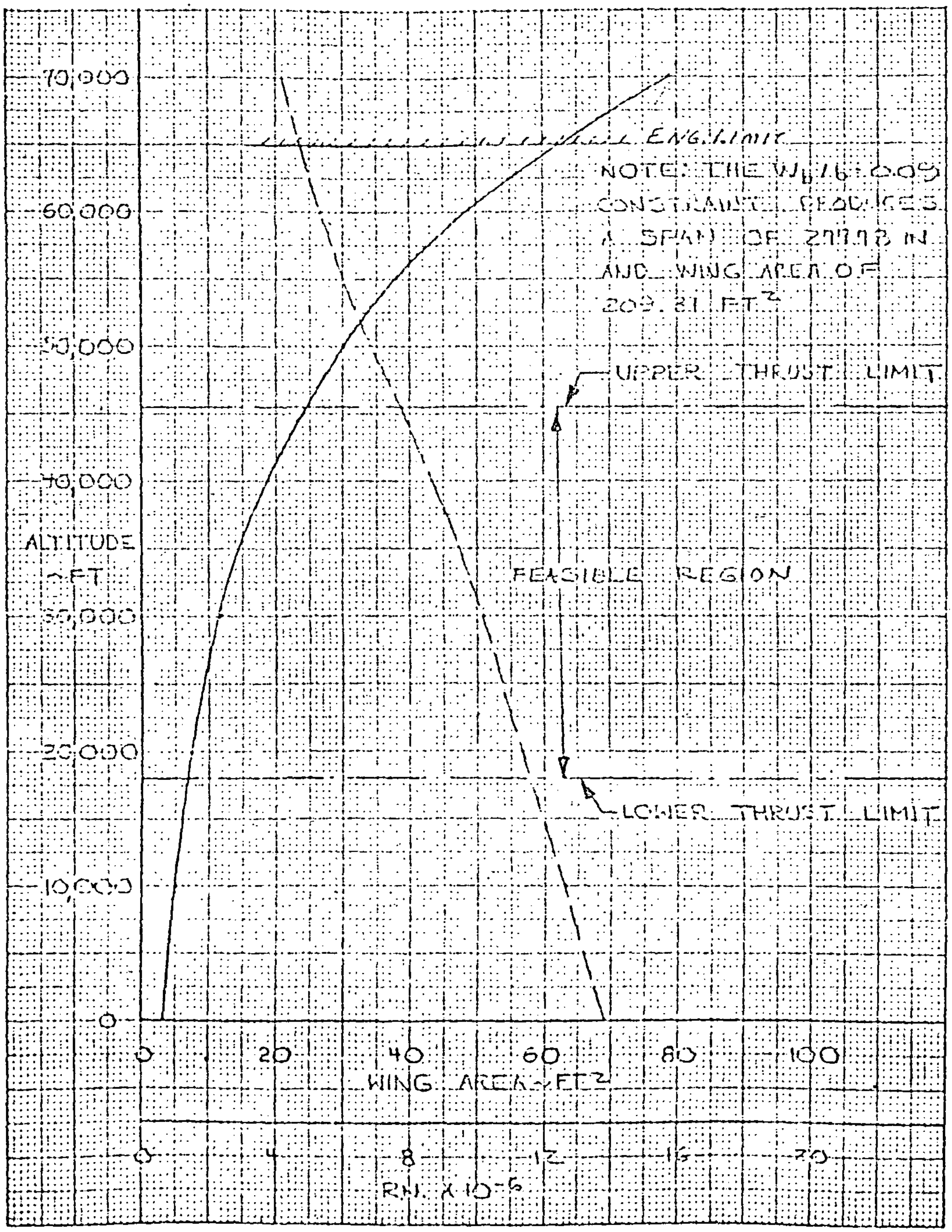

Figure 3-15. NASA Wing Study, Sizing Study for Wing No. 6 .

horizontal tail volume coefficients for most applications should be at least 0.60 to 0.80. This criterion would limit most wing sizes to less than 45 square feet. In only one application, involving wing 5 (which had laminar airfoils) was a deviation on tail volume coefficient permitted down to 0.40, close to that of a similar vehicle in existence. An additional flight limitation was the thrust-limited maximum altitude at the designated design Mach number and lift coefficient.

The results of this portion of the study were then examined for compatibility with the BQM-34E fuselage crossover, center of gravity, and tail arms by means of three-view design layouts. The design layouts included the following range of feasible wing areas for each application:

WING NO.	WING AREAS, SQUARE FEET
1	30 to 50
2	26 to 50
3	20 to 28
4	40 to 60
5	40 to 60
6	25 to 35

3.2 POINT DESIGNS

The preliminary design guidelines for developing feasible designs for each of the six applications consisted of the following:

a. Wing crossover structure close to that of the basic vehicle.

b. Wing c/4 close to Station No. 264 to achieve reasonable center-of-gravity balance.

c. Horizontal volume coefficient, $\overline{V}_H \geq 0.6$ to 0.8.

d. Vertical volume coefficient $\overline{V}_V \geq 0.08$.

e. Revision of fuel system to about 400-pound fuel capacity.

f. Air launch primary, ground launch secondary.

g. Conventional aluminum riveted construction or equivalent.

h. Conventional ailerons plus stabilizer tail.

i. MARS or standard parachute recovery secondary.

It was apparent at the onset of this study that a high-wing configuration could more easily be developed than could a low-wing configuration. However, it was considered desirable to achieve a low-wing capability, since this would be more representative of transport configurations.

WEIGHTS ANALYSIS

The weight of the basic BQM-34E, less wing and target augmentation equipment, is tabulated below:

ITEM	WEIGHT (pounds)
Wing Group	
Tail Group	50.0
Body Group	273.3
Takeoff and Recovery Equipment	122.0
Propulsion	427.0
Lube and Fuel System	36.1
Electrical	139.4
Controls	36.7
Guidance	42.8
Electronics	50.6
Environmental Protection Equipment	10.1
Weight Empty - Revised	(1188.0)
Unusable Fuel and Oil	15.2
Refrigerant System	20.6
Zero Fuel Weight - Revised	(1223.8)
Internal Fuel	274.0
Refrigerant	8.3
Gross Weight - Revised	(1506.1)
Basic Items Removed	
Wing	142.2
Target Augmentation	171.8

Modifications Weight Summary

Estimated weight for anticipated modifications to the BQM-34E are tabulated below:

ITEM	WEIGHT (pounds)
NASA Payload	250.0
Two Span Ailerons	20.0
Additional Fuel	76.0
Additional Tankage	24.0
High-Lift Devices	50.0
MARS Recovery System	50.0
Wing Crossover Adapter	50.0
Revised Air Launch Fittings	10.0
Area Rule Modifications	50.0
Ballast Provisions	100.0
Total Modification Weight	(680.0)

Estimated Modified Vehicle Gross Weight

The estimated vehicle gross weights for each wing configuration are tabulated below:

CONFIGURATION	WEIGHT (pounds)
Configuration 1 (S_W = 30 ft.^{2})	
BQM-34E GW Revised	1506.1
Modifications	680.0
Wing	156.0
Gross Weight	(2340.1)
Configuration 2 (S_W = 30 ft.^{2})	
BQM-34E GW Revised	1506.1
Modifications	680.0
Wing	159.0
Gross Weight	(2345.1)

CONFIGURATION	WEIGHT (pounds)
Configuration 3 (S_W = 24 ft.^{2})	
BQM-34E GW Revised	1506.1
Modifications	680.0
Wing	128.0
Gross Weight	(2314.1)
Configuration 4 (S_W = 40 ft.^{2})	
BQM-34E GW Revised	1506.1
Modifications	680.0
Wing	199.0
Gross Weight	(2385.1)
Configuration 5 (S_W = 60 ft.^{2})	
BQM-34E GW Revised	1506.1
Modifications	680.0
Wing	226.0
Gross Weight	(2412.1)
Configuration 6 (S_W = 35 ft.^{2})	
BQM-34E GW Revised	1506.1
Modifications	680.0
Wing	136.0
Gross Weight	(2322.1)

Performance Envelopes

The general performance and typical NASA research mission capabilities of each wing application developed from the design study were examined in this portion of the study (Figures 3-16 through 3-27).

NOTE

The notation for each design includes a wing number corresponding to its application in Table 1-1. The dash number denotes wing area; i.e., 1-30 is wing 1 with a 30-square-foot wing.

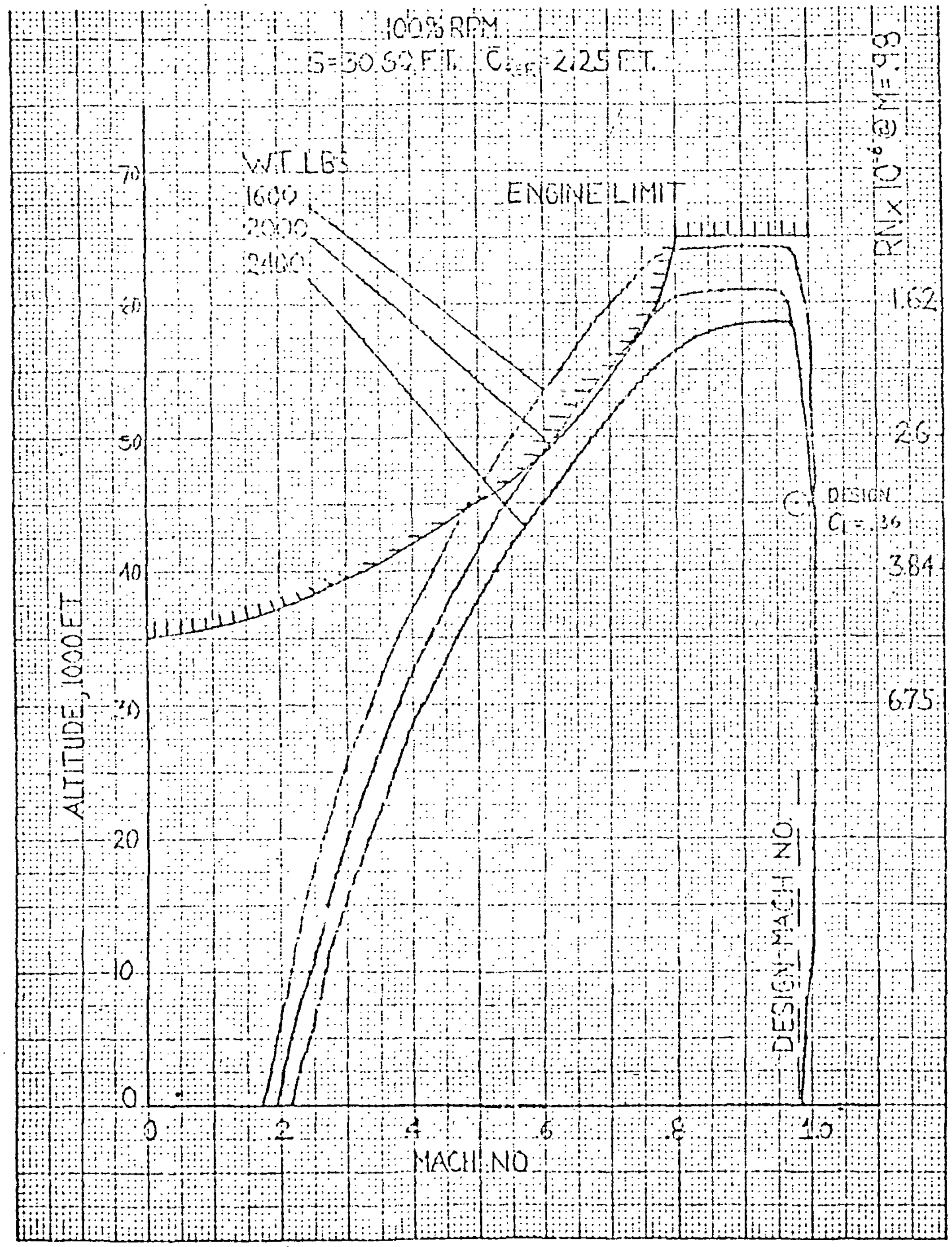

Figure 3-16. No. 1-30 Mach Number vs. Altitude

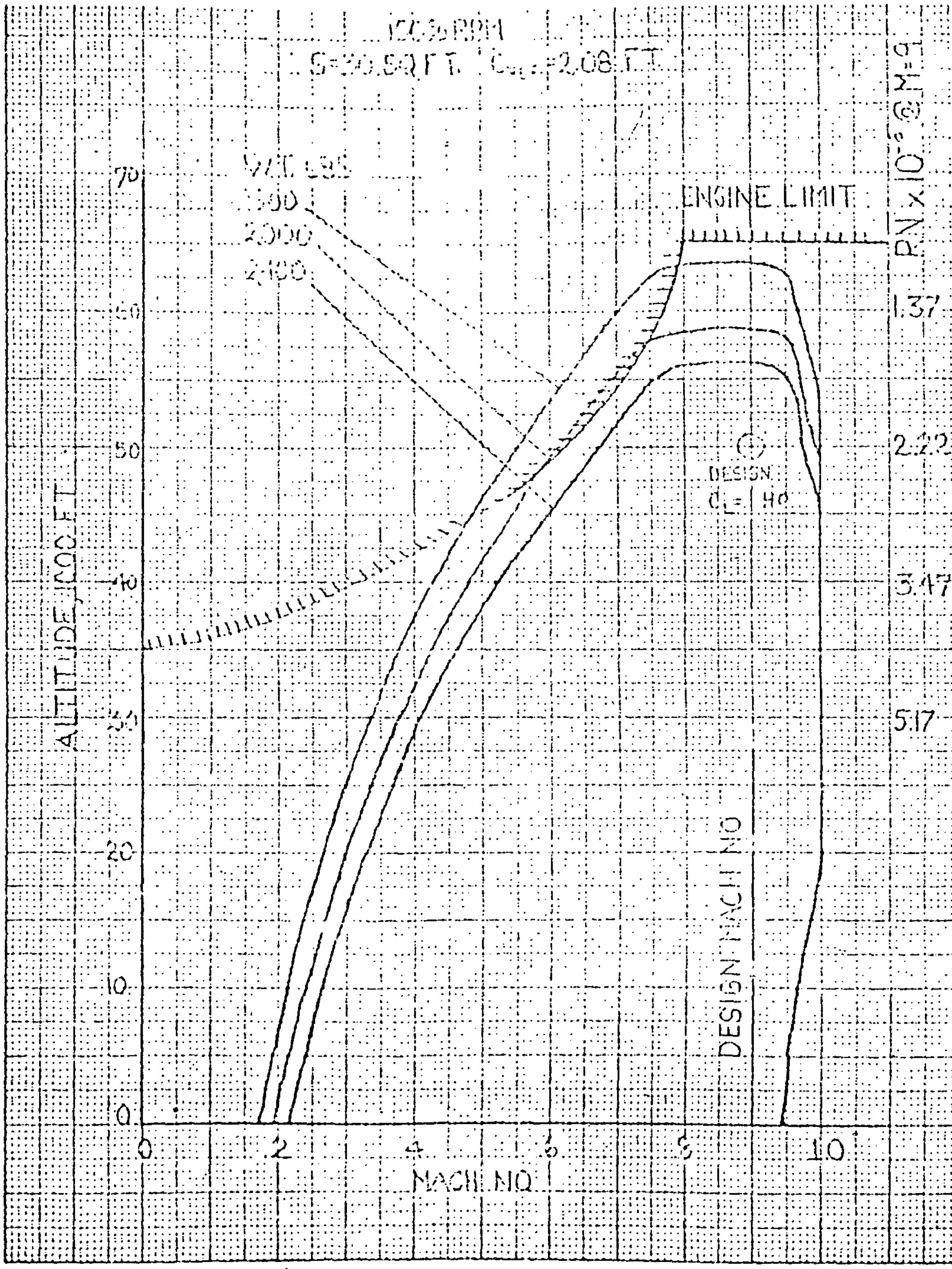

Figure 3-17. No. 2-30 Mach Number vs. Altitude

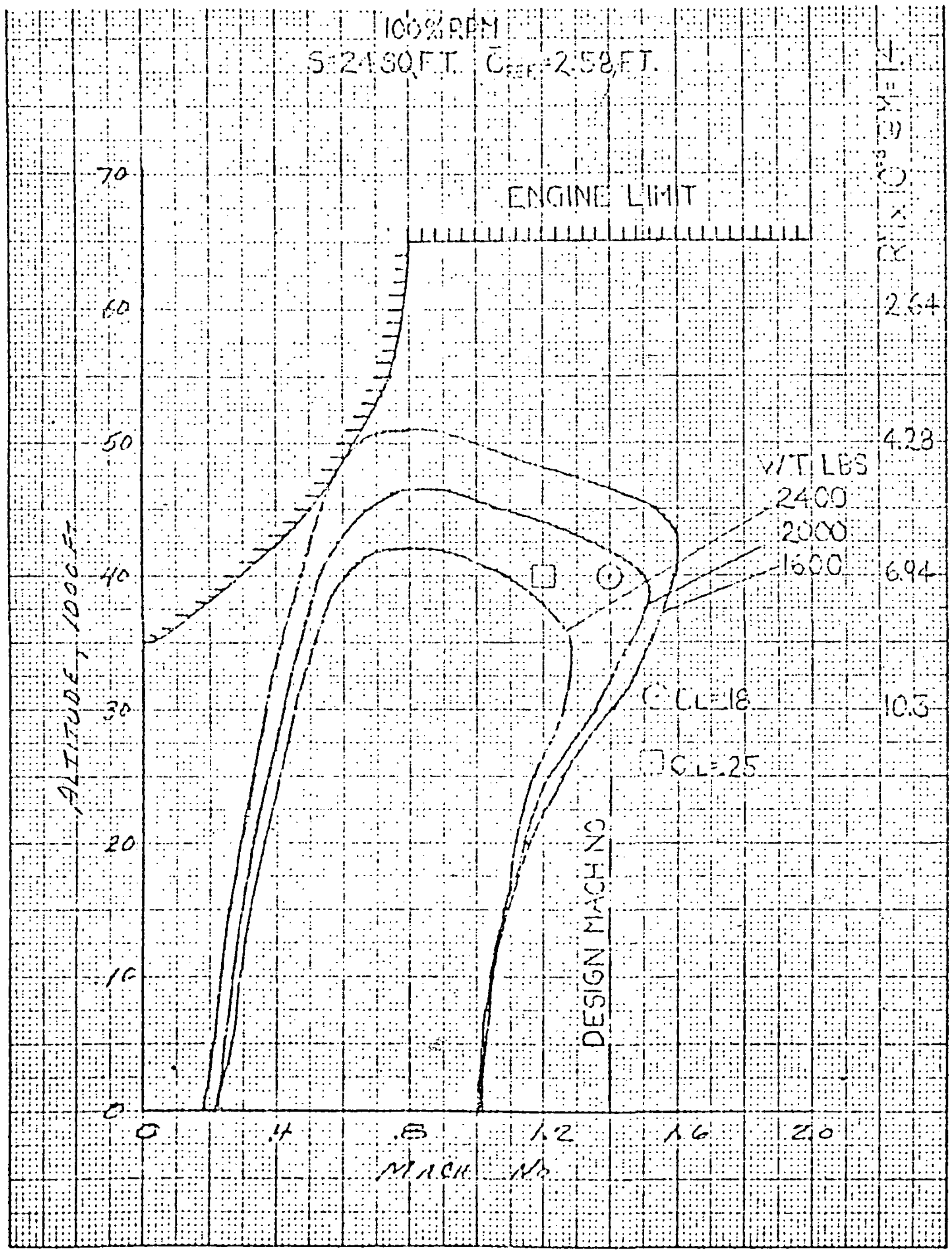

Figure 3-18. No. 3-24 Mach Number vs. Altitude

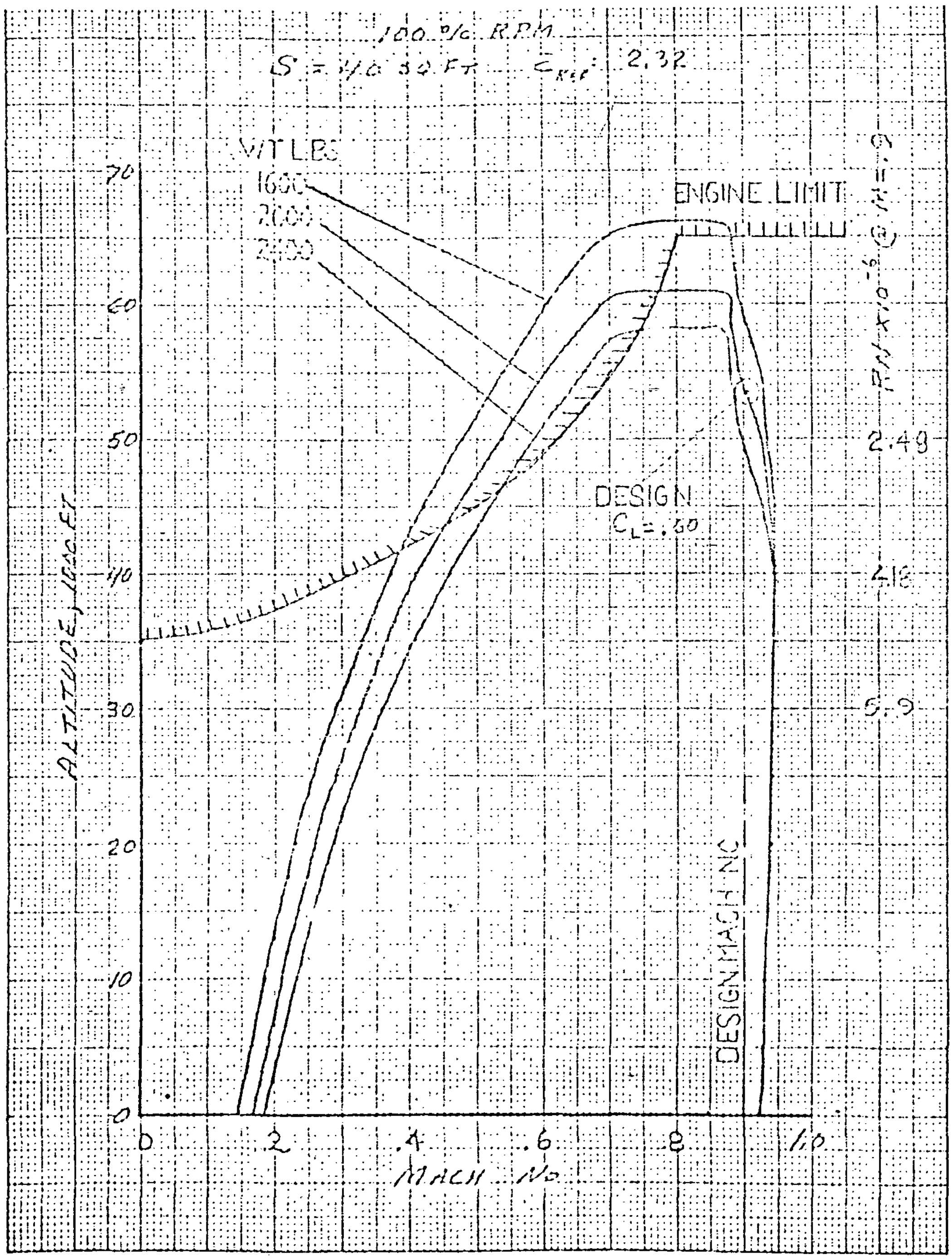

Figure 3-19. No. 4-40 Mach Number vs. Altitude

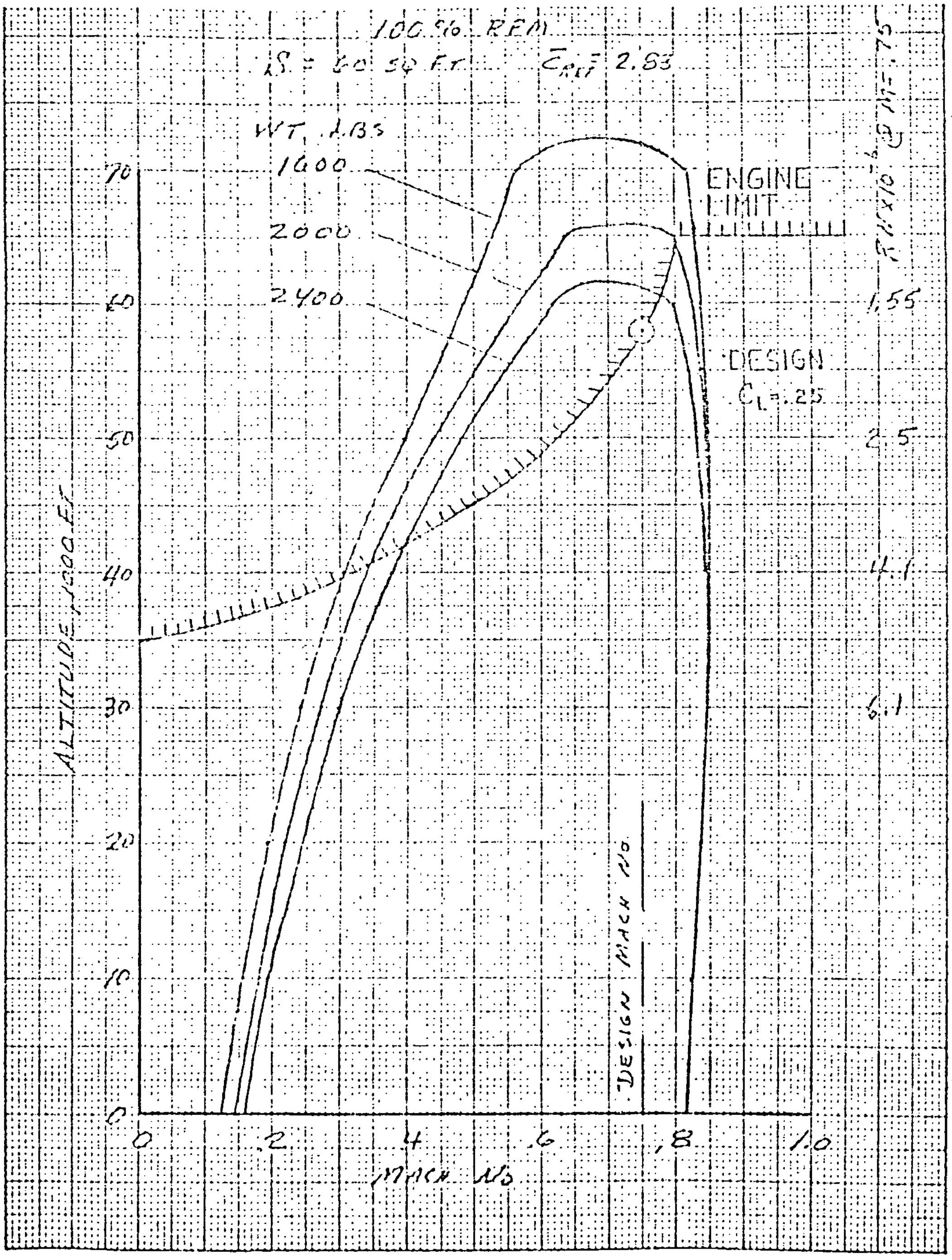

Figure 3-20. No. 5-60 Mach Number vs. Altitude

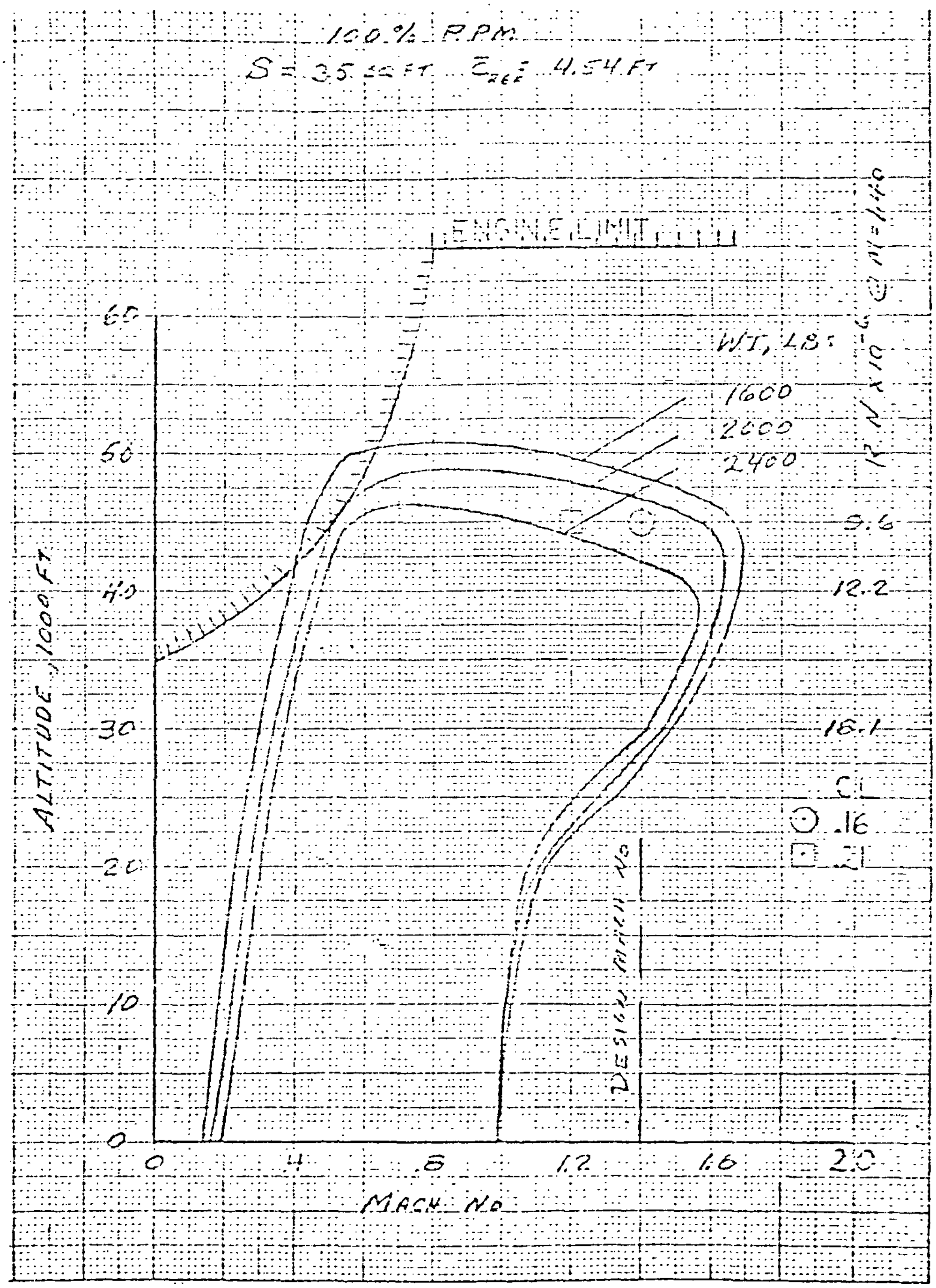

Figure 3-21. No. 6-35 Mach Number vs. Altitude

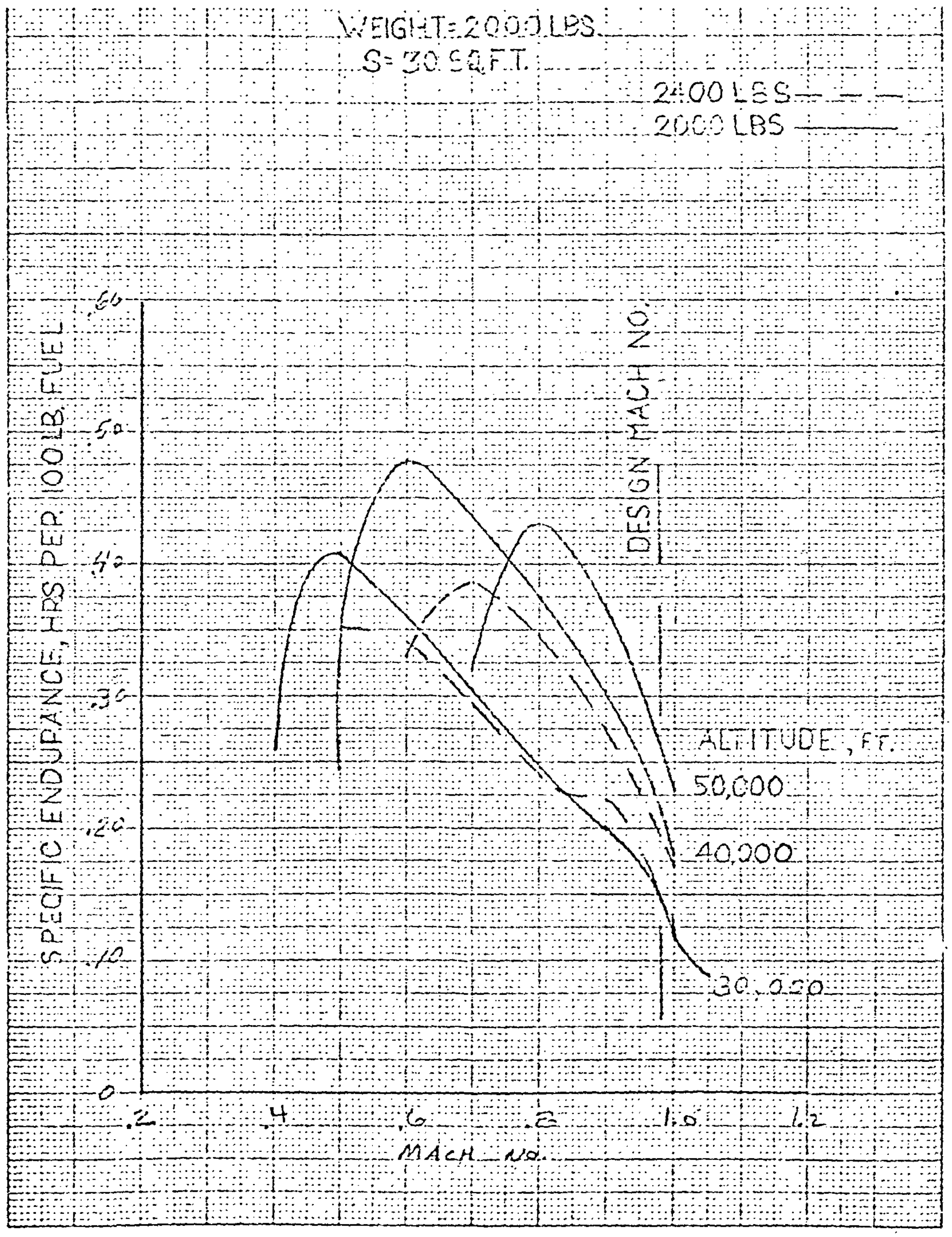

Figure 3-22. No. 1-30 Specific Endurance

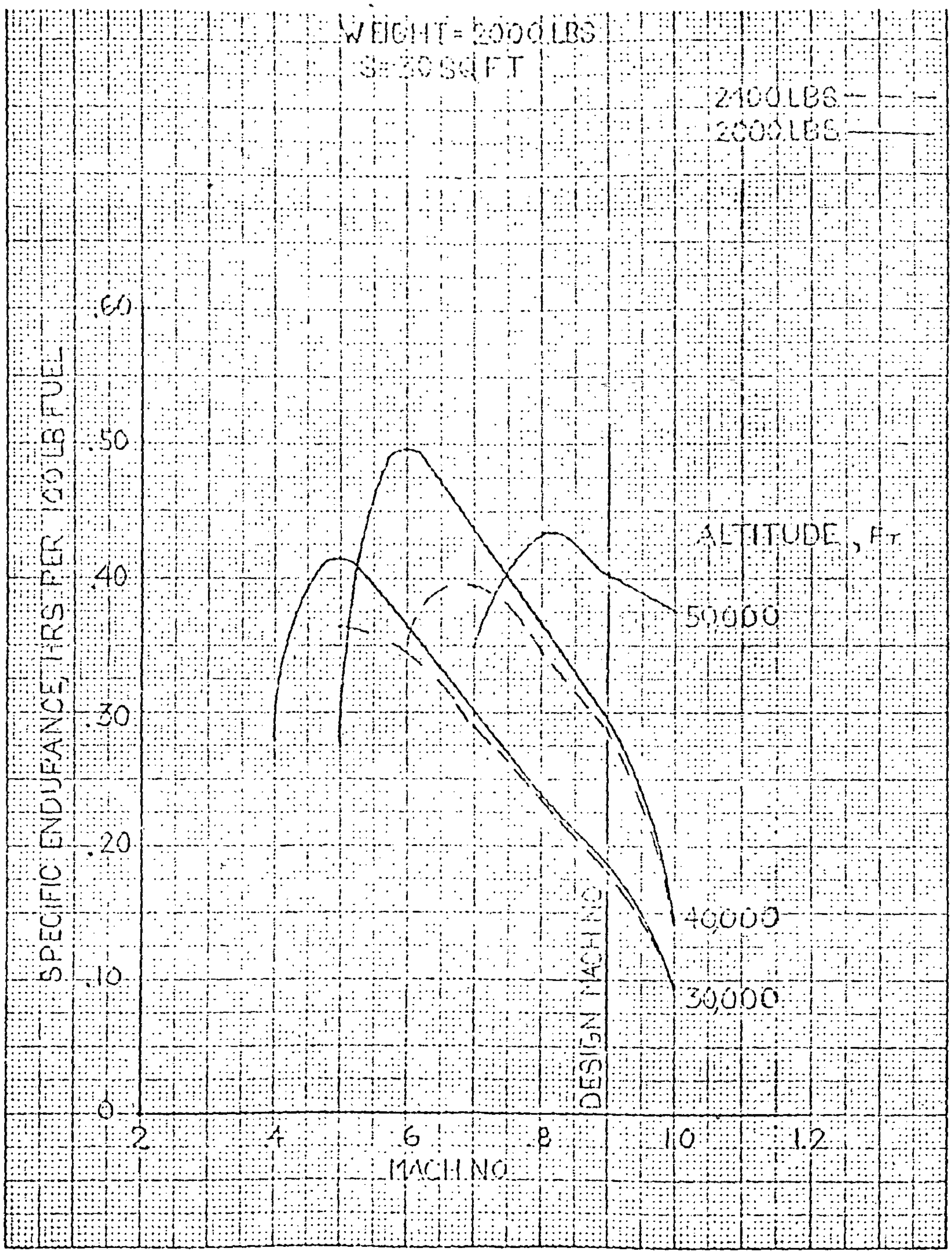

Figure 3-23. No. 2-30 Specific Endurance

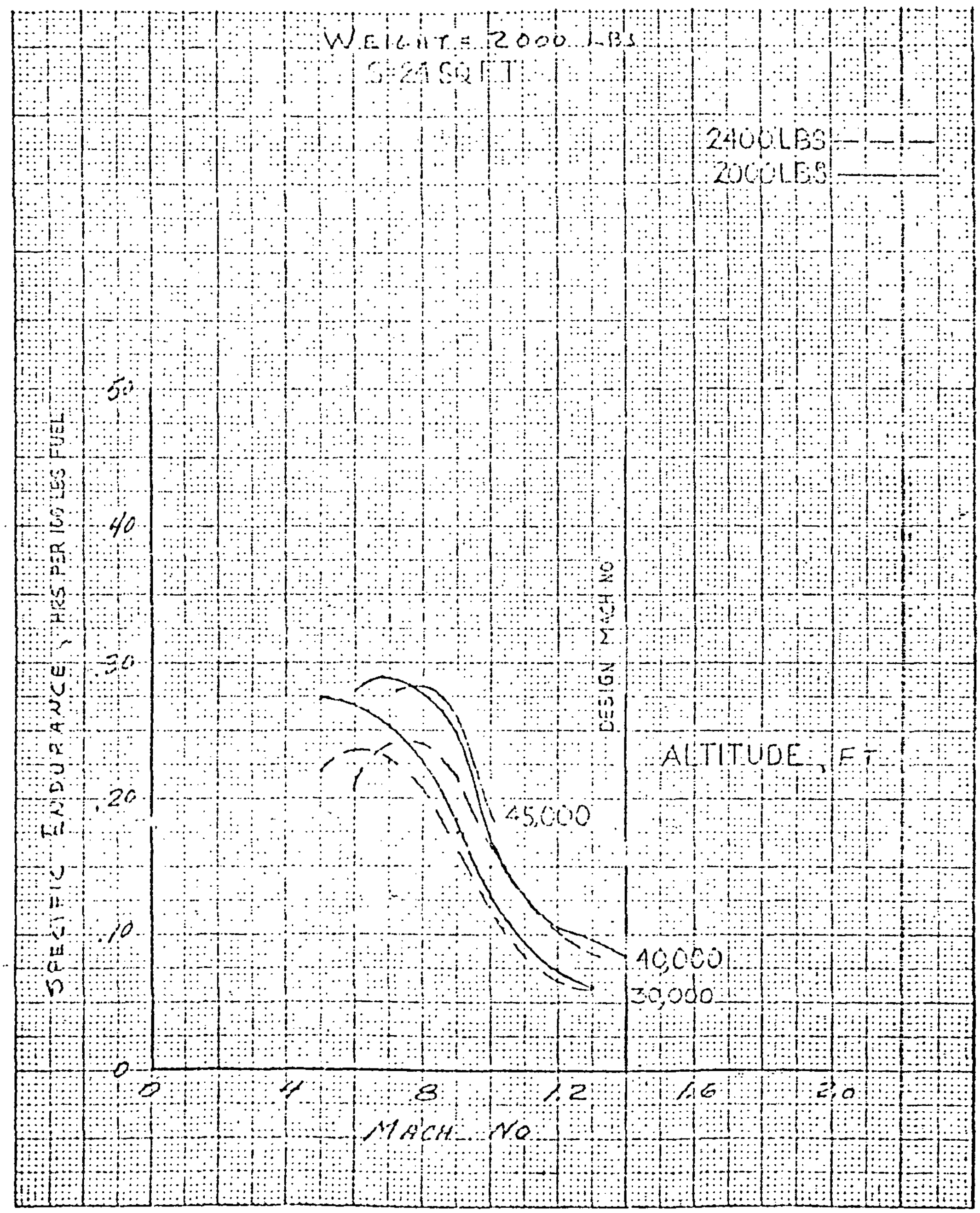

Figure 3-24. No. 3-24 Specific Endurance

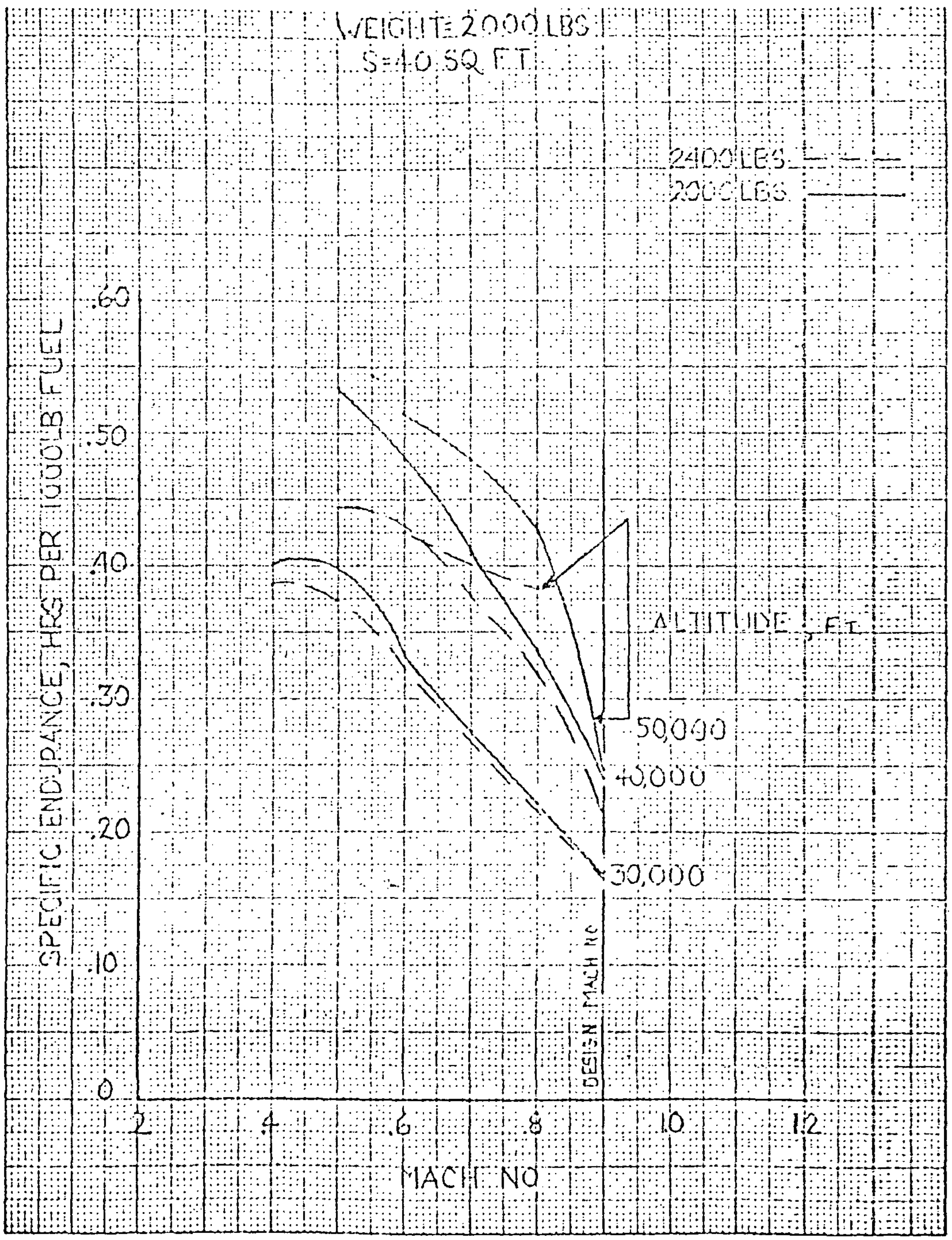

Figure 3-25. No. 4-40 Specific Endurance

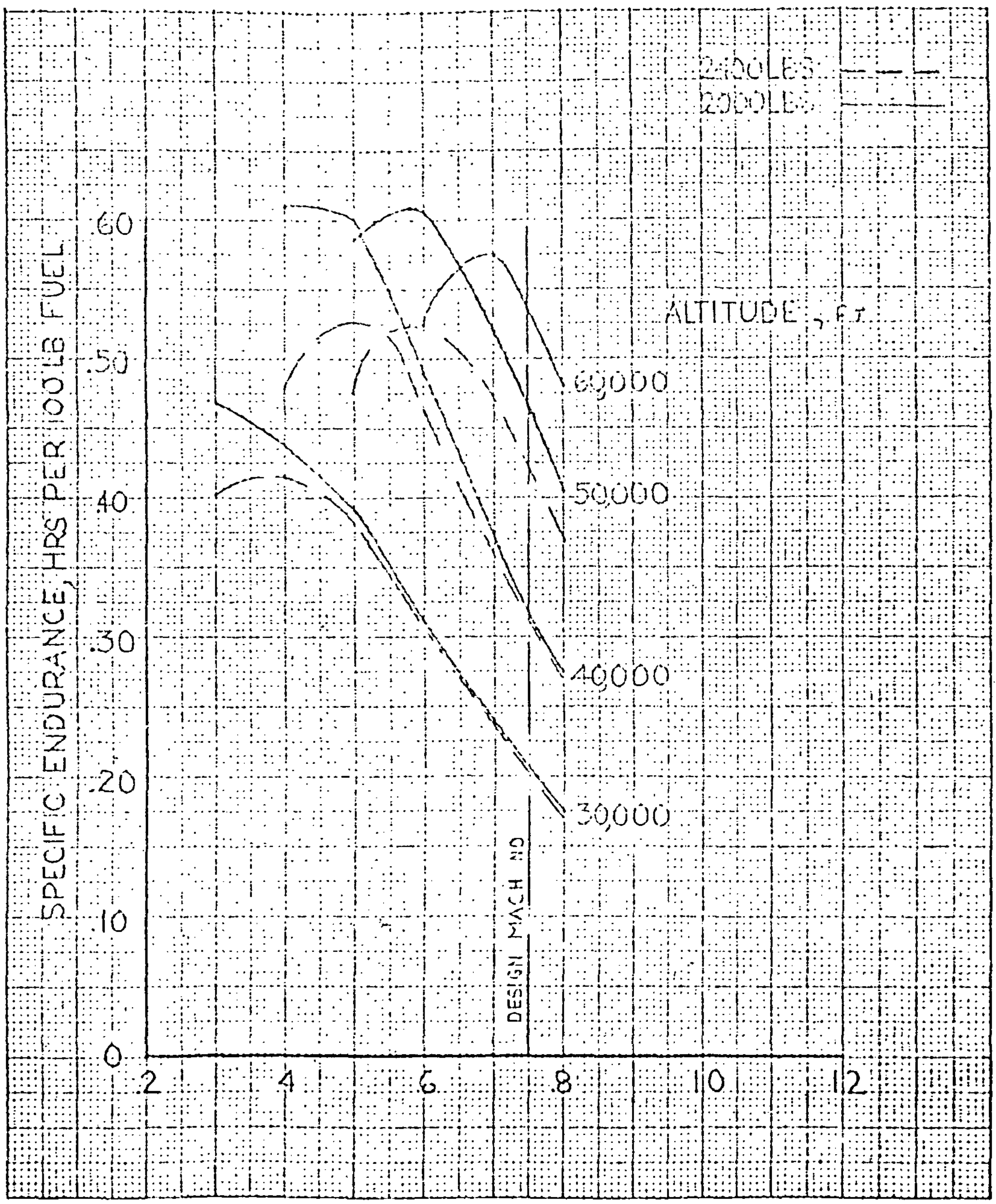

Figure 3-26. No. 5-60 Specific Endurance

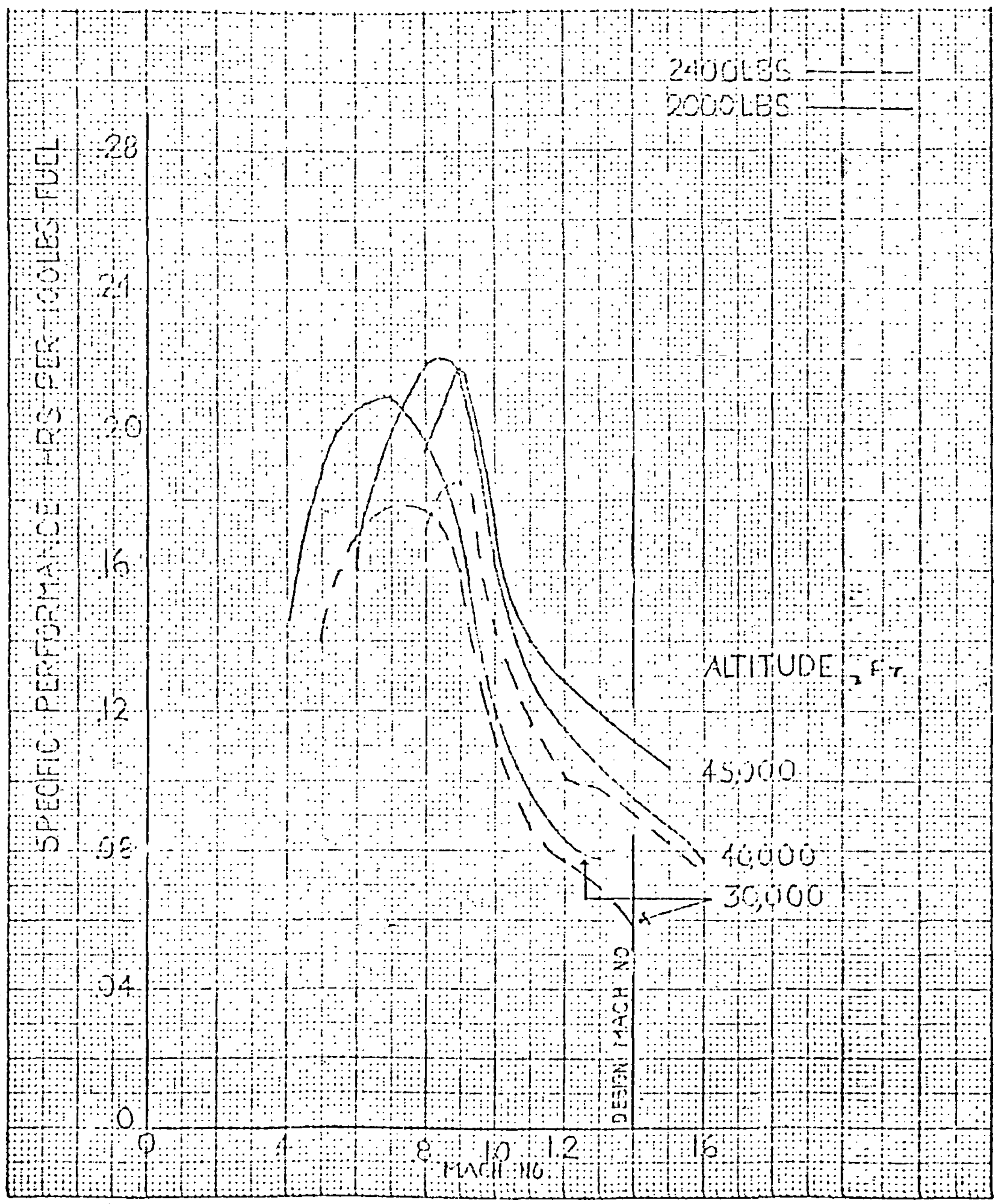

Figure 3-27. No. 6-35 Specific Endurance

The performance evaluation was preceded by estimates of the required longitudinal aerodynamic coefficients versus Mach number and angle of attack. Available methods included in the AAF Datcom Handbook, NASA Reports, and Teledyne Ryan estimation methods were applied directly as necessary to generate aerodynamic coefficients for this study. For most of the subject configurations, wind tunnel test data, due to compressibility and flow separation phenomena, were available as the data basis.

The results of the flight envelope capabilities evaluation of each point design, at three typical weights, are included in Figures 3-16 through 3-26. Typical NASA research mission capabilities are presented in Tables 3-1 through 3-6. Examples of the subsonic drag buildup for each of the wing configurations are included in Tables 3-7 through 3-12 at design altitudes. The supersonic wave drag and subsonic drag divergence phenomena were estimated by available Teledyne Ryan Advanced Systems empirical methods.

The applicable longitudinal coefficients versus Mach number for each of the subject configurations utilized to determine the flight performance envelopes are included in Figures 3-28 through 3-44.

The flight performance capabilities of each configuration were determined by means of the computerized Teledyne Ryan performance programs.

Area Rule Modifications

The distribution of volume in terms of cross-sectional area versus length was identified for each of the six-point designs. It was noted that the equivalent body fineness ratio of each point design was quite high, so that even without ideal area rule modifications this research vehicle would be expected to have low wave drag, i.e.:

CONFIGURATION	EQUIVALENT BODY F.R.
1-30	13.0
2-30	12.6
3-24	13.9
4-40	12.2
5-60	10.0
6-35	13.8

The variation of cross-sectional area of the selected configuration 1-30-2 can be compared with a recommended and an ideal zero-lift distribution in Figures 3-52 and 3-53.

TABLE 3-1

NASA RESEARCH MISSION TABULATION,
WING NO. 1-30, MACH 0.98 TRANSPORT

MISSION SEGMENT	SEGMENT DESCRIPTION	t (min.)	WEIGHT (lb.)	R (nm)
1	Warmup and launch at 10,000 ft.	0.0	45.0	0.0
2	Max. climb to 45,000 ft. at Mach 0.9	2.2	58.1	18.0
3	Design cruise at Mach 0.98 at 45,000 ft.	25.8	246.9	242.0

Launch Weight: 2342.1 lb.
Fuel Weight: 350.0 lb.
Zero Fuel Weight: 1992.1 lb.

TABLE 3-2

NASA RESEARCH MISSION TABULATION,
WING NO. 2-30, MACH 0.90 TRANSPORT

MISSION SEGMENT	SEGMENT DESCRIPTION	t (min.)	WEIGHT (lb.)	R (nm)
1	Warmup and launch at 10,000 ft.	0.0	45.0	0.0
2	Max. climb to 50,000 ft. at Mach 0.9	3.83	90.4	32.9
3	Design cruise at 50,000 ft. at Mach 0.9	49.9	214.6	429.0

Launch Weight: 2345.1 lb.
Fuel Weight: 350.0 lb.
Zero Fuel Weight: 1995.1 lb.

TABLE 3-3

NASA RESEARCH MISSION TABULATION, WING NO. 3-24, AIR-TO-AIR RPV

MISSION SEGMENT	SEGMENT DESCRIPTION	t (min.)	WEIGHT (lb.)	R (nm)
1	Warmup and launch at 10,000 ft.	0.0	45.0	0.0
2	Max. climb to 40,000 ft.	2.55	70.8	21.9
3	Design cruise at Mach 1.4 at 40,000 ft.	12.38	234.2	165.6

NOTE: Add 50.5 pounds of fuel to increase segment No. 3 to 15 minutes.

Launch Weight: 2314.1 lb.
Fuel Weight: 350.0 lb.
Zero Fuel Weight: 1964.1 lb.

TABLE 3-4

NASA RESEARCH MISSION TABULATION, WING NO. 4-40, ENDURANCE TURBOJET

MISSION SEGMENT	SEGMENT DESCRIPTION	t (min.)	WEIGHT (lb.)	R (nm)
1	Warmup and launch at 10,000 ft.	0.0	45.0	0.0
2	Max. climb to 50,000 ft.	4.54	99.7	43.4
3	Design cruise at Mach 0.9 at 50,000 ft.	47.3	205.3	406.0

Launch Weight: 2385.1 lb.
Fuel Weight: 350.0 lb.
Zero Fuel Weight: 2035.1 lb.

TABLE 3-5

NASA RESEARCH MISSION TABULATION,
WING NO. 5-60, ENDURANCE TURBOFAN

MISSION SEGMENT	SEGMENT DESCRIPTION	t (min.)	WEIGHT (lb.)	R (nm)
1	Warmup and launch at 10,000 ft.	0.0	45.0	0.0
2	Max. climb to 55,000 ft.	5.13	105.9	34.3
3	Design cruise at 55,000 ft., at Mach 0.75	58.0	199.1	418.11

Launch Weight: 2412.1 lb.
Fuel Weight: 350.0 lb.
Zero Fuel Weight: 2062.1 lb.

TABLE 3-6

NASA RESEARCH MISSION TABULATION,
WING NO. 6-35, SST CONFIGURATION

MISSION SEGMENT	SEGMENT DESCRIPTION	t (min.)	WEIGHT (lb.)	R (nm)
1	Warmup launch at 10,000 ft.	0.0	45.0	0.0
2	Max. climb to 40,000 ft.	2.84	78.7	26.2
3	Design cruise at Mach 1.4 at 40,000 ft.	12.54	226.3	167.5

NOTE: Add 44.3 pounds fuel to achieve 15-minute segment No. 3.

Launch Weight: 2322.1 lb.
Fuel Weight: 350.0 lb.
Zero Fuel Weight: 1972.1 lb.

TABLE 3-7

PROFILE DRAG BUILDUP, MODEL 1-30

COMPONENT	$\Delta t/c_{max.}$	(t/c)	AWet (sq. ft.)	ℓ Ref (ft.)	RN x 10^{-6}	C_f x 10^{-4}	K_f (L, R1)	$\frac{A_w}{S_{Ref}}$	ΔC_{D_o}	f
Wing:										
Inner Panel	60	0.11	20.0	3.90	5.28	32	1.32	0.67	0.0028	
Outer Panel	38	0.08	37.2	1.79	2.42	37	1.48	1.24	0.0068	
Horizontal	32	0.035	11.0	1.45	1.96	39	1.34	0.37	0.0019	
Vertical	40	0.003	13.6	2.71	3.67	35	1.34	0.45	0.0021	
Fuselage			102.4	28.25	38.26	25	1.15	3.41	0.0098	
Nacelle (Eng.)			44.5	13.5	18.28	26	1.20	1.48	0.0046	
Base Drag									0.0015	
Antennas									0.0010	
Total			228.7						0.0305	

Mach No.: 0.90
Altitude: 45,000 feet

RN/ft.: 1.3545

S. Reference: 30.0 sq. ft.
$\overline{C}$ Reference: 2.25 feet

TABLE 3-8

PROFILE DRAG BUILDUP, MODEL NO. 2-30

COMPONENT	$\Lambda t/c_{max.}$	(t/c)	AWet (sq. ft.)	ℓ Ref (ft.)	RN x 10^{-6}	C_f x 10^{-4}	K_f (L, R1)	$\frac{Aw}{S_{Ref}}$	ΔC_{D_o}	f
Wing:										
Inner Panel	60	0.12	24.81	4.27	5.78	32	1.32	0.83	0.0035	
Outer Panel	30	0.09	37.29	1.68	2.28	38	1.48	1.24	0.0070	
Horizontal	32	0.035	11.0	1.45	1.96	39	1.34	0.37	0.0019	
Vertical	40	0.003	13.6	2.71	3.67	35	1.34	0.45	0.0021	
Fuselage			102.4	28.25	38.26	25	1.15	3.41	0.0098	
Nacelle (Eng.)			44.5	13.5	18.28	26	1.20	1.48	0.0046	
Base Drag									0.0015	
Antennas									0.0010	
Total			233.6						0.0314	

Mach No: 0.90
Altitude: 45,000 feet

RN/ft.: 1.3545

S. Reference: 30.0 sq. ft.
$\overline{C}$ Reference: 2.08 feet

TABLE 3-9

PROFILE DRAG BUILDUP, MODEL NO. 3-24

COMPONENT	$\Lambda t/c_{max.}$	(t/c)	AWet (sq. ft.)	ℓ Ref (ft.)	RN x 10^{-6}	C_f x 10^{-4}	K_f (L. R1)	$\frac{Aw}{S_{Ref}}$	ΔC_{D_o}	f
Wing:										
Inner Panel	59	0.05	18.86	4.00	5.42	32	1.32	0.79	0.0034	
Outer Panel	37	0.045	22.84	1.97	2.67	36	1.46	0.95	0.0050	
Horizontal	32	0.035	11.0	1.45	1.96	39	1.34	0.46	0.0024	
Vertical	40	0.003	13.6	2.71	3.67	35	1.34	0.57	0.0027	
Fuselage			102.4	28.25	38.26	25	1.15	4.27	0.0123	
Nacelle (Eng.)			44.5	13.5	18.28	26	1.20	1.85	0.0058	
Base Drag									0.0019	
Antennas									0.0013	
Total			213.2						0.0348	

Mach No.: 0.90
Altitude: 45,000 feet

RN/ft.: 1.3545

S. Reference: 24.0 sq. feet
$\overline{C}$ Reference: 2.58 feet

TABLE 3-10

PROFILE DRAG BUILDUP, MODEL NO. 4-40

COMPONENT	$\Lambda t/c_{max.}$	(t/c)	AWet (sq. ft.)	ℓ Ref (ft.)	RN x 10^{-6}	C_f x 10^{-4}	K_f (L, Rl)	$\frac{Aw}{S_{Ref}}$	ΔC_{D_o}	f
Wing:										
Inner Panel	58	0.11	32.6	4.54	6.15	31	1.33	0.82	0.0034	
Outer Panel	32	0.08	55.8	1.78	2.41	37	1.51	1.40	0.0078	
Horizontal	32	0.035	11.0	1.45	1.96	39	1.34	0.28	0.0015	
Vertical	40	0.003	13.6	2.71	3.67	34	1.34	0.34	0.0015	
Fuselage			102.4	28.25	38.26	25	1.15	2.56	0.0074	
Nacelle (Eng.)			44.5	13.5	18.28	26	1.20	1.11	0.0035	
Base Drag									0.0012	
Antennas									0.0008	
Total			259.9						0.0271	

Mach No.: 0.90
Altitude: 45,000 feet

RN/ft.: 1.3545

S, Reference: 40.0 sq. feet
$\bar{C}$ Reference: 2.32 feet

TABLE 3-11

PROFILE DRAG BUILDUP, MODEL NO. 5

COMPONENT	$\Lambda t/c_{max.}$	(t/c)	AWet (sq. ft.)	ℓ Ref (ft.)	RN x 10^{-6}	$C_f \times 10^{-4}$	K_f (L, R1)	$\frac{Aw}{S_{Ref}}$	ΔC_{D_o}	f
Wing:	24	0.14	117.7	2.48	2.80	37	1.57	1.96	0.0114	
Inner Panel Outer Panel										
Horizontal		0.035	11.0	1.45	1.64	40	1.34	0.18	0.0010	
Vertical		0.003	13.6	2.71	3.06	35	1.34	0.23	0.0011	
Fuselage			102.4	28.25	31.89	25	1.15	1.71	0.0050	
Nacelle (Eng.)			44.5	13.5	15.24	27	1.20	0.74	0.0024	
Base Drag									0.0008	
Antennas									0.0005	
Total			289.5						0.0222	

Mach No.: 0.75
Altitude: 45,000 feet

RN/ft.: 1.129

S. Reference: 60.0 sq. feet
$\overline{C}$ Reference: 2.83 feet

TABLE 3-12

PROFILE DRAG BUILDUP, MODEL NO. 6-35

COMPONENT	$\Lambda t/c_{max.}$	(t/c)	AWet (sq. ft.)	ℓ Ref (ft.)	RN x 10^{-6}	$C_f \times 10^{-4}$	K_f (L, Rl)	$\frac{A_w}{S_{Ref}}$	ΔC_{D_o}	f
Wing										
Inner Panel	54	0.05	31.71	5.63	7.62	30	1.24	0.906	0.0034	
Outer Panel	33	0.04	22.36	2.30	3.11	36	1.41	0.639	0.0032	
Horizontal	32	0.035	11.0	1.45	1.96	39	1.34	0.314	0.0016	
Vertical	40	0.003	13.6	2.71	3.67	34	1.34	0.388	0.0018	
Fuselage			102.4	28.25	38.26	25	1.15	2.93	0.0084	
Nacelle (Eng.)			44.5	13.5	18.28	26	1.20	1.27	0.0040	
Base Drag									0.0014	
Antennas									0.0008	
Total			225.57						0.0246	

Mach No.: 0.90
Altitude: 45,000 feet

RN/ft.: 1.3545

S. Reference: 35.0 sq. feet
$\bar{C}$ Reference: 4.54 feet

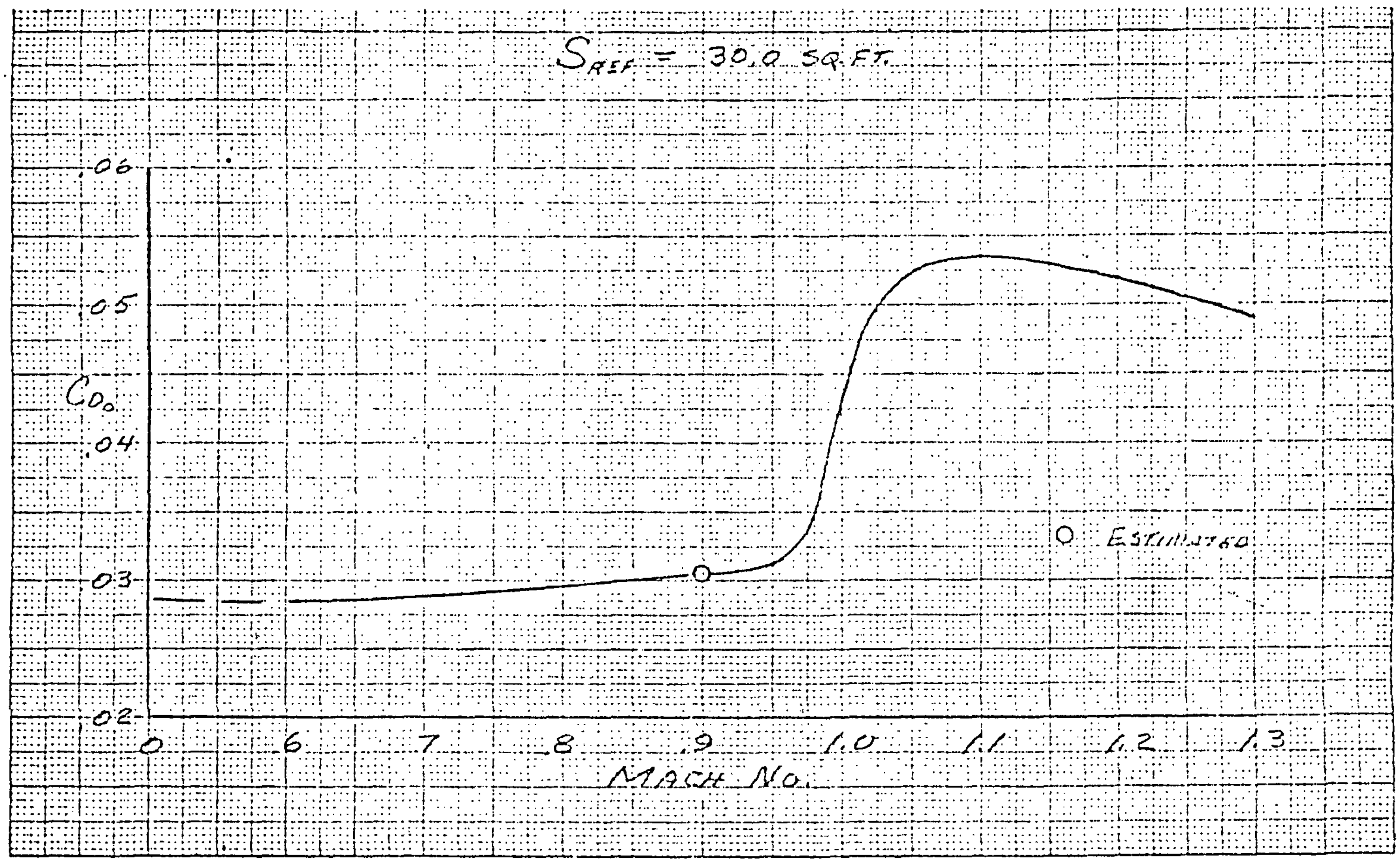

Figure 3-28. No. 1-30 C_{D_0} vs. Mach Number

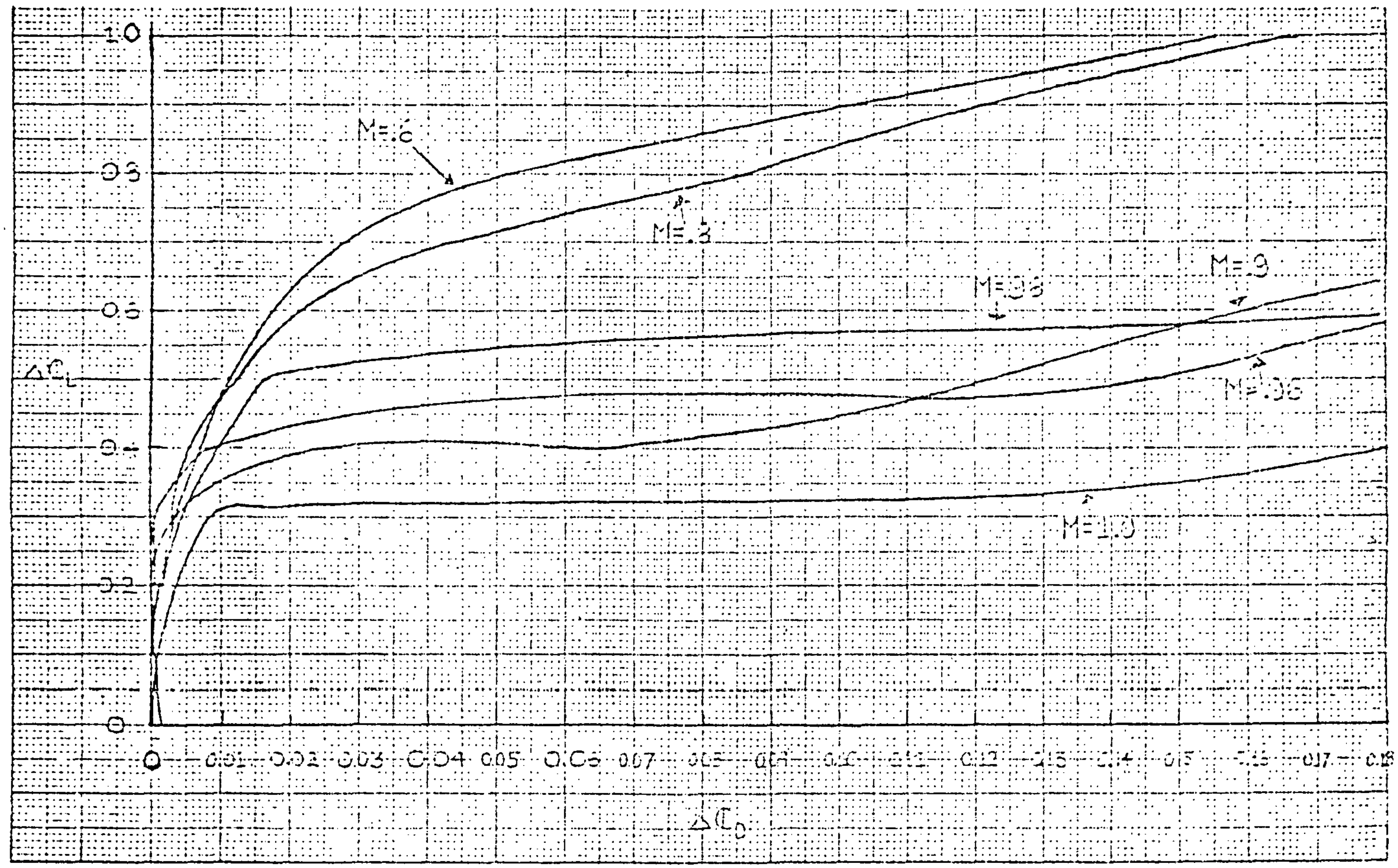

Figure 3-29. No. 1-30 Induced Drag Coefficient vs. Mach Number

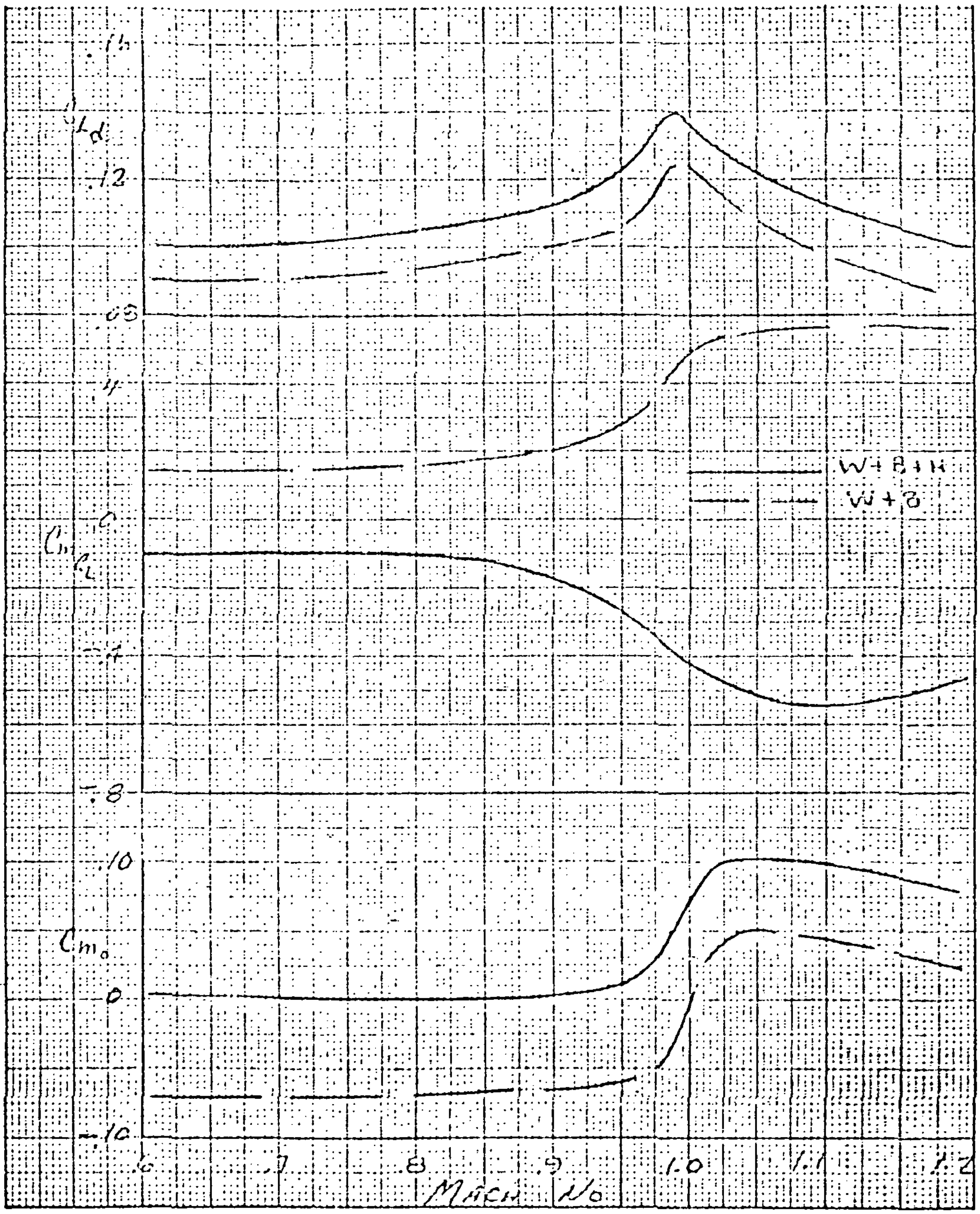

Figure 3-30. No. 1-30 Longitudinal Characteristics

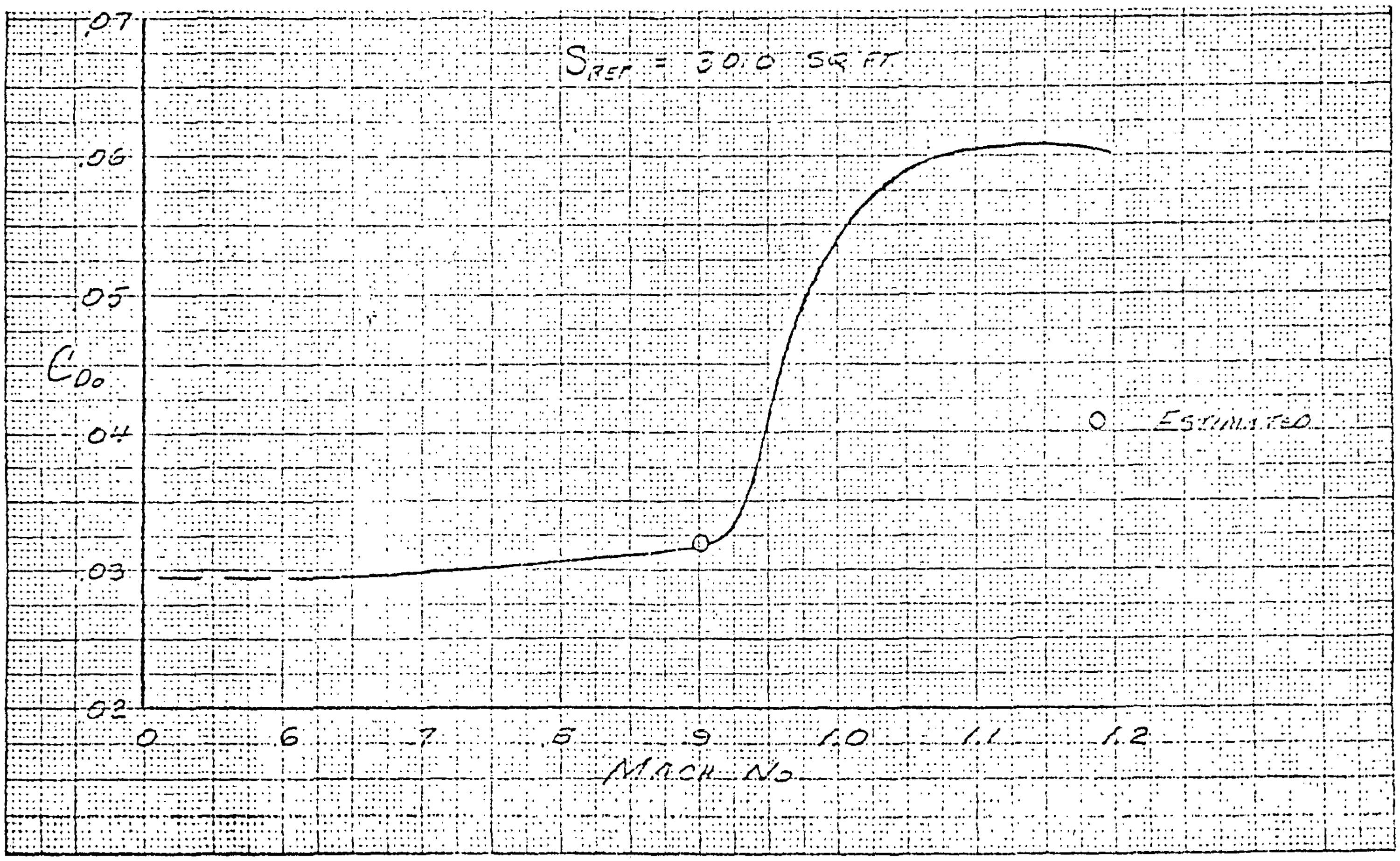

Figure 3-31. No. 2-30 C_{D_0} vs. Mach Number

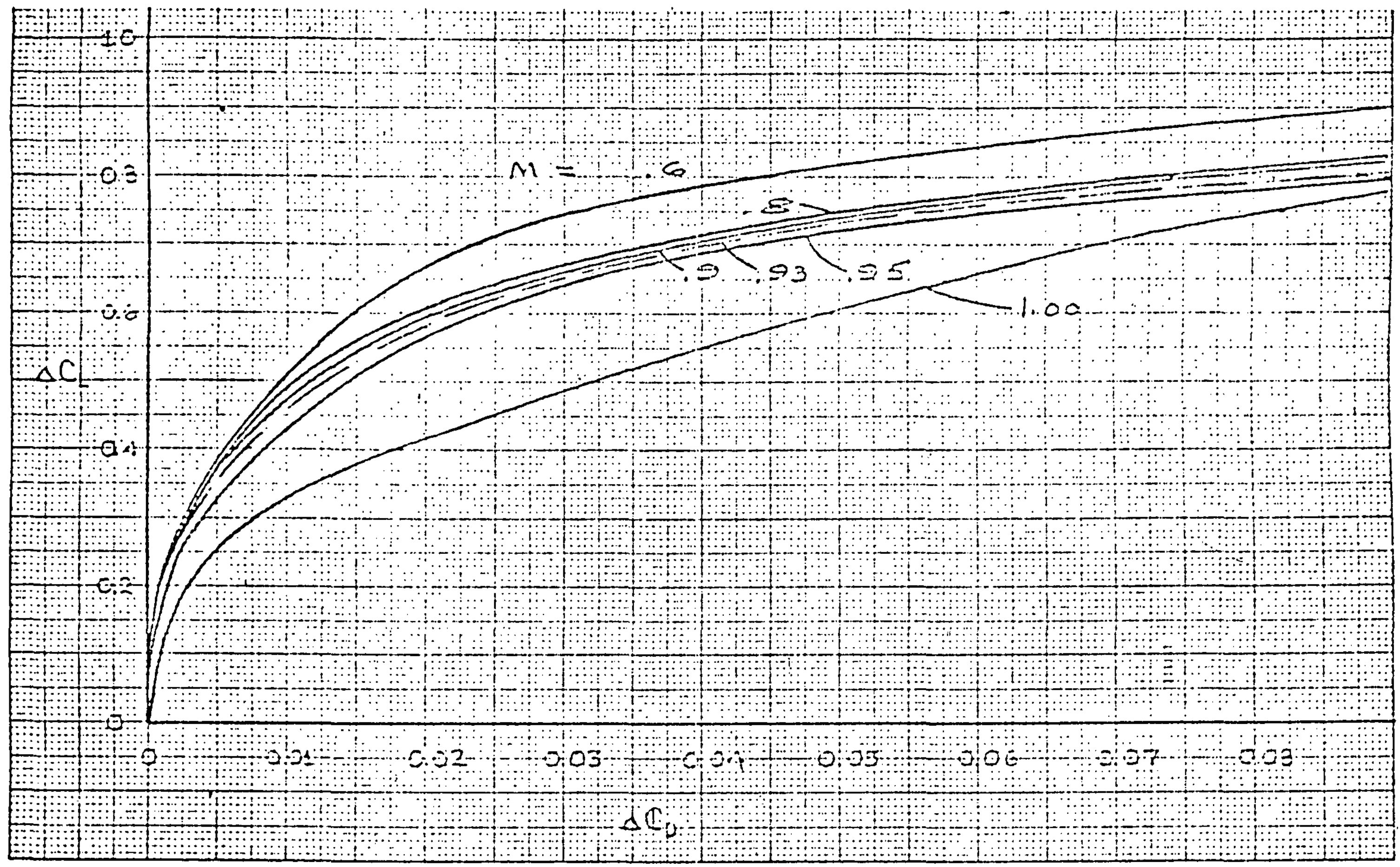

Figure 3-32. No. 2-30 Induced Drag Coefficient vs. Mach Number

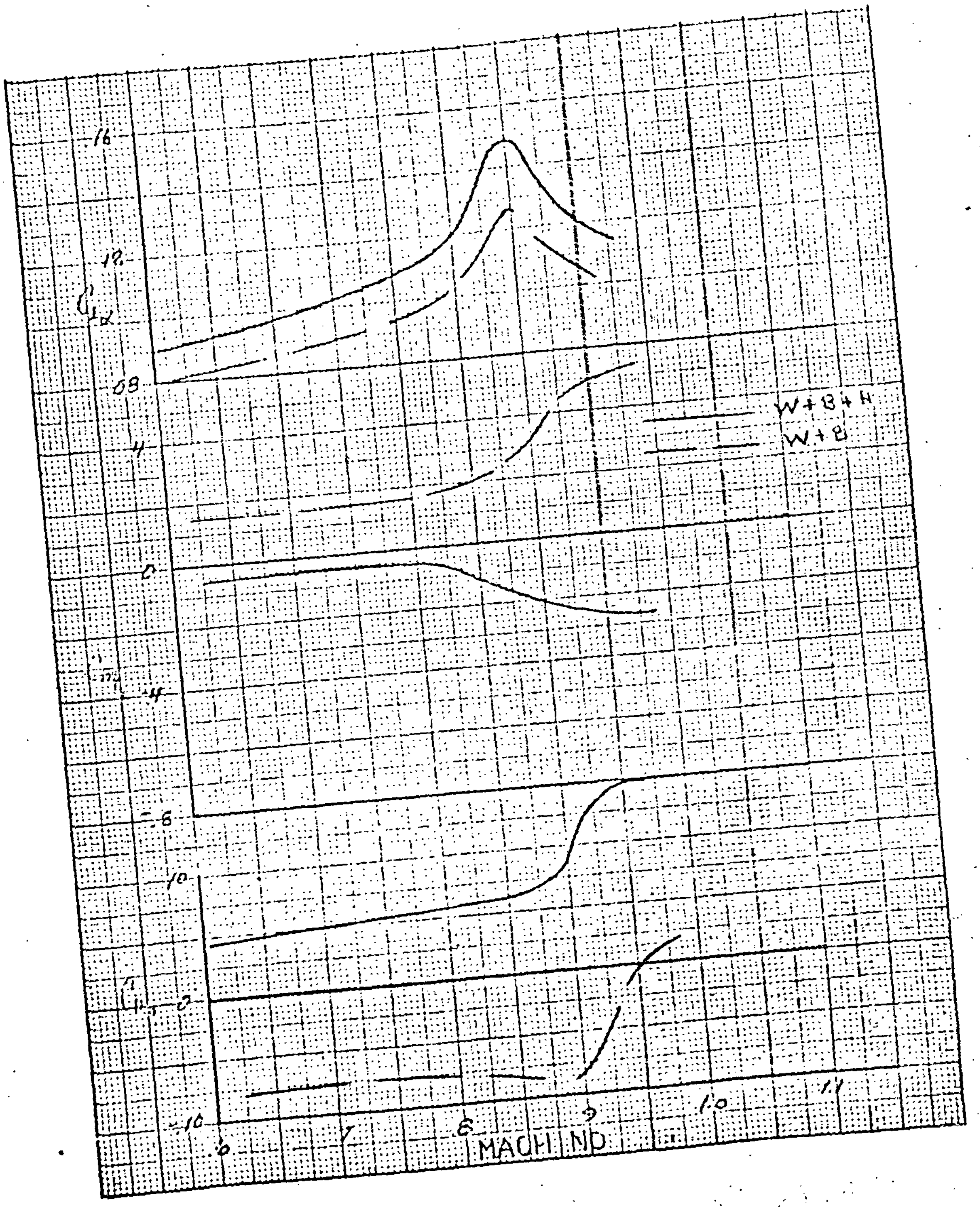

Figure 3-33. No. 2-30 Longitudinal Characteristics

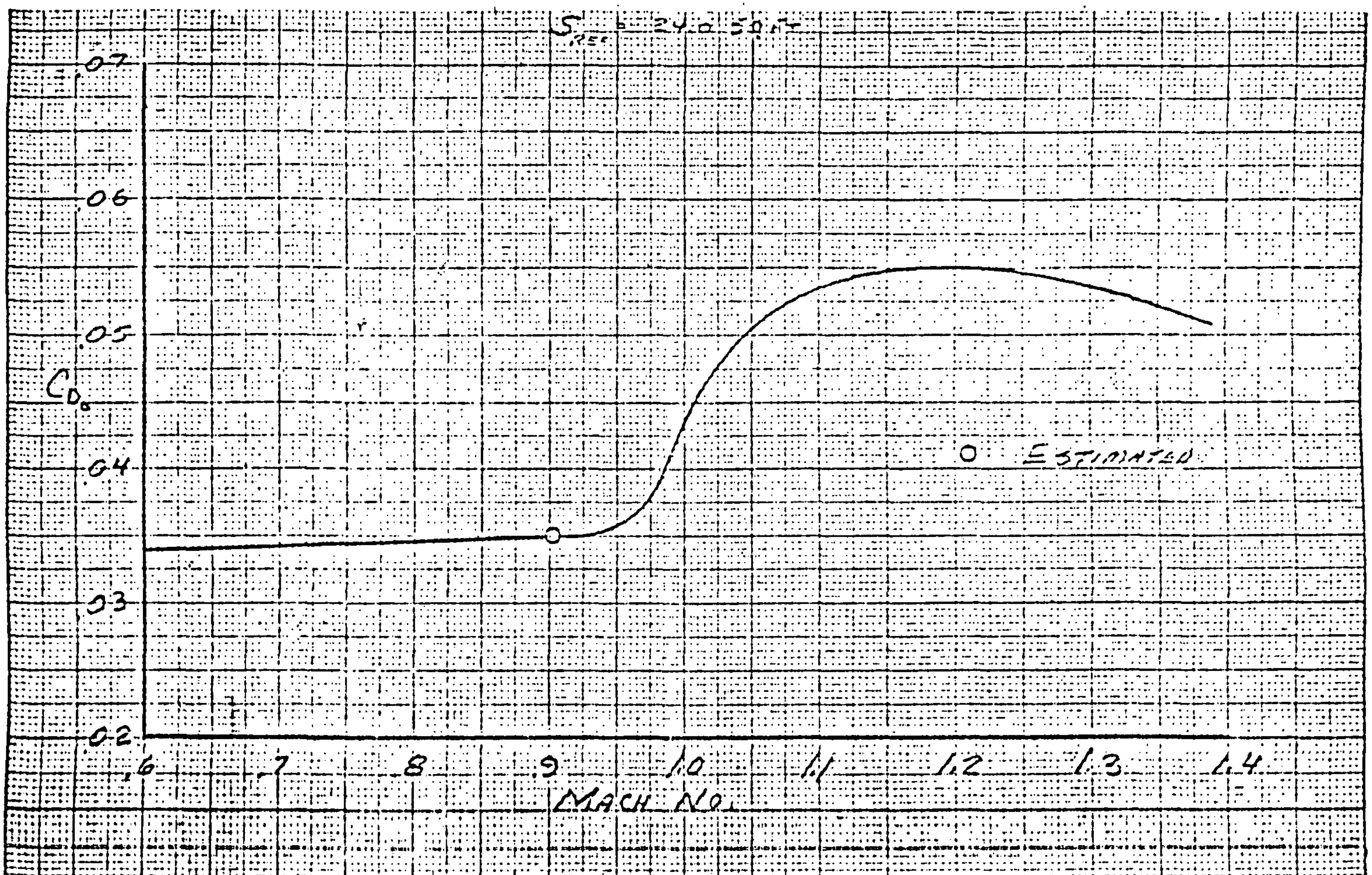

Figure 3-34. No. 3-24 C_{D_0} vs. Mach Number

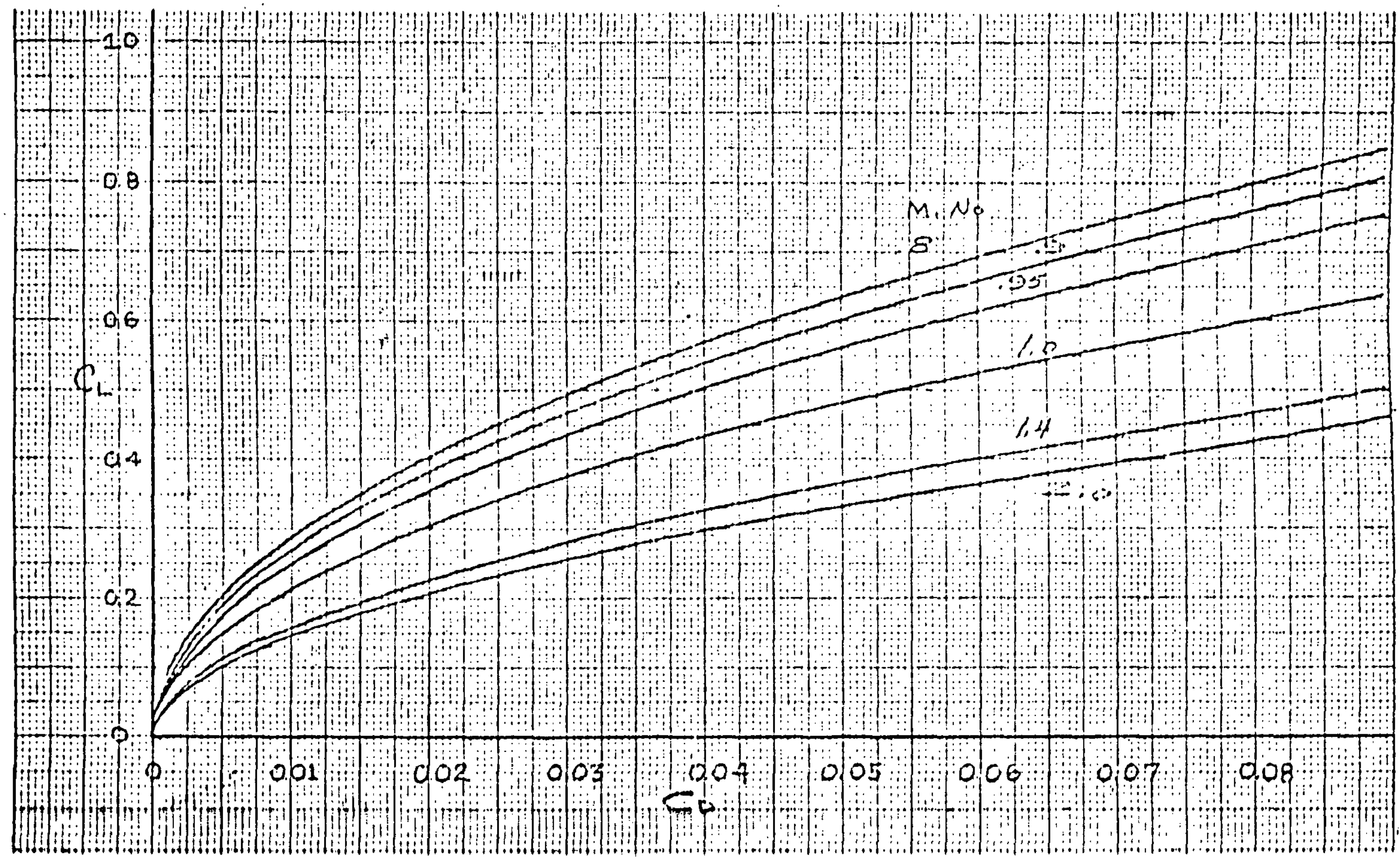

Figure 3-35. No. 3-24 Induced Drag Coefficient vs. Mach Number

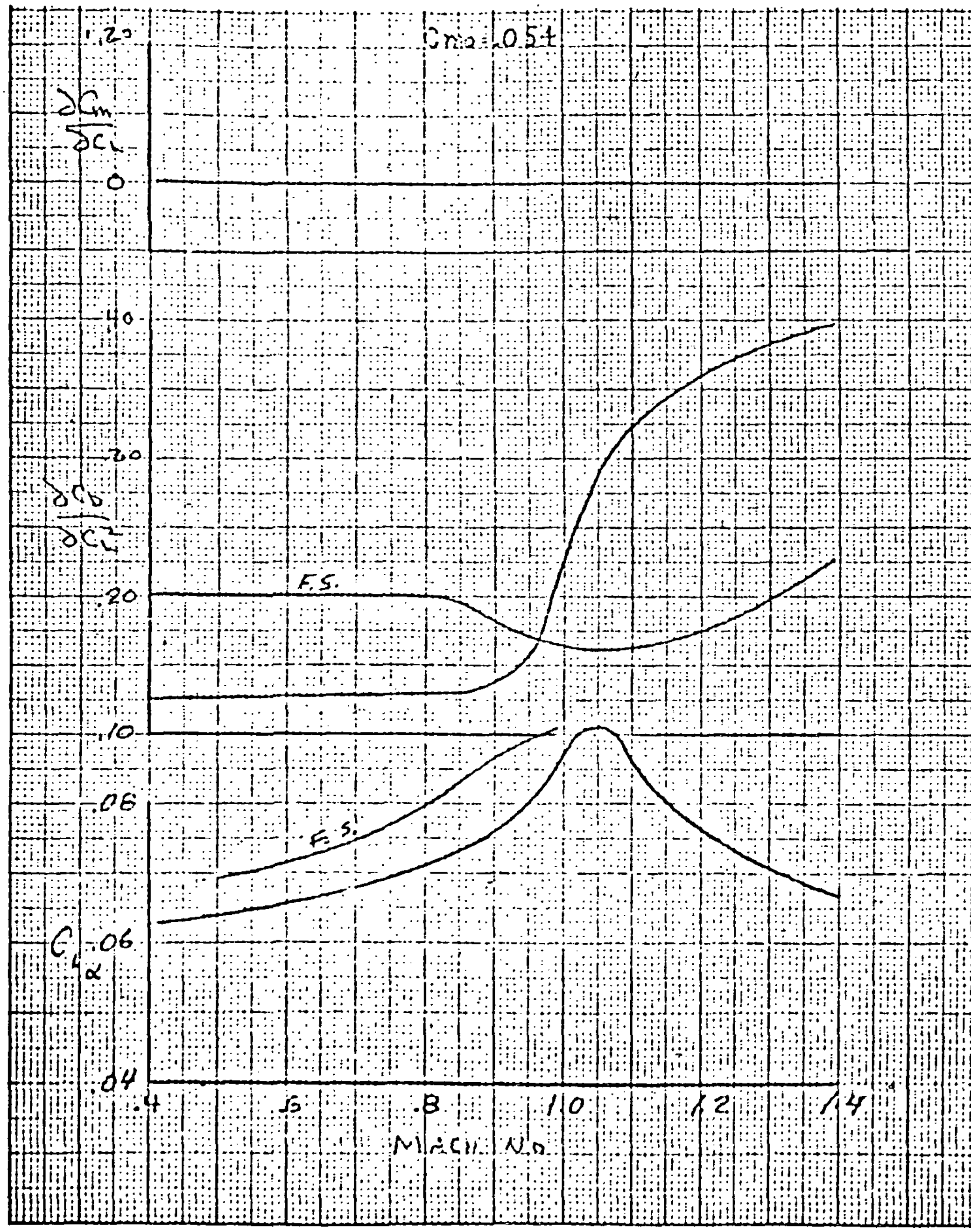

Figure 3-36. No. 3-24 Longitudinal Characteristics

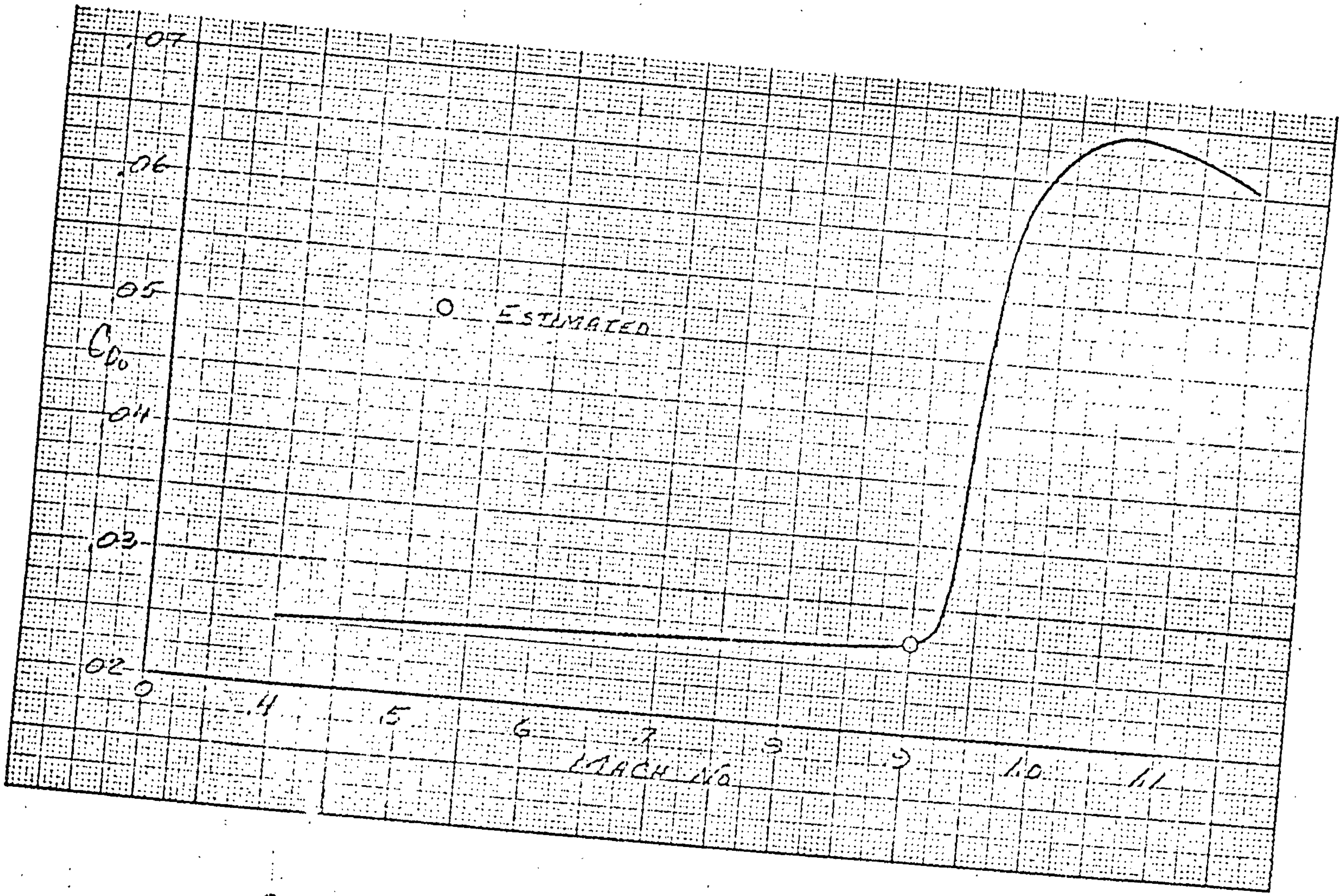

Figure 3-37. No. 4-40 C_{D_0} vs. Mach Number

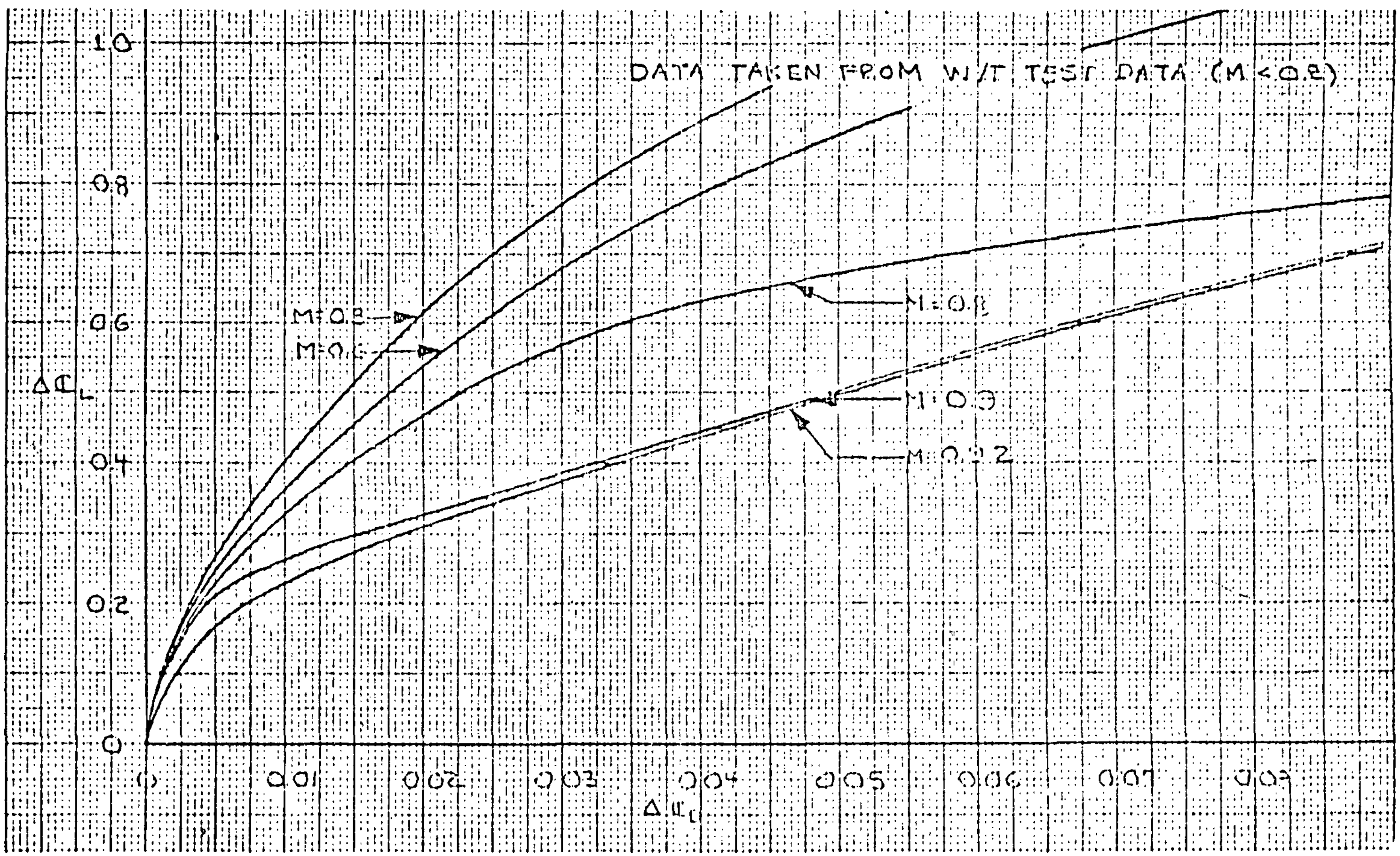

Figure 3-38. No. 4-40 Induced Drag Coefficient vs. Mach Number

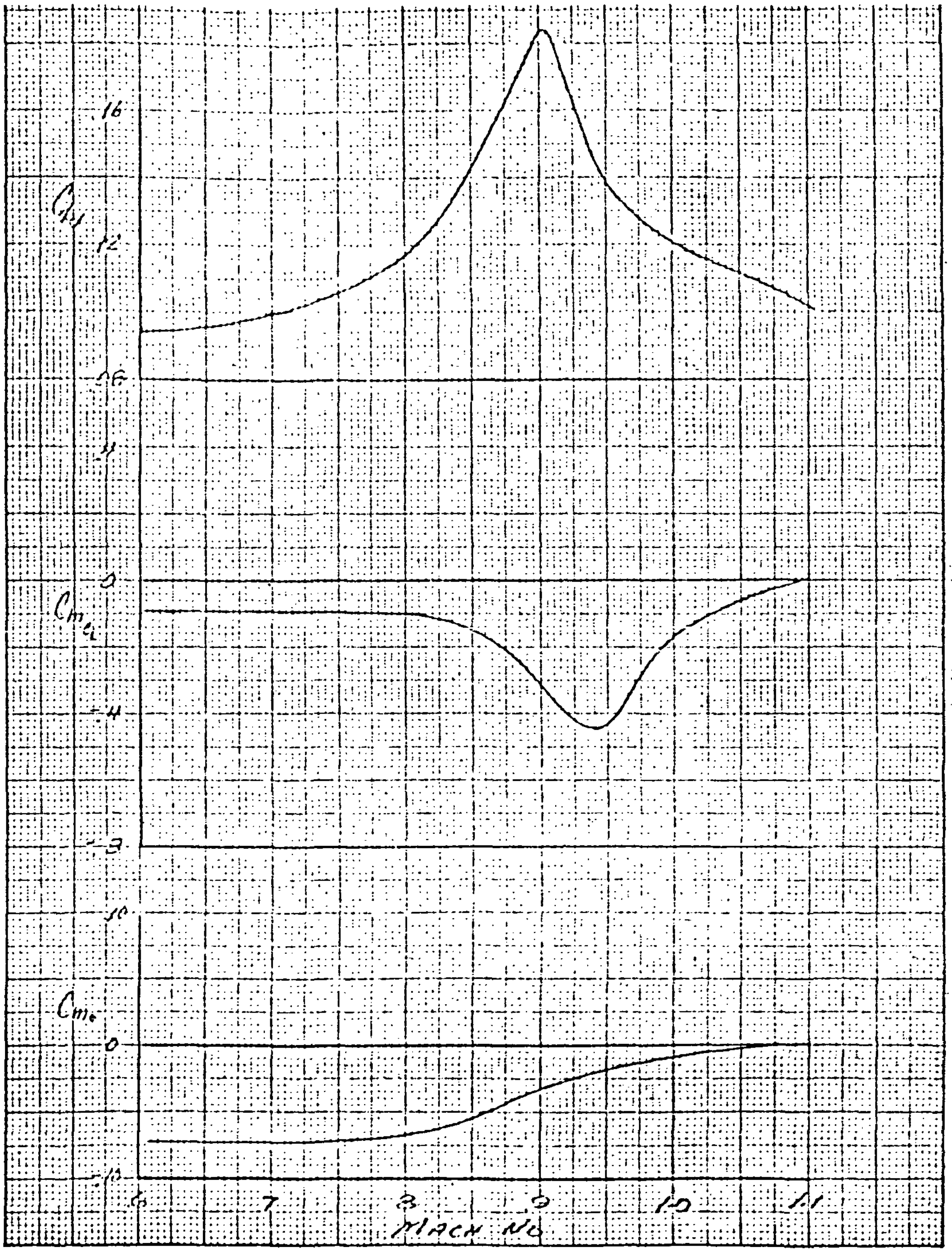

Figure 3-39. No 4-40 Longitudinal Characteristics

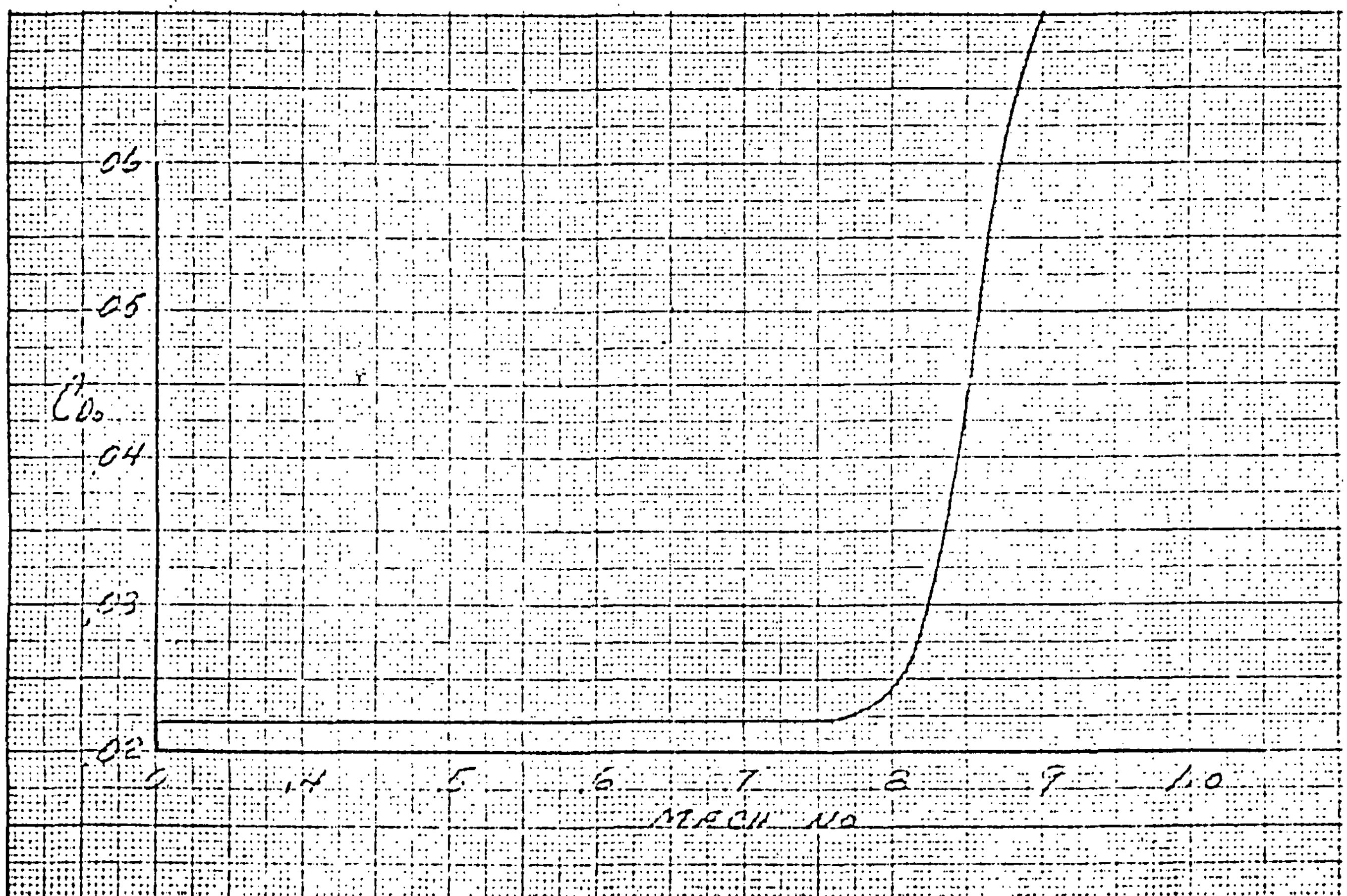

Figure 3-40. No. 5 C_{D_0} vs. Mach Number

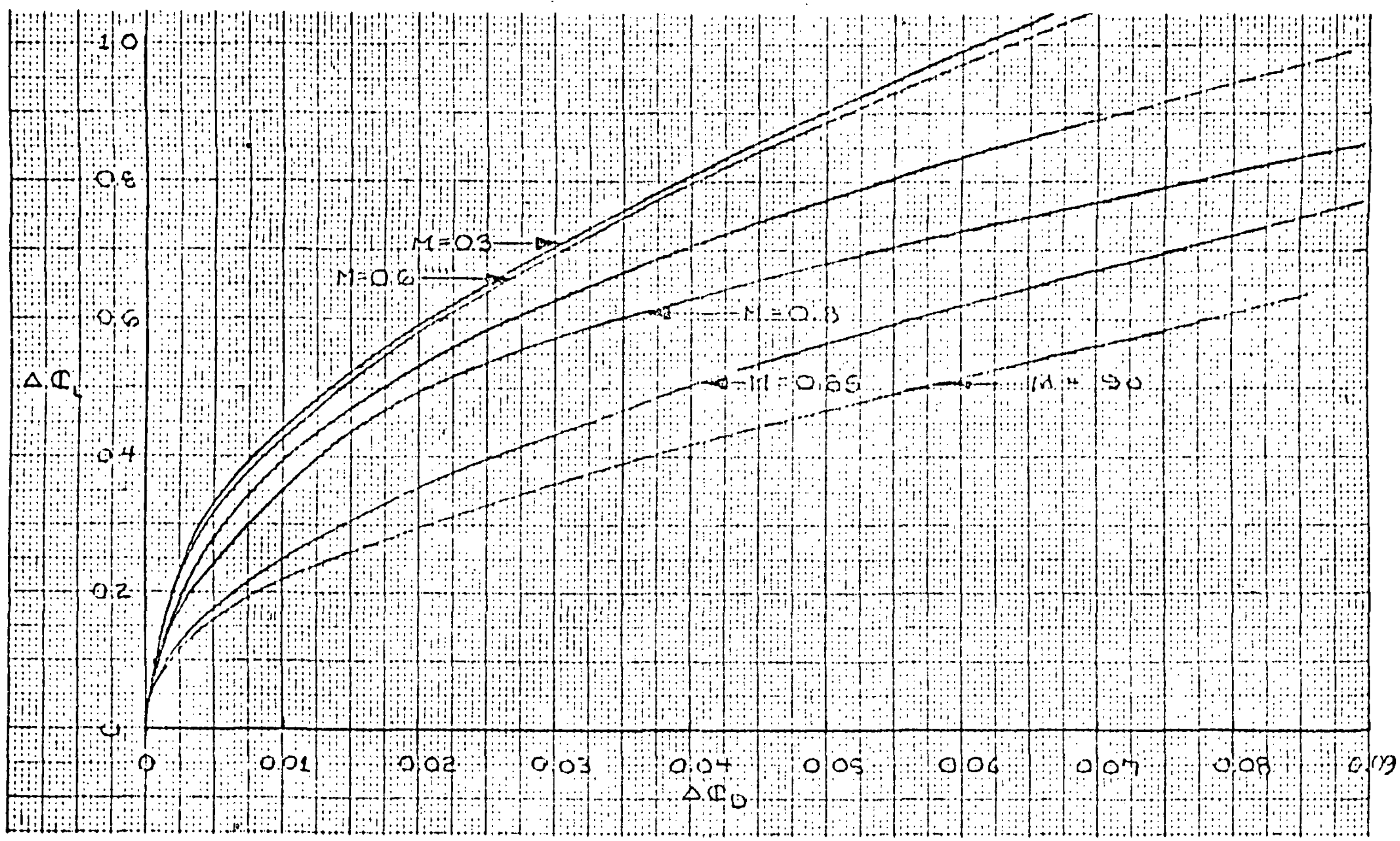

Figure 3-41. No 5-60 Induced Drag Coefficient vs. Mach Number

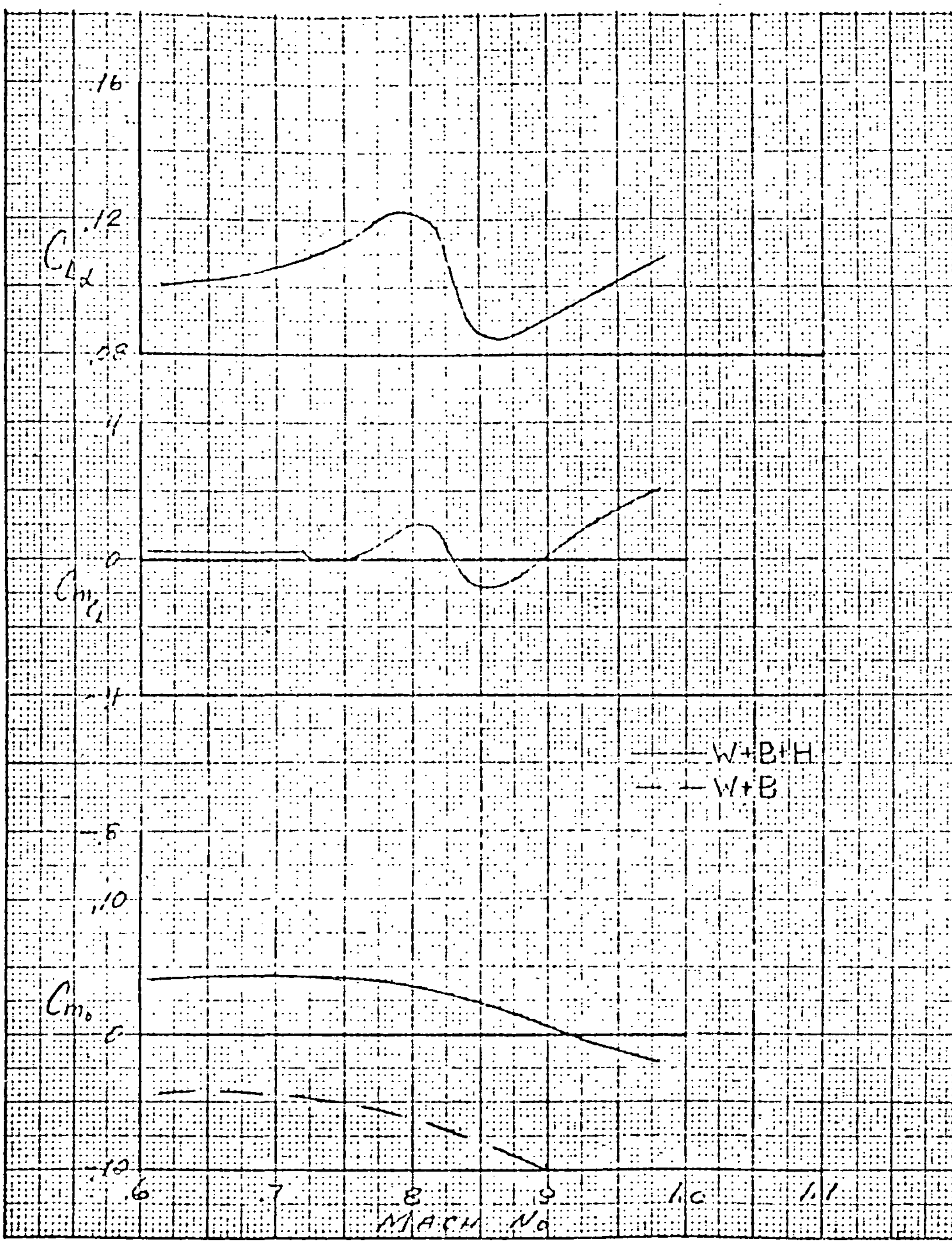

Figure 3-32. No. 5-60 Longitudinal Characteristics

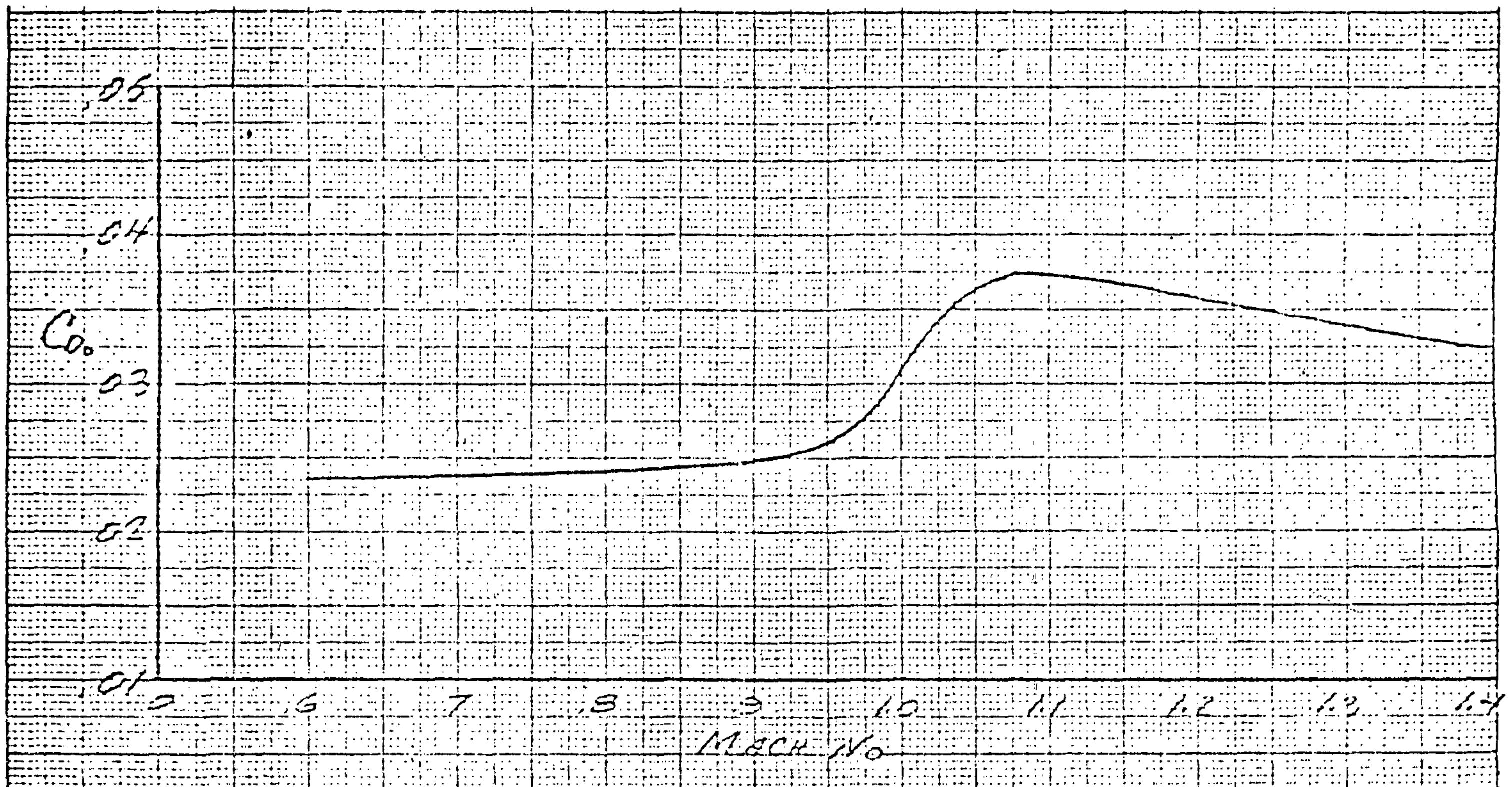

Figure 3-43. No. 6-35 C_{D_0} vs. Mach Number

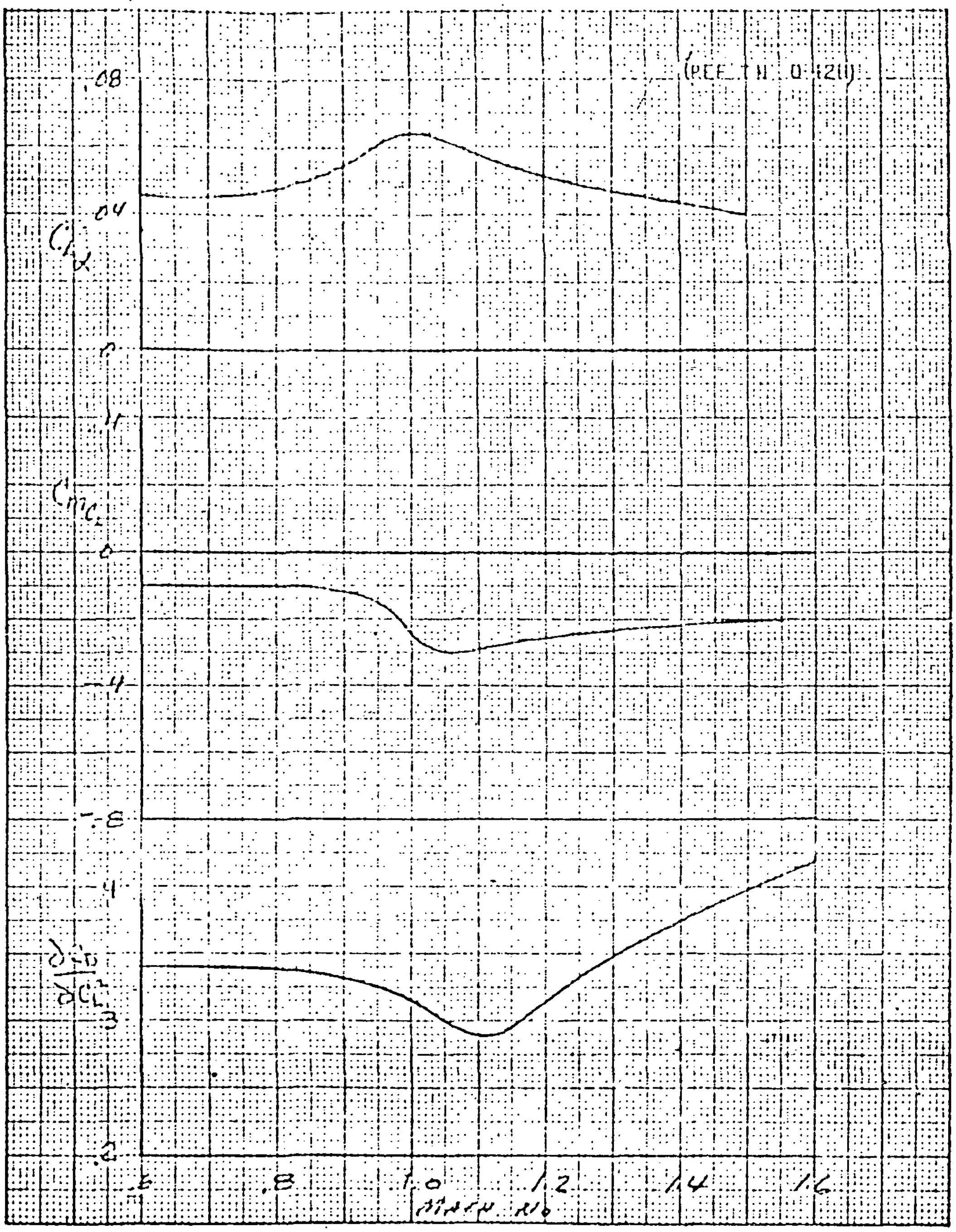

Figure 3-44. No. 6-35 Longitudinal Characteristics

To achieve an ideal distribution of volume, the fine-body cross-sectional area would have to be almost doubled. A very reasonable compromise, well suited to the Mach range of this research drone and designated as "minimum area rule fairings", is illustrated in Figure 3-51. The shoulder fairings provide the least interference with access doors and launch and recovery fittings. In any case, this does not appear to be a serious consideration for this particular configuration, due to its inherently high equivalent body fineness ratio.

3.3 RESEARCH CONFIGURATION

The results of the wing parametric and sizing analyses summarized in Table 3-13 were included in an interim report to NASA (ASTM 72-22). From this data, a representative research drone configuration (Figure 3-45) was selected for more in-depth engineering studies, to be presented in the ensuing sections. The results of structural and design studies, as well as pertinent features of a command and guidance system capable of accomplishing a variety of NASA research tasks, is included in Paragraphs 3.3.1 through 3.3.7. Various tests required to achieve assurance of success are summarized in Paragraph 3.4.

3.3.1 Wing Location

Four wing location concepts were investigated, all with the same basic wing planform (configuration 1, 30 square feet) which was selected from the previous six-wing parametric study. These four were identified as configuration 1-30-1, 1-30-2, 1-30-3, and 1-30-4 (Figures 3-46 and 3-47), as shown in Table 3-14.

A tradeoff study was performed to select the best all-around method of wing installation (Figure 3-47). Many parameters were considered, but they were reduced to four significant ones: transport geometric simulation, vehicle performance, estimated cost, and operational factors. Transport simulation consisted of determining how closely the design of the drone could be scaled to be representative of the proposed supercritical wing transports. Flight duration, stability, drag, etc., were considered under the vehicle performance aspect. In the cost estimate, configurations were considered in the light of Teledyne Ryan's experience with them, their total costs, and other factors. Air launch and recovery difficulties, as well as the chance of damage in case of ground impact, were considered in the operational aspect of the study. The results (Figure 3-47) indicate that configuration 1-30-2, the low midwing, is the best, with configuration 1-30-1 the second best. Since both of these configurations were of interest to NASA, they were both investigated as

TABLE 3-13

NASA POINT DESIGN SUMMARY

Based on BQM-34E with basic empennage (250-pound payload and 350 pounds fuel, design load factor ±5 g)

NUMBER	APPLICATION	A.R - Λ - λ	$t_{CR}/t/C_t$	DESIGN M. NO/C_L	GROSS WEIGHT (pounds)	WING AREA (sq. ft.)	TAIL VOL. COEFF. (EXISTING TAIL) $\bar{V}_H$	TAIL VOL. COEFF. (EXISTING TAIL) $\bar{V}_V$	TIME ON STATION (minutes)	AIRFOILS
1	Sonic Transport	7 - 38 - .35 C/2	.11/.07	.98/.36	2342.1	30.0	.93	.12	25.8 at 45,000 feet	Supercritical
2	Mach.9 Transport	8 - 30 - .38 C/2	.12/.08	.90/.40	2345.1	30.0	1.10	.12	49.9 at 50,000 feet	Supercritical
3	Air-to-Air	4 - 40 - .38 LE	.05/.04	1.40/.60	2314.1	24.0	1.11	.24	12.38 at 40,000 feet	Supersonic
4	Endurance Turbojet	9 - 35 - .30 C/4	.12/.06	.90/.50	2385.1	40.0	.72	.075	47.30 at 53,000 feet	Supercritical
5	Endurance Turbofan	9 - 25 - .30 C/4	.14/.12	.75/.60	2412.1	60.0	.41*	.04*	58.0 at 58,000 feet	Laminar
6	SST Delta Transport	2.5 - 51 - .13 LE	.03/.03	1.40/.25	2322.1	35.0	1.11	.25	12.54 at 45,000 feet**	Supersonic
Basic	BQM-34E	2.5 - 53 - .30 LE	.03/.03	1.60/.25	2305	32.0	.586	.20	13.8 at 58,000 feet	Supersonic

*Revised Tail Required.
**Add 50 pounds fuel to achieve 15 minutes.

TABLE 3-14.
CONFIGURATION LIST

NO. SYSTEM = CONFIGURATION NO. - WING AREA - WING LOCATION*

NO.	DESCRIPTION
1-30-1	STANDARD-LENGTH FUSELAGE WITH WINGS FROM 1-30-2 BOLTED TO NEW TORQUE BOX LOCATED ON ORIGINAL UPPER WING ATTACH POINTS
1-30-2	STANDARD-LENGTH FUSELAGE, LOW MID-WING BOLTED TO SIDE OF FUSELAGE
1-30-3	STRETCHED FUSELAGE WITH WING BOX THROUGH STRETCHED SECTION
1-30-4	STANDARD-LENGTH FUSELAGE WITH WING FROM 1-30-3 LOCATED BELOW FUSELAGE AND FAIRED IN WITH FAIRING SIMILAR TO THAT OF EXISTING DROP TANK

* INDICATED
1. HIGH WING
2. LOW WING ON FUSELAGE
3. LOW WING ON STRETCHED FUSELAGE
4. LOW WING BELOW FUSELAGE

WING
- GROSS AREA: 30 SQ. FT.
- AIRFOIL: SUPERCRITICAL T/C 11% ROOT 7% TIP
- ASPECT RATIO: 7.0
- TAPER RATIO: .35

TAIL – HORIZONTAL
- GROSS AREA: 9.1
- NET EXPOSED AREA: 5.5 SQ. FT.
- AIRFOIL: NACA-65003.5 (MODIFIED) TIP WITH NACA-65005 (MODIFIED ROOT Y_F = 10.10)
- ASPECT RATIO: 3.5
- INCIDENCE: ALL MOVABLE
- TAPER RATIO 0.40
- DIHEDRAL: 0
- STABILIZER HINGE AXIS: X_F 359.56
- VOL. COEFF: .983

TAIL – VERTICAL
- GROSS AREA: 8.65 SQ. FT.
- AIRFOIL: NACA65-003 (MODIFIED)
- ASPECT RATIO: (GEOMETRIC) 1.2
- TAPER RATIO: 0.30
- RUDDER HINGE AXIS: 85% CHORD
- NET EXPOSED AREA: 6.8 SQ. FT.
- VOL. COEFF. .125

POWER PLANT
- CONTINENTAL (YJ69-T-406 CAE MODEL 356/34A)
- RATED THRUST 1840 LB. SEA LEVEL STATIC

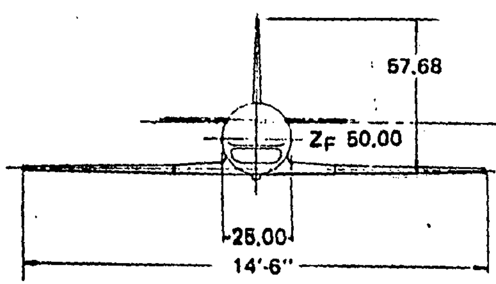

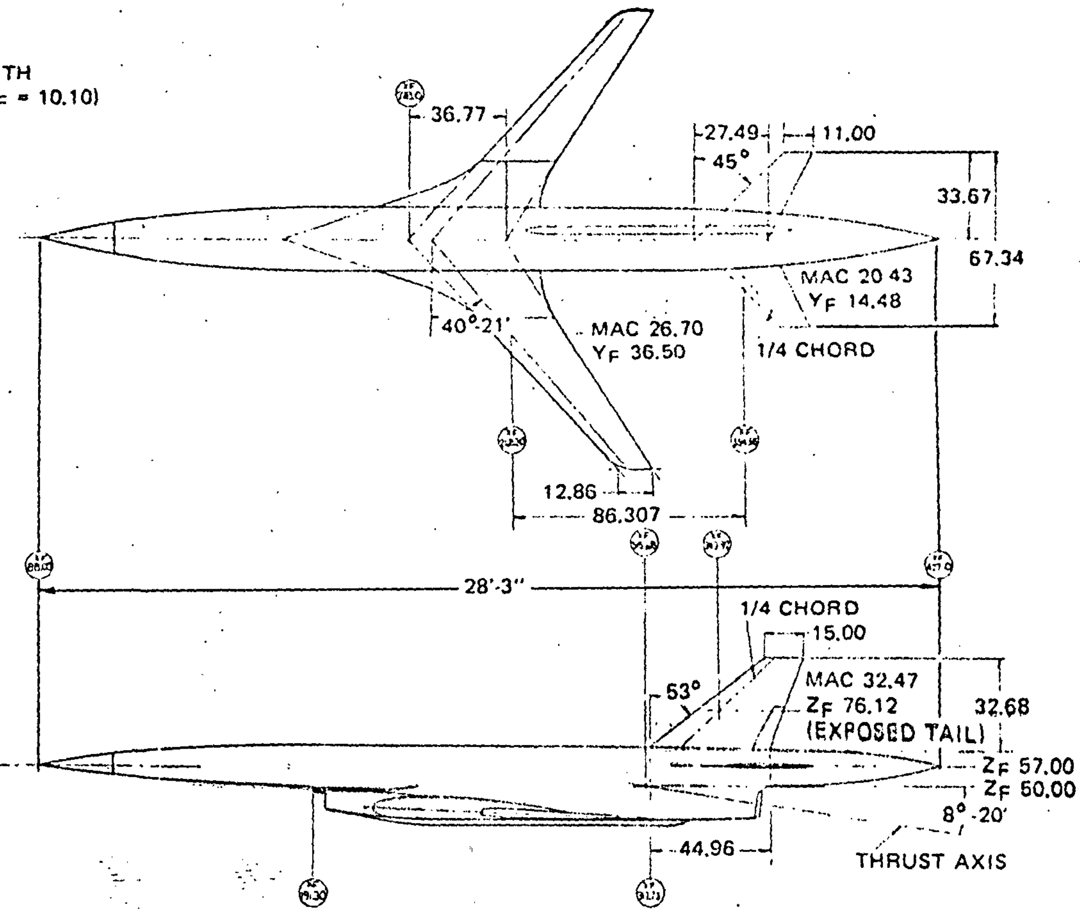

Figure 3-45. General Arrangement, 1-30-2

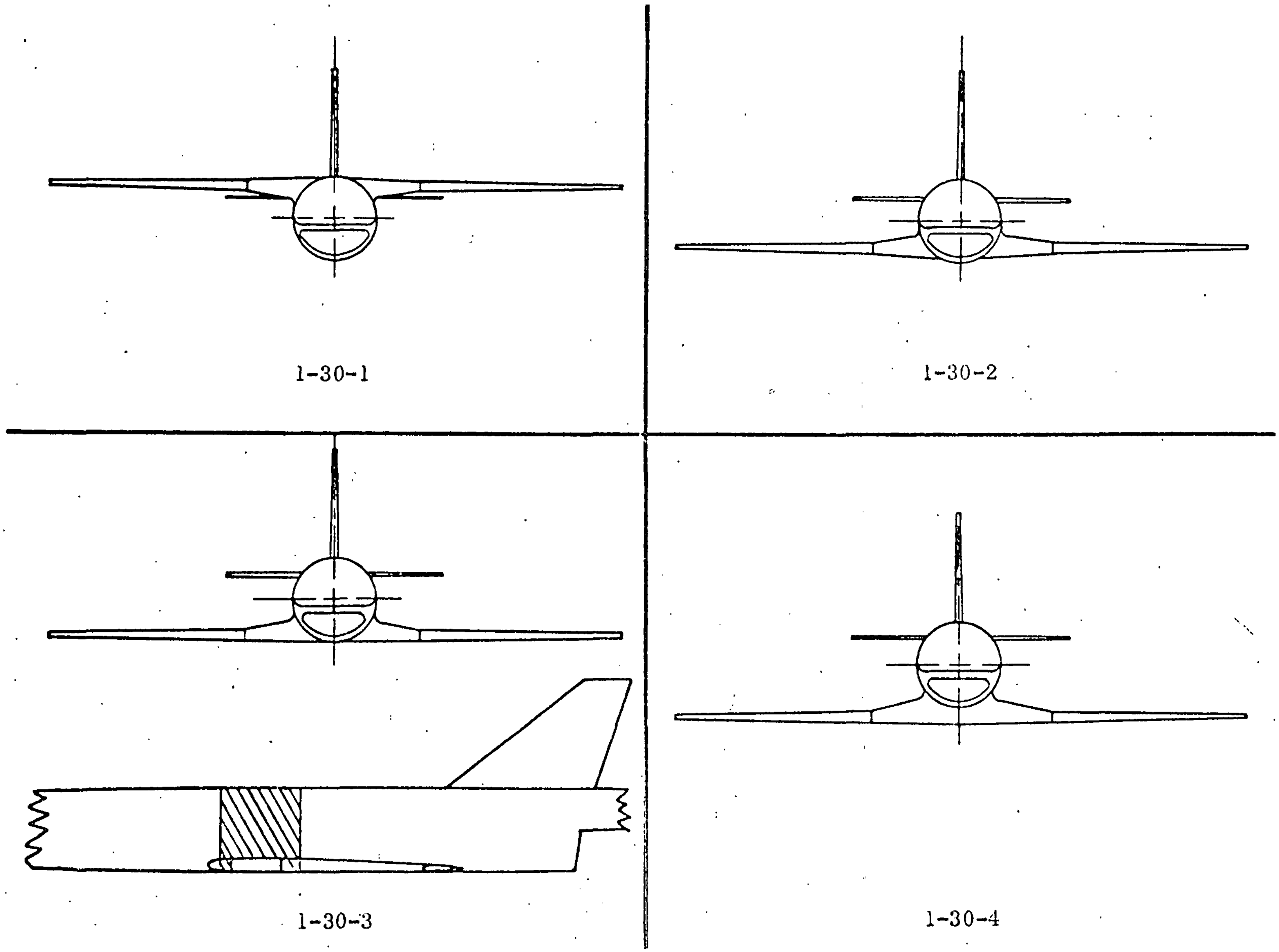

Figure 3-46. Design Alternatives

CONFIG. NUMBER	TRANSPORT SIMULATION	VEHICLE STABILITY AND PERFORMANCE	MANUFACTURING COST	OPERATIONAL FACTORS
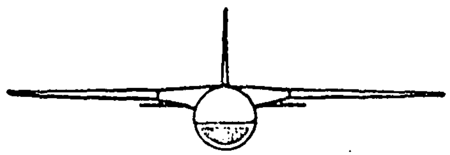 1-30-1	4	2	☆	2
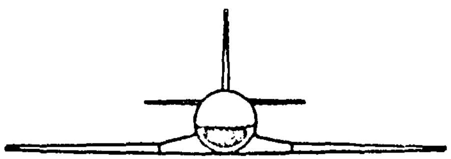 1-30-2	☆	☆	3	☆
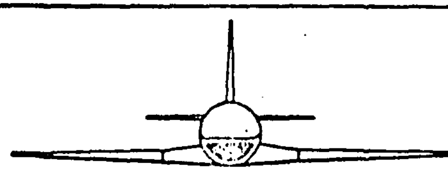 1-30-3	2	3	4	4
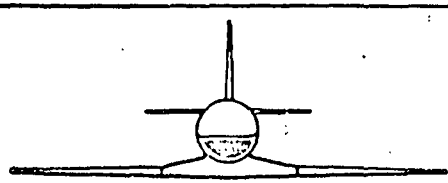 1-30-4	3	4	2	3

Figure 3-47. Wing/Fuselage Configuration Tradeoff

to the method of construction. In addition, it was determined from NASA that the ability to convert one vehicle from a low wing to a high wing (configuration 1-30-2 to 1-30-1) would be desirable from a research viewpoint. This capability was also included in the investigation.

The stretched fuselage configuration 1-30-3, with a low wing, was discarded because of cost, air launch difficulty, center-of-gravity travel, and some increase in wetted area. Its only real advantage was increased fuel volume for longer flight duration. Configuration 1-30-4 was discarded because of increased drag due to an increase in the frontal area and a greater chance of wing damage in case of ground impact.

Low-Wing Attachment (Configuration 1-30-2)

This configuration requires modifications to the existing BQM-34E in the area of the fuselage fuel tank in order to mount the wing panels externally. The modification will consist of removing two sheet metal frames at XF 250.060 and XF 258.340. Three heavier machined frames located at XF 247.800, XF 254.000, and XF 260.200 (Figure 3-48) will replace the frames. The replacement frames will be within the existing tank skin line, thereby avoiding any fuel tank sealing problems. A suitable material thickness will be built into the frames to withstand the loads imposed from wing bending and torsion as well as the heavy bosses required for concentrated bolt locations. The wing panel will be tension bolted to these frames through adapter fittings located outside the tank skin. This machined adapter (Figure 3-48, Section B-B) will be bolted to the internal frames at six places, two in each frame, with 7/16-inch-diameter, 300,000-psi, heat-treated bolts. To mount the wings to the adapter fitting, 5/16-inch-diameter, 300,000-psi, heat-treated bolts are used. The desired wing incidence and dihedral will be incorporated into the adapter fitting. Minor incidence and dihedral changes can be made by machining alternate adapter fittings as required.

High Wing (Configuration 1-30-1)

This configuration can be considered as an alternate to the low-wing configuration as the primary vehicle. As an alternate to configuration 1-30-2, the high-wing location can be created by removing the wings and adapter fittings from configuration 1-30-2 and installing a new, machined, wing carrythrough box (Figure 3-49). This torque box will fit between the existing fuel tank top and the parachute riser trough. It will bolt into the top of the machined frames added for configuration 1-30-2. Twelve barrel nut and wing attach studs are furnished to allow interchangeable

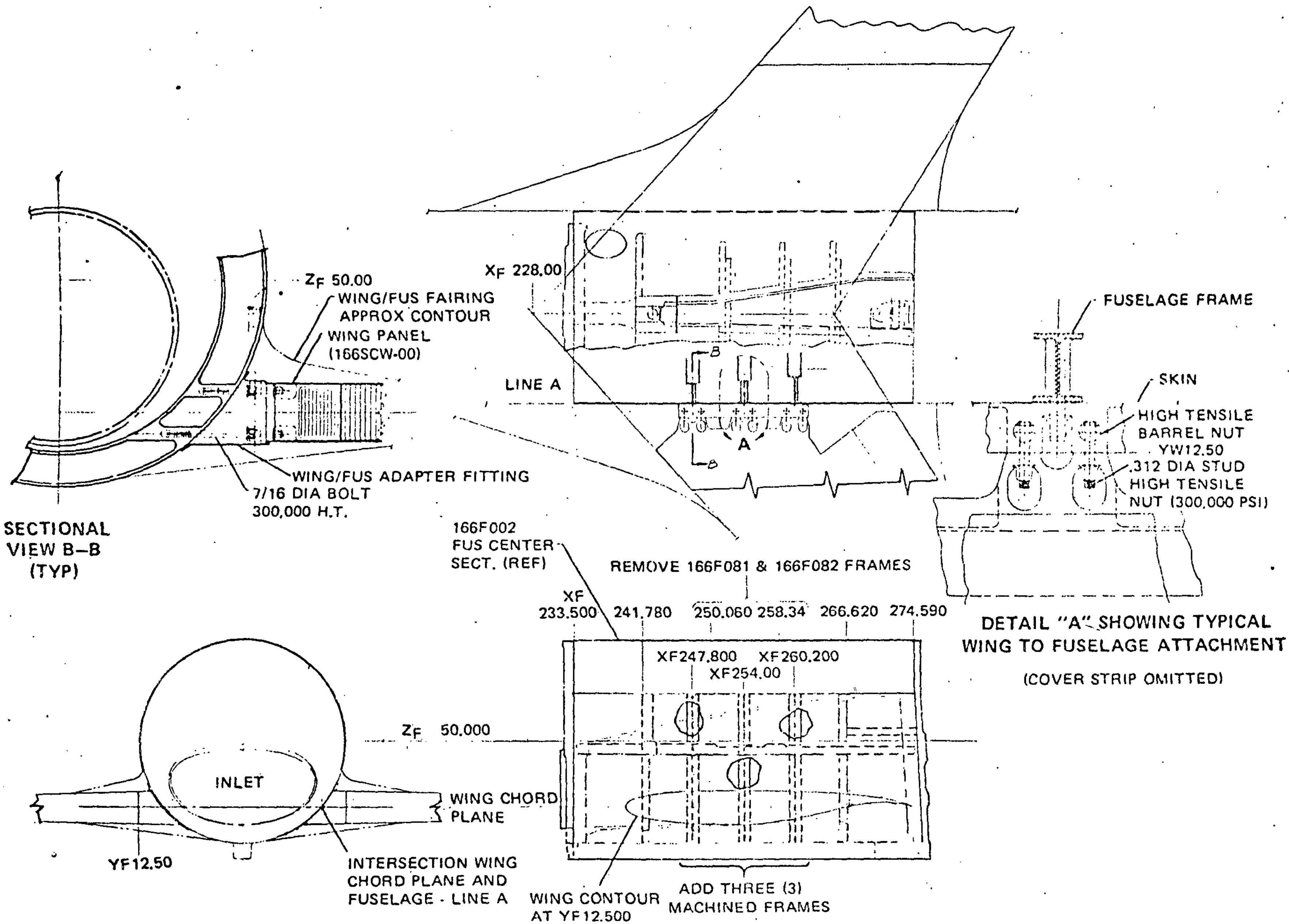

Figure 3-48. Wing Installation and Fuselage Modification 1-30-2

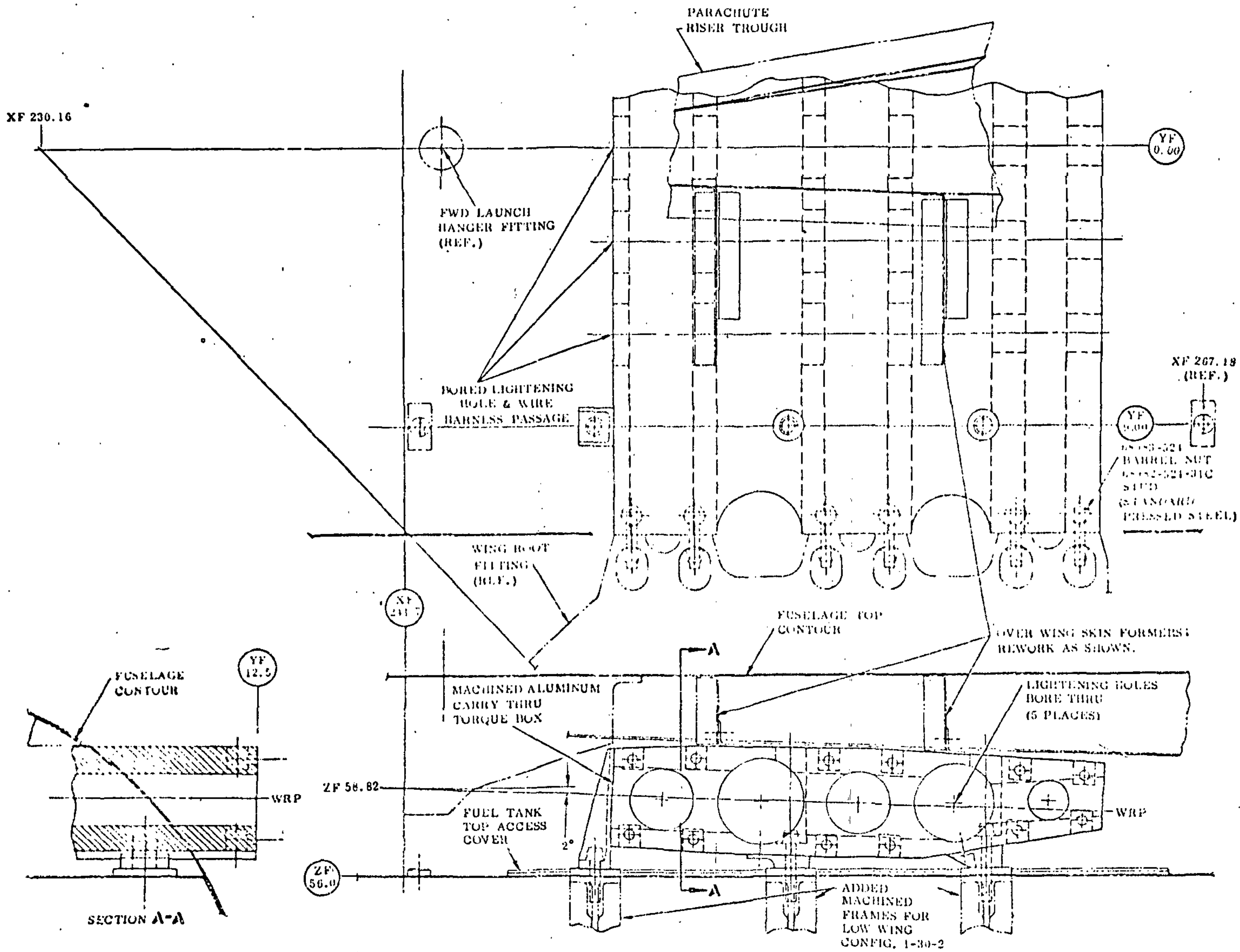

Figure 3-49. Wing Installation and Fuselage Modification 1-30-1

installation of each wing panel. Lightening holes are provided in the torque box to allow wire and plumbing passage and a reduction in weight.

Fuel and Payload Provisions

Configuration 1-30-1, High Wing (Figure 3-49). - The fuel for this configuration is stored in the regular fuselage tank, with optional fuel available in the nose and a small tank behind the wing carrythrough box. Assuming JP-5 fuel at approximately 6.8 pounds per gallon, the fuel weight for each tank is as follows:

Main tank in fuselage	263 pounds
Auxiliary in nose	70 pounds
Auxiliary behind wing box	20 pounds
Total	353 pounds

The pressurized payload provisions are all in the nose equipment compartment, and available space exists around the essential equipment located in the compartment. Available and optional volume locations and sizes may be summarized as follows:

Nose cone (available)	0.30 cu. ft.
Cooling system removed (optional)	0.75 cu. ft.
Shaker unit removed (optional)	0.60 cu. ft.
103-gallon fuel tank removed (optional)	1.40 cu. ft.
Miscellaneous volumes (available)	1.10 cu. ft.
Total	4.15 cu. ft.

In addition to the nose compartment volume, there is approximately 0.5 cubic foot available around the wing carrythrough box if the optional fuel tank is removed. This area is unpressurized.

Configuration 1-30-2, Low Wing (Figure 3-48). - The fuel and payload provisions are essentially the same as those of configuration 1-30-1, with the exception of the space above the fuel tank. Since no wing carrythrough box is required, the fuel load can be increased by approximately 20 pounds in the auxiliary tank over the main tank, thereby providing a total fuel capacity of 373 pounds. In the case of payload provision, if the fuel tank above the main tank is removed the available unpressurized payload volume is approximately 1.0 cubic foot. A detailed inboard profile of this arrangement is illustrated in Figure 3-50.

Area Rule Modifications

Vehicle area ruling can be accomplished by installing external fairings on the fuselage/wing joints. The fairings will be fiber-glass structures (Figure 3-51) held to the fuselage with screws. Points requiring frequent service may require special access doors through the fairings. Typical vehicle area distributions are shown in Figures 3-52 and 3-53, and variations of these can be achieved by redesigned fairings.

3.3.2 Wing Design and Construction

Structural Arrangement

The wing (Figure 3-54) is a tapered, swept wing with a supercritical airfoil section, 11 percent thick at the root and 7 percent at the tip. The sweep angle is 40 degrees 21 minutes at the wing quarter chord. Inboard and outboard ailerons are utilized, along with a hinged leading edge capable of moving up and down.

The primary bending and torsional structure of the wing is composed of a full-depth honeycomb box bounded by sheet metal channel spars at 15 and 60 percent chord. A machined aluminum root fitting is located at the root of the bending box, allowing wing removal from the mating fuselage fitting. The trailing-edge fixed structure is of fiber glass and is removable for control system access. A sheet metal, removable, leading edge is furnished for access to the movable leading-edge controls. The wingtip is a foam-filled, fiber-glass shell bolted to the torque box closeout rib.

Variable-Stiffness Wings

The honeycomb torque box wing construction (Figure 3-55) will permit wings of varying stiffness to be designed and built without any major tooling change. This type of wing has nearly all of the bending and torsional material concentrated in the upper and lower skins, which are bonded to the full-depth aluminum honeycomb core. By altering the modulus of elasticity, thickness, and (in the case of fiber materials) the fiber orientation from the wing elastic axes, the properties of these skins can be varied considerably. Computer programs such as SQ5, LAP*,

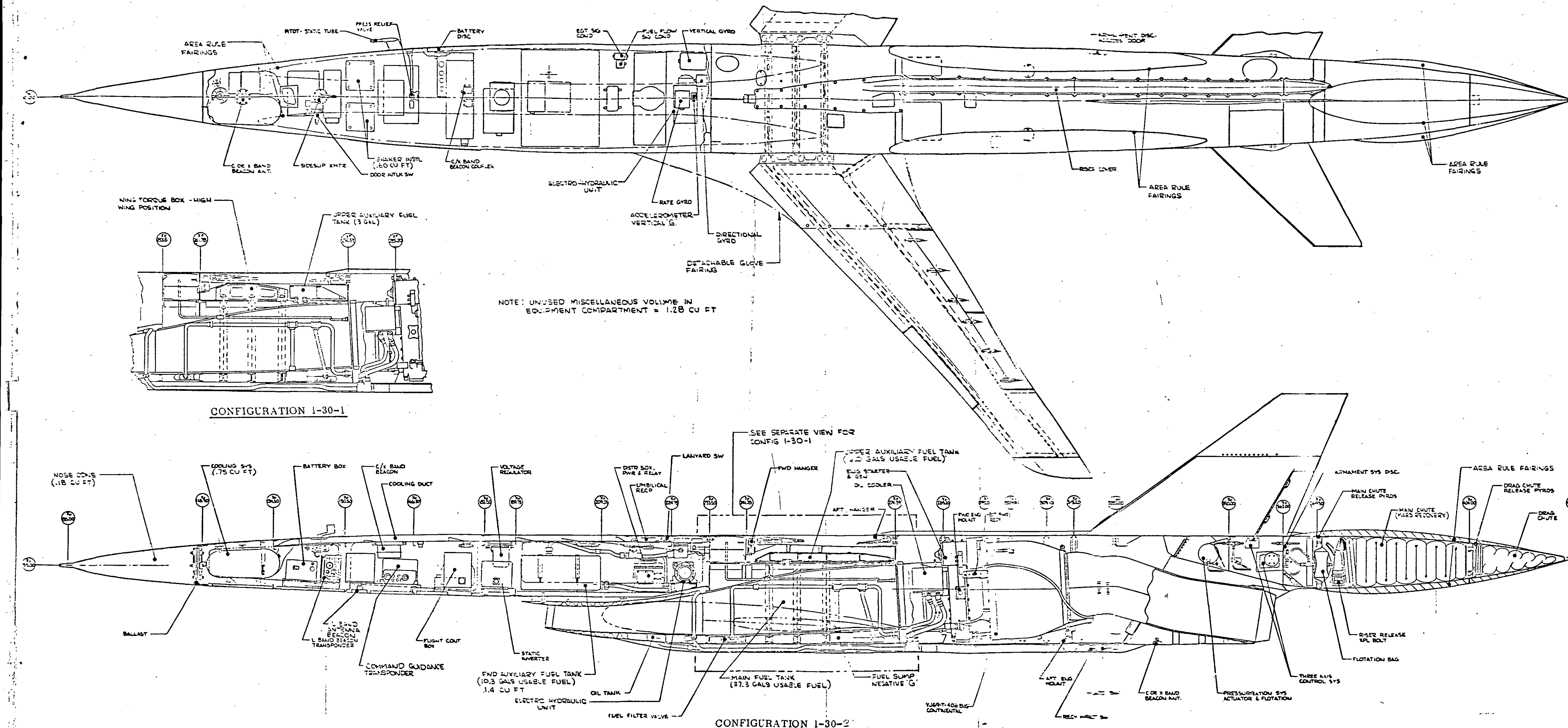

Figure 5-50. Inboard Profile, Configurations 1-30-1 and 1-30-2

Page Intentionally Left Blank

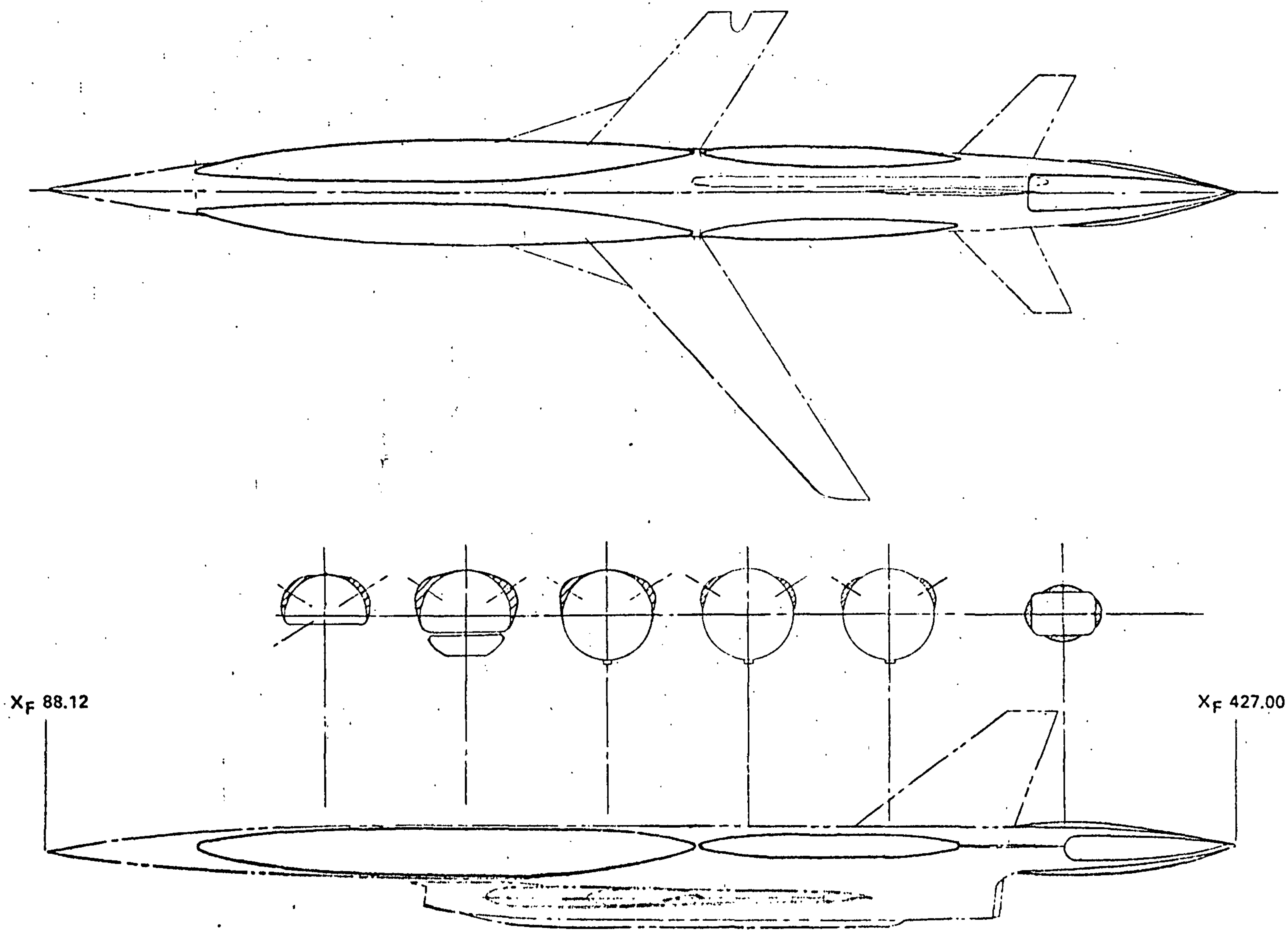

Figure 3-51. Area Rule Modifications

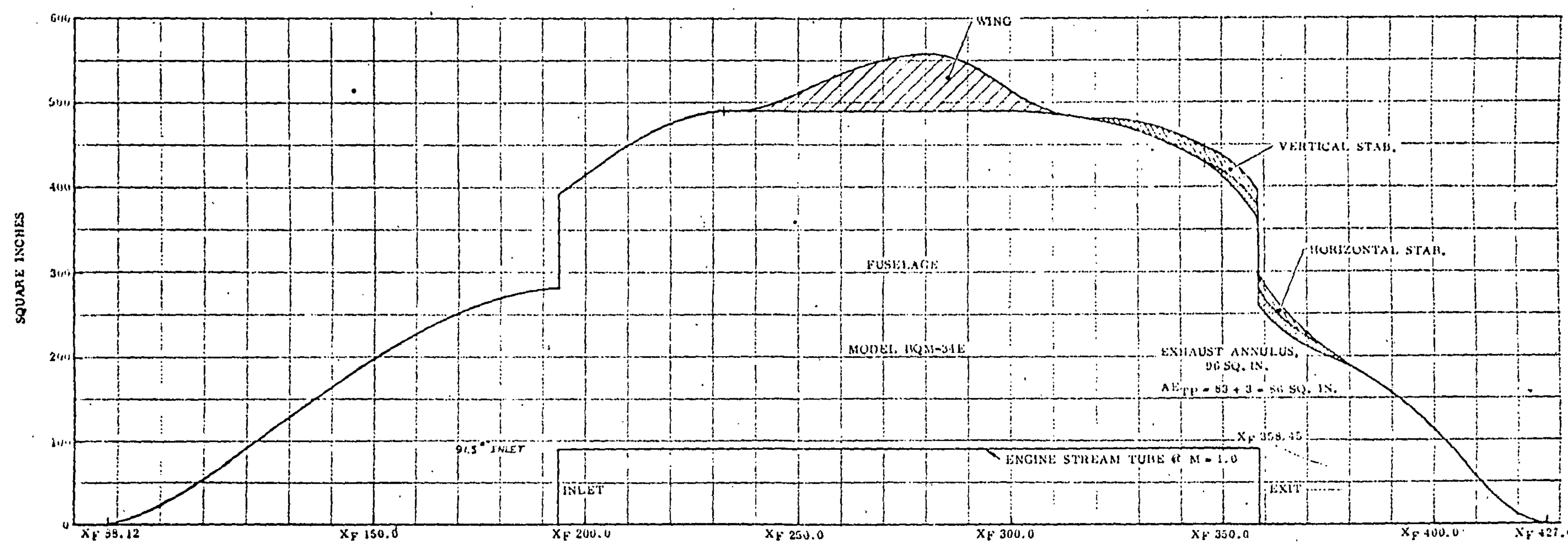

Figure 3-52.   Area Distribution for the Basic BQM-34E

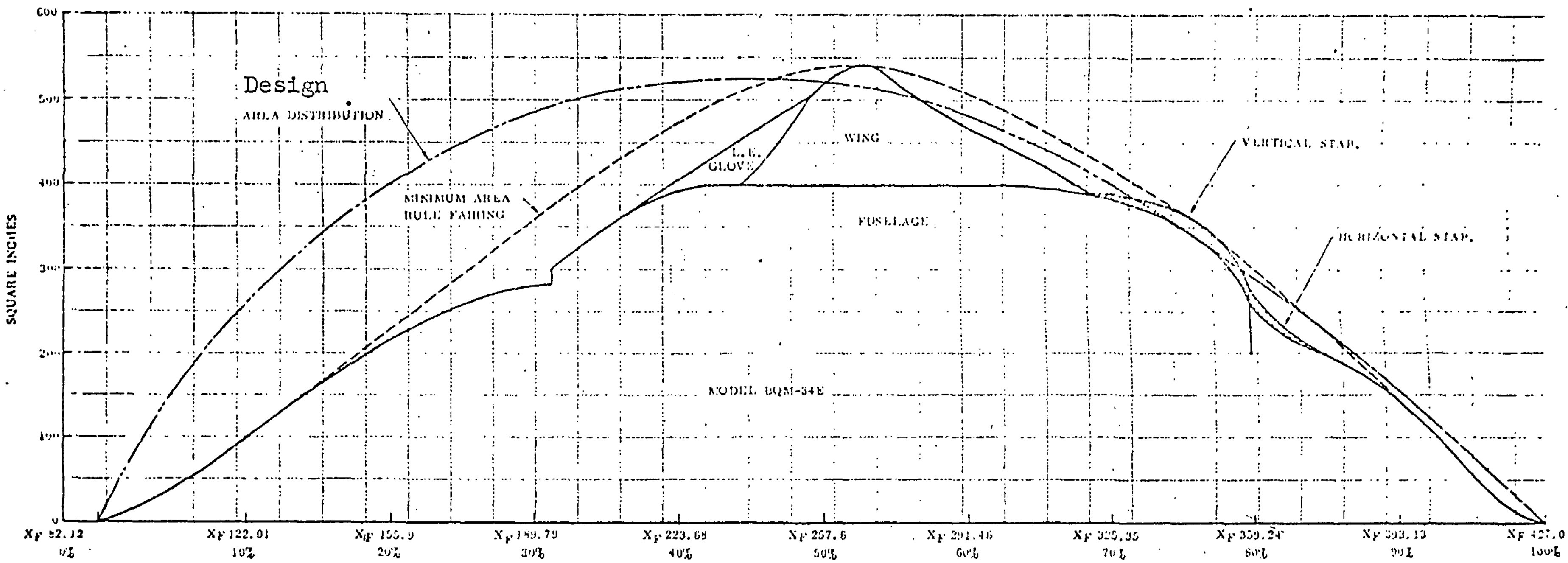

Figure 3-53. Area Distribution, Configuration 1-30-2 NASA Research Wing, Model 166

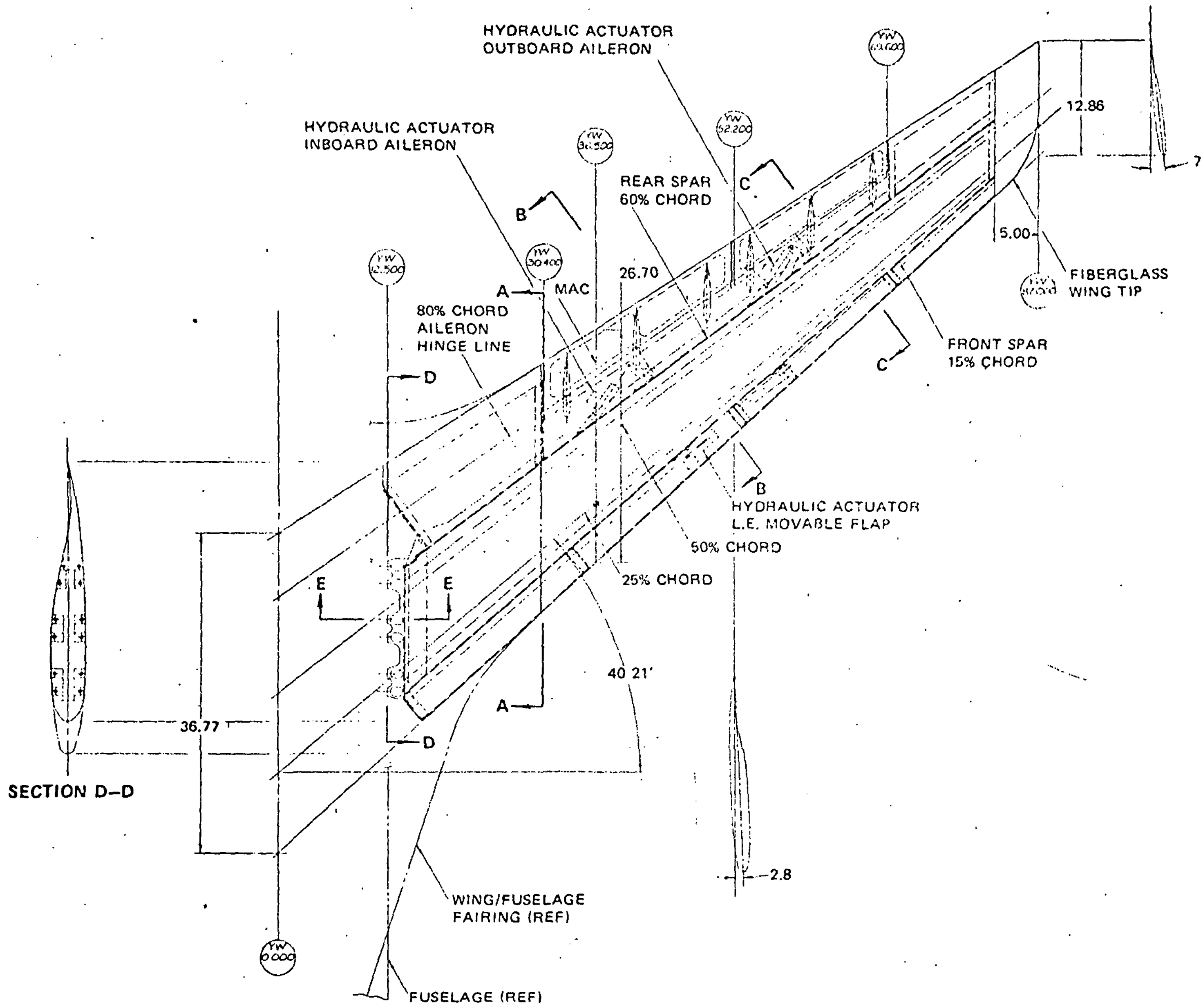

Figure 3-54. Wing Plan Form Structural Arrangement

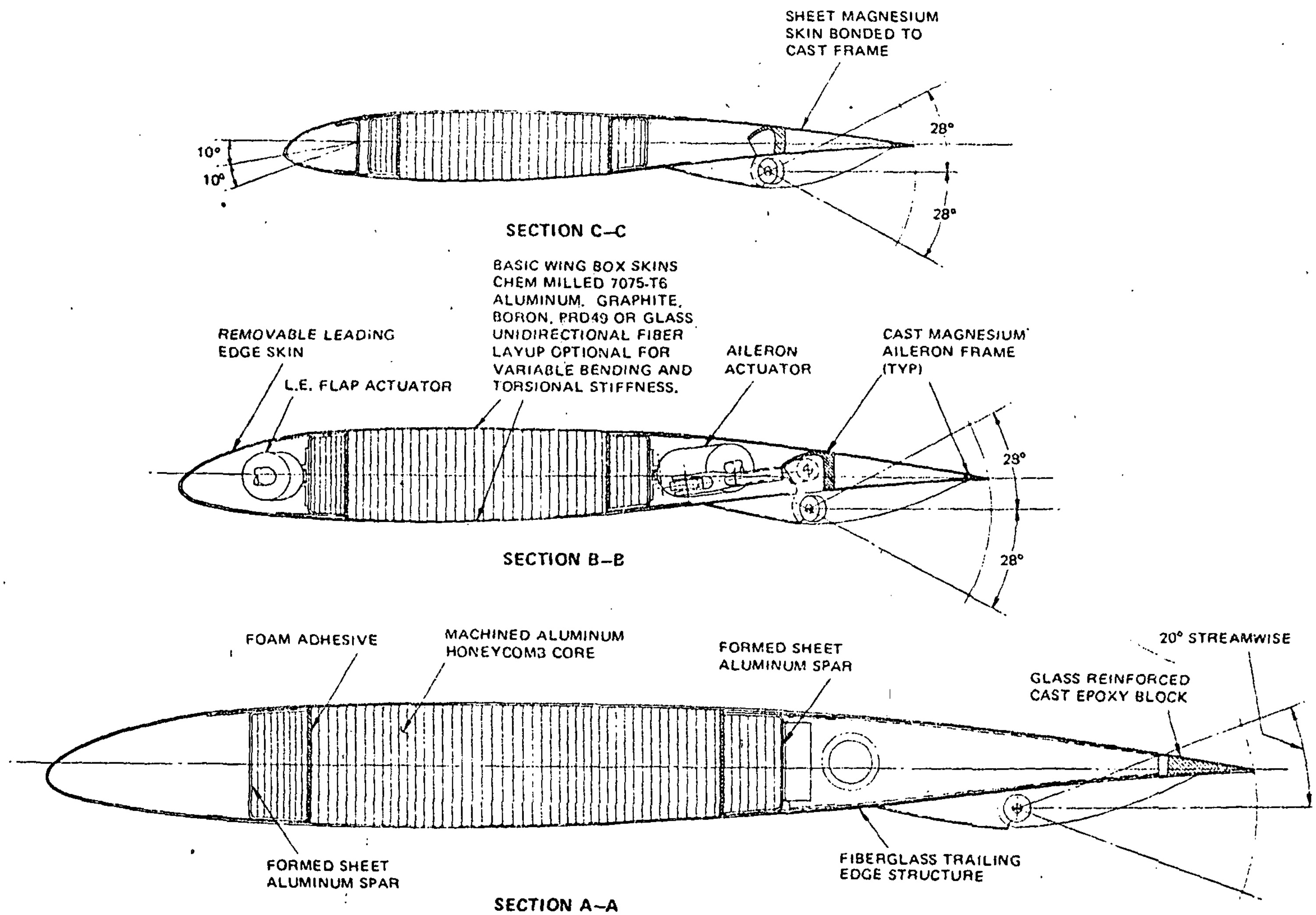

Figure 3-55. Wing Structural Cross Sections

box beam, NASTRAN, and WAVES I are available and have been used to aid in the design of this type of wing. Candidate skin materials, each having certain structural features, are glass fiber, magnesium, aluminum, PRD-49 fiber, boron fiber, steel, and graphite fiber. The materials used for skins outside the bending torque box need not change. The honeycomb and channel spars will likely remain aluminum, although other materials may be considered, depending upon wing requirements.

3.3.2.1 Preliminary Structural Design Criteria

The basis for the preliminary structural design criteria for the modified BQM-34E research vehicle with the NASA supercritical wing shall be the structural design criteria for the basic aircraft. The criteria presented herein shall be utilized for preliminary sizing of the structure. As refinements in structural, mass and aerodynamic characteristics are developed, these criteria may likewise be modified.

Results of a flutter study will dictate wing stiffness requirements to ensure a flutter and divergence design without control reversal. The 15 percent margin (1.15 times maximum operating speeds) required by MIL-A-8870 (for manned aircraft) shall be considered a requirement for the wing. The empennage already possesses this margin.

The Mach-altitude envelopes for the standard BQM-34E and the research vehicle with the supercritical wing are presented in Figure 3-56. The V_H curve for the modified aircraft was generated by using a constant dynamic pressure curve (equivalent to Mach 0.95 at sea level) up to Mach 0.98, then a constant Mach number to upper altitudes. V_L for the modified craft was generated in the same fashion, with the constant dynamic pressure curve corresponding to Mach 1.05 at sea level. Constant Mach number for V_L is attained at Mach 1.08.

Sea-level V-n diagrams for both symmetrical and unsymmetrical flight are presented in Figures 3-57 and 3-58 for the basic BQM-34E. Figures 3-57(b) and 3-58(b) only (the two lower envelopes) shall also be applicable for the craft with the supercritical wing.

Gross Weights

The gross weights for structural design of the BQM-34E are presented in Table 3-15. The structural design gross weight for the craft with the supercritical wing shall be the same as that for the standard BQM-34E with external tank (i.e., free flight ~ 2500 pounds, ground launch ~ 2900 pounds, etc.).

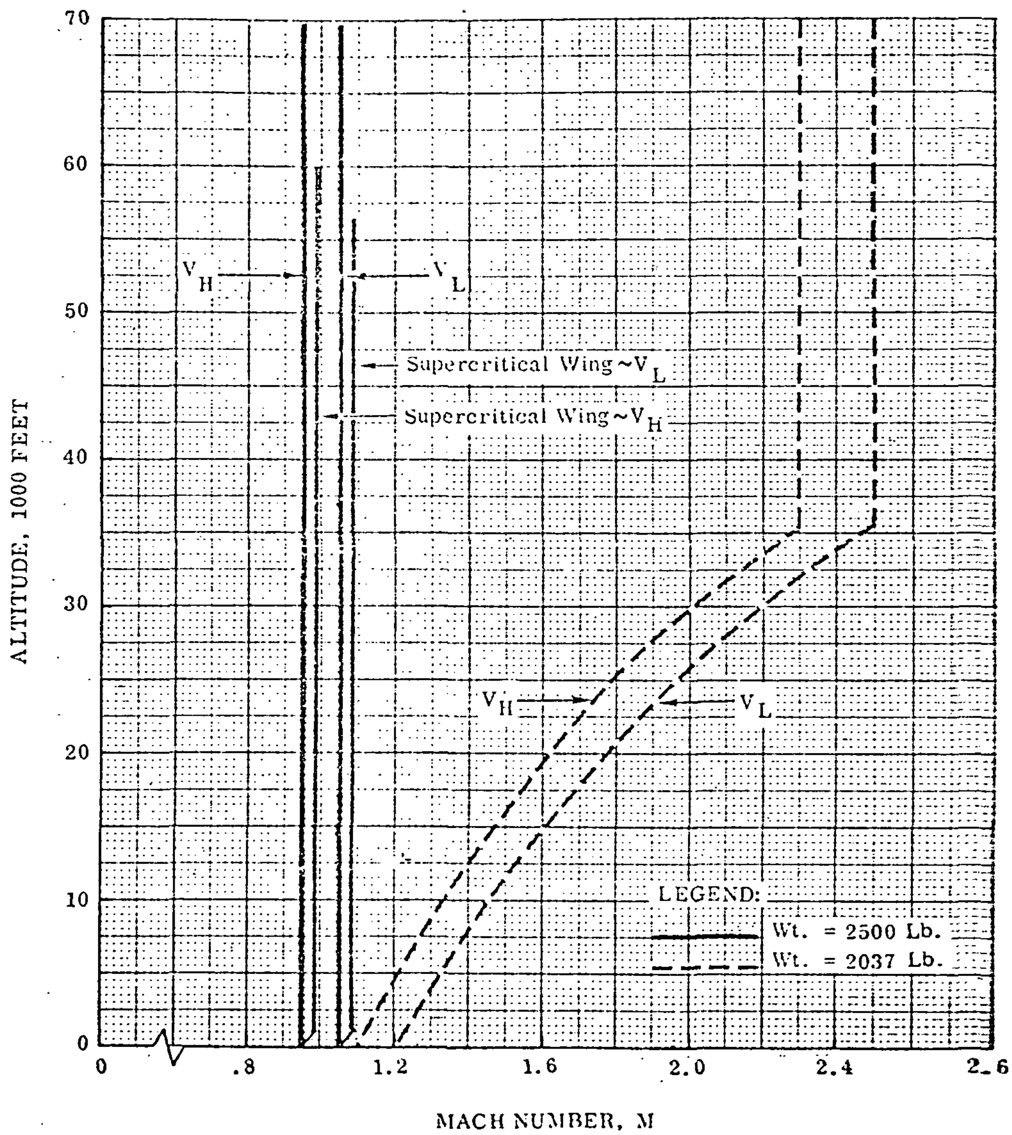

Figure 3-56. Mach Number vs. Altitude

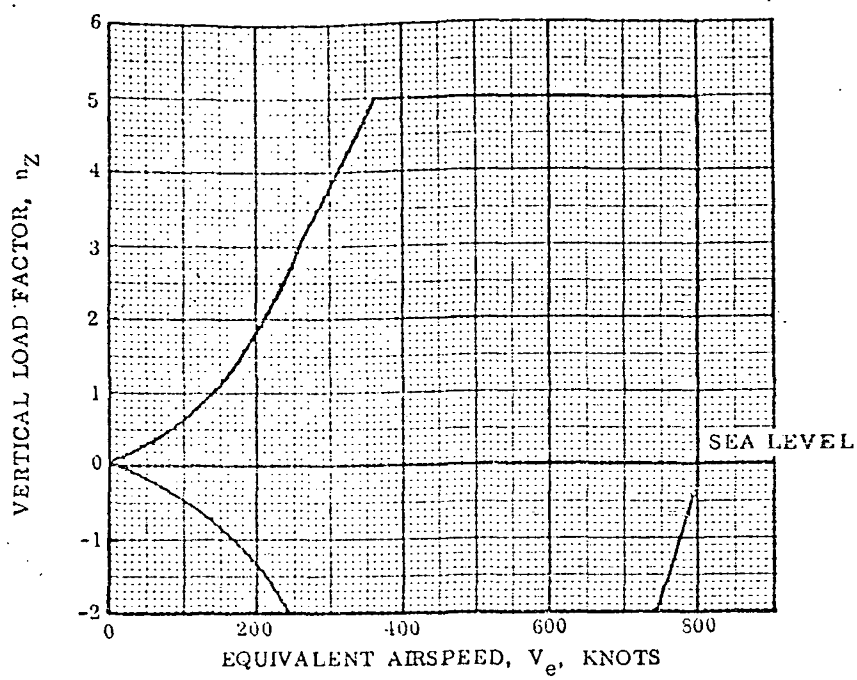

(a). Gross Weight = 2037 Lb.

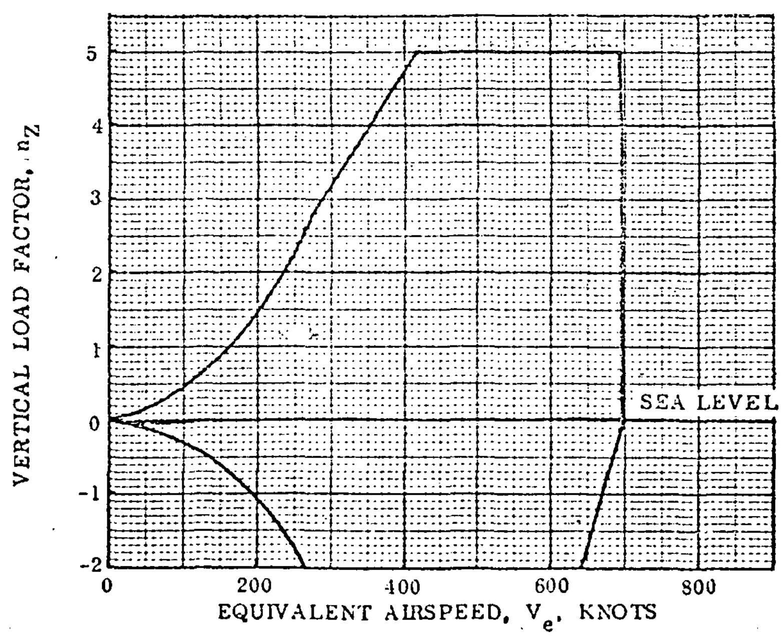

(b). Gross Weight = 2500 Lb.

NOTE:
(b) is applicable only to the craft with the supercritical wing.

Figure 3-57. V-n Diagrams - Symmetrical Maneuvers, Model BQM-34E

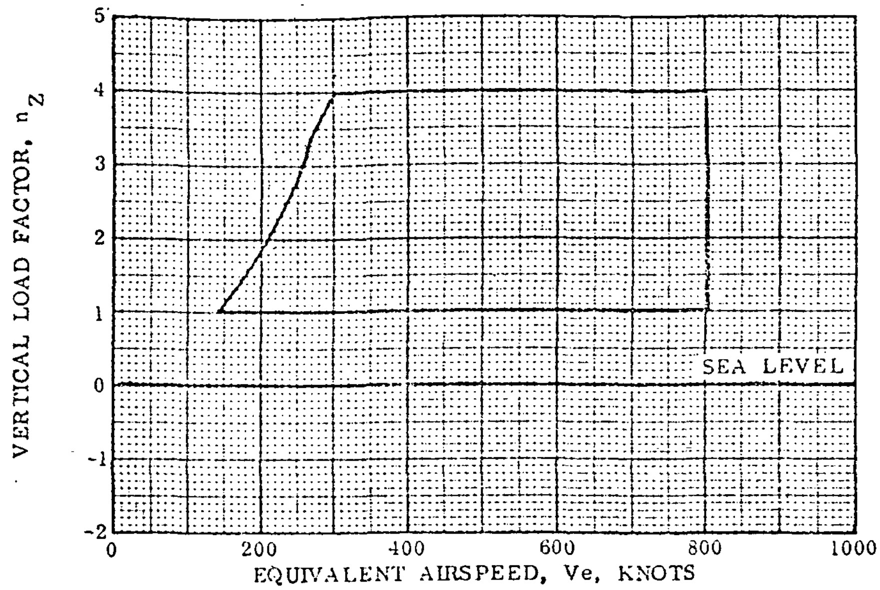

(a). Gross Weight = 2037 Lb.

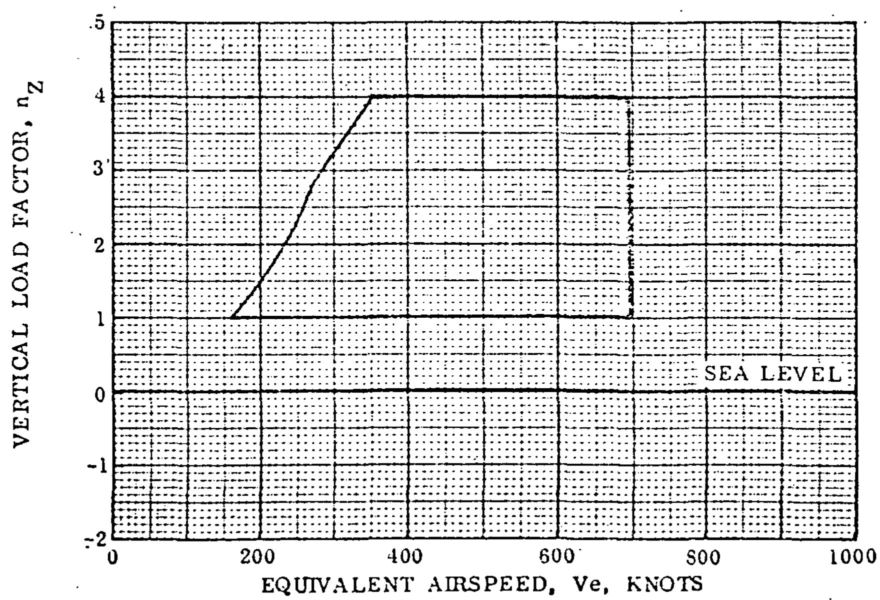

(b). Gross Weight = 2500 Lb.

NOTE:
(b) is applicable only to the craft with the supercritical wing.

Figure 3-58. V-n Diagrams - Unsymmetrical Maneuvers, Model BQM-34E

TABLE 3-15
STRUCTURAL DESIGN CRITERIA SUMMARY, PARACHUTE RECOVERY

CONDITION	DESIGN GROSS WEIGHT (pounds)	ULTIMATE FACTOR OF SAFETY	MAXIMUM LIMIT LOAD FACTOR			COMMENTS
			n_x	n_y	n_z	
FREE FLIGHT	2500 2037	1.25				Subsonic Supersonic
Symmetrical Maneuvers					-2.0 to 5.0	$\dot{\omega}_{max}$ = 1.5 rad./sec.^{2}, basic
Asymmetrical Maneuvers					1.0 to 4.0	
Gust						27 fps (EAS) at V_H
CAPTIVE FLIGHT	2544	1.50				
Taxi, Takeoff, Landing			±2.50	±1.50	-3.0 to 6.0	For design of attachments and sway braces. Loads act simultaneously.
Gust						50 fps (EAS) at V_H of DP-2E,
PARACHUTE RECOVERY		1.25				
Drag Parachute Deployment	1250 to 2028		-12.0*	±3.0*	6.00*	Based upon 15,000-lb. parachute load.
Main Parachute Deployment	1922					Based upon 12,000-lb. parachute load.
GROUND LOADS		1.50				
Ground Launch	2900					Includes JATO unit and external fuel tank.
	2100		7.00*	±1.50*	2.40*	Includes JATO unit. Ground launch loads and load factors based upon JATO thrust of 14,000 pounds plus engine thrust.
Ground Impact (1)	1400		±6.0	±3.0	12.0	
Ground Handling Loads						
Shipping	1900		±4.0	±1.33	±2.0	n_z acts alone and in combination with horizontal load factors.
Hoisting	2944		±0.4	±0.4	2.67	
Jacking	2544		±0.5	±0.5	2.0	
Carting	2544		±2.0	±1.33	2.0	
WATER LOADS						
Water Impact	1720	1.25	±3.0	±4.0	7.5	Load factors act independently.

NOTE: For flight with external fuel tank (2500 lb.), V_H and V_L are Mach 0.95 and Mach 1.05. For flight without external fuel tank (2037 lb.), V_H and V_L follow constant dynamic pressure lines from Mach 1.1 to Mach 2.3 and from Mach 1.2 to Mach 2.5, as shown.

* Used for equipment installation.

(1) The XBQM-34E was designed for ground impact. Although the requirement for ground impact was not carried over to the BQM-34E criteria, the strength inherent with the original design still exists.

Center-of-Gravity Envelope

The center-of-gravity range for free-flight structural design conditions shall be 15 to 50 percent of the wing mean aerodynamic chord.

Flight Loads Criteria

Free-Flight Balanced Maneuver. - Loads shall be determined at critical points on and within the V-n diagram (Figure 3-57(b)) for the symmetrical balanced condition described in Paragraph 3.2.1 of MIL-A-8861. This condition has zero pitching acceleration, and the pitching velocity shall be obtained by solution of the expression $q = (g/V_T)\ (n_Z - 1)$, where V_T is the true velocity.

Free-Flight Maneuver with Specified Pitching Acceleration. - Loads shall be determined on or within the V-n diagram for the symmetrical maneuver, with specified pitching acceleration described in Paragraph 3.2.2.1 of MIL-A-8861. This condition shall have a basic pitch acceleration of 1.5 rad./sec.^{2} and the values of pitching velocity specified by Figure 2 of MIL-A-8861.

Free-Flight Accelerated Roll. - Loads shall be determined at speeds to V_L and at initial load factors between 1.0 and 4.0 g for the accelerated roll maneuver described in Paragraph 3.3.1.1 of MIL-A-8861. The V-n diagram for roll maneuvers is shown on Figure 3-58(b).

Control System Limitations. - The above structural design free-flight maneuvering criteria have been selected to provide adequate margins beyond those maneuvers attainable in flight with an operational flight control system, provided that system has characteristics similar to that on the standard BQM-34E.

Free-Flight Gust Encounter. - Free-flight gust load factors shall be determined by the discrete gust analysis described in Paragraph 3.5 of MIL-A-8861. The gust velocities specified in the referenced paragraph are unreasonably high for an unmanned recoverable vehicle. An analysis was therefore performed on the BQM-34E flight profiles to determine a more rational value. The analysis showed that a gust of 27 feet per second would be encountered (on the average) once in 10 sorties of the mission which was determined critical (low-altitude dash mission). This value shall be used as the free-flight gust velocity at V_H.

Captive-Flight Design Conditions. - The loads imposed on the BQM-34E by the attachment fittings and sway braces shall be calculated using the load factors specified in Table 3-15. The gust load factors in captive flight shall be determined using the methods and gust velocities presented in Paragraph 3.5 of MIL-A-8861, where the forward speeds are those appropriate to the launch aircraft.

Design Features Affecting Determination of Critical Conditions. - A large part of structural design is governed by parachute recovery and surface-impact conditions. Since the basic craft was designed for high supersonic speeds, the lifting surfaces have small thickness-to-chord ratios; this results in design of these surfaces for rigidity as well as strength. The fact that the craft is designed for higher speeds, dynamic pressures, and load factors than the carrier aircraft tends to make captive-flight conditions noncritical, except for local attachments. A result of these design features is to make this type of craft less critical for certain conditions than would be the case for a conventional, piloted aircraft.

Elevated-Temperature Criteria. - Combined aerodynamic loading and heating were investigated for the following conditions for the basic BQM-34E:

a. Mach 0.55 at sea level.

b. Mach 1.05 at sea level.

c. Mach 2.5 at 35,500 feet.

These points were shown to be critical during preliminary design studies on the BQM-34E. Since the craft with the supercritical wing will not operate outside the above points, they shall be utilized as criteria for the modified aircraft also.

Ultimate Factors of Safety. - The ultimate factor of safety shall be 1.25 for free-flight and recovery conditions and 1.5 for captive flight.

Parachute Recovery Loads Criteria

Drag Parachute Deployment. - A 15,000-pound drag load shall be considered for structural design during drag parachute deployment. This load shall act anywhere rearward within a 5-degree angle to the line of flight. A gross weight of 2028 pounds was investigated for the BQM-34E. In addition, a gross weight of 1250 pounds was also investigated in order to provide a maximum longitudinal load factor for equipment installation.

Main Parachute Deployment. - During main parachute deployment, large loads are transmitted to the craft through the forward and aft main parachute bridles. For structural design of the BQM-34E, a main parachute load of 12,000 pounds shall be considered to act in the fuselage plane of symmetry at angles between the vertical and directly aft. Gross weights up to 1922 pounds apply for main parachute deployment on the BQM-34E.

Paragraph 3.7.2.1.1 of the BQM-34E detail specification (Teledyne Ryan Specification No. SD-2019 R-1) states that the parachute shall be suitable for lowering the craft at a maximum sinking speed of 20 feet per second with no fuel abaord. This is adopted as a parachute design criterion. The sink speed measured during qualification testing was 17.2 feet per second, based on a suspended weight of 1400 pounds. This is equivalent to a sink speed of 19.1 feet per second for a suspended weight of 1720 pounds.

Ultimate Factor of Safety. - The ultimate factor of safety shall be 1.25 for parachute recovery conditions.

Ground Loads Criteria

Ground loads are incurred in two separate phases: ground launch and ground handling. The original criteria (for the BQM-34E) included a requirement for ground impact which has subsequently been deleted. However, structural strength for this condition, which is defined in Table 3-15, still exists.

Ground Launch Criteria. - The ground launch weights are shown in Table 3-15. The limit design thrust of the JATO unit shall be taken as 14,000 pounds.

Loads shall be determined for the specified conditions at center-of-gravity locations determined by weight analysis. In addition, loads shall be determined for actual weights and center-of-gravity locations for a range of mission weight distributions.

Ground Handling Criteria. - Loads shall be determined for shipping, hoisting, jacking, and carting. The weights and load factors for these conditions are presented in Table 3-15.

Ultimate Factors of Safety. - The ultimate factor of safety shall be 1.5 for ground launch (bottle ignition) and ground handling and 1.25 for ground launch (bottle burnout).

Water Loads Criteria

Water-Impact Load Factors. - For water impact, the structural design load factors listed in Table 3-15 are 7.5 vertical, ±3.0 longitudinal, and ±4.0 lateral. These criteria, which were used for both the XBQM-34E and the BQM-34E, were based upon calculated values (and past experience) and were demonstrated to be adequate during controlled drop tests and during XBQM-34E flight operations.

Gross Weight and Center-of-Gravity Locations. - Water-impact loads shall be determined for the weight shown in Table 3-15 and for the center-of-gravity location determined by weight analysis. In addition, loads shall be determined for actual weights and center-of-gravity locations for a range of mission weight distributions.

Sea Conditions. - Since the craft is an unmanned vehicle descending on a parachute rather than a seaplane landing at relatively high velocities, no investigation of the effects of different sea states on water-impact loads has been made. The criteria contained herein are intended to provide structural integrity for landing under reasonable sea states (3 or below).

Ultimate Factor of Safety. - The ultimate factor of safety shall be 1.25 for the water-impact condition.

3.3.2.2 Supplement to Preliminary Structural Design Criteria

This supplement is to be utilized in the event that a mid-air recovery system (MARS) is to be incorporated on the modified BQM-34E research vehicle. The MARS will be identical to the system incorporated on the BQM-34F; hence this criteria is developed from the BQM-34F criteria.

The major change required to convert the recovery system from the standard drag-main parachutes (on the BQM-34E) to the drag-main/engagement system (on the BQM-34F) is the exchange of parachutes and attachment of the slightly longer container. Hence, the preliminary structural design criteria for the BQM-34E research vehicle are applicable to all aspects of the vehicle operation except for MARS. The preliminary structural design criteria for the craft with MARS are summarized in Table 3-16.

Drag Parachute Deployment

The drag-parachute deployment criteria for the research vehicle shall remain unchanged.

TABLE 3-16

STRUCTURAL DESIGN CRITERIA SUMMARY, MARS RECOVERY

CONDITION	DESIGN GROSS WEIGHT (pounds)	ULTIMATE FACTOR OF SAFETY	MAXIMUM LIMIT LOAD FACTOR n_x	n_y	n_z	COMMENTS
FREE FLIGHT		1.25				
Complete Target	2500					Subsonic (with fuel pod)
	2037					Supersonic (without fuel pod)
Symmetrical Maneuvers					-2.0 to 5.0	$\dot{\omega}_{max}$ = 1.5 rad./sec.^{2}, basic
Asymmetrical Maneuvers					1.0 to 4.0	
Gust						27 fps (EAS) at V_H
CAPTIVE FLIGHT	2544	1.50				
Taxi, Takeoff, Landing			± 2.50	± 1.50	-3.0 to 6.0	For design of attachments and sway braces. Loads act simultaneously.
Gust						50 fps (EAS) at V_H of DP-2E.
PARACHUTE RECOVERY		1.25				
Drag Parachute Deployment	1250 to 2028		-12.0*	± 3.0*	6.00*	Based upon 15,000-lb. parachute load.
Main/Engagement Parachute Deployment	1922					Based on test or analysis (Minimum load of 12,000 lb. per BQM-34E criteria.)
HELICOPTER RETRIEVAL	1571 to 1720	1.50				
Pickup and Towing						Maximum load factor of 2.0 acting within 45° of positive Z axis of target.
Docking			0	0	2.0	
			0	± 1.0	1.0	
			± 1.0	0	1.0	
GROUND LOADS		1.50				
Ground Launch	2900					Includes JATO unit and fuel pod.
	2100		7.00*	± 1.50*	2.40*	Includes JATO unit.
						Ground launch loads and load factors based upon JATO thrust of 14,000 pounds plus engine thrust.
Ground Handling Loads						
Shipping	1900		± 4.0	± 1.33	±2.0	n_z acts alone and in combination with horizontal load factors.
Hoisting	2944		± 0.4	± 0.4	2.67	
Jacking	2544		± 0.5	± 0.5	2.0	
Carting	2544		± 2.0	± 1.33	2.0	
WATER LOADS						
Water Impact	1720	1.25	± 3.0	± 4.0	7.5	Load factors act independently.

NOTE: For flight with fuel pod (2500 lb.), V_H and V_L are M .95 and M 1.05. For flight without fuel pod (2037 lb.), V_H and V_L follow constant dynamic pressure lines from M 1.1 to M 2.3 and from M 1.2 to M 2.5.

*Used for equipment installation.

Page Intentionally Left Blank

Main/Engagement Parachute Deployment. - Main/engagement parachute criteria are summarized in Table 3-16. Loads generated from these criteria shall not be less than those for a standard (no-MARS) system.

Additional Loading Conditions - Helicopter Retrieval Loads Criteria

In the event that MARS is incorporated into the BQM-34E research vehicle, the structure shall be capable of sustaining loads developed during helicopter pickup, towing, and docking operations.

Gross Weights and Center-of-Gravity Locations. - Helicopter retrieval loads shall be determined for the range of weights shown in Table 3-16 and for the center-of-gravity locations determined by weight analysis.

Helicopter Pickup and Towing. - The maximum load factor acting at the center of gravity of the vehicle during helicopter pickup and towing shall be 2.0. The line of action of the pickup or towing force shall be considered to lie anywhere within a cone generated at 45 degrees to the positive Z axis of the aircraft. These criteria are based on past experience and have been used successfully on other Teledyne Ryan pilotless aircraft.

Docking. - The maximum load factors for docking are presented in Table 3-16.

Ultimate Factor of Safety. - The ultimate safety factor shall be 1.5 for retrieval conditions.

3.3.3 Structures and Weights

3.3.3.1 Wing Location Structural Evaluation

The four different structural design configurations (Paragraph 3.3.1) for joining the wing to the fuselage were evaluated in depth. The configurations are quantitatively rated and ranked in an orderly fashion to help facilitate a design decision.

The fuselage structure evaluated reacts the wing and provides overall bending and shear continuity to the fuselage. This portion of the fuselage contains fuel, and sealing is a consideration. The structure affected by the trade includes fuselage skin, frames, bulkheads, longerons, and fittings in the center section region between Stations 235.5 and 274.59.

Other systems which may be affected by the wing location are the fuel plumbing and sealing, the inlet duct, and the electrical harnesses.

Design Alternatives (See Referenced Drawings)

The four wing locations evaluated are as described below:

a. Configuration 1-30-1, standard fuselage. Wing center box with provisions for attaching to the original wing mounting points on the fuselage.

b. Configuration 1-30-2, standard fuselage. Low midwing bolted to side of fuselage. (A continuous wing would interfere with the inlet duct.)

c. Configuration 1-30-3, stretched fuselage. New center plug with provisions for attaching low midwing of continuous construction.

d. Configuration 1-30-4, standard fuselage. Wing located below fuselage.

Method of Evaluation

Each configuration was evaluated for the following items, called figures of merit:

a. Weight (pounds) of airframe

b. Vehicle aerodynamic performance

c. Costs

d. Manufacturing schedule

e. Operational characteristics

Certain parameters were associated with each merit item. These parameters are shown in Table 3-17. Merit points were assigned to each parameter on the basis of its relative importance.

The advantages and disadvantages for each configuration were compared and ranked in a matrix. Table 3-18 is a tabulation of the comparison. The relative importance of each parameter and its influence on the design decision were accounted for with this table.

TABLE 3-17

FIGURES OF MERIT, ASSOCIATED PARAMETERS, WEIGHTING FACTORS

Figure of Merit	Parameters	Points
Weight (100 pts)	o Weight	100
Aero-Performance (100 pts)	o A_W (Sq. Ft.) Wetted Area	25
	o F.R. Equiv. - body fineness ratio	25
	o $\overline{V}_H$ Horizontal Tail Vol.	25
	o $\overline{V}_V$ Vertical Tail Vol.	25
Unit Costs (100 pts)	o Fabrication Complexity*	Total 100
	o Quality Assurance*	
	o Producibility*	
	o Ability to Hold Tolerance*	
Manufacturing Schedule (100 pts)	o Fabrication Complexity	35
	o Geometric Restrictions	25
	o Quality Assurance	5
	o Ability to Hold Tolerance	10
	o Producibility	35
Operational Characteristics (100 pts)	o Susceptibility to Damage	40
	o Maintainability, Repairability, and ease of field assembly	
	o Reliability	10
	o Safety	20

*Parameters which affect more than one figure of merit

TABLE 3-18

COMPARISON MATRIX

Configuration / Parameter	1-30-1 High Wing	1-30-2 Low Wing	1-30-3 New Center Plug	1-30-4 Bottom Fuselage
Unit Costs:				
Fabrication Complexity	• New center box for wing attachment. • Rework fairing • Low number parts • Least complexity rank .05	• 3 new fuselage frames. • New wing attach ftn'gs., (L, H, & R.H.) • New frame tie bars • New fairing at wing old location • Moderate number of parts and complexity rank .10	• New frames, skins, longerons, and fittings • New section of inlet duct • Provisions for keel continuity • Fuel sealing provisions • Electrical harness splices required • Large size of parts and highest complexity rank .65.	• Modification to existing fuselage frames • New external structure attached to fuselage bottom for wing mount • Provisions for keel continuity Rank .20
Producibility	• Least tooling costs and mfg. time Rank .10	• Moderate tooling costs and mfg. time Rank .20	• High degree of tooling costs, set-up and mfg. time, trimming, drilling, forming and finishing. Rank .40	• Next to highest tooling costs and mfg. time Rank .3

TABLE 3-18 (Continued)

COMPARISON MATRIX

Configuration / Parameter	1-30-1	1-30-2	1-30-3	1-30-4
Ability to hold tolerances	• Moderate degree required to align wing properly. Rank .1	• Moderate degree for frames and wing attach ftgs. Rank .2	• High degree to align plug with fuselage and wing. Rank .40	• Next to highest degree for proper wing alignment. Rank .3
Quality Assurance	• Good Rank .10	• Good to fair Rank .20	• Poor to fair Rank .40	• Fair Rank .30
Material Cost	$250.00/lb.	$250.00/lb.	$250.00/lb.	$250.00/lb.
Operational Characteristics:				
Susceptability to damage	• As good as original Rank .067	• Low wing more likely to sustain damage dur-surface landing. Rank .167	• Longer fuselage and lower wing more vulnerable during surface landing. Rank .30	• Wing under fuselage is highly exposed to damage during surface landing. Rank .466
Maintainability, Repairability, ease of assy. in field	• Can easily replace center box and make repairs. Rank .10	• Fuselage ft'gs. difficult to align in field to restore wing alignment. Rank .2	• Better than -4 Rank .3	• Wing alignment difficult to restore in field Rank .4

TABLE 3-18 (Continued)

COMPARISON MATRIX

Configuration / Parameter	1-30-1	1-30-2	1-30-3	1-30-4
Reliability	• This config. and -2 are considered equally reliable	• Eqval to -1	• Better than -4	• Least reliability
	Rank .125	Rank .125	Rank .35	Rank .40
Safety	• Good as original design	• As good as -1	• Has greatest impact on other systems.	• Better than -3
	Rank .1	Rank .1	Rank .5	Rank .3
Aero Performance:				
Wetted Area, ΔA_W	• No change	• No Change	• Greatest	• Greater than -1 & -2.
	Rank 0.0	Rank 0.0	Rank .787	Rank .213
Equiv. finess body ratio	Rank .252	Rank .252	Rank .270	Rank .225
Horiz. Tail Vol., $\bar{V}_H$	Rank .25	Rank .25	Rank .25	Rank .25
Vert. Tail Vol., $\bar{V}_V$	Rank .25	Rank .25	Rank .25	Rank .25
Weight/Costs:				
ΔWeight	0	30	55	35
Relative costs	1.0	1.25	1.50	1.10
Added costs	1.0	30.00	55.00	35.00
Weighing ratio	.01	.25	.45	.29

The final evaluation of each configuration was based on the number of merit points earned. Each point is a mark against the configuration. The candidate design with the lowest total was considered the best selection. Table 3-19 is a summation of points for each configuration.

Final Selection

The evaluation of the alternative configurations is summarized as follows:

a. The high wing, configuration 1-30-1, scores best, except for the fact that this location is not typical for transports.

b. Fabrication of a new center plug and stretching of the fuselage are quite expensive relative to the other configurations. The increased wetted area gives it a poor aerodynamic ranking. Fabrication complexity and impact on other systems rank high relative to the alternative configurations.

c. In configuration 1-30-4, the bottom of the fuselage does not score well aerodynamically and ranks third from an operational standpoint.

d. Configuration 1-30-2 is the most feasible wing location, based on the total evaluation of all items.

3.3.3.2 Structural Analysis

A structural analysis was performed on the fuselage center section to substantiate the feasibility of mounting the NASA research wing to the BQM-34E fuselage. The internal load distribution generated by the wing reactions on the fuselage was determined, and an estimate was made of modifications required.

For analysis purposes, the fuselage center section between XF 233.5 and XF 274.59, where the wing is located, was isolated in a structural model. The wing introduces large concentrated loads, at the attachment points, which are required to be distributed into the shell. In addition, this section provides overall bending and shear continuity to the fuselage. It also affords fuel containment and is subjected to fuel pressure.

Configuration 1-30-2 (wing bolted to fuselage side) was analyzed in detail. The structural concept requires a two-piece wing, consisting of a left and right-hand panel. Wing continuity or carrythrough structure is

TABLE 3-19

EVALUATION

OBJECTIVE: Determine Most Feasible Wing Location																
		Aero. Perf'm.			Mfg. Schedule				Operational Charac.							
Configuration	Weight-Cost Evaluation Factor	Wetted Area	Equiv. Body Fineness Ratio	Tail Vol.	Fabrication Complexity	Production	Ability to hold tolerance	Quality Assurance	Susceptibility to damage	Repairability, ease of assy.	Reliability	Safety	Total Evaluation	Remarks	Selection
1-30-1 High Wing	1.0	0	6.3	*	1.75	2.5	1.0	.5	2.68	3.0	1.25	2.0	21.98	• Not typical for transparts	
1-30-2 Low Wing	25	0	6.3	*	3.5	5.0	2.0	1.0	6.68	6.0	1.25	2.0	58.73	• Typical for transparts	Final Choice
1-30-3 New Center Plug	45	19.675	6.75	*	22.75	12.5	4.0	2.0	12.0	9.0	3.5	10.0	147.175	• Provides for additional fuel • High fineness ratio	
1-30-4 Bottom Fuse.	29	5.325	5.56	*	7.0	7.5	3.0	1.5	18.64	12.0	4.0	6.0	99.615	• High frontal area	

* Same for all

provided by the fuselage, which is modified to accommodate the wing. This modification consists of the following items:

a. Three new frames, which serve as the main carrythrough structure.

b. A left and right-hand wing attachment fitting. These fittings comprise the structural link between the wing and the fuselage.

c. The tie bars which connect the ends of the horseshoe-shaped frames and provide fuel-containing facilities to replace the original wing structure which performed this function.

Construction consists of a conventional semimonocoque frame/longeron shell structure. The material is aluminum alloy. Drawing No. 166SCW014 depicts the configuration.

The fuselage structure in the region of the wing attachment is idealized into an analysis model which describes the geometry, reactions, materials, and the structural elements. The finite elements include rods, bars, and shear panels. These elements and the computer program formulations are described in Reference 11. The program computes displacements, reactions, and internal loads on the finite elements. The wing reactions are applied as concentrated loads at the attachment points. The portion of structure between XF 233.5 and XF 274.59 is isolated into the analysis model (Reference Drawing No. 166SCW014). Appropriate reactions are provided at these stations.

Input

The structural analysis input data consists of the following items:

a. Geometry

b. Idealization

c. Structural elements and sizes

d. Material properties

e. Reactions (constraints)

f. External loads

These items are described and presented on the following pages for the different structural configurations used in this feasibility study.

Geometry. - Center Section

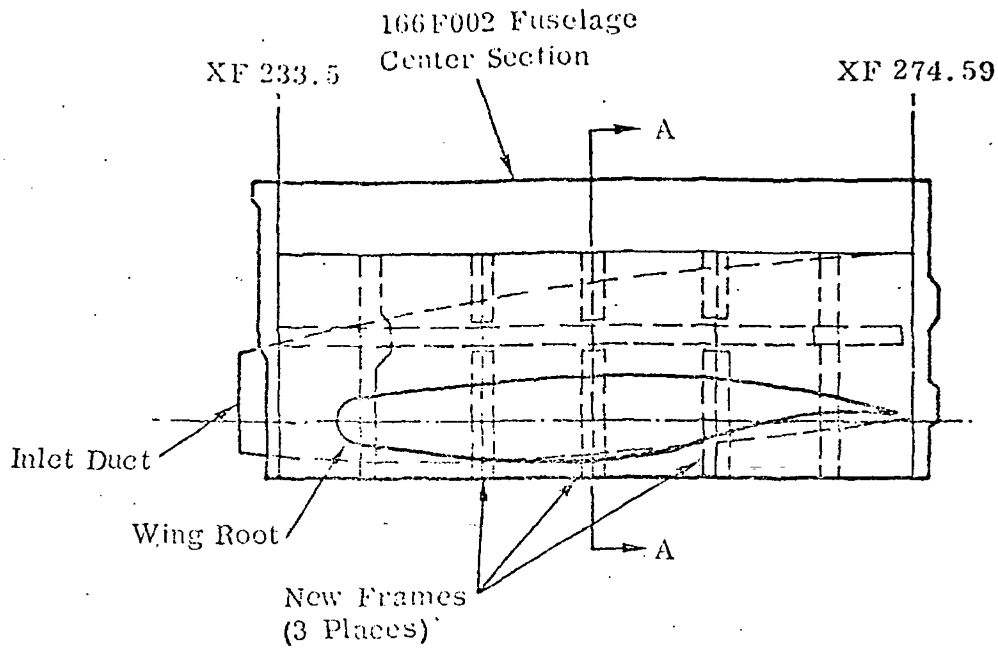

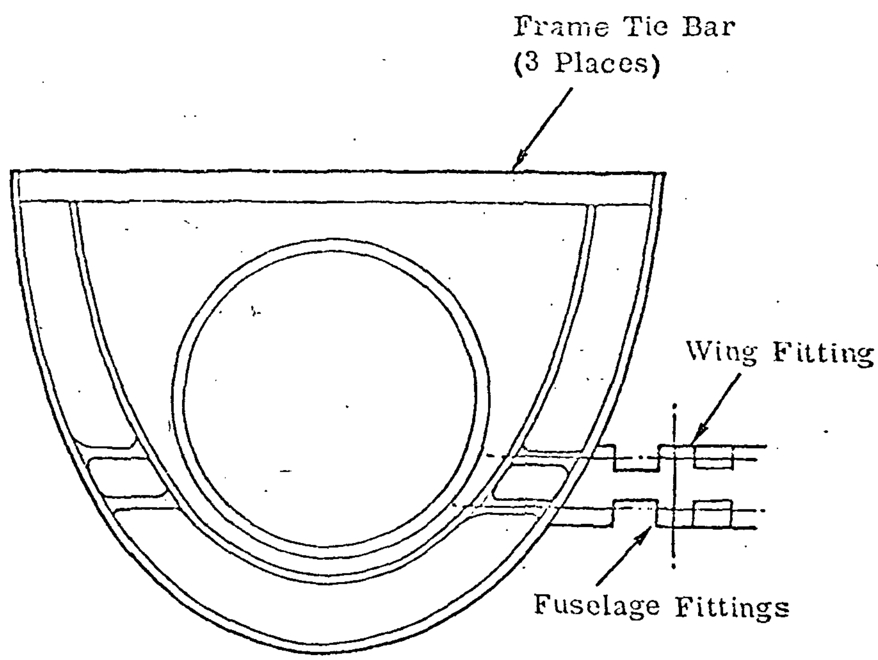

SECTION A-A

Grid Points and Shear Panels.

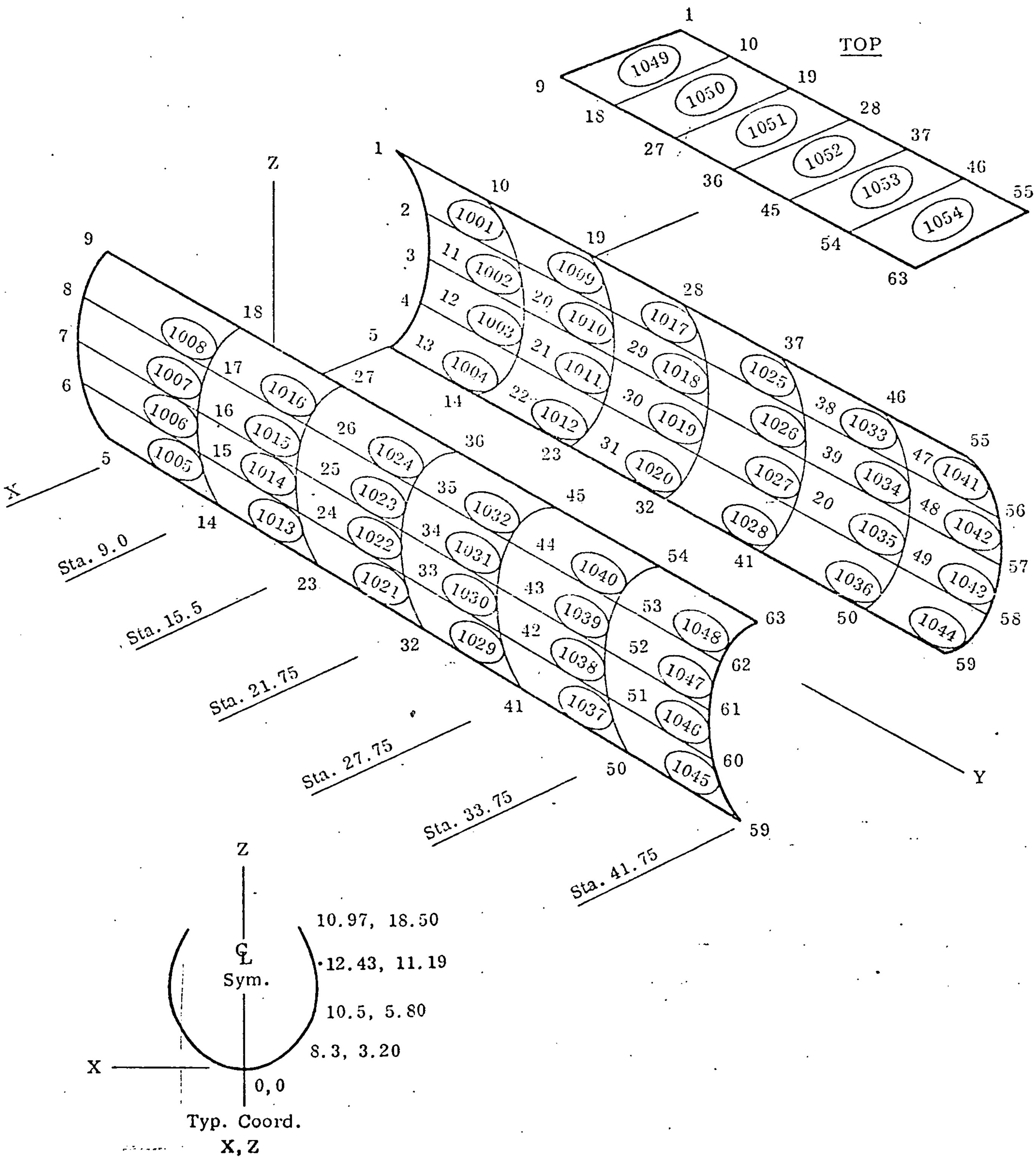

Rods and Bars.

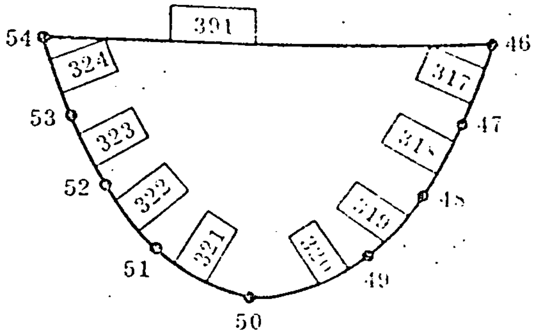

Sta. 33.75

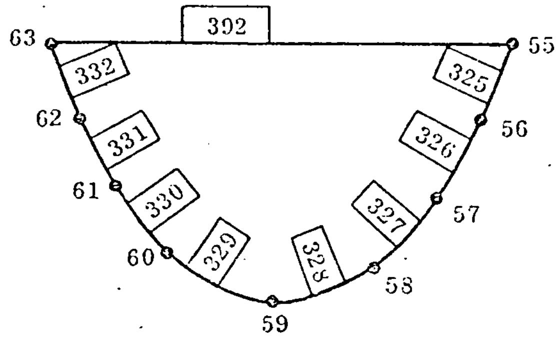

Sta. 41.75

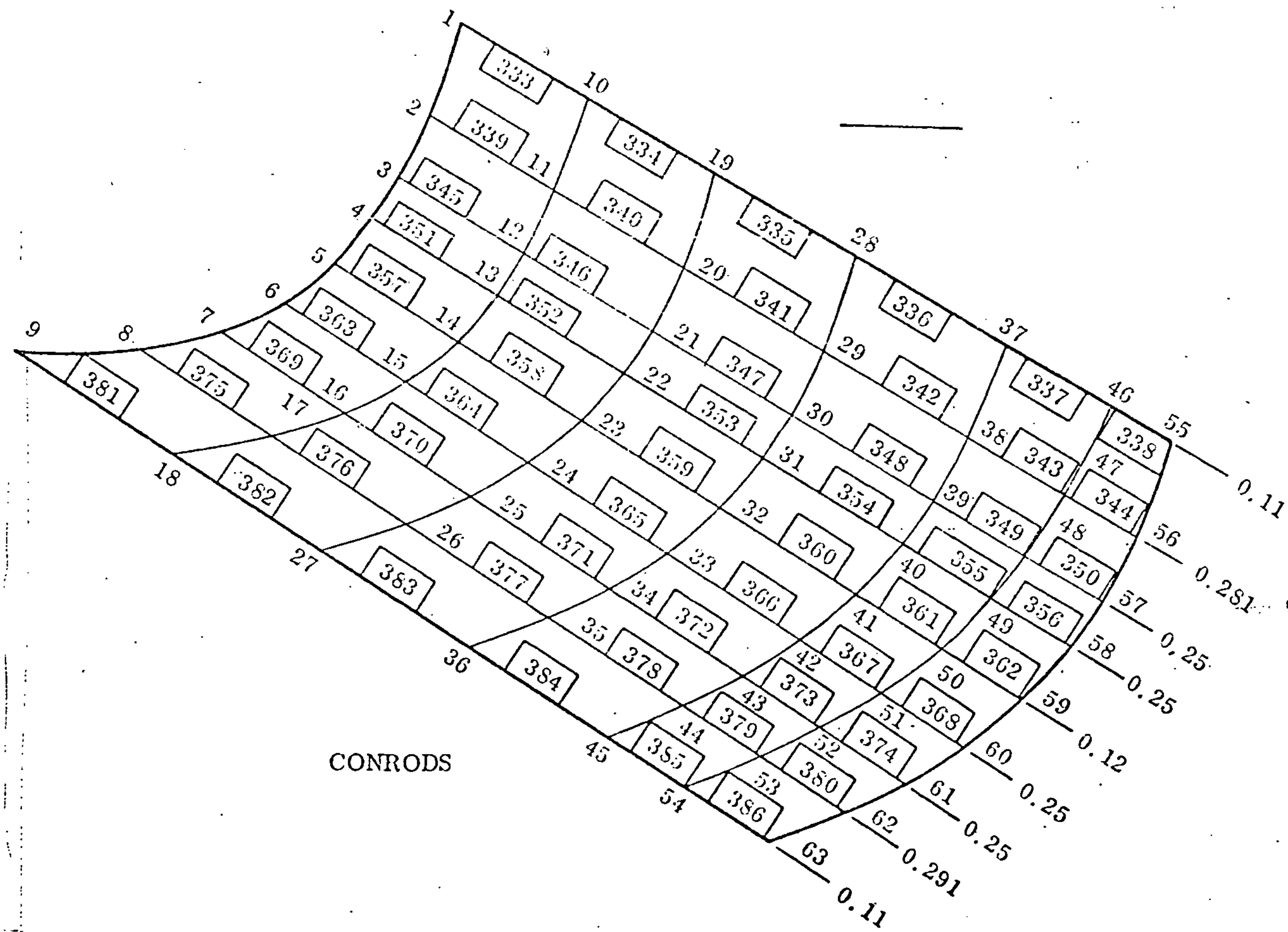

Rods and Bars.

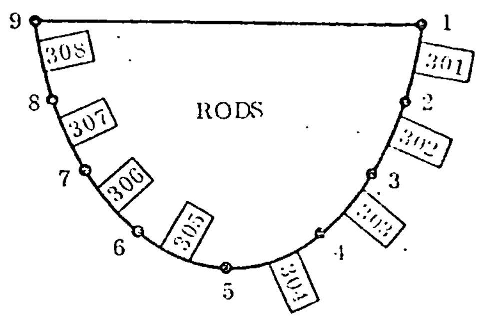

Sta. 0.0

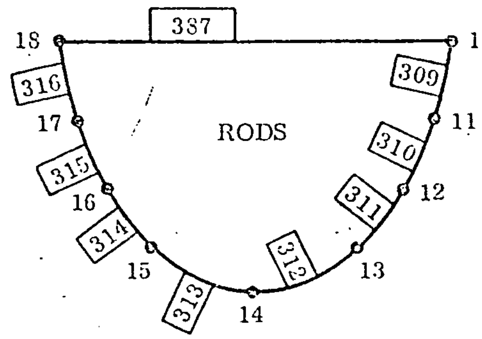

Sta. 9.0

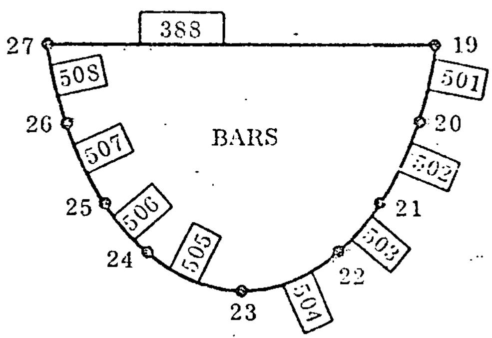

Sta. 15.5

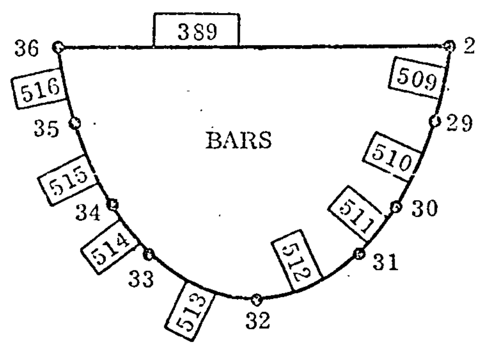

Sta. 21.75

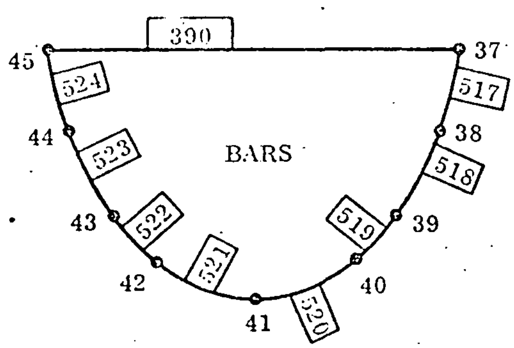

Sta. 27.75

Analysis - Configuration 1-30-2

External Loads. - Loads representing the 5-g symmetrical maneuver flight condition are applied to the center section. Wing bending and shear loads are distributed equally to the three fuselage frames. Torsion is reacted by the frames at the forward and aft spars.

Fuselage bending and shear resulting from loads applied on the forward fuselage are applied at XF 233.5. The section is fixed at XF 274.59.

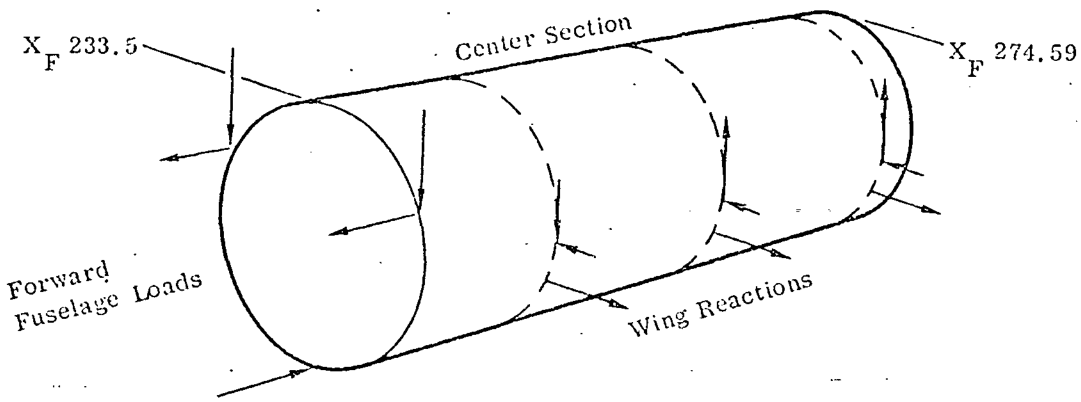

Wing Root Loads (Ultimate)

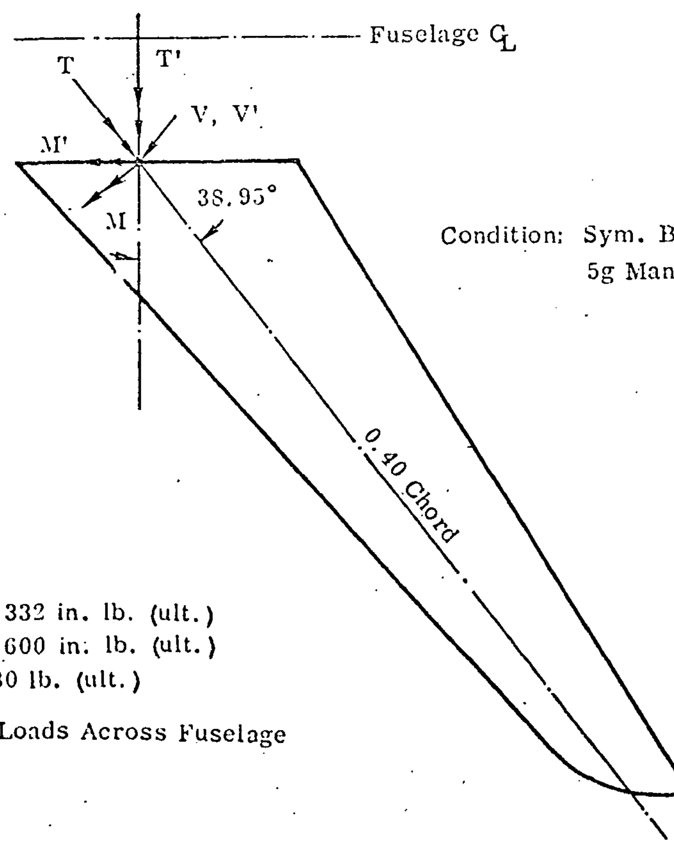

Condition: Sym. Balanced 5g Maneuver

M = 379,332 in. lb. (ult.)
T = -15,600 in. lb. (ult.)
V = 8,130 lb. (ult.)

Resolve Loads Across Fuselage

$$M' = M \cos\theta - T \sin\theta$$
$$= 379332 \cos 38.95° - 15600 \sin 38.95°$$
$$= 285196 \text{ in. lb. (ult.)}$$

$$T' = T \cos\theta + M \sin\theta$$
$$= 15600\ (0.77769) + 379332\ (0.62864)$$
$$= 250595 \text{ in. lb. (ult.)}$$

$$V' = 8130 \text{ lb. (ult.)}$$

Loads - Wing Reactions on Fuselage. - Assume M' and V' are shared equally at three frames.

$$M/\text{Frame} = \frac{M'}{3} = \frac{285196}{3}$$
$$= 95065 \text{ in. lb. (ult.)}$$

$$P_V/\text{Frame} = \frac{V'}{3} = \frac{8130}{3}$$
$$= 2710 \text{ lb. (ult.)}$$

M/frame is coupled into the frame as shown below.

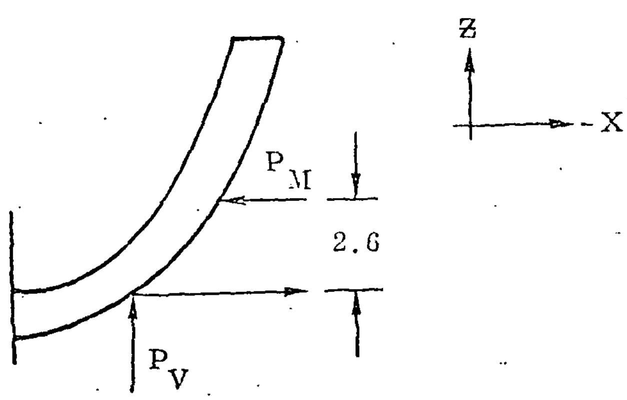

$$P_M = \frac{95065}{2.6} = 36563 \text{ lb. (ult.)}$$

Torsion, T', is coupled between the forward and aft frames.

Torsion

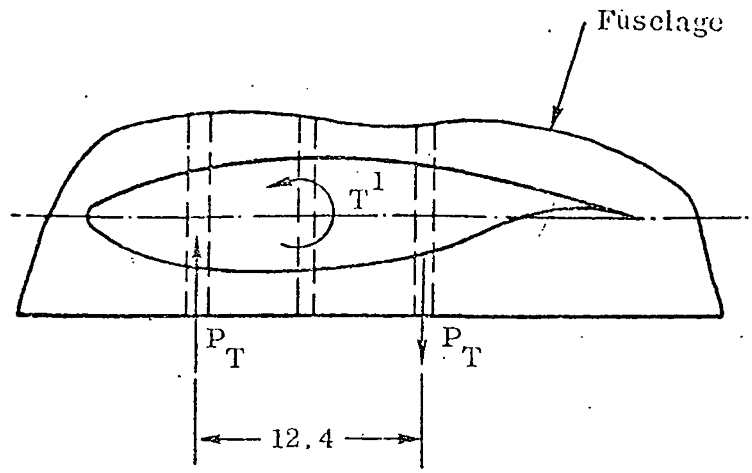

$$P_T = \frac{T'}{12.4} = \frac{250595}{12.4}$$

$$= \pm 20209 \text{ lb. (ult.)}$$

SUMMARY OF APPLIED WING LOADS ON FUSELAGE (ULTIMATE)

GRID POINT*	X (lb.)	Y	Z (lb.)
21 (25)	36563	0	-
22 (24)	-36563	0	22920
30 (34)	36563	0	-
31 (33)	-36563	0	2710
39 (43)	36563	0	-
40 (42)	-36563	0	17500

*See Idealization
(25) indicates opposite hand grid point

Forward Fuselage Loads

XF 233.5 shear and bending (limit)

M = -170645 in.lb. 5-g sym. maneuver

V = -3015 lb.

The loads are increased to ultimate and panel pointed as shown below.

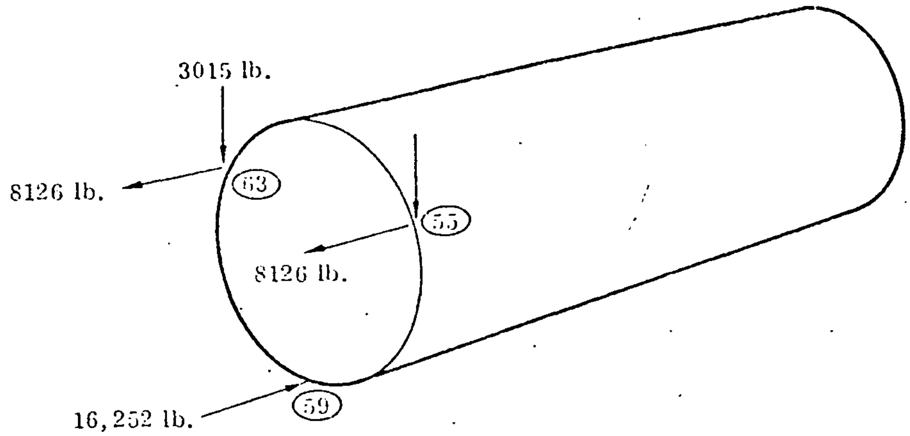

Reactions

The section is constrained at XF 274.59 at grid points shown.

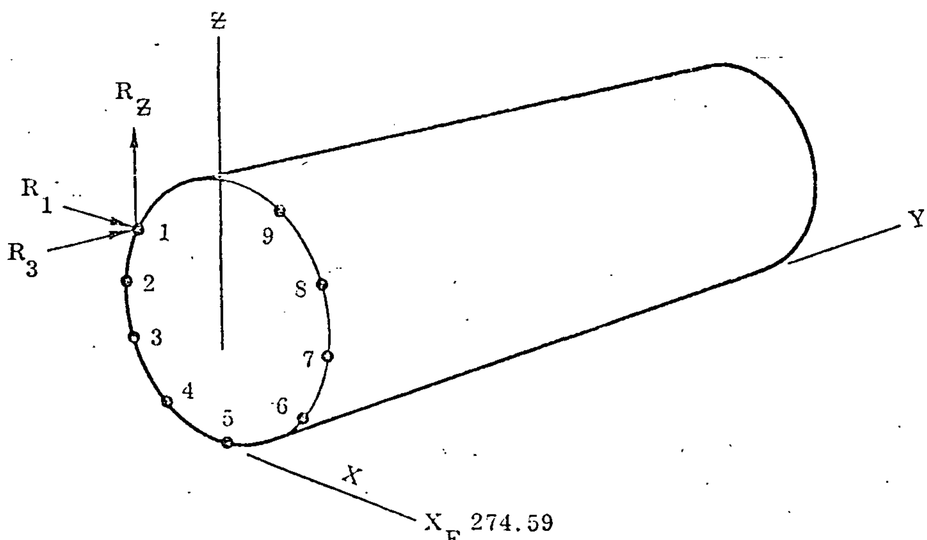

Material Properties

Material is 7075-T6 al. aly.

F_{tu} = 73000 psi

F_{cy} = 65000 psi

F_{su} = 43000 psi

E = 10.5×10^6 psi

G = 3.9×10^6 psi

Output. - The results of the computer analysis include the following data:

a. Internal forces and stresses in bars, rods, and shear panels.

b. Deflections

c. Reactions

These results are summarized and presented in the following pages. Only the significant loads are shown. The detailed output for each element is included in Reference 12.

Output - Longeron Loads. - Critical longeron loads are tabulated below.

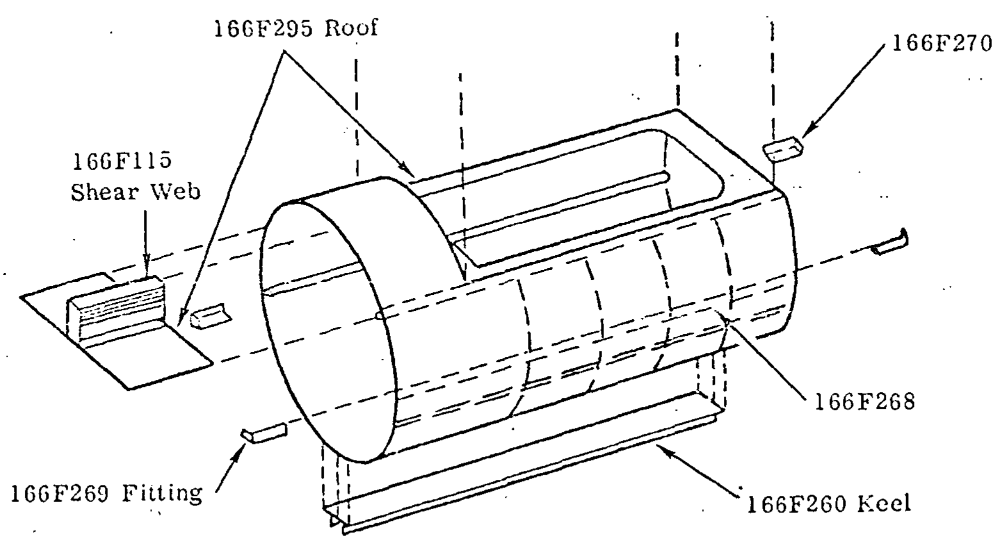

LONGERON PART NO.	ELEMENT NO.	LOAD (lb., ult.)
166F295	334	19317 Ten.
166F268	339	15266 Ten.
166F260	361	-16252 Comp.

Skin Shear Loads. - Critical skin shear loads are shown below.

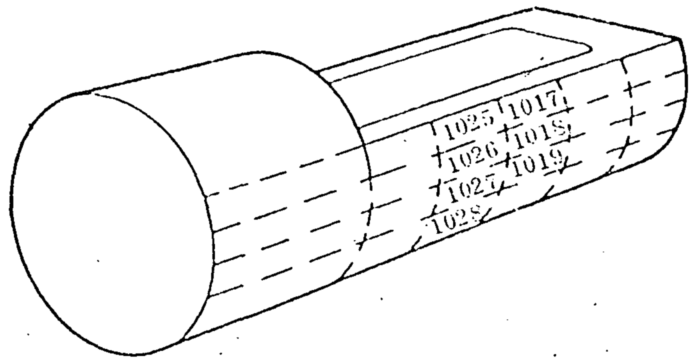

ELEMENT NO.	STRESS (psi, ult.)	SHEAR FLOW (lb./in., ult.)
1017	11926	596
1018	26659	1333
1019	17150	856
1025	11237	562
1026	36762	1838
1027	20728	1036
1028	2416	121

Frame Loads. - The forward wing attachment frame internal loads are shown below. Loads are symmetrical about the vertical and centerline.

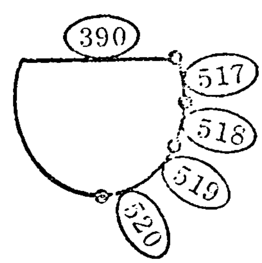

ROD NO.	M (ult.) (in./lb.)	P_{axial} (lb., ult.)	SHEAR (lb., ult.)
390		-4875	
517	-36741		4600
518	-56590	9628	3160
519	48568	-5314	-29125
520	12000	11189	5299

Reactions

Ultimate reactions are shown below. Loads are symmetrical about the vertical centerline.

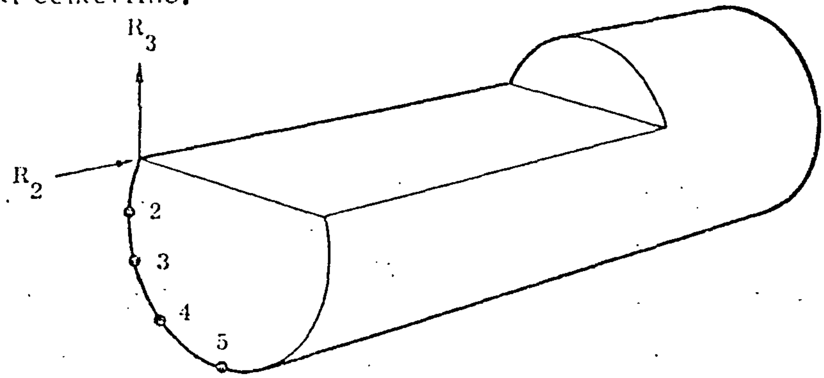

GRID POINT NO.	R_2 (ult.) (pounds)	R_3 (ult.) (pounds)
1	-13715	-1671
2	-16150	-2374
3	6086	-923
4	16106	-183
5	15348	73

Output - Deflections. - Displacements along the bottom and based on ultimate loads, are shown below.

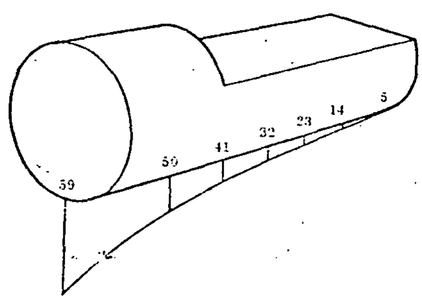

GRID POINT NO.	DISPLACEMENT (inches)
5	0.0
14	-0.070
23	-0.202
32	-0.424
41	-0.682
50	-1.010
50	-1.698

Stress Analysis

A stress analysis was made on the critical structural elements to determine their ability to carry the loads shown on the preceding pages. The most critical elements are certain panels that comprise the fuselage shell and the frames which react the wing loads. The skins undergo severe diagonal tension, and it is recommended the 0.050-inch basic skin be reinforced with an 0.012-inch doubler over several panels. The frames experience large bending loads and must be adequately stiff to prevent large wing deflections.

Part No. 166F268 Longeron

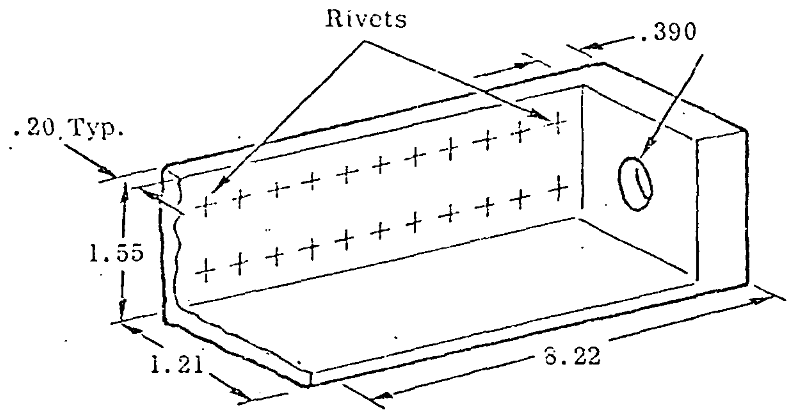

Tension across net section:

$$P = 15266 \text{ lb. (ult.)}$$

$$A = 0.542 \text{ in.}^2$$

$$f_t = \frac{P}{A} = \frac{15266}{0.542}$$

$$f_t = 28166 \text{ psi}$$

$$F_{tu} = 76000 \text{ psi}$$

$$MS = \frac{76000}{28166} - 1 = 1.69$$

The tension fitting end of the longeron is analyzed as an angle-type fitting with a NAS626 bolt, using methods of Reference 3.

$$A = 1.55 - \frac{0.20}{2} = 1.45 \qquad \gamma_i = \frac{0.375}{2} = 0.1875$$

$$B = 1.21 - \frac{0.20}{2} = 1.11 \qquad \gamma_o = \frac{0.646}{2} = 0.322$$

$$C = 0.61 - \frac{0.20}{2} = 0.51 \qquad t_w = 0.20$$

$$a = \frac{A + B}{\pi} = 0.815 \qquad Ag = \pi\, a\, t_w = 0.512$$

$$d = a - \left(\frac{C + D}{2}\right) = 0.3005 \qquad c = 0.637a = 0.5191$$

$$I = 0.298\, a^3\, t_w = 0.0322$$

Wall Stress

Axial load, f_{tu}:

$$f_{tu} = \frac{P}{Ag} = \frac{16150}{0.512} = 31543 \text{ psi (ult.)}$$

Bending stress, f_{bu}:

$$M = P\,(c-b) = 16150\,(1.5191 - 0.3005)$$

$$M = 3530 \text{ in./lb. (ult.)}$$

$$f_{bu} = \frac{M\,c}{I} \qquad c = \frac{a}{2} = 0.407$$

$$f_{bu} = \frac{3530\,(0.407)}{0.0322}$$

$$f_{bu} = 44618 \text{ psi (ult.)}$$

Net Stress:

$$f_{total} = f_{tu} + f_{bu}$$

$$= 31543 + 44618$$

$$= 76161 \text{ psi (ult.)}$$

$$F_{bu} = F_{tu}\, 1.25 = 95000 \text{ psi}$$

$$MS = \frac{95000}{76161} - 1 = \underline{0.247}$$

End Pad Stress, f_{bue}:

$$\frac{\gamma_i}{a} = 0.230 \qquad \frac{a-d}{\gamma_o} = 1.599 \qquad \frac{t_e}{t_w} = 1.95$$

$$\therefore K_1 = 1.55,\ K_2 = 0.55$$

$$f_{bue} = \frac{P}{t_e^2} K_1 K_2 = \frac{16150\,(1.55)\,(0.55)}{0.39^2}$$

$$f_{bue} = 91103 \text{ psi}$$

$$F_{bue} = 76000\,(1.5) = 114000$$

$$MS = \frac{114000}{91103} - 1 = \underline{0.25}$$

Wing Attachment Frame. - The frame experiences critical loads at the wing attachment.

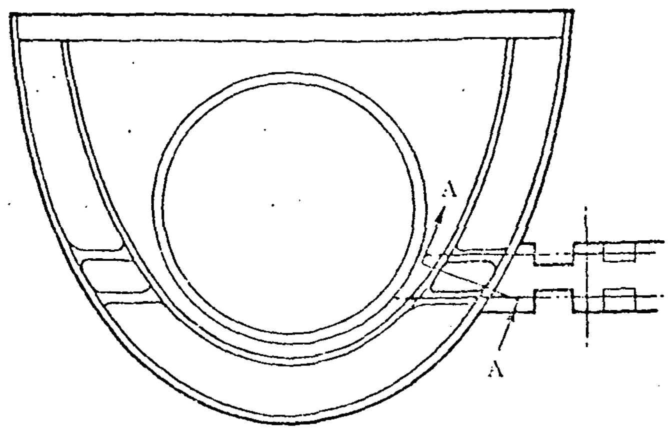

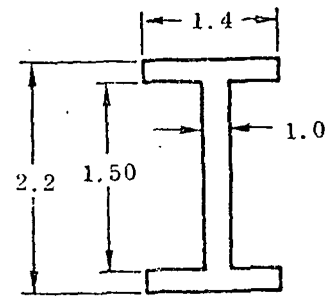

Loads (ult.) @ A-A:

$M = 56590$ in./lb.

$P = 9628$ lb. (axial)

$V = 3160$ lb. (shear)

Sec. A-A

$I = 1.23$ in.^{4}

$A = 3.1$ in.^{2}

Bending @ A-A:

$$f_b = \frac{Mc}{I} + \frac{P}{A} = \frac{56590\ (1.1)}{1.23} + \frac{9628}{3.1}$$

$f_b = 53715$ psi (ult.)

$F_{tu} = 76000$ psi

$$MS = \frac{76000}{53715} - 1 = \boxed{0.41}$$

Part No. 166F260 Keel. - The keel originally served to distribute the vertical reaction of the external fuel tank to frames and to react bending loads. Its function in the NASA research vehicle is primarily as a longeron for fuselage bending loads.

Geometry:

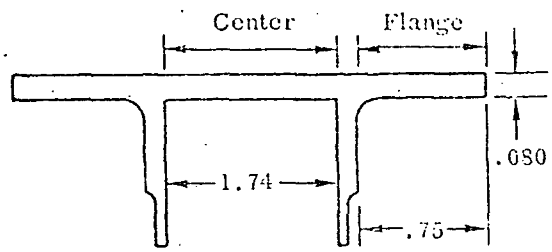

Material: 7075-T651
Area = .648 in.^{2}

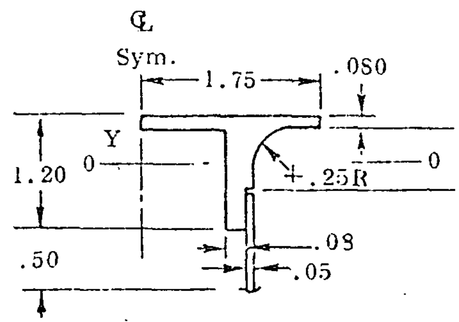

Material = 7075-T651

Area = 0.648 in.^{2}

Maximum compression, f_c:

$$P = -16252 \text{ lb. (ult.)}$$

$$f_c = \frac{P}{A} = \frac{16252}{0.648}$$

$$f_c = 25080 \text{ psi (ult.)}$$

Allowable compressive load, F_{ccr}:

$$F_{ccr} = \frac{K_c \pi^2 E}{12\,(1-u^2)} \left(\frac{t}{b}\right)^2$$

K_c = 4.0 for center
K_c = 0.43 for flange } Reference 4; Table 7

b = 1.74 in. for center

b = 0.75 in. for flange

u = 0.30

E = 10.5×10^6 psi

t = 0.08 in.

$$F_{cr_{center}} = \frac{4\ \pi^2\ 10.5 \times 10^6}{12\ (1 - 0.3^2)} \left(\frac{0.08}{1.74}\right)^2 = 80247 \text{ psi} > F_{cy}$$

$$F_{cy_{flange}} = \frac{0.43\ \pi^2\ 10.5 \times 10^6}{12\ (1 - 0.3^2)} \left(\frac{0.08}{0.75}\right)^2 = 46430 \text{ psi}$$

Margin of safety:

$$MS = \frac{46430}{25080} - 1 = \boxed{0.851}$$

Skin Panels. - The skin panels which comprise the fuselage shell experience high shear flows during the 5-g symmetrical maneuver. These loads are mainly due to coupling out of the wing torsion into the shell.

Geometry:

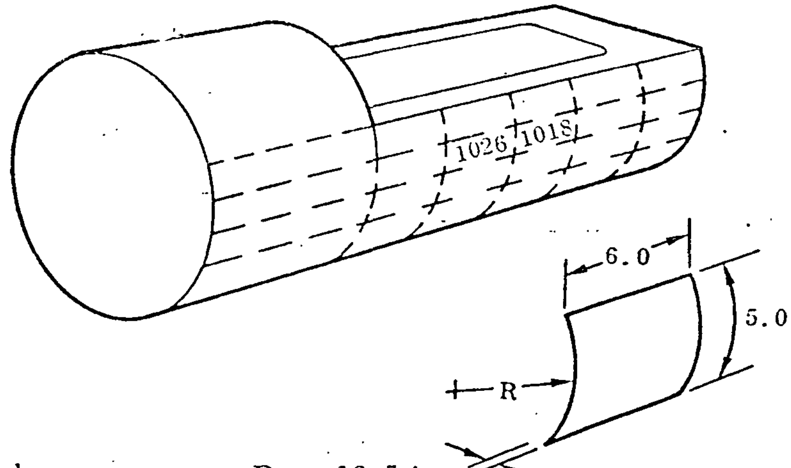

Material 7075T6 Clad

R = 12.5 in.
t = 0.062 in. (doubler added)

Loads; elements 1026 and 1018 are critical:

$$q\ 1026 = 1838 \text{ lb./in. (ult.)}$$

$$q\ 1018 = 1333 \text{ lb./in. (ult.)}$$

Shear stress, f_s:

$$f_s = \frac{q}{t} = \frac{1838}{0.062}$$

$$f_s = 29645 \text{ psi}$$

Shear buckling allowable, F_{scr}:

$$F_{scr} = K_s E \left(\frac{t}{b}\right)^2$$

$$\frac{a}{b} = \frac{6}{5} = 1.2$$

$$\frac{b^2}{Rt} = \frac{5^2}{12.5\ (0.062)} = 32.25$$

$\therefore K_s = 14$ (Reference 5, page 396)

$$E = 10.5 \times 10^6$$

$$F_{scr} = 14 \times 10.5 \times 10^6 \left(\frac{0.062}{5}\right)^2$$

$$F_{scr} = 22638 \text{ psi}$$

$\therefore$ semitension field

$$\frac{f_s}{F_{scr}} = \frac{29645}{22638} = 1.31$$

$\therefore k = 0.12$ (Reference 5; page 407)

$$\frac{ta}{Ae} = \frac{0.062\ (6)}{0.542} = 0.69$$

$$\tan \alpha = 0.98 \text{ (Reference 5; page 408)}$$
$$\alpha = 44°25'$$

$$F_{sw} = 32800 \text{ psi (panel allow, Reference 5; page 410)}$$

Panel margin of safety:

$$MS = \frac{32800}{29645} - 1 = \underline{|0.10}$$

3.3.3.3 Structural Configuration

The structural configuration selected for the NASA research wing is shown in Figure 3-54. The wing consists of the following items:

a. Wing structural box

b. A machined root rib

c. Leading edge

d. Trailing edge

e. Wingtip

f. Leading and trailing edge flaps

g. Ailerons

The wing box is of full-depth sandwich honeycomb construction. Its tapered skins are adhesive bonded to the core. Lightweight sheet metal spars bonded to the skins and core form the spanwise sides of the box. The root rib is attached to the inboard ends of the skins, core, and spars. Provisions are at the outboard ends for attaching a fiber-glass wingtip. The leading and trailing edges attach at the spar flanges, flush with the center-box skins to form a smooth, aerodynamic surface. Movable surfaces are appropriately hinged from the leading edge spar and frames housed in the trailing edge. The wingtip and trailing edge are of fiber-glass construction. The remaining wing structure, including the honeycomb core, is of aluminum alloy construction.

The movable surfaces are actuated by hydraulic units located in the leading and trailing edges. Appropriate pushrods, bell cranks, and fittings link each movable surface to its actuator. A wing fillet fairing is provided.

A qualitative evaluation of the configuration indicates that the weight-cost comparison relative to other concepts is good. Fabrication complexity is not great, and susceptibility to damage compares with alternative designs. Teledyne Ryan Engineering and Manufacturing have had much experience with this type of structural configuration as fabricated from both metallic and advanced composite materials. Technical risks are not high.

The configuration has a multiplicity of load paths, and any local damage is not likely to affect surrounding structure. Wing bending, shear, and torsion loads are carried by the center box. The root rib redistributes these loads and reacts them into the fuselage attachment bolts. Loads on movable surfaces and leading and trailing edges are distributed directly into the wing box. Loads on the actuating systems are not severe. Adequate space exists for installation of the actuator systems, and ease of accessibility is provided.

The concept offers an aerodynamic surface with a high degree of smoothness and lends itself to fabrication.

3.3.3.4 Mass Properties

The weight and balance for the NASA wing feasibility study (low wing) is presented in Table 3-20. The base vehicle is the BQM-34E (Reference 7), modified to include the new wing, control surfaces and controls, MARS system and repositioning of the wing and area rule fairings. The payload consists of a shaker installation and available volume located at Body Station 213. The density used for this volume is 45 pounds per cubic foot. Additional allowances for payloads are covered in Paragraph 3.3.2.

The center-of-gravity travel is considered to be for level flight and to be linear from a zero-fuel-weight configuration (29.93 percent MAC) to a gross-weight configuration (10.56 percent MAC). With the present systems and payloads, no ballast is required. If any equipment is modified, replaced, or removed, further study should be made to determine the effects on the center-of-gravity travel and the possibility of ballast.

TABLE 3-20

WEIGHT AND BALANCE SUMMARY,
NASA WING STUDY (LOW WING)

	WT. (1)	WEIGHT (Lbs.)	HORIZONTAL ARM (In.)	HORIZONTAL MOMENT (In.-Lb.)	VERTICAL ARM (In.)	VERTICAL MOMENT (In.-Lb.)
Aerodynamic Surfaces	(+5.8)	(214.10)	(290.6)	(62223)	(47.2)	(10116)
Wing (New incl. Fairing)	+5.8	162.40	270.9	43994	41.0	6658
Fin (1)	0	31.73	346.4	10990	73.1	2320
Stabilizer (1)	0	19.97	362.5	7239	57.0	1138
Body	(+12.7)	(271.61)	(245.8)	(67043)	(51.6)	(14005)
Nose (1)	0	101.02	181.9	18378	54.2	5471
Center (1 + Mod)	+12.7	115.39	264.2	30484	48.0	5548
Tail (1)	0	55.20	329.4	18181	54.1	2986
Take-Off & Recovery	(+43.7)	(165.28)	(373.5)	(62563)	(56.9)	(9405)
Take-Off (1)	0	6.88	257.4	1771	60.5	416
Recovery (2)	+43.7	158.40	383.8	60792	56.7	8989
Propulsion	(+18.1)	(498.20)	(287.1)	(143042)	(49.3)	(24546)
Air Breathing Sys(1)	0	443.40	291.5	129250	49.4	21896
Fuel & Lub (1+Mod)	+18.1	54.80	251.7	13792	48.4	2650
Power Generating System	(0)	(125.40)	(219.8)	(27560)	(55.2)	(6917)
Electrical - AC(1)	0	12.20	184.0	2245	54.6	666
Electrical - DC(1)	0	113.20	223.6	25315	55.2	6251
Orientation Contr	(+42.0)	(77.80)	(316.0)	(24587)	(48.5)	(3772)
Stabilator & Rudder	0	35.80	353.2	12645	57.3	2050
Leading Edge Flaps (New)	+14.0	14.00	276.8	3875	41.0	574
Aileron (New)	+28.0	28.00	288.1	8067	41.0	1148
Guidance & Electronics (New)	(-41.0)	(89.00)	(171.7)	(15248)	(53.5)	(4761)
Environmental Protection (1)	(0)	(19.70)	(285.9)	(5632)	(50.8)	(1000)
Hydraulic System (New)	(+20.0)	(20.00)	(240.8)	(4816)	(49.8)	(996)
Payload (New)	(+119.9)	(119.93)	(166.1)	(19923)	(53.8)	(6451)
Shaker Inst'l	+ 95.1	95.13	153.9	14641	54.0	5137
Avail @ Body Sta 213	+ 24.8	24.80	213.0	5282	53.0	1314
Area Rule Fairing (New)	(+ 23.3)	(23.3)	(260.6)	(6072)	(55.0)	(1281)
Forward		14.4	205.0	2952	55.0	792
Mid		5.0	312.0	1560	55.0	275

TABLE 3-20 (Continued)

WEIGHT AND BALANCE SUMMARY, NASA WING STUDY (LOW WING)

	WT. (1)	WEIGHT (Lbs.)	HORIZONTAL ARM (In.)	HORIZONTAL MOMENT (In.-Lb.)	VERTICAL ARM (In.)	VERTICAL MOMENT (In.-Lb.)
Aft		3.9	400.0	1560	55.0	214
Miscellaneous (1)	0	(3.30)	(169.4)	(559)	(112.7)	(372)
Weight Empty	(+244.5)	(1627.62)	(269.89) (31.16%)(3)	(439268)	(51.38)	(83622)
Unusable Fuel	(1.1)	(5.1)	(241.6)	(1232)	(42.9)	(219)
Main (1)	0	4.0	272.0	1038	40.5	162
Aux#1 (2)	+.7	0.7	199.8	140	50.0	35
Aux#2 (New)	+.4	0.4	260.2	104	55.4	22
Unusable Oil (1)	0	(2.3)	(299.0)	(688)	(43.0)	(99)
Oil - Usable (1)	0	(9.3)	(221.5)	(2060)	(43.0)	(400)
Zero Fuel Weight	(+245.6)	(1644.32)	(269.56) (29.93%)	(443248)	(51.29)	(84340)
Fuel (JP-5) Gal	(+110.8)	(373.8)	(244.7)	(91457)	(50.1)	(18730)
Main (1) 38.7	0	263.0	254.2	66855	48.7	12303
Aux#1 (2) 10.3	+ 70.0	70.0	199.8	13986	52.6	3682
Aux#2 (New) 6.0	+ 40.8	40.8	260.2	10616	56.0	2240
Refrigerant (1)	0	(8.3)	(128.8)	(1069)	55.3)	(459)
Gross Weight	(+356.4)	(2026.42)	(264.39) (10.56%)	(535774)	(51.09)	(103529)
LEMAC = 261.57 MAC = 26.70						

(1) Report No. TRA 16644-22, Actual Weight Report for BQM-34E Supersonic Aerial Target, Serial No. BQ-16181, dated 4 May 1972.

(2) Report No. TRA 16644-25, Actual Weight Report for BQM-34F Supersonic Aerial Target, dated 4 February 1972.

(3) Percent mean aerodynamic chord (MAC).

3.3.3.5 Advanced Composite Components

The capabilities of advanced composite materials in airframe structures can be demonstrated by the application of these materials to small components, such as a skin panel, flap, aileron, rudder, or part of an empennage. The development of advanced composite technology has progressed along these lines, and many do's, don'ts, and warnings have evolved from these types of application programs. The technical approach to achievement of a design objective with advanced composite materials may be summarized as follows:

a. Design/analysis

b. Fabrication

c. Test

Design/Analysis

This phase of the technical approach begins with a structural configuration and a design criterion. From this, geometry, external loads, sizes, and advanced composite material properties are generated. Figure 3-59 shows an outer wing panel fabricated from composite materials by Teledyne Ryan. This panel is a component on Teledyne Ryan's AQM-34R drone. An automated, iterative, design/analysis procedure shown in Figure 3-60 was used to substantiate the outer wing panel design. The procedure involved three separate but coupled types of analysis: laminate, structural, and flutter.

Each analysis required a computer program. The analysis cycle involved an inner strength loop and an outer flutter loop. The inner loop started with the laminate analysis program, which was used to generate stiffness matrices for the plate elements used in the structural analysis program. Ply orthotropic material properties, ply orientations, and allowable strain data were part of the input. Information from this phase was used as input in the structural analysis program to determine internal loads. The internal loads on the finite elements were then cycled back into the laminate program and were used to perform a point stress analysis of the laminate. Each ply in the laminate was analyzed for its critical failure mode, and margins of safety were calculated.

The structure was idealized into an analysis model which described the wing geometry, reactions, materials, and the structural elements. The finite elements included rods, shear panels, and plates. The composite

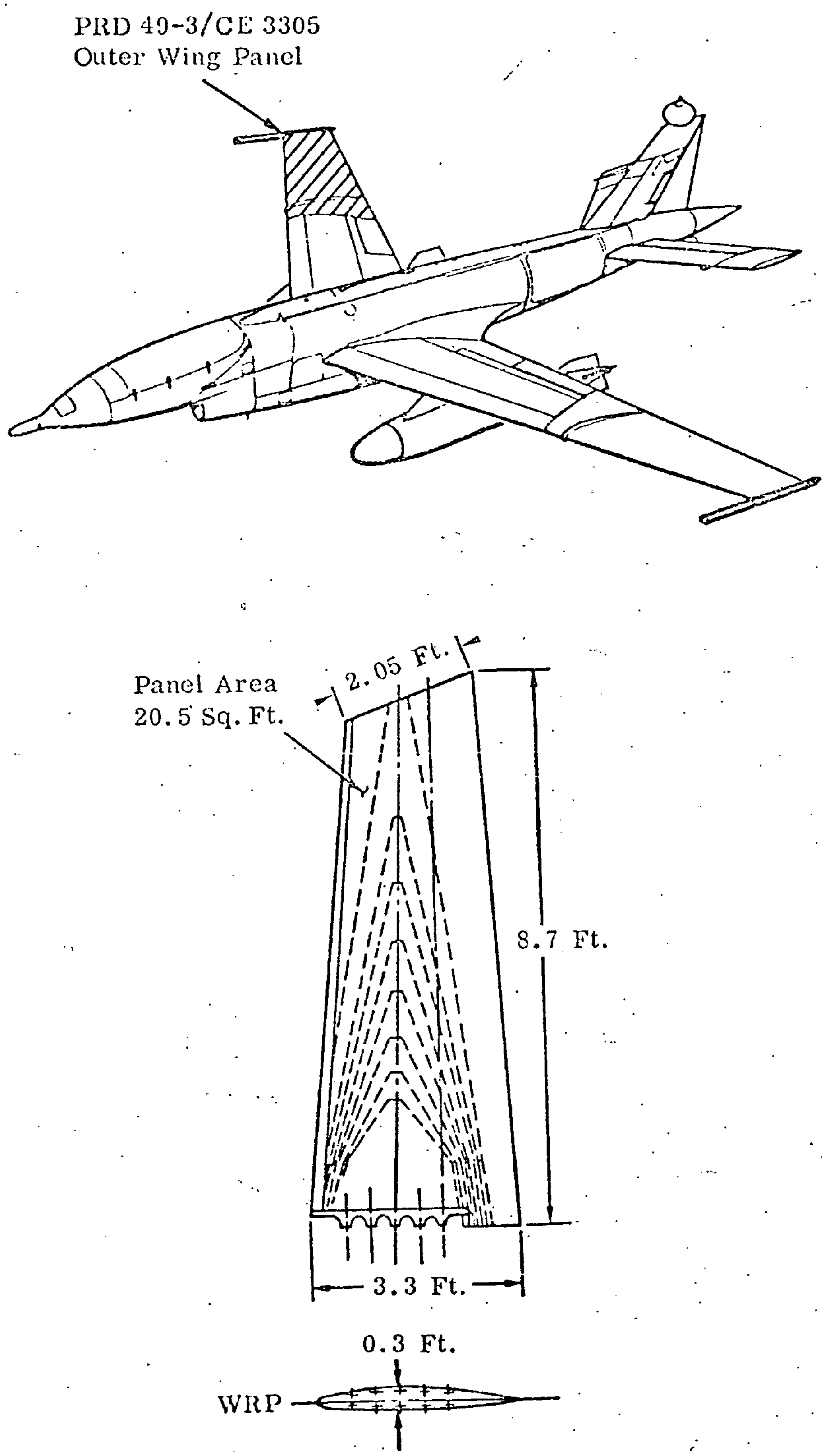

Figure 3-59. Model AQM-34R Drone

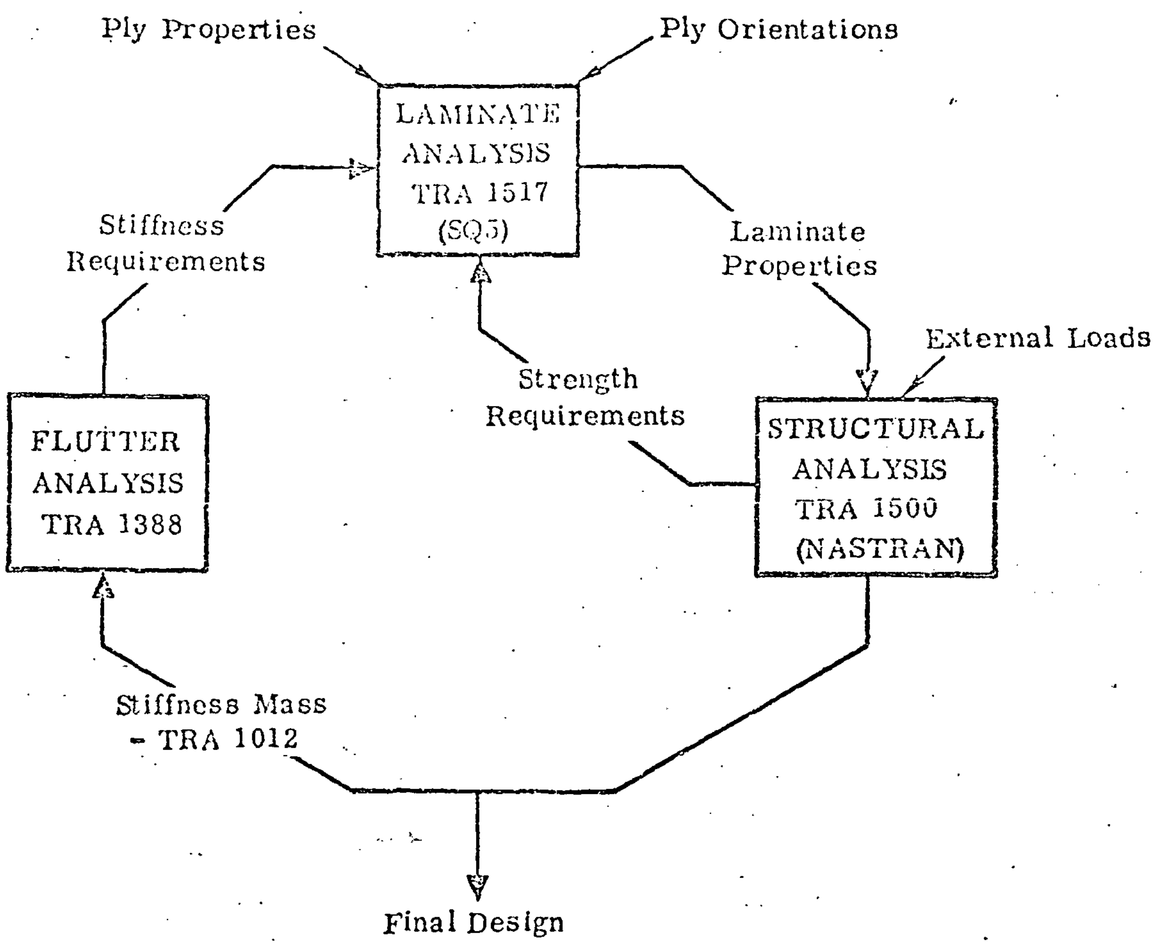

Figure 3-60. Analysis Approach and Cycle

laminated skins were represented as orthotropic triangular membrane elements. The program computed displacements, reactions, and internal loads for the design load conditions. The loads on the composite skins were cycled into the laminate analysis program, and a point stress analysis was performed. Figure 3-61 shows the structural analysis procedure. An elastic-axis beam representation of the structure was used in the flutter analysis loop utilized. Orthotropic beam elements were employed to determine EI and GJ stiffness properties.

Detail analyses were also performed on adhesive bond lines, joints, and stability failure modes.

Fabrication

This phase of the technical approach includes the following broad items:

a. Materials and test program

(1) Characterization of a resin system

(2) Tests to determine the mechanical properties of the material system to establish design allowables

(3) Development of adhesive data

(4) Development of tests and specifications

b. Manufacturing and quality control

(1) Fabrication techniques

(2) Autoclave versus vacuum bagging

c. Tooling development

(1) Structural concepts - tradeoffs

(2) Tooling materials

d. Manufacturing engineering

(1) Tolerance requirements

(2) Bonding processes

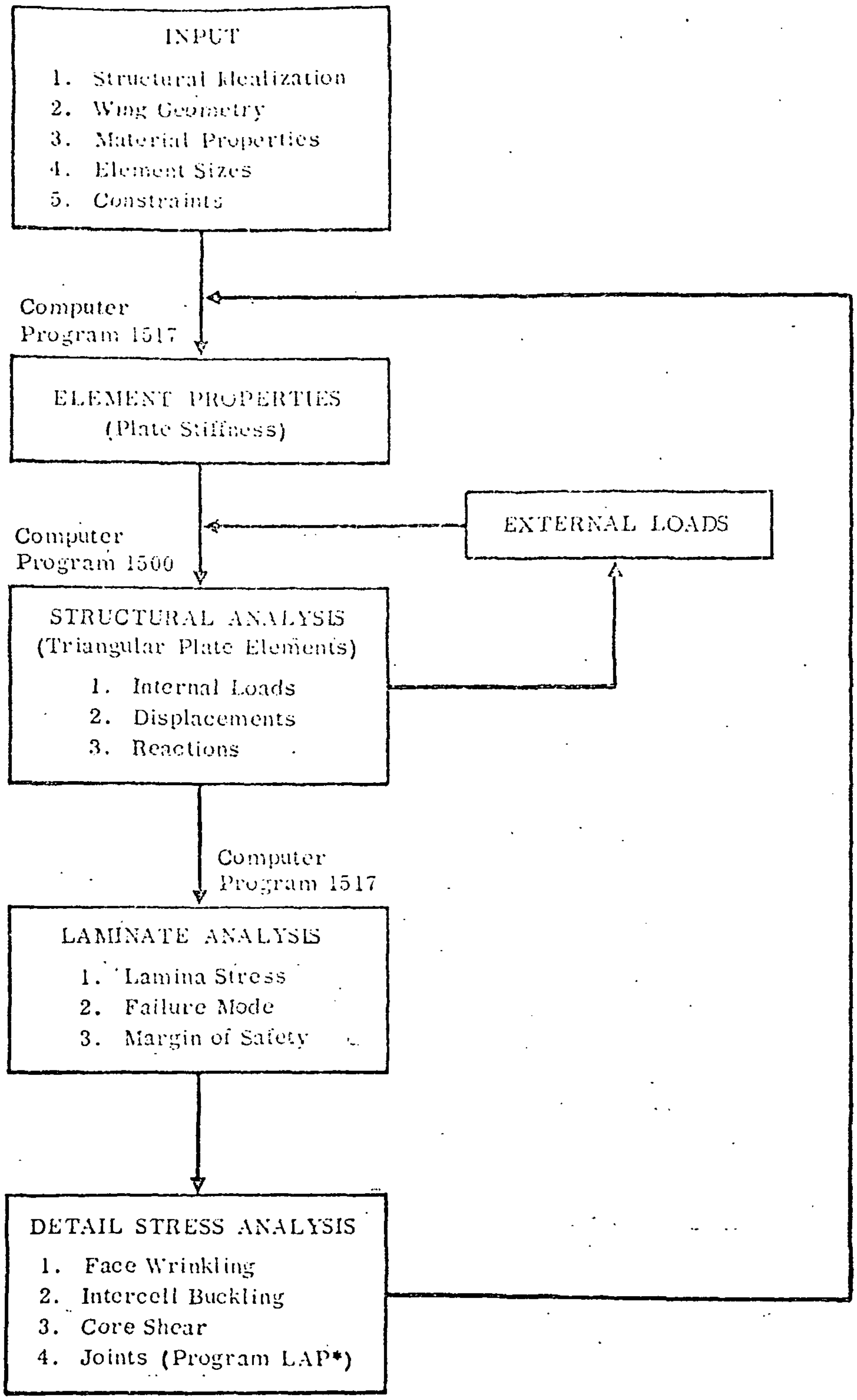

Figure 3-61. Structural Analysis Procedure

(3) Drilling, cutting, trimming, and routing

(4) Assembly techniques

c. Quality Control

(1) Receiving and inspection meetings

(2) Nondestructive test methods

(3) Process control

(4) Fabrication control

Tests

Component testing involves static and flight test programs.

The static test is conducted to determine the flightworthiness of the component. The test substantiates the strength and stiffness integrity of the component. The test may or may not be carried out to failure.

A flight test program is conducted to evaluate the environmental effects under actual flight conditions. The need for protective environmental coatings can be determined, and any evidence of excessive deflections or structural deterioration can be noted.

Representative panels of a wing or fuselage shell, such as stringer, plates, and skin-stringer combinations, are subjected to compressive and shear loads which demand consideration of their behavior in the design loading ranges. Those structural elements may be tested with conventional laboratory equipment with the use of conventional testing techniques. Initial buckling data, overall panel stiffness, ultimate strengths, and failure modes may be obtained and correlated with theoretical predictions.

Teledyne Ryan has had considerable experience in the development and application of advanced composite components for supersonic drone aircraft. A boron horizontal stabilator for the BQM-34E (supersonic Firebee II) was designed, fabricated, and ground tested. Later, Teledyne Ryan designed, fabricated, and tested three ultrahigh-modulus, graphite/epoxy, horizontal stabilators. One unit successfully passed static and dynamic tests. The remaining surfaces were flight tested at Point Mugu, California.

The application of advanced composites to the BQM-34E horizontal stabilators resulted in a 40 percent weight reduction for the boron unit and 50 percent weight reduction for the graphite component over the existing metallic component. This, in turn, permitted a reduction in ballast weight located in the vehicle nose. The thin aerodynamic surfaces on the BQM-34E are stiffness-critical; hence, the advanced composite materials could be used efficiently.

One advantage of flight testing components fabricated from new and untried materials on an unmanned vehicle, such as the BQM-34E, is that the consideration of pilot safety is not involved.

3.3.3.6 Variable Stiffness

Concepts for varying the wing bending and torsional stiffness may be classified in three board categories:

a. Mechanical (arrangement of structural elements)

b. Material changes

c. Combination of mechanical/material

Bending stiffness, EI, and torsional stiffness, GJ, are manifestations of a mechanical/material system integrated into a structure. E and G moduli are associated with the material, thickness, etc., implicit in the structural arrangement. Quantitatively, I and J are expressed as follows:

$$I = \Sigma A_i Y_i^2$$

$$J = \frac{4 A^2}{\oint \frac{ds}{t}}$$

Ai = Area of bending cap material

Yi = Distance from neutral axis to centroid of Ai

A = Enclosed area of a torque cell

$\oint \frac{ds}{t}$ = Line integral around the periphery of the cell walls of thickness t

Concepts for mechanically varying wing stiffness of necessity involve these parameters.

Figures 3-62 through 3-68 illustrate concepts that will achieve variations in bending and torsional stiffness. The following constraints are assumed to be common for all the methods:

a. The wing planform and aerodynamic shape must be maintained.

b. The leading and trailing edges, flaps, ailerons, and control systems remain unchanged.

c. The external loads are the same (same strength requirements for all concepts).

d. Stiffness variations are achieved with the wing box.

Mechanical Methods

The following schemes are included in this approach:

a. Variable spar cap and/or stringer areas (removable slugs)

b. Skin covers , replaceable, with different thicknesses

c. Variable torque box size

d. For wings with many shear webs or stringers, a mechanical means for deactivating these elements to become structurally ineffective

Removable spar cap slugs influence the bending stiffness two ways. As the area changes, the distance between its centroid and the bending axis changes. Increased area causes an increase in centroid distance, with a cumulative effect on the area moment of inertia. Wing mass will change; however, its distribution can be controlled by selective area changes. Inertia effects on aeroelastic characteristics should not differ widely.

Skin covers which can be replaced by others of different thicknesses will influence torsion chiefly. The line integral $\frac{ds}{t}$ will vary with a change in t. An increase in t will give a corresponding increase in torsion stiffness. Inertia distribution will not change significantly.

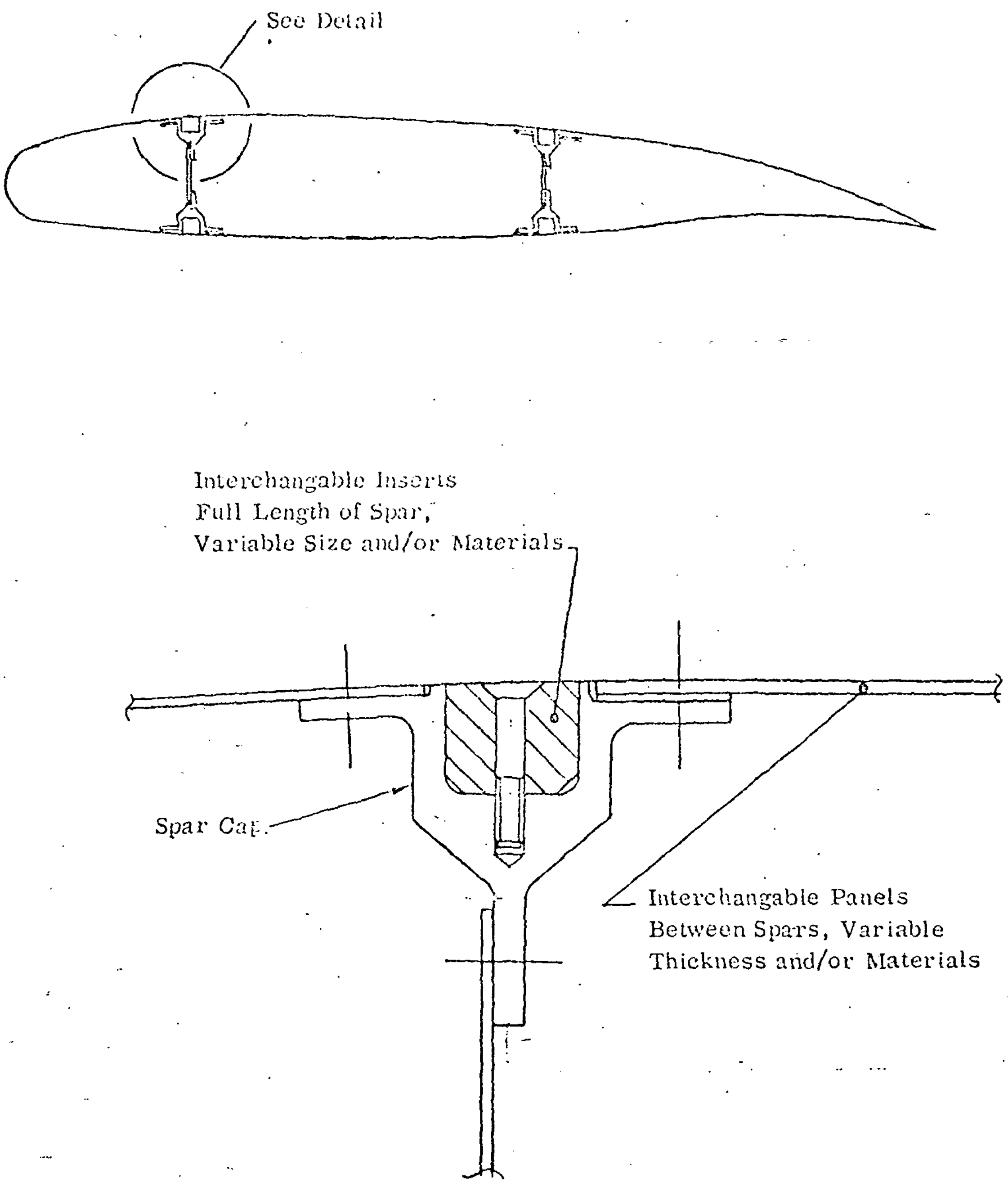

Figure 3-62. Concept 1, Variable Wing Stiffness

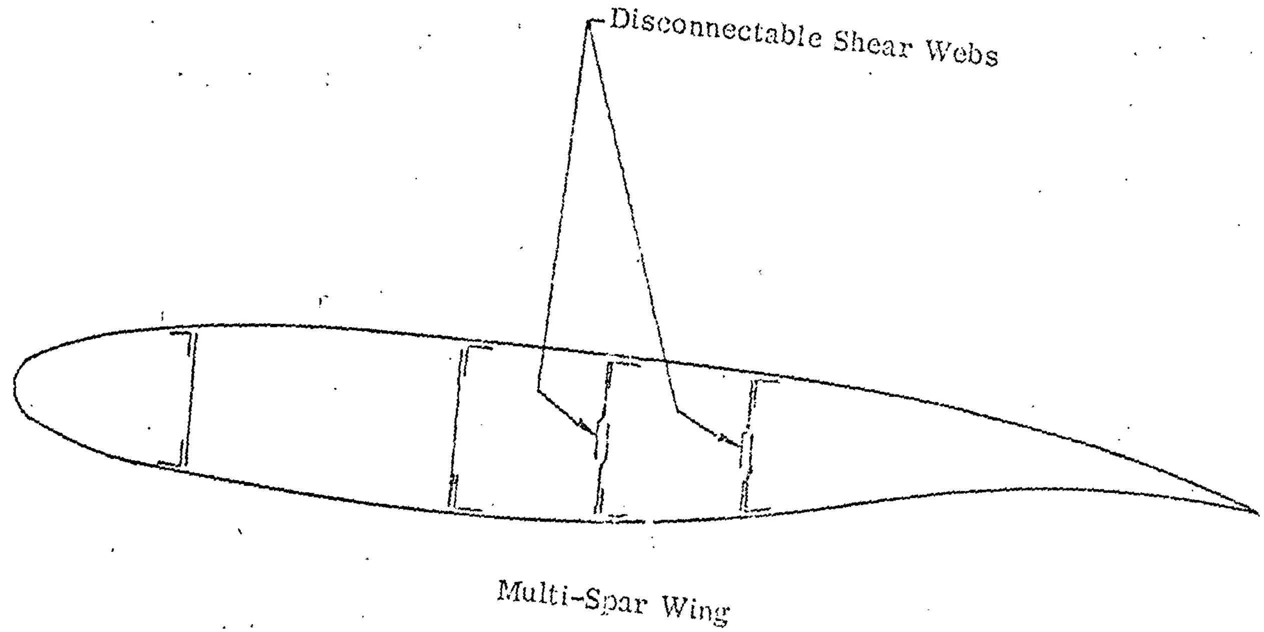

Figure 3-63. Concept 2, Variable Wing Stiffness

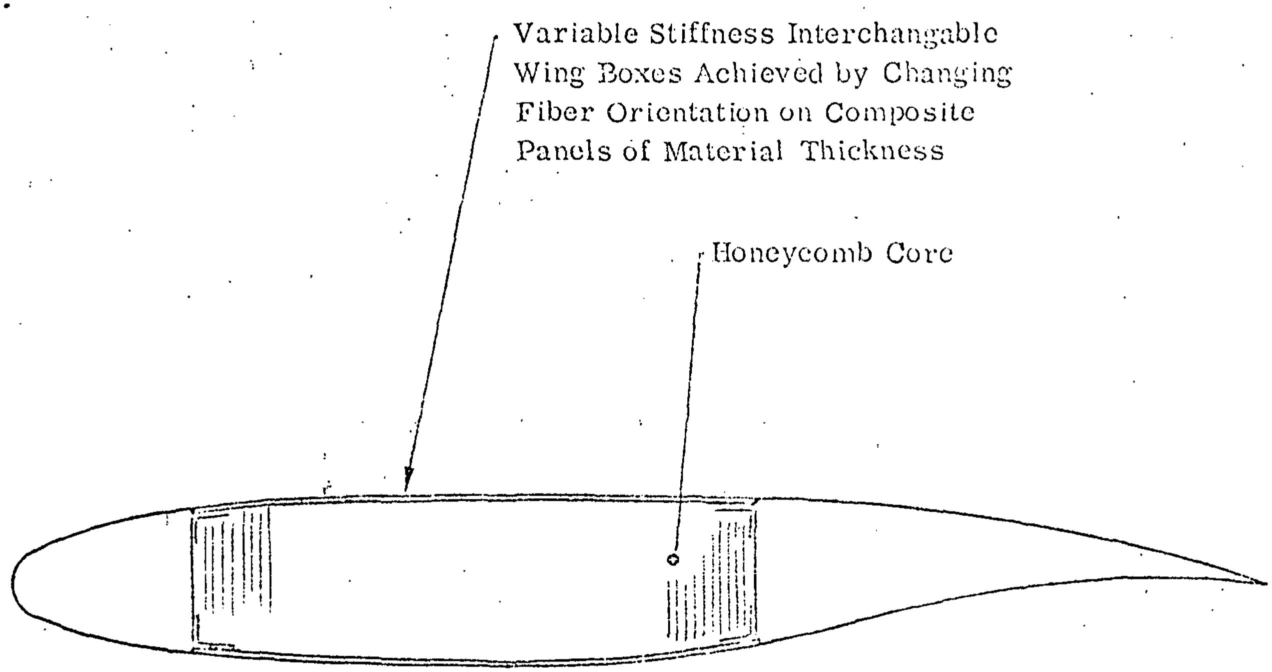

Figure 3-64. Concept 3, Variable Wing Stiffness

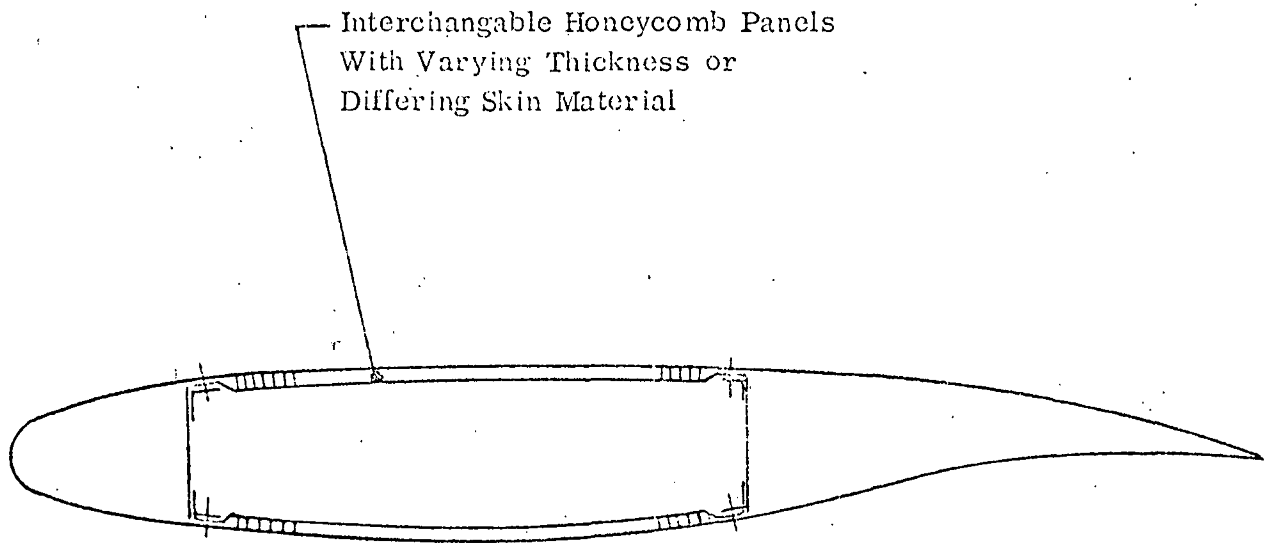

Figure 3-65. Concept 4, Variable Wing Stiffness

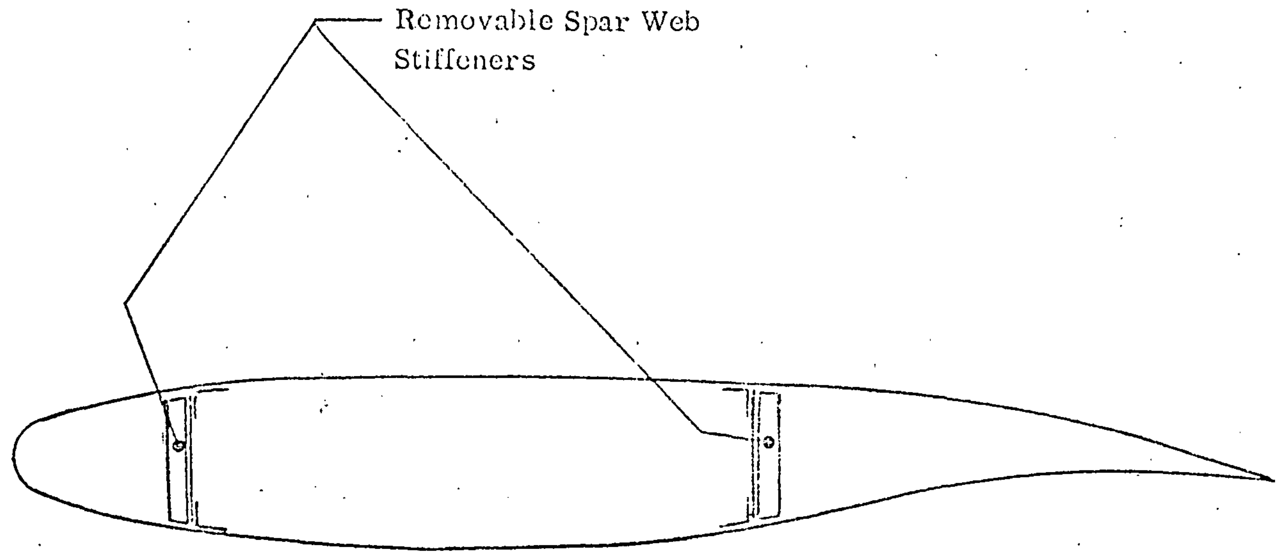

Figure 3-66. Concept 5, Variable Wing Stiffness

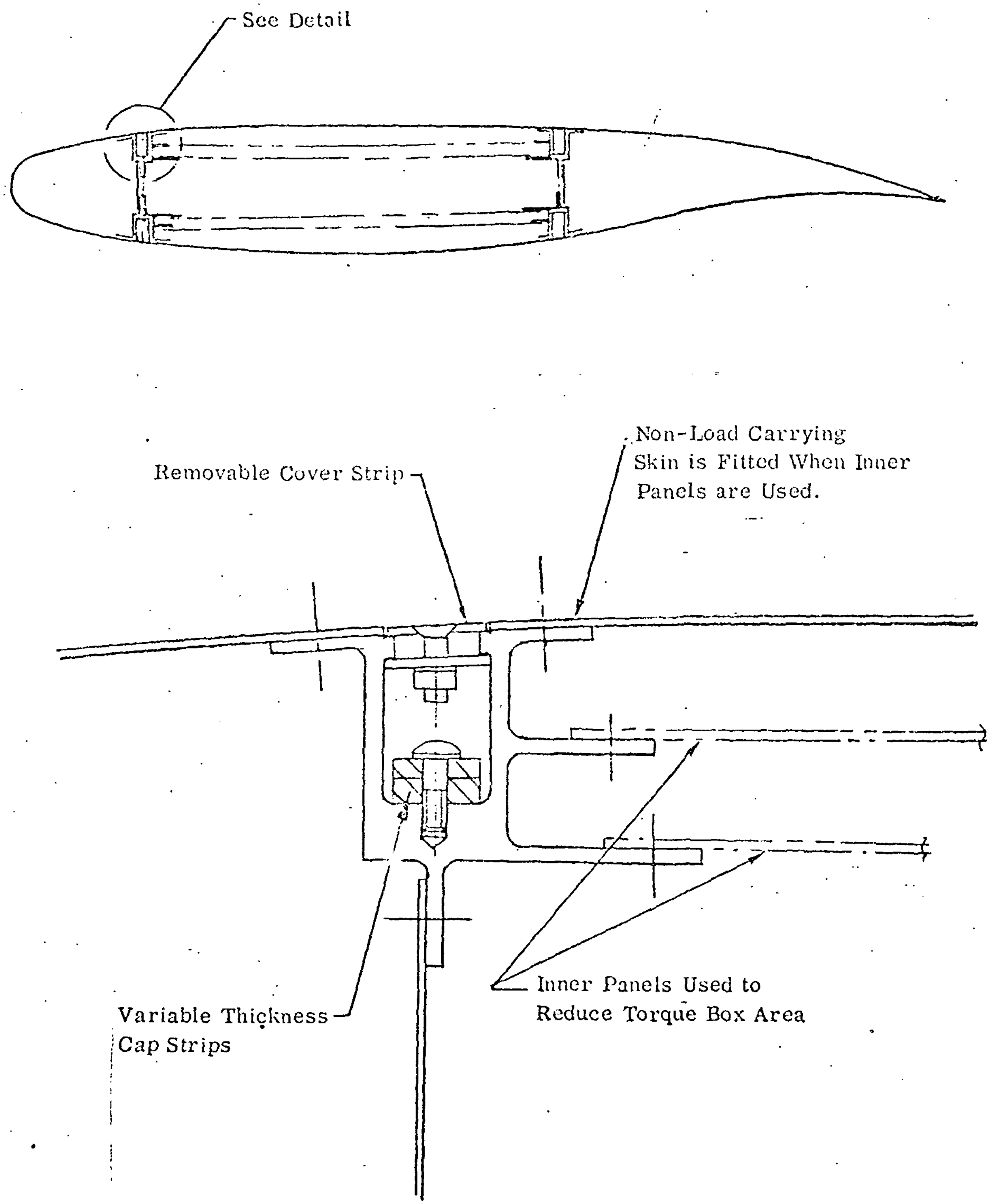

Figure 3-67. Concept 6, Variable Wing Stiffness

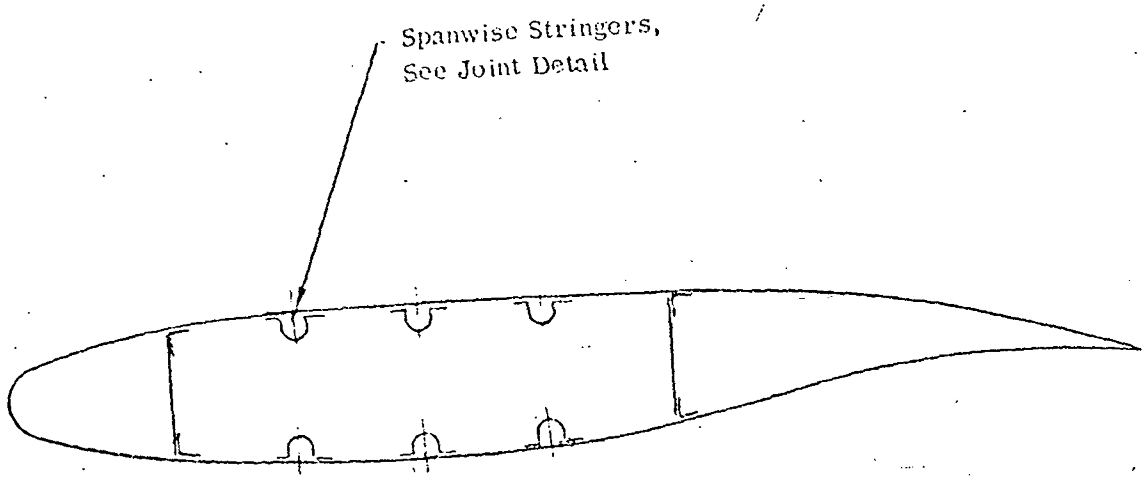

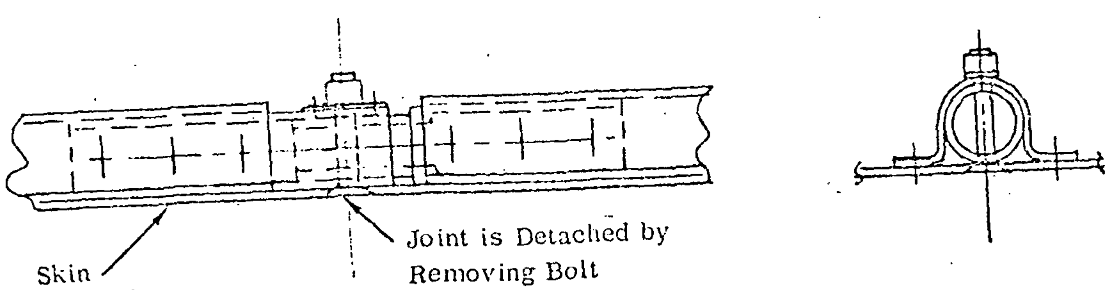

DETACHABLE STRINGER JOINT

Figure 3-68. Concept 7, Variable Wing Stiffness

Changing of the enclosed area of the torque cell is a very effective way to change the torsional stiffness, which is a function of area squared. This scheme, in conjunction with changing of the cell wall (skin) thickness, will yield a wide variation in stiffness. Deactivation of structural elements is another approach tantamount to removal of stringer areas and changes in torque cell size.

The mechanical methods vary in cost, weight, fabrication complexity, ease of assembly, and reliability. This is also true for development and test programs required to substantiate the concepts.

Material Changes

The use of advanced composite materials to achieve a variation in structural response cannot be overemphasized. The orthotropic properties of these materials make them superior to isotropic materials (metallics) to tailor a structure to specific strength and stiffness requirements. These requirements can be controlled through selection of the materials and lamination patterns.

Advanced composite materials offer four sources of design freedom which may be utilized to tailor any desired stiffness. These sources are as follows:

a. Material selection

(1) E-glass-epoxy

(2) Graphite-epoxy

(3) Boron-epoxy

b. Lamina (ply) orientation

c. Lamina thickness

d. Number of plies (lamina)

Figure 3-69 illustrates the wide variation in EI and GJ properties that may be achieved in a design. These curves are for a wing component designed by Teledyne Ryan. All of the curves will meet a common strength requirement. Figure 3-69 indicates that EI can be varied from 12.5 to 92.5 x 10^6 at the wing root. The weight change is not significant.

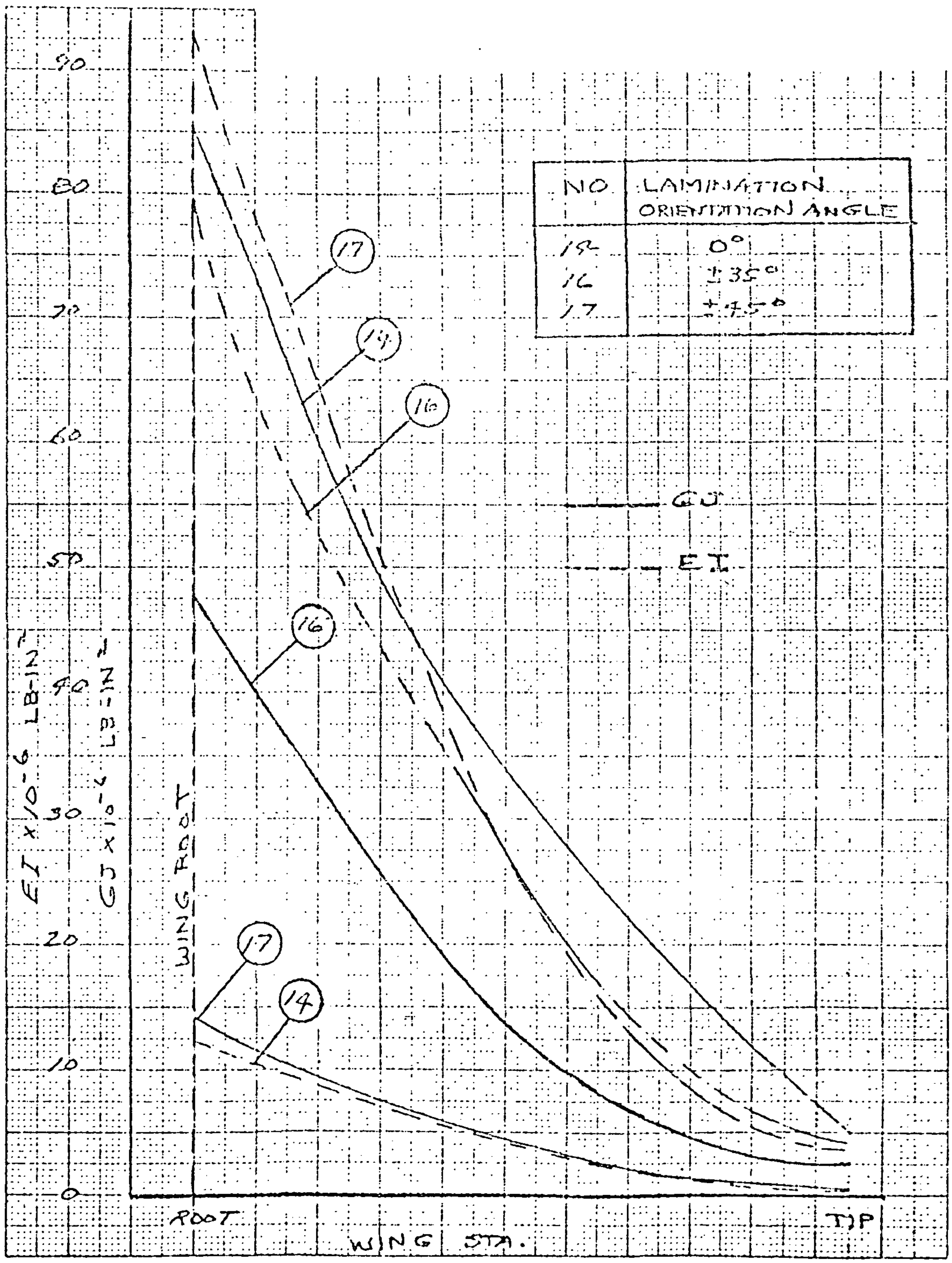

Figure 3-69. Wing Stiffness Variation, Model 147TF Composite Skins

Structural configurations into which advanced composite materials may readily be integrated with controlled stiffness properties are as follows:

a. Wing box full-depth honeycomb core construction with adhesive bonded composite skins.

b. Removable skin covers with honeycomb panels fabricated with composite facings.

The tailorability and versatility of composite materials permit the design of a structure for specific stiffness characteristics and strength requirements unmatched by other materials.

3.3.4 Stability and Control

3.3.4.1 Longitudinal Characteristics

A preliminary analysis of the research configuration (1-30-2) equipped with the high-aspect-ratio, supercritical wing has been conducted to determine the estimated static longitudinal stability level and trim capability. The results indicate that this configuration, with the existing horizontal tail, should have approximately the same stability margin as the NASA full-scale flight research configuration as well as adequate control power to trim the lift coefficient up to approximately 0.80.

Data and Method

The data available for the study is unpublished. It consisted of a plot of $C_{m_{C_L}}$ for the wing-body and wing-body-tail (Figure 3-70). The wing for the research configuration was assumed to be an exact scale of that of a NASA wind tunnel model, so that the aerodynamic coefficients for the wing could be applied directly. No corrections were applied to account for differences in fuselage characteristics, and rigid aerodynamic data were used throughout. The static stability of the research configuration was estimated on the basis of this data. The trim requirements at the higher lift coefficients were evaluated by the use of the wind tunnel data, since the pitching moment data are nonlinear with increasing lift coefficient.

Longitudinal Stability

Wing-Body. - The lift-curve slope of the horizontal tail of the NASA model was calculated from the tail incremental stability contribution and subtracted from the measured lift-curve slopes of the wind tunnel test data to determine the wing-body lift-curve slope. The wing-body pitching moment derivative $C_{m_{\alpha WB}}$ was then determined from $(C_{m_{C_L}})_{W+B}$.

Horizontal Tail. - The horizontal-tail contribution to C_{m_α} was obtained by correcting standard BQM-34E data in the presence of the body for the geometric changes of the new wing.

Downwash slope, $d\epsilon/d\alpha$, was calculated by available empirical methods to be 0.31 for low speed. Calculation of downwash by the same method for the NASA model tail location was approximately 5 percent larger than for the BQM-34E tail location. The low-speed downwash was modified by the lift-curve slope ratio to obtain the downwash as a function of Mach number. For the NASA configuration, $d\epsilon/d\alpha$ at Mach 0.90 was calculated to be 0.46. An independent check based on stabilizer incidence effectiveness yielded 0.46. The accuracy of this correlation is probably fortuitous but is nonetheless encouraging. A value of horizontal tail dynamic pressure ratio of 0.90 was assumed and applied with $(1 - d\epsilon/d\alpha)$ to obtain the horizontal-tail stability contribution in the presence of the wing.

Neutral Point. - The static stability margin was then calculated from

$$C_{m_{C_L}} = \frac{C_{m_{\alpha\ WBT}}}{C_{L_{\alpha\ WBT}}}$$

and the neutral point from

$$No = 0.25 - C_{m_{C_L}}$$

The calculated stability margin is shown in Figure 3-71 in comparison with that for the NASA model. For similar tail volume coefficients (0.925 for the BQM-34E versus 0.91 for the NASA model) and for similar vertical displacements of the horizontal tail relative to the wing chord plane, one would expect similar stability levels.

The allowable center-of-gravity range is also shown in Figure 3-71. For conservatism, the most aft center of gravity was established $0.05\bar{c}$ forward of the most forward neutral point.

The most forward center of gravity was established for the condition of -10 degrees elevator deflection and a trim lift coefficient of 0.80. Use

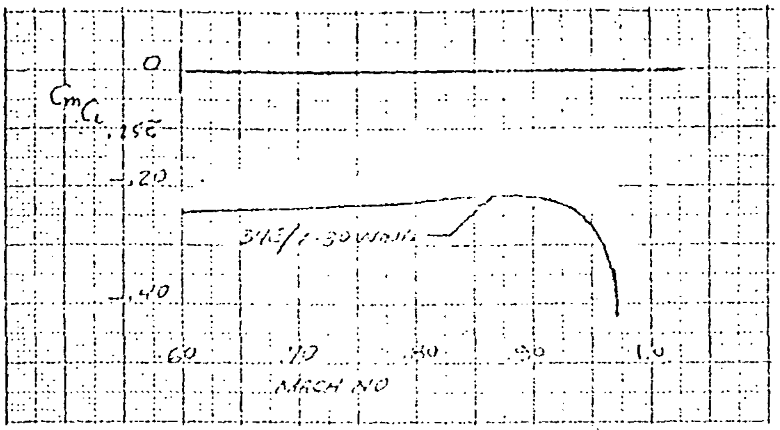

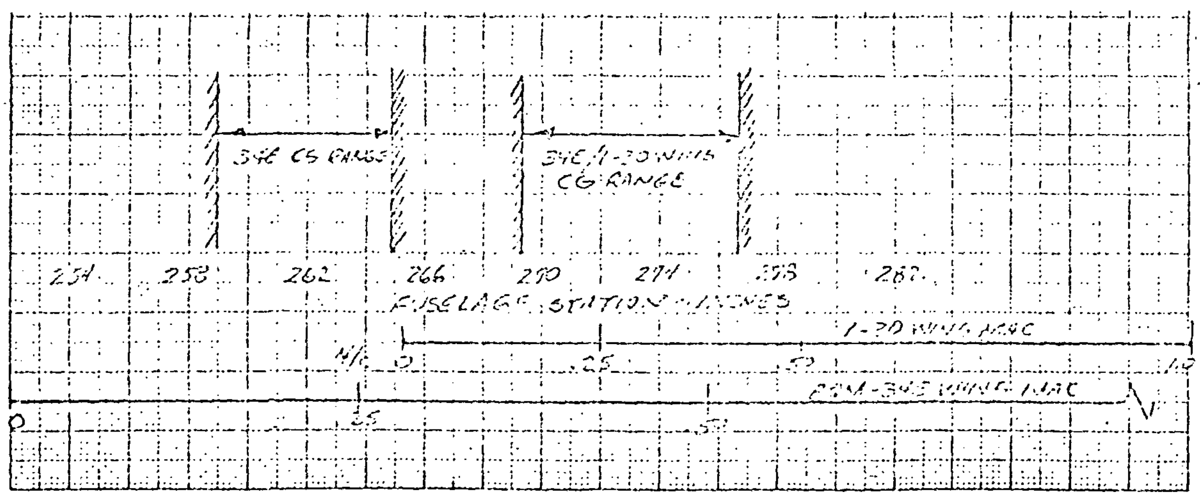

Figure 3-71. Estimated Static Stability and CG Range

was made of the wind tunnel data plots in these calculations because of the nonlinearities in the pitching moment data at high lift coefficients. The allowable center-of-gravity range shown in Figure 3-71 is shifted approximately 10 inches aft of the standard BQM-34E range, but ballast requirements should be alleviated by the more rearward wing location.

Trim Characteristics

Elevator deflections required to trim are shown for a nominal center-of-gravity location of $0.25\bar{c}$ in Figure 3-72 as a function of Mach number and lift coefficient. The nonlinear pitching moment data were again used in these calculations. No corrections were applied to the pitching moment data due to configuration differences because of the similarity in stability and downwash previously established.

The limit C_L boundary shown in Figure 3-72 represents the limit of linearity in the lift-curve slope data. These values of C_L correspond closely with an abrupt positive break in the pitching moment data. The steepness of this boundary at the design Mach number of 0.98 indicates the need for additional wind tunnel data in the transonic and low supersonic Mach range. Based on the assumptions of the analysis, adequate trim power is available for the useable range of lift coefficients. Engine thrust effects were not included in the trim equations.

An indication of maneuver capability is shown in Figure 3-73. Normal load factor is shown versus altitude for a gross weight range of 1800 to 2400 pounds. The lift coefficient at each Mach number corresponds to the limit C_L boundary of Figure 3-73.

Conclusions

Based on the results of this preliminary analysis, the existing BQM-34E horizontal tail appears adequate for both longitudinal stability and trim, in conjunction with the supercritical wing configuration designated as configuration 1-30-2. Actual downwash data should be available for more refined analyses, and inclusion of aeroelastic effects should be considered if flight at high dynamic pressures is envisioned.

NASA wind tunnel data indicate nonlinear pitching moments at a high lift coefficient. A better definition of this characteristic, by means of wind tunnel tests of a scale model of the research drone, would be desirable in the transonic Mach number range.

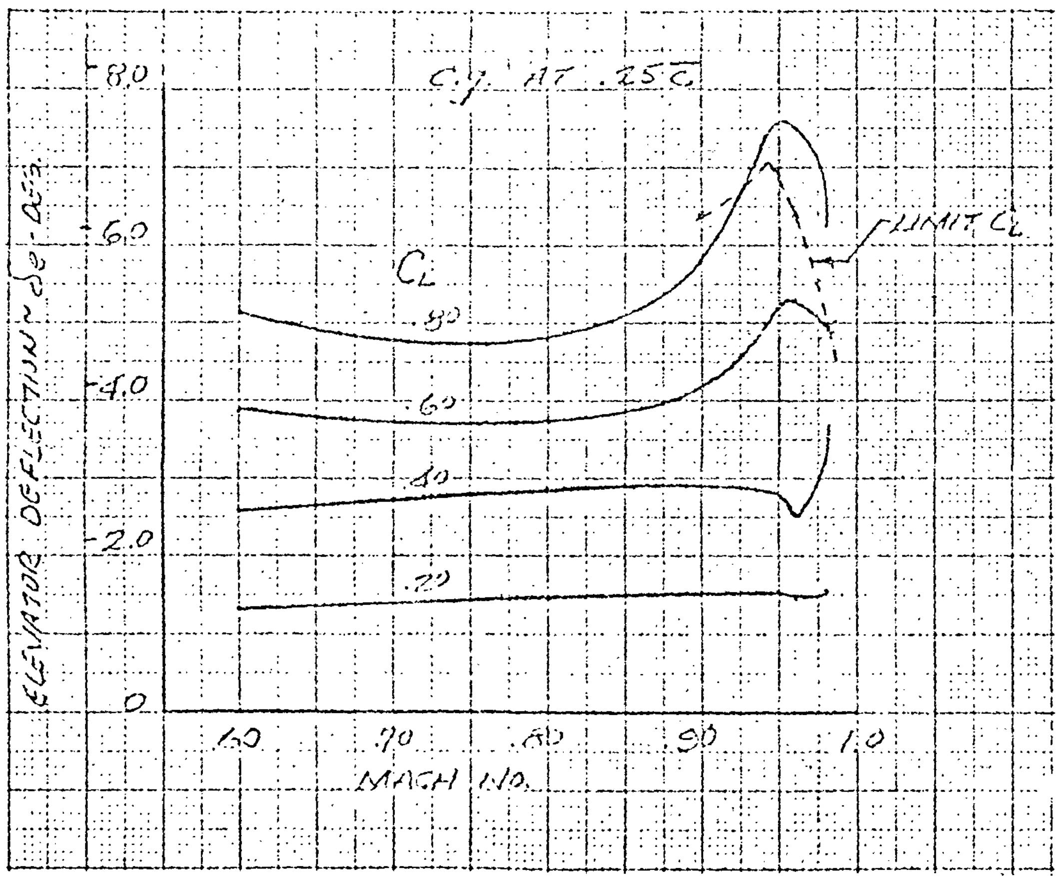

Figure 3-72. Model BQM-34E With Supercritical Wing 1-30, Elevator Angle Required for Trim

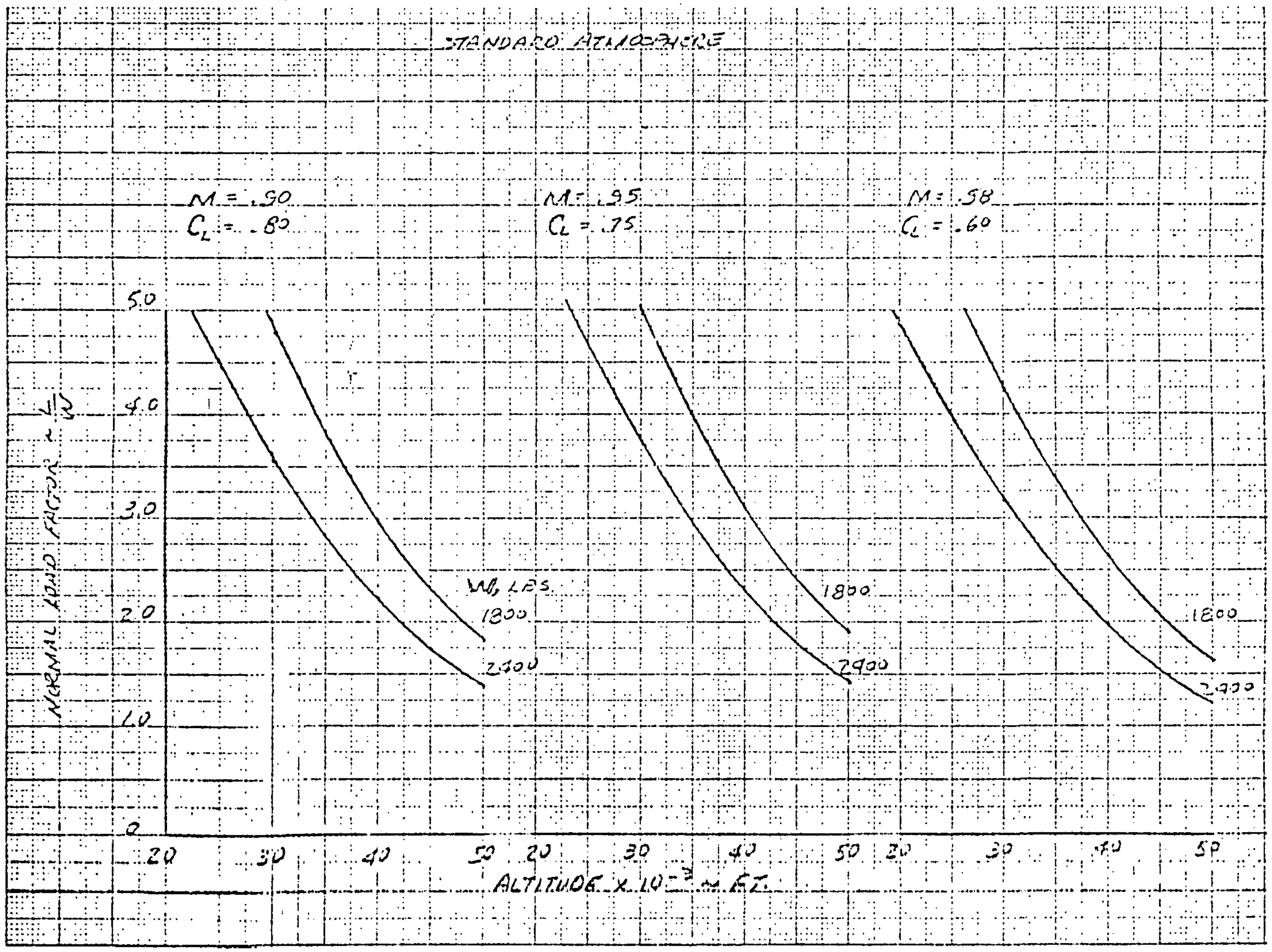

Figure 3-73, Model BQM-34E With Supercritical Wing 1-30, Estimated Maneuver Capability

Fore-Body Effects

An estimate has been made, by means of Datcom methods, of the effect of lengthening the fuselage on the static longitudinal stability of the subject research configuration.

Lift and pitching moment characteristics of the nose and forebody are discussed in Paragraph 4.3.2.1 of Datcom, and the following equations are given to determine the increments of the lift and pitching moment curve slopes:

$$C_{L_\alpha} = \frac{2(k_2 - k_1)\, S_o}{V_b^{2/3}}, \text{ per radian}$$

$$C_{m_\alpha} = \frac{2(k_2 - k_1)}{V_b} \int_0^{x_o} \frac{dS_x}{d_x} (\ell_b - x)\, dx, \text{ per radian}$$

The nose and forebody are considered as the fuselage section forward of the wing-fuselage juncture. The equations above, evaluated for a body length of 12.6 feet, give the following:

C_{L_α} = 0.00321 per degree, based on wing geometry.

C_{m_α} = 0.00491 per degree, based on wing geometry, relative to base of forebody.

As a check on the validity of the method, the equations were also used to calculate the stability level of the entire fuselage, and a comparison was made with wind tunnel test data:

	DATCOM (REFERENCE 1)	TEST DATA (REFERENCE 2)
C_{L_α} per deg.	0.0023	0.0025
C_{m_α} per deg.	0.0112	0.0130 $M < 0.40$

Based on the data from either source, the effective center of pressure of the fuselage is about one MAC forward of the nose, indicative of the couple produced by bodies in potential flow. If the moment due to the nose lift is doubled to approximate a couple and a viscous cross-flow term is added, the resulting moment curve slope is on the order of 0.0105, which is in fair agreement with the above values.

The effect of additional fuselage length was determined by adding constant-area sections forward of the base of the forebody and determining the increment in lift and moment due to the additional volume.

$$C_{m_\alpha} = \frac{C_{m_{\alpha_{vol}}} \times V_b}{57.3\, S_w \bar{c}} = 0.0002191\, V_b \text{ (moments referred to nose base)}$$

$$C_{L_\alpha} = \frac{C_{L_{\alpha_{vol}}} \times V_b^{2/3}}{57.3\, S_w} = 0.0004062\, V_b^{2/3}$$

$$\Delta C_{m_\alpha} = C_{m_{\alpha_x}} - C_{m_{\alpha_{x=0}}}$$

$$\Delta C_{L_\alpha} = C_{L_{\alpha_x}} - C_{L_{\alpha_{x=0}}}$$

where x represents the additional fuselage length.

The moments were then referenced to the center of gravity, and the increment in static stability was determined from

$$\frac{\Delta dC_m}{dC_L} = \frac{\Delta C_{m_\alpha}}{\Sigma C_{L_\alpha} + \Delta C_{L_\alpha}} - \frac{dC_m}{dC_L} \frac{1}{1 + \dfrac{\Sigma C_{L_\alpha}}{\Delta C_{L_\alpha}}}$$

where

$$\frac{dC_m}{dC_L} = -0.05 = \frac{\Sigma C_{m_\alpha}}{\Sigma C_{L_\alpha}}$$

$$\Sigma C_{m_\alpha} = C_{m_{\alpha_B}} + C_{m_{\alpha_W}} + C_{m_{\alpha_H}}$$

$$\Sigma C_{L_\alpha} = C_{L_{\alpha_B}} + C_{L_{\alpha_W}} + C_{L_{\alpha_H}}$$

The results over the subsonic range of Mach number, where the static margin is smallest, are shown in Figure 3-74. A 1-foot increase in fuselage length reduces the static margin by almost 2 percent.

The maximum dynamic pressure was determined from the speed-altitude and corresponds to a Mach number of 1.36 at 10,000 feet.

3.3.4.2 Lateral-Directional Stability

A brief analysis has been conducted to evaluate the lateral-directional static stability of the BQM-34E equipped with the supercritical wing designated configuration 1-30-2. The results indicate that the BQM-34E vertical tail will provide positive directional stability but that it may be marginal at low Mach numbers. Utilization of the directional stability augmentation system may be desirable for satisfactory stability characteristics at low speeds and high angles of attack.

Dihedral Effect

C_{ℓ_β} was estimated for configuration 1-30-2 by subtracting the estimated vertical tail contribution from NASA wind tunnel model data and adding the contribution of the BQM-34E vertical tail. The change in C_{ℓ_β} due to the low-wing location was estimated by an empirical expression in Etkin, p. 486. The resulting level of C_{ℓ_β} is shown in Figure 3-75.

Directional Stability

Comparison of the vertical tail geometry of the NASA model and the BQM-34E shows approximately the same tail volume coefficient, $\overline{V} = 0.13$,

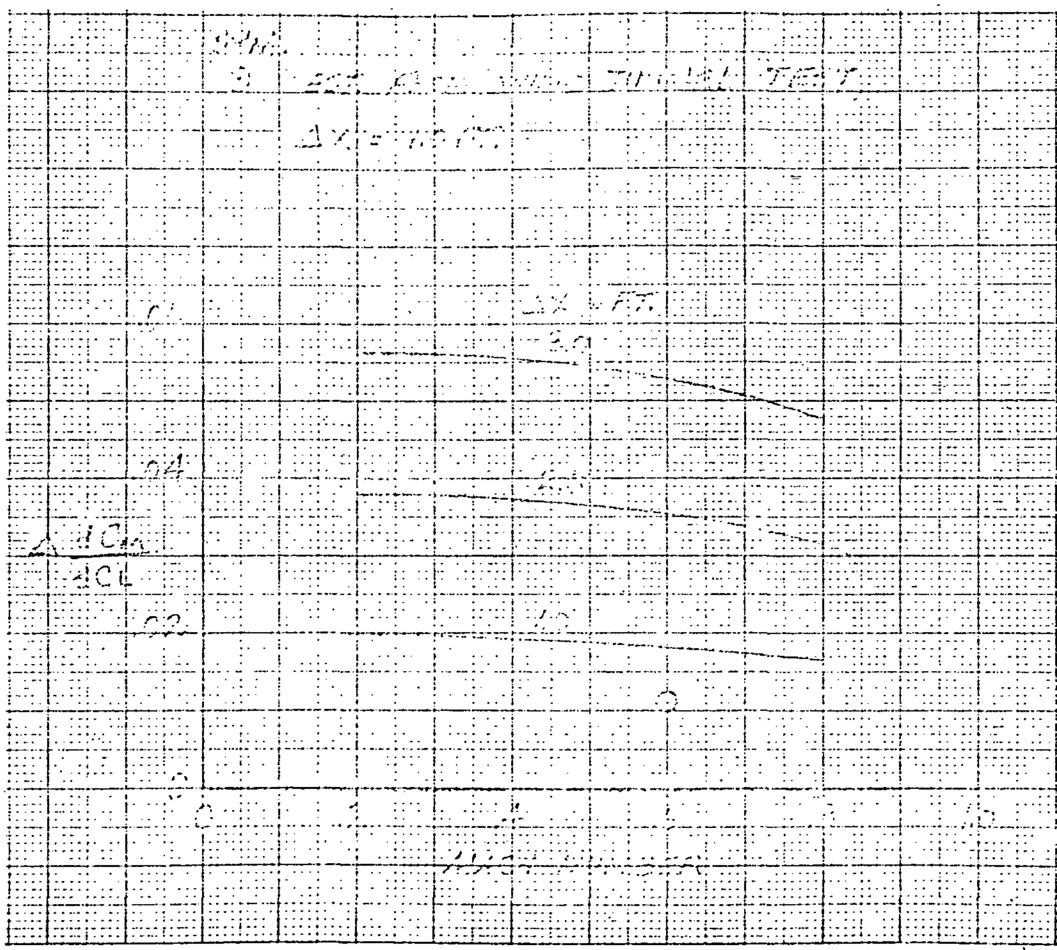

Figure 3-74. Model BQM-34E Estimated Change in Stability due to Added Fuselage Section Forward of Wing

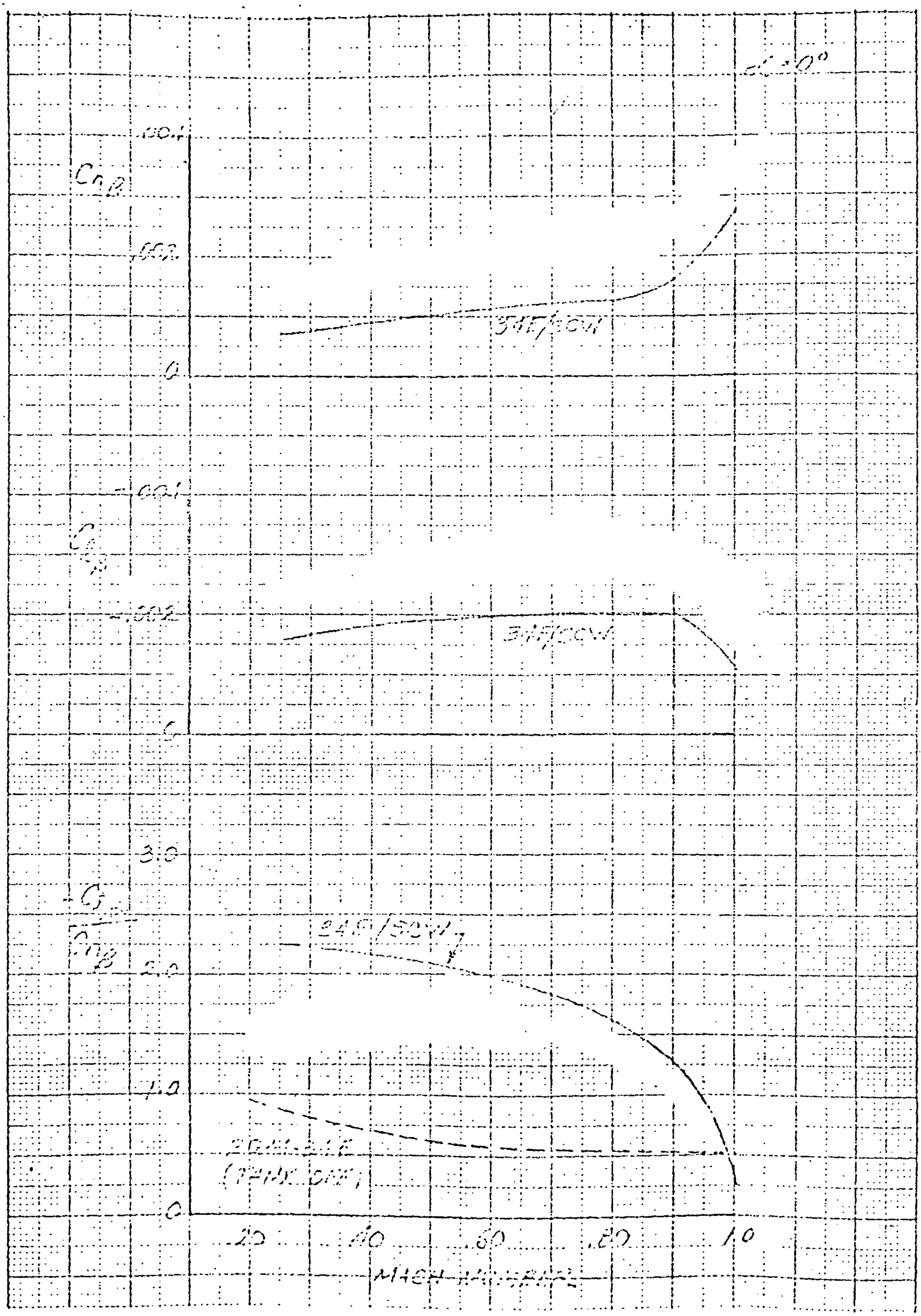

Figure 3-75. Model BQM-34E With Supercritical Wing, Comparison of Lateral-Directional Stability Derivatives

for the same ratio of exposed area to gross tail area as established by the BQM-34E. The NASA model vertical tail contribution to C_{n_β} could not be determined accurately in the absence of tail-off data, but it is estimated to be approximately 15 percent more effective than the BQM-34E vertical due to a higher aspect ratio and lower sweep angle. This results in a reduction in C_{n_β} of 0.00078 for the subject configuration, as shown in Figure 3-75. Also shown in the figure is the ratio of C_{ℓ_β} to C_{n_β}, which is an indicator of dutch roll characteristics. This ratio is about the same for the subject configurations in the design Mach number range. However, at low Mach numbers corresponding to launch airspeeds, the ratio increases and approaches that for the basic BQM-34E with the external tank on. Experience with air launch of the BQM-34E indicated a need for high directional stability. The directional stability augmentation system is used for this purpose for the tank-on configuration and may be desirable for the research configuration utilizing a standard BQM-34E vertical tail. The directional stability can be increased by approximately 0.0016 and will increase C_{n_β} to a level equal to or higher than the NASA model data. Other factors would influence the closed-loop and dynamic stability characteristics, such as yaw due to roll control, higher roll and yaw inertias, and higher roll damping from the supercritical wing.

The effects of angle of attack were not checked, but the increase in C_{ℓ_β} with α for the NASA configuration indicates that a higher level of C_{n_β} than that provided by the basic BQM-34E vertical tail may be desirable.

3.3.5 Mission Performance

The performance capabilities of configuration 1-30-2 in the Mach-altitude plane was included in the point design summary of Paragraph 3.2, Figures 3-17 and 3-22. In addition to this, an actual time history of an example mission at maximum power was made for both a ground launch and an air launch at 10,000 feet. These results, shown in Figure 3-76, indicate that this vehicle should be able to provide on-station mission data at speeds close to Mach 0.98 for over 20 minutes. Additional performance capabilities are illustrated in Figures 3-77 and 3-78.

3.3.6 Command and Control

The preceding discussion has been concerned mainly with the feasibility of modifying the BQM-34E airframe for research applications. This section discusses the other vehicle subsystems, primarily avionics, which must also be modified. These subsystems include the data transmission links, automatic flight control, and secondary power (which is not

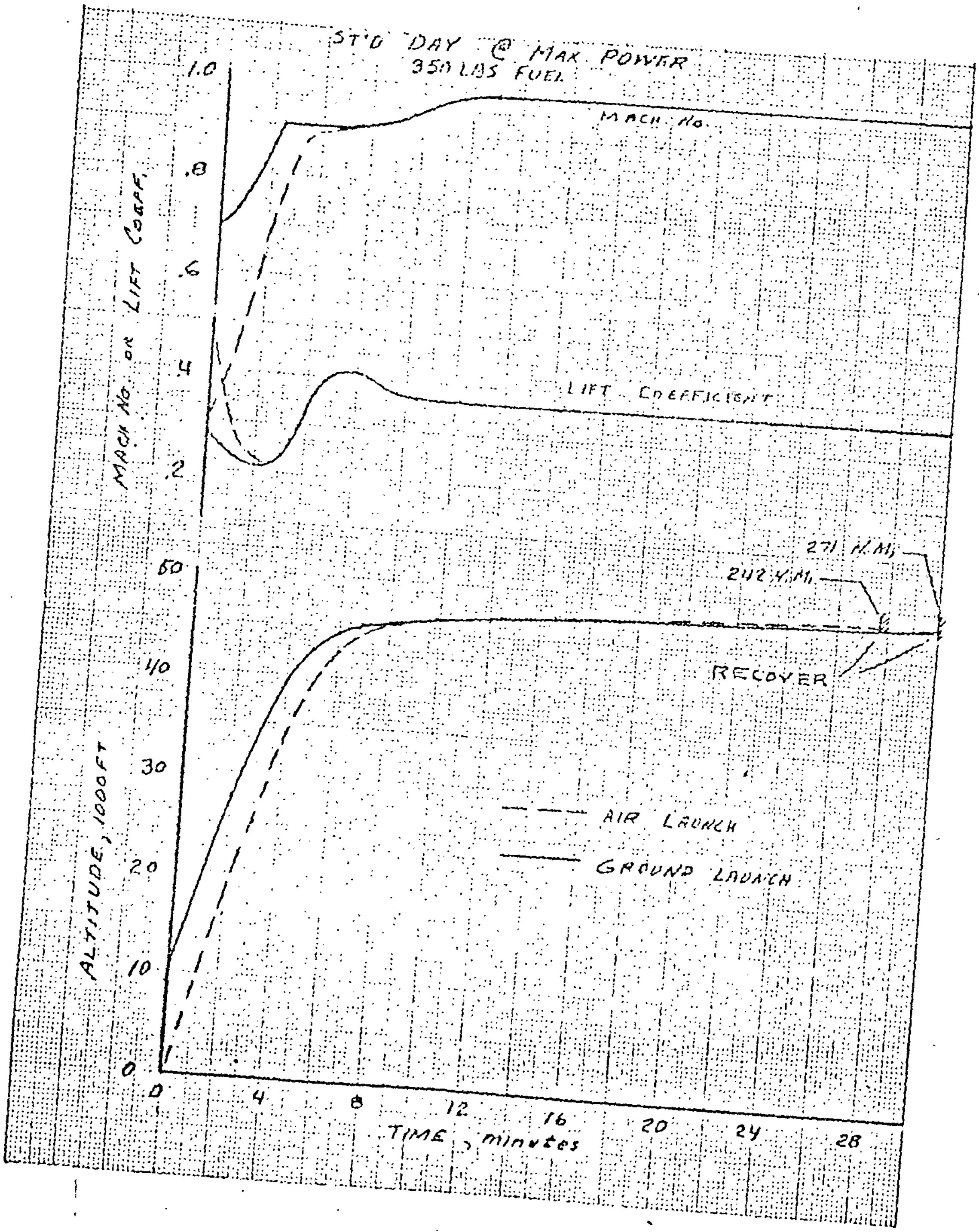

Figure 3-76. No. 1-30-2 Time History of a Typical NASA Research Mission

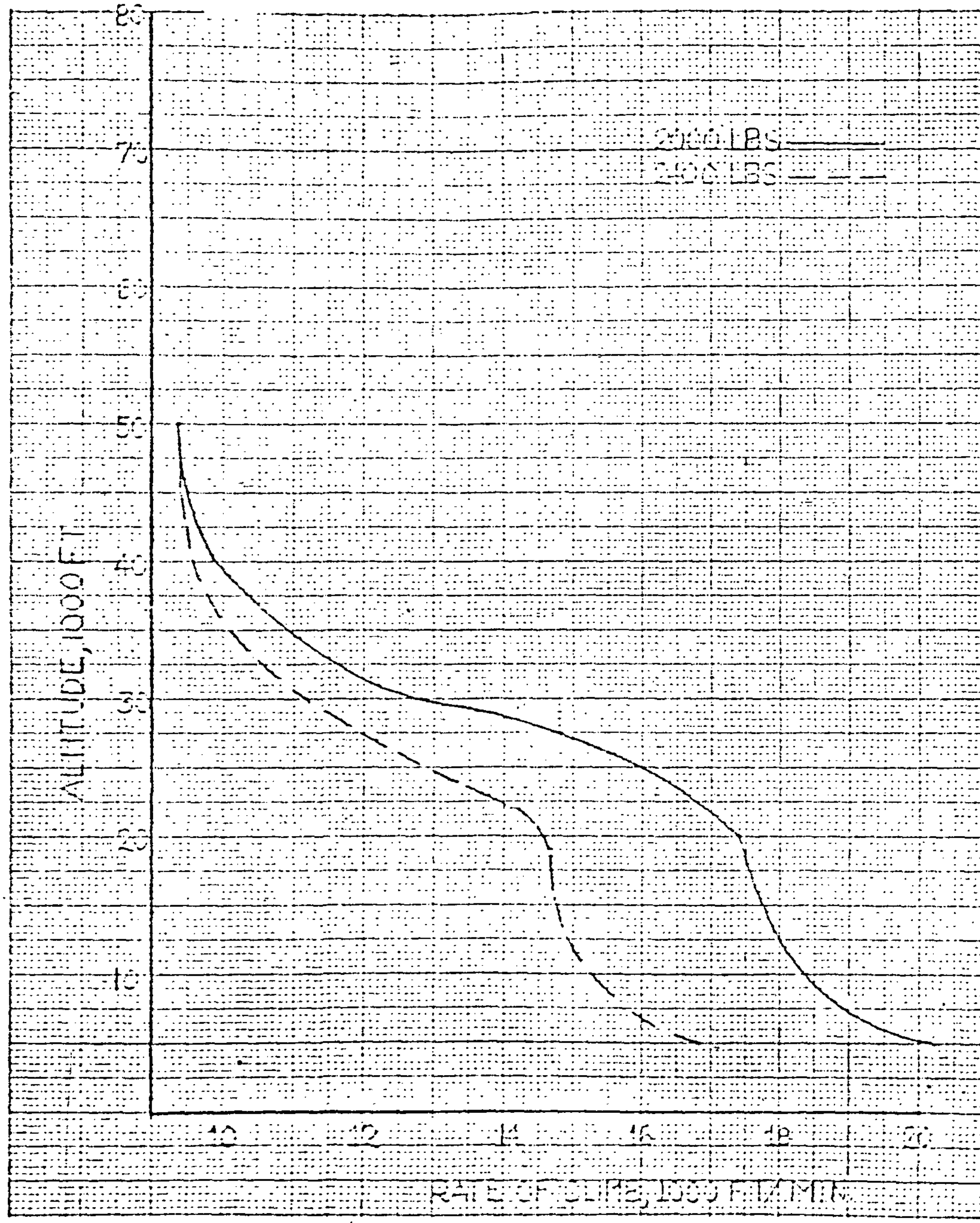

Figure 3-77. No. 1-30 Maximum Rate-of-Climb vs. Altitude

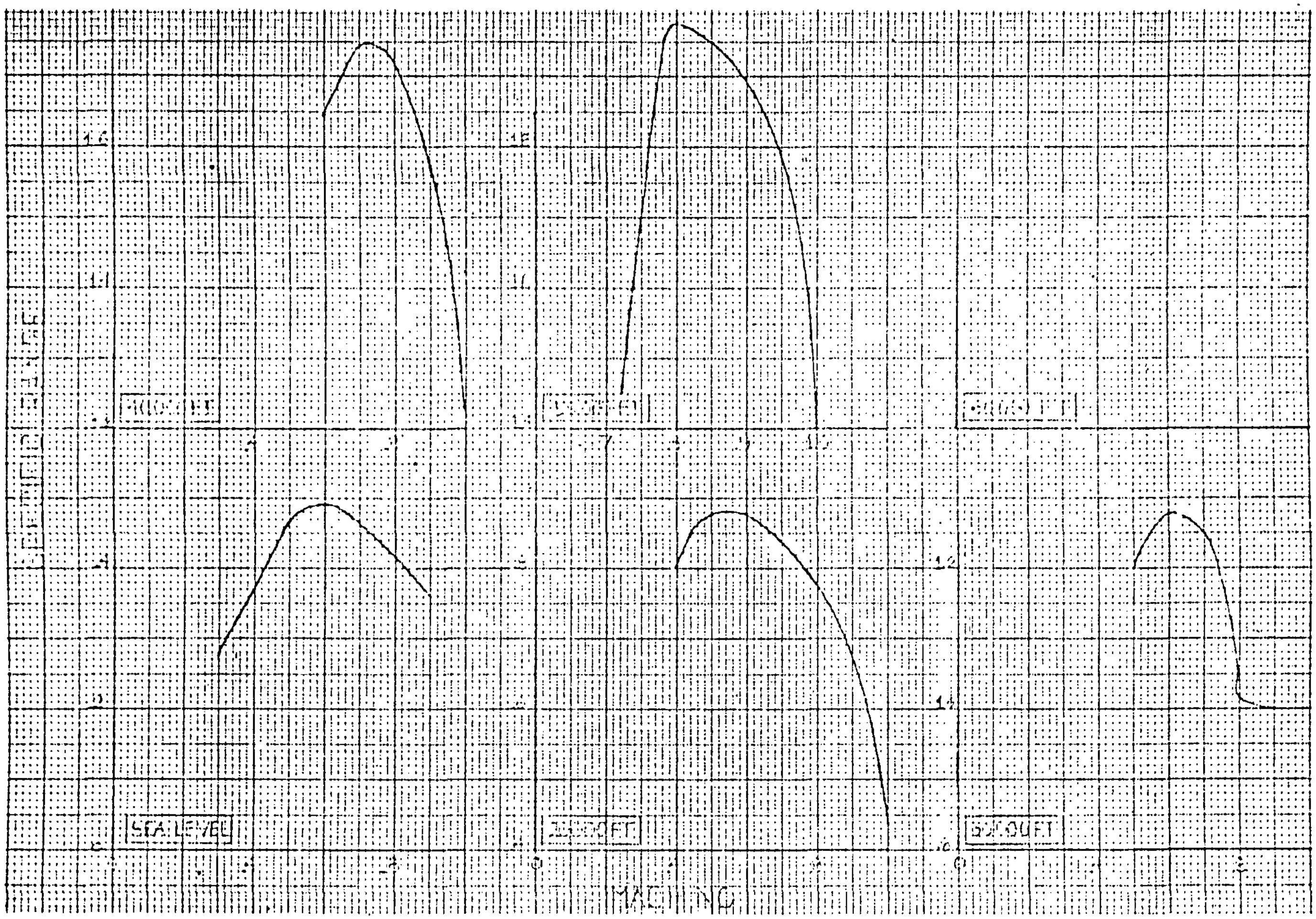

Figure 3-78. No. 1-30 Specific Range vs. Mach Number, 2000 Lb.

commonly included under the avionics label). The propulsion and recovery subsystems remain unaltered. Analysis of the ground-based portion of the vehicle control system was beyond the scope of the study. However, the influence of the availability and performance of ground equipment on the airborne equipment had to be considered for completeness.

A simplified functional block diagram of the airborne subsystems (less airframe) is shown in Figure 3-79. Of the 12 functional blocks shown, three are new (for wing controls) and one is modified (automatic flight control system (AFCS)); the remainder are unchanged from the target configuration with one qualification. The recommended command guidance transponder has not yet flown in the BQM-34E/F; however, it has flown in several versions of the BQM-34A subsonic drone. The functional modifications for installing the transponder amount to interfacing with the AFCS; hence, the modification is allocated to the AFCS.

The difference between the E (Navy) and F (Air Force) models of BQM-34E lies in the target augmentation equipment complement. Hence, with these equipments removed, the models are virtually identical.

The target command and control system is designed to be operated by military personnel having a minimum of training. The operators are generally not pilots. The controls available to the operator are discrete (i.e., relay closure) commands, limited flight data for performance monitoring, and a vehicle tracking display. The commands are limited to such as TURN RIGHT, TURN LEFT, CLIMB, DIVE, turning equipment on or off, initiation of the recovery mode, etc. Each maneuver command energizes a potentiometer in the drone autopilot, which is set prior to flight to a specific command voltage. The autopilot responds to the commands in a proportional manner. For example, the autopilot responds to a turn command with a constant-altitude turn whose roll angle (and consequently turn rate and load factor) is proportional to the preset voltage.

Once initiated, the turn relay remains latched until it is disabled by a STRAIGHT AND LEVEL command. The latter command represents zero roll angle to the autopilot. The turn command potentiometer voltage can, therefore, represent any roll angle from 0 through about 85 degrees, as limited by maximum load factor, although only one value can normally be commanded during a flight. (In special modes, an alternate level can be selected.) The autopilot responds to CLIMB and DIVE commands, in a similar manner, as altitude change commands. Mach number can also be controlled, although it is normally not commanded directly by the operator. He does so by keeping engine rpm (i.e., a discrete command

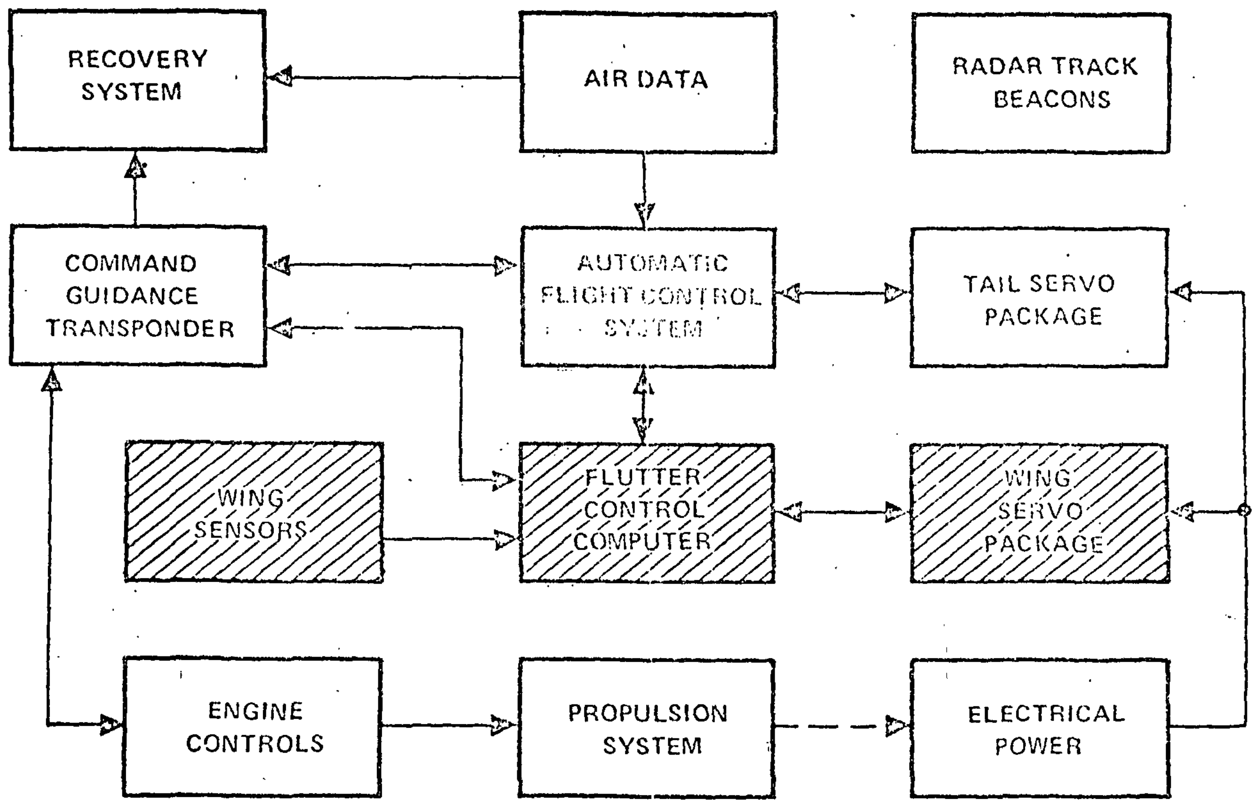

NOTE:
NEW AFCS (MODIFIED)

Figure 3-79. Avionics Functional Block Diagram of throttle rate) while monitoring engine rpm and Mach number on flight data readout. Other displayed flight data parameters include pitch and roll attitude, altitude, and heading. For a complete discussion of the target control system, see References 17 and 18.

A proportional command capability is achieved by replacing the discrete command link with one having continuously variable data channels, as in telemetry data, and introducing the command variables into the autopilot in lieu of potentiometer voltages. Hence, the autopilot responds to a continuously variable voltage command that is controllable from the ground.

Avionics Reconfiguration

The avionics (including secondary power and servoactuators) set required for research operations are derived from the basic BQM-34E/F target avionics in the following manner:

a. The target augmentation and scoring equipments are removed. These include such items as radar augmentors and antennas, infrared sources, miss distance sensors, and tow-target equipments.

b. The standard command receiver and telemetry transmitter are replaced by a command guidance transponder and possibly a small, wide-band telemetry transmitter.

c. An electrically driven hydraulic power supply is added for the wing control surface actuators. A small electronic unit housing the flutter mode control computer and ancillary AFCS interface is added.

d. The resulting equipment complement is rearranged within the compartment to utilize the available space to better advantage. The cooling system was retained somewhat arbitrarily since it is not required, except at the highest Mach numbers. For many research operations, the cooling system space can be occupied by other equipment.

Command Guidance Data Links

The command guidance data links provide the means for communicating with the vehicle for purposes of control and remote measurement. The important link parameter is its frequency bandwidth or channel capacity, which denotes the amount of data that the link can transmit. The factors that determine the bandwidth required are the number of parameters to be transmitted (i.e., the number of channels), their resolution or accuracy, and their frequency content, which is also bandwidth.

Multiple channels are obtained either by dividing the available bandwidth into narrower bands (frequency-division multiplexing) and transmitting all parameters simultaneously or by transmitting samples of each parameter sequentially (time-division multiplexing) or a combination of the two (sub-multiplexing). Most available drone control systems use time-division multiplexing. The important factor in time-division multiplexing (TDM) becomes the sampling or update, which must be at least twice as high as the bandwidth of interest of the parameter to be transmitted.

The bandwidth and sampling rate required of the drone data links depend on the guidance and control philosophy employed. The philosophy determines which control laws are mechanized and whether control loops are closed in the air or on the ground (whether by man or computer). Such alternatives are indicated in Figure 3-80. In the figure, the width of the data link arrows is proportional to the bandwidth required. The basic vehicle control loops are indicated in the four blocks with their relative frequency ranges indicated. The AFCS outer loops include airspeed, altitude, and heading control and phugoid modes. These control parameters are used in a typical target. The difference between the top two blocks is proportional command versus preset discrete commands. AFCS inner loops include short-period dynamics, stability augmentation, and handling qualities. This is the loop in which a man operates in an aircraft without an autopilot. Note that the inner loop control frequencies are an order of magnitude greater than the outer loop frequencies. Wing flutter mode control loops (and body bending as well) involve frequencies that are another order of magnitude greater than those of the inner loops.

The sampling rate on the telemetry must be somewhat greater when the flight control computations are performed on the ground rather than in the air to prevent the overall transport delays in the closed loop from distoring the response or causing oscillations. The increase would be on the order of a factor of two to four times as great. Similarly, the quantization level (digital resolution) is important, because too large an increment can cause limit cycling. For example, if roll attitude were to be quantized over 180 degrees with an 8-bit word (256 increments), then the resolution would be 0.7 degree. This could produce a small-amplitude limit cycle of a similar magnitude. Hence, a longer word, say 10 bits, would be desirable.

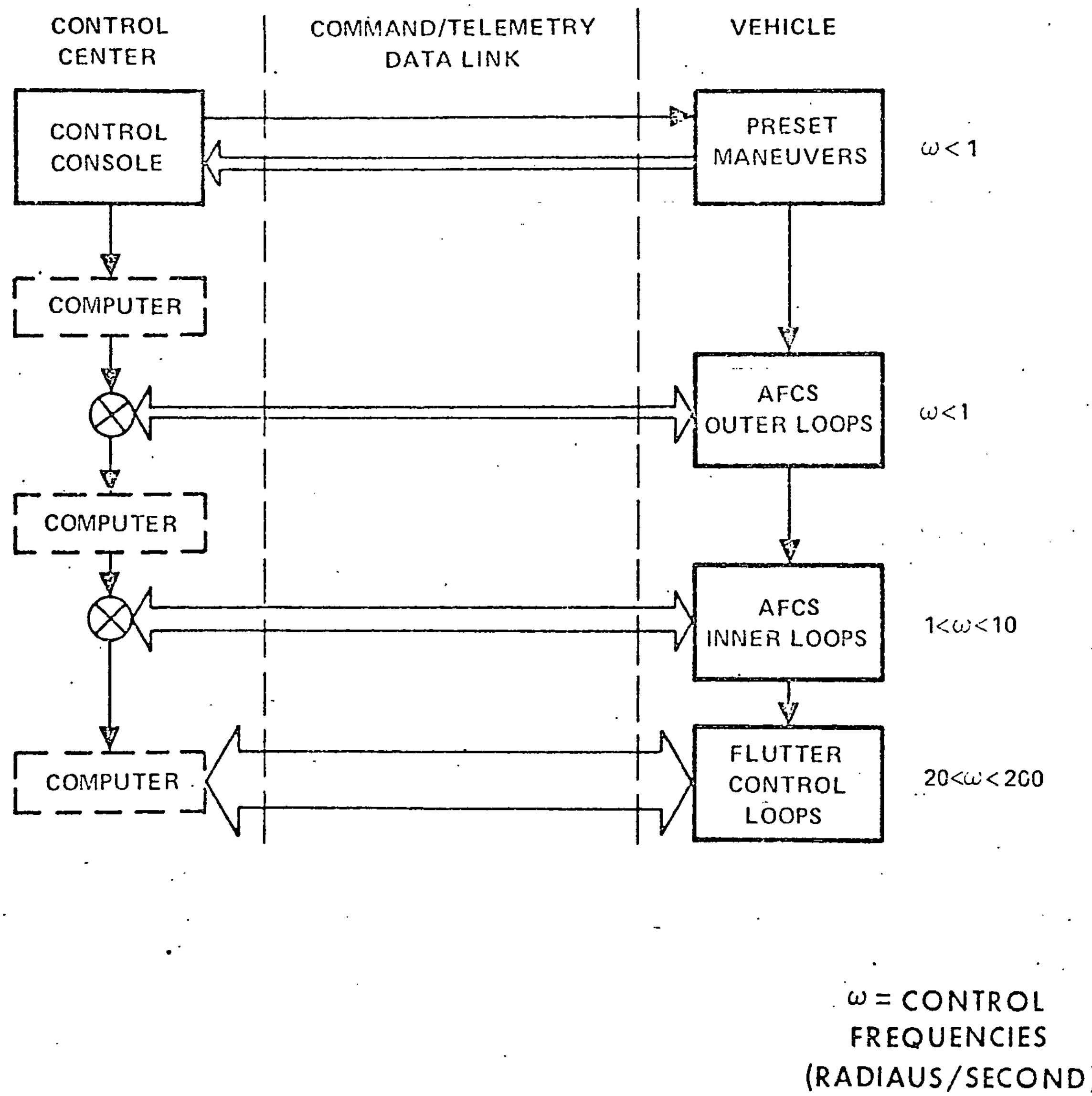

Figure 3-80. Guidance and Control Concepts

The command guidance equipments most often used today for drone control are listed in Table 3-21. Each of these equipments is capable of handling the research application with respect to controlling vehicle maneuver dynamics for either ground or airborne computation. However, with respect to the capability of handling wing-flutter and body-bending mode control, each would be limited to first modes at best, particularly with ground computation, because the closed-loop delay times become significant at such frequencies. Possible solutions to the latter problem are as follows:

a. Develop or adopt a new or wider bandwidth telemetry link.

b. Modify the existing links to increase their bandwidths.

c. Compute only in the vehicle and transmit the flutter data to the ground for monitoring purposes over a separate dedicated (standard) telemetry link.

The options are listed in order of decreasing cost, schedule impact, and flexibility.

The main differences between the equipments listed in Table 3-21 are in the tracking function and relative cost. The Vega system uses the local tracking radar as a host for its telemetry carrier, the Motorola system has an integral tracking radar (with lower power and accuracy), and the Babcock telemetry link is separate from the local tracking radar. The Motorola system also has an integral control and display console, which the other two do not. The equipments are listed in order of generally increasing cost, although the first two are significantly lower than Motorola because of their lesser complexity.

Automatic Flight Control System

The BQM-34E/F AFCS provides control of vehicle altitude, Mach number, pitch, and roll attitude plus three-axis stability augmentation. A detailed description of the AFCS function and performance can be gained from References 17 through 19.

Since the target AFCS was not designed for research applications, it lacks some of the flexibility and capability which are desirable. However, for the application being considered, it can satisfy the immediate requirements with some relatively simple modifications.

TABLE 3-21
COMMAND GUIDANCE EQUIPMENTS

EQUIPMENT	CHANNELS AVAILABLE	UPDATE RATE (PRR SECOND)	RESOLUTION	REMARKS
VTCS (VEGA TARGET CONTROL SYSTEM)	8/16 PROPORTIONAL 64/128 DISCRETE	320* MAX. 20* TYP.	10 BITS	USED BY AFFDL AT EDWARDS AFB AND NAVY
BABCOCK BCRD-31	8 WORDS	75 MAX.	8 BITS	USED BY NASA FRC AT EDWARDS AFB AND NWC, CHINA LAKE
ITCS (INTEGRATED TARGET CONTROL SYSTEM - MOTOROLA AN/USW-3 CV)	15 WORDS	90 MAX.	9 BITS	NAVY, IN TEST

NOTE:

* DEPENDENT ON HOST TRACKING RADAR PRF

The options available are as follows:

a. Retain the AFCS as is, except for modifications for proportional command inputs.

b. Augment the option 1 AFCS with the necessary computation and logic for new modes.

c. Retain the AFCS for launch and recovery, but bypass the sensor and/or computer sections with airborne or ground-based alternate equipment for the test portion of flight.

d. Replace the existing AFCS with a new one having capabilities more suitable to the application.

In general, the options are listed in order of increasing capability, cost, and development time. Teledyne Ryan has successfully flown aircraft employing options a, b, and d. NASA Flight Research Center (Edwards AFB) is about to fly a spin test vehicle using option c without AFCS.

The recommended course of action is option b. The sorts of modifications required within the AFCS are outlined as follows. The longitudinal and lateral axes are sufficiently separable functionally to be considered individually. A simplified block diagram of the longitudinal axis, including representative modifications, is shown in Figure 3-81. The sensors currently used (air data, vertical gyro, rate gyro, and normal accelerometer) are those which would be expected in a research vehicle.

Existing command inputs (continuously variable) include Mach number, altitude, and attitude. Rate or acceleration command mode can be obtained by introducing switching logic prior to the stability augmentation summing junction. The command would be shaped prior to summation to provide the proper response characteristics, in the manner of command augmentation. In operation, the altitude, Mach, and attitude inputs would be diverted to the synchronize mode, so that reversion to one of those modes would not cause a switching transient.

The figure also shows aileron servo inputs, to indicate how collective ailerons or flaps could be driven for direct-lift control studies.

The lateral axis (modified) is depicted in Figure 3-82. It consists of the yaw and roll axes plus the flutter mode control subsystem. The yaw axis is shown as it currently exists with two exceptions: provisions for yaw command are included, and the sideslip sensor is used for control only

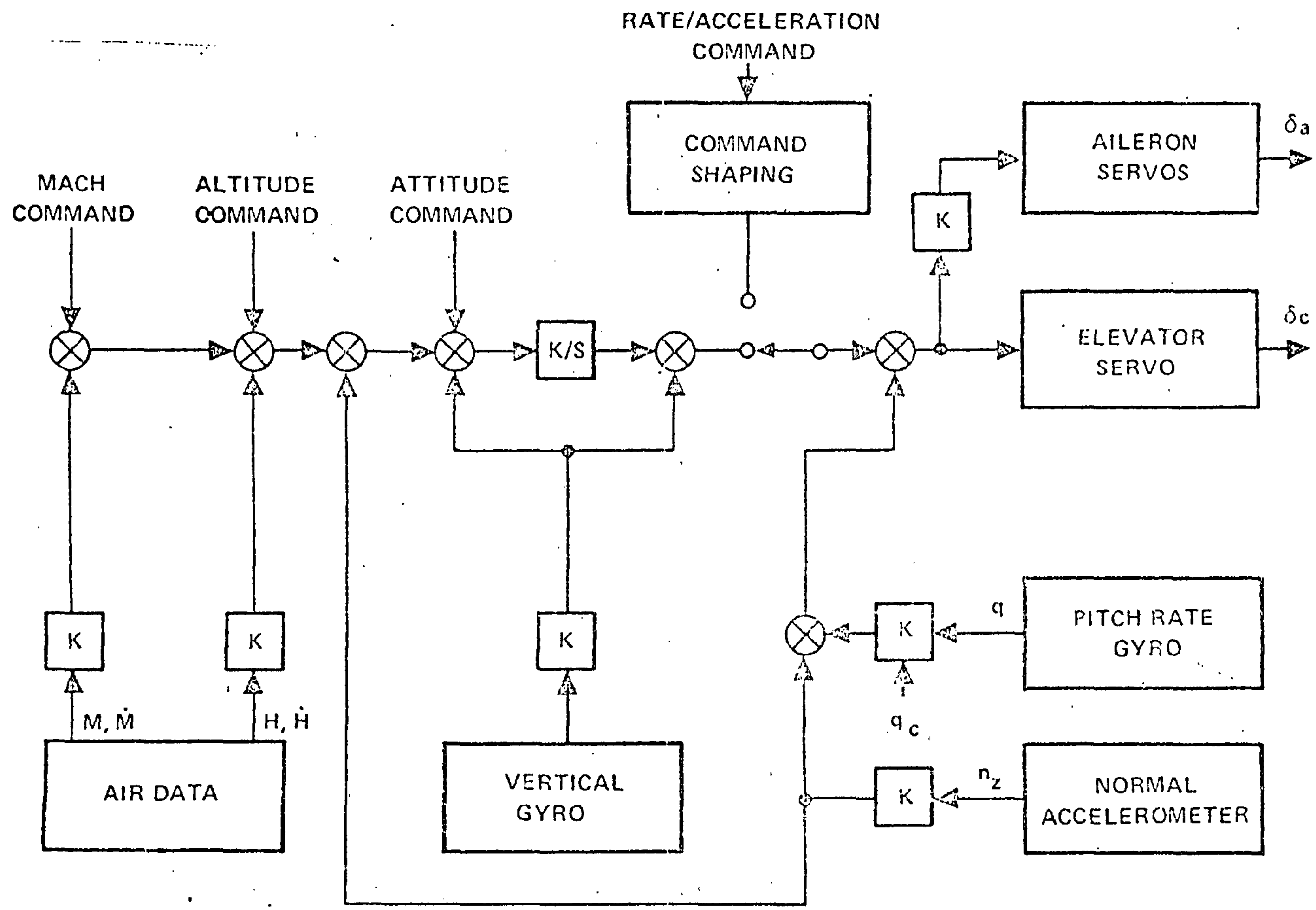

Figure 3-81. Longitudinal Axis AFCS Channel

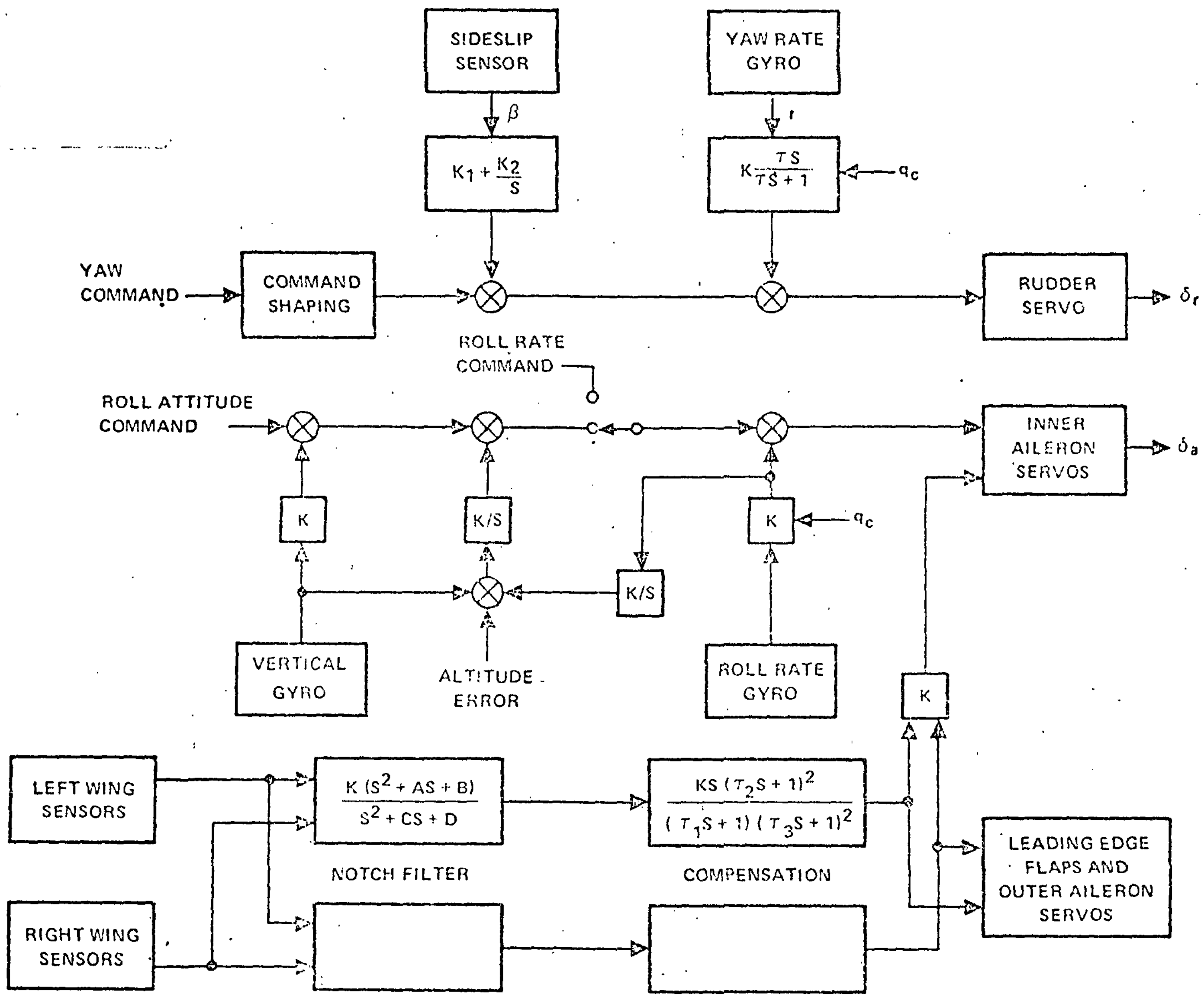

Figure 3-82. Lateral Axis AFCS Channel

when the external belly fuel pod is attached. The roll axis is also shown as it currently exists with two exceptions: provisions for roll rate command are included, and the output drives aileron servos rather than the existing rolling tail servos. The tail would then operate purely as an elevator.

The flutter mode control loop consists of a number of wing-mounted sensors (accelerometers and possible rate gyros), a compensation filter network (approximately fifth order), and wing-surface servoactuators. The filter mechanization in analog form is straightforward. It would consist of several operational amplifiers and a resistor-capacitor pair for each filter element. The filter characteristics (i.e., gain and time constants) can be made variable and can be controlled remotely if needed. For example, each axis of the stability augmentation system has a variable-gain element which is controlled by a voltage. The control parameter is dynamic pressure, but a remote command, being a voltage, could also control it. Because the flutter mode frequencies of interest approach 30 Hz, which could overtax the existing data links, and because the filter design is straightforward, the onboard mechanization is recommended.

Secondary Power

The BQM-34E/F secondary power is derived from an engine-driven dc generator, which also serves as the engine start motor. Hydraulic power for the control-surface actuators is provided by an electrically driven supply. The servoactuators and power supply form an integral, self-contained unit, which is also a structural member of the airframe.

Additional hydraulic power will be required for the wing actuators. The existing supply is sized for the tail actuation requirement; hence, it does not have any significant reserve capacity. The engine has only one power takeoff pad, which is used by the generator. Therefore, since an engine-driven hydraulic pump is not possible, the alternative is to provide an electrically driven hydraulic supply. A number of such supplies are used on missile and reentry vehicles. They are small enough to fit easily into the drone. Further, sufficient electrical power is available to drive one.

The hydraulic power requirements have been estimated as follows: the maximum aileron hinge moments for the inner and outer ailerons and leading-edge flaps are 1500, 1000, and 500 inch-pounds, respectively; the frequency response of the outer aileron/leading-edge flap pair should be at least 100 radians per second at the first order break; and the inner aileron response should be about 20 radians per second. The existing hydraulic system supplies two actuators having 4000 inch-pounds of stall torque and one (rudder) having 900 inch-pounds of torque stall. All servos have a first-order lag of slightly greater than 20 radians per second.

A very gross comparison of power requirements can be obtained by multiplying stall torque by frequency response for each servoactuator and summing. When this is done for the wing set and tail set, the ratio of wing power/tail power is approximately two.

The electrical input to the tail hydraulic pump is 20 amperes at 28 volts dc. It supplies 0.6 gallon per minute at 1000 psi. Data on two available electrically driven power supplies is presented below. Note that this data indicates that the power supplies can provide 2-1/2 times the power of the existing supply.

TYPE	USED ON	PRESSURE	FLOW	ELECTRICAL INPUT
Pesco Model 165-100	Martin hypersonic lifting body	1500 psi	1.0 gpm	28 Vdc 38 amp.
Pesco Model 144-300	Minuteman Third Stage	1500 psi	1.0 gpm	28 Vdc 38 amp.

The available electrical power, summarized in Table 3-22, is adequate for driving either supply while retaining a reserve for additional equipment.

Conclusions

The feasibility of converting the BQM-34E/F avionics from a target-oriented to a research-oriented configuration has been analyzed with the following results:

a. The modifications are confined primarily to the automatic flight control system and to equipment relocation.

b. Command guidance data links with adequate capacities for research applications are available.

TABLE 3-22

SECONDARY POWER

- AVAILABLE GENERATOR CAPACITY 200A @ 28 VDC

  BASIC VEHICLE LOAD

  WARMUP. 134A

  CRUISE. 94A

- WING ELECTROHYDRAULIC SYSTEM 40-58A (ESTIMATED)

  RESIDUAL CAPACITY

  WARMUP. 29-11A

  CRUISE. 66-48A

c. The control laws are well understood, and their mechanizations are within the current state of the design art and hardware capability.

d. Adequate electrical and hydraulic power are available.

3.4 SUPPORT STUDIES

3.4.1 Wind Tunnel Tests

To assure a high probability of success of new or revised RPVs, it is recommended that aerodynamic test data be obtained in each of the critical flight regimes. This will provide not only a verification of estimated aerodynamic, stability, and control coefficients but, in addition, will make possible realistic preflight simulations, including nonlinear effects due to compressibility and separation phenomena.

For the subject vehicle, this would include low-speed transonic as well as supersonic wind tunnel test data of scale models, as required, close to flight Reynolds numbers. Although new vehicle checkouts usually include engine inlet tests, boundary-layer gutter optimization, etc., it is felt that this is not likely to be required for the subject application. The basic inlet configuration is designed to operate, with reasonable compromise, in both the subsonic as well as the supersonic regime. (Mach 2.0 tests indicated a mild instability.)

A requirement for pressure taps to provide good chordwise and spanwise load data is always desirable, from an analytical viewpoint, in both aerodynamic and load analyses. However, this requirement is seldom implemented, because of economic and time constraints.

Typical flight modes of a new wing to be critically examined by means of wind tunnel tests would include the following:

a. Low-speed launch mode, Mach 0.1 to 0.4, free-fall stability and trim at near zero lift.

b. High-speed launch mode, Mach 0.6 to 0.8 (only if required).

c. Maximum climb trim and stability, Mach 0.4 to M_{max}.

d. Cruise trim, stability, and control, Mach 0.4 to M_{max}.

e. Maximum load factor (turn mode).

f. Power-off glide characteristics, Mach 0.8 to 0.2.

g. Recovery mode, drag chute.

h. Maximum trim C_L versus Mach number.

i. Captive-flight loads on carrier aircraft.

3.4.2 Flight Assurance Summary

Reliability

Flight-phase and recovery-phase inherent reliability predictions for the NASA-configured BQM-34E have been completed. These predictions were developed from BQM-34E reliability prediction mathematical models, with adjustments for the currently planned changes to the Navy vehicle. Sixty-five minutes (1.083 hours) flight phase, and 22 minutes (0.368 hour) recovery phase durations (Navy prediction profiles) were used to provide a comparison of the two vehicles. The maximum phase durations were selected to provide a conservative estimate of inherent reliability. The results are as follows:

	NASA BQM-34E	NAVY BQM-34E
Flight phase	97.90%	98.04%
(With cooling system installed)	97.79%	97.93%
Recovery phase	99.42%	99.63%
Recovery and retrieval (combined)	98.0 %	--

These values are for the air vehicle shown in Figures 3-83 through 3-84.

The flight phase includes the period from launch to the initiation of recovery procedures. The recovery phase includes the period from the initiation of recovery procedures until the air vehicle is in a position to start the retrieval operation. For this analysis, the worst-case condition of parachute descent to a water landing was assumed.

Since there is no reliability model for a Navy MARS retrieval system, data from other programs in which the MARS system is used was examined. A combined recovery and retrieval reliability of 98.0 percent is indicated.

The NASA BQM-34E predictions are based on the system changes discussed in the following subparagraphs.

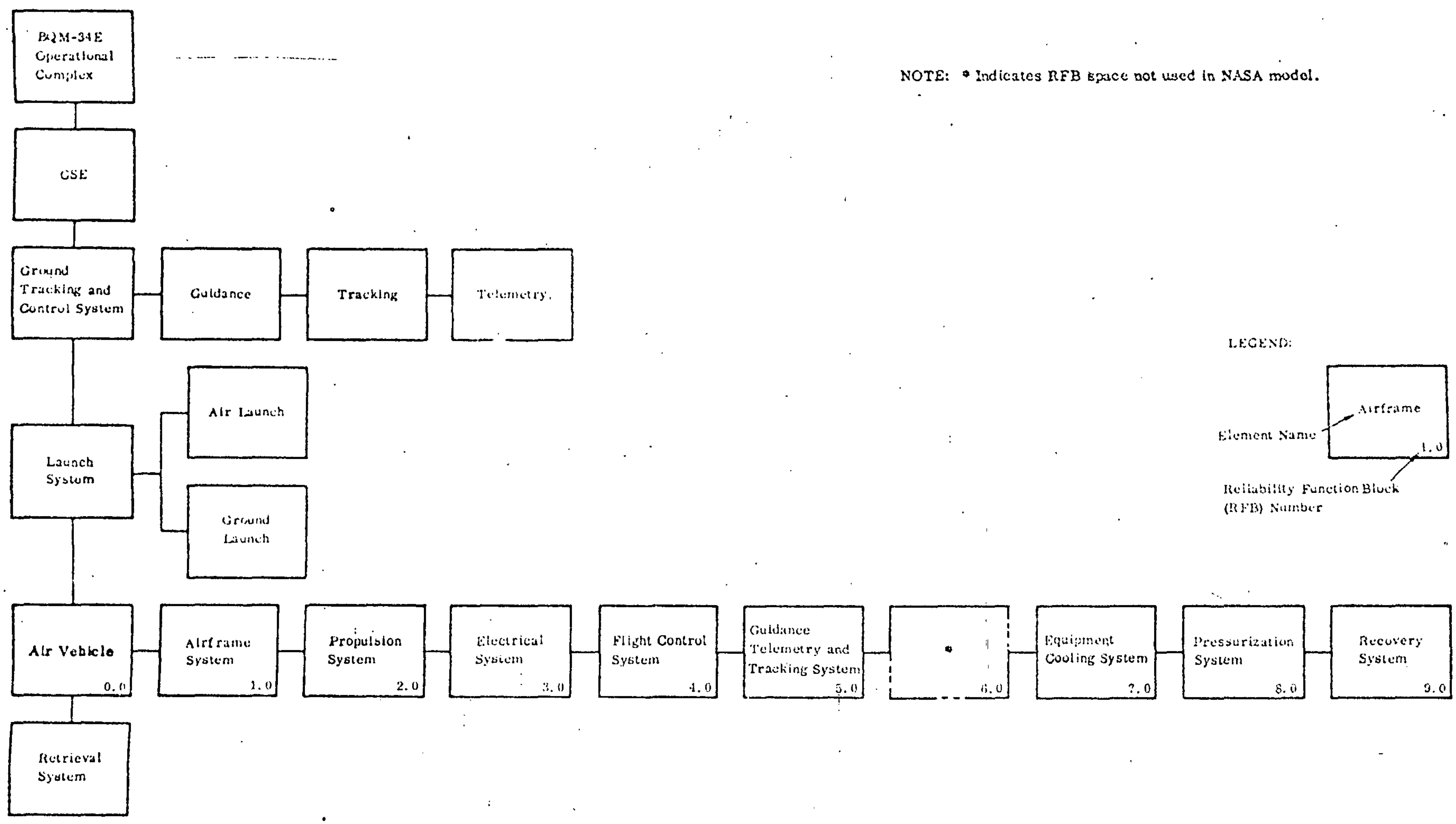

Figure 3-83. Model BQM-34E Reliability Functional Block Diagram, Operational Complex

"Page missing from available version"

page 172

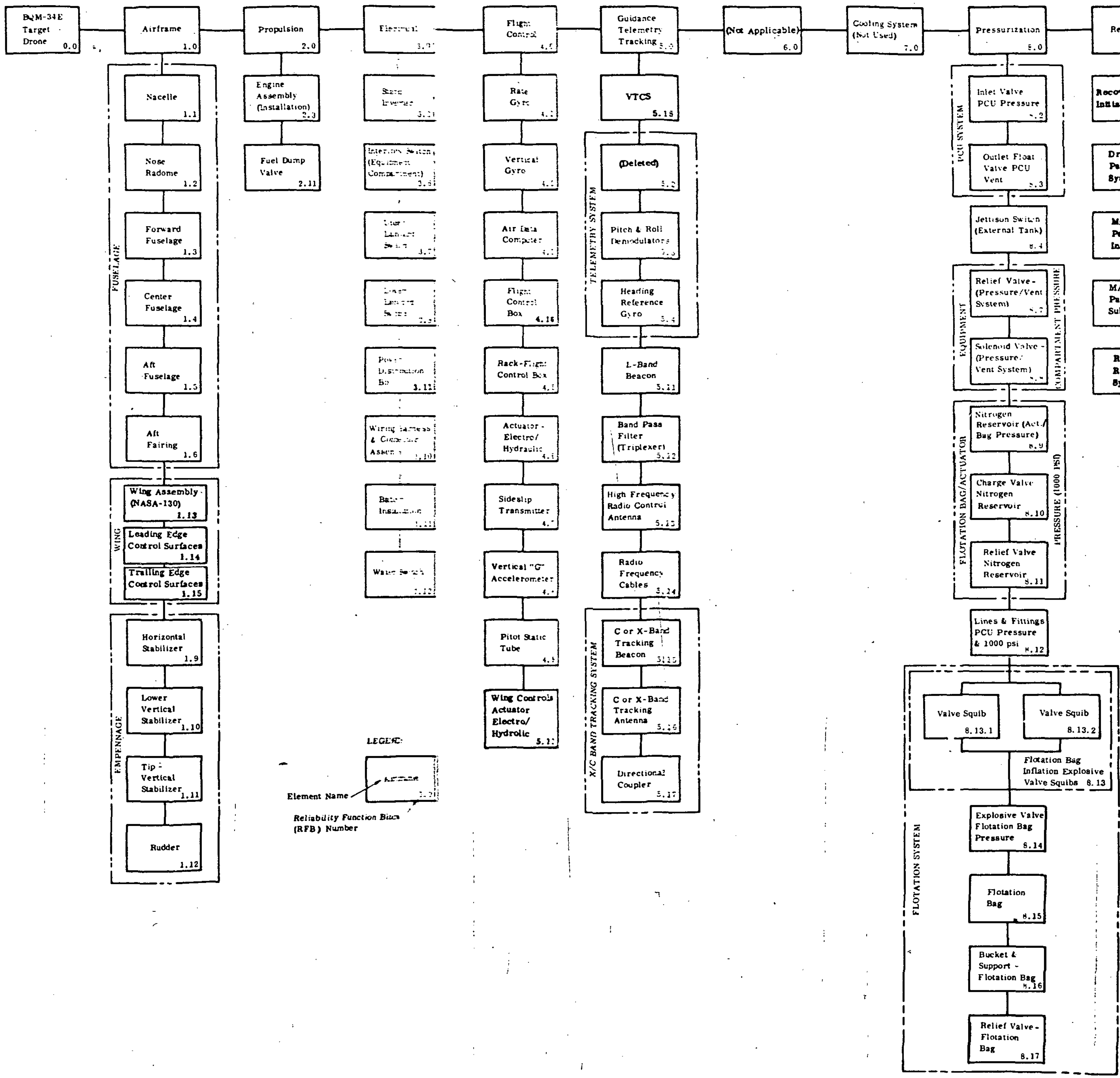

Figure 3-84. NASA Research Vehicle Recovery Phase Reliability, Functional Block Diagram

"Page missing from available version"

PAGE 174

Airframe. - The NASA-130 wing is substituted for the Navy wing. It is assumed that the failure rate is equal to four times the Navy wing failure rate due to added complexity and planned flights approaching the wing structural limits. Planned flights beyond the structural limits have been excluded from this analysis and will require further study during the design phase.) Four wing trailing-edge control surfaces, each with a failure rate equal to one horizontal stabilizer, are added, as well as two wing leading-edge control surfaces, each with a failure rate equal to one rudder.

Propulsion System. - No change is made in the propulsion system.

Electrical System. - The Air Force power distribution box failure rate is substituted for that of the Navy power distribution box to provide for potential increased functional requirements.

Flight Controls. - An electrohydraulic actuator with a failure rate equal to those of existing electrohydraulic actuators is added for wing control surfaces. Additional flight control box functions, with a combined failure rate equal to the combined failure rate of the existing pitch command assembly and 0.5 times the existing relay logic assembly, is provided.

Guidance, Telemetry, Tracking. - The existing radio receiver and telemetry transmitter are replaced by the (Vega) VTCS, and an α sensor with a failure rate equal to that of the existing β sensor is added.

Equipment Cooling. - This system is not currently planned for use; however, air vehicle reliability is shown for both cases (i.e., without or with the cooling system installed) in the event that supersonic flights may later require the system be installed.

Recovery. - The Air Force MARS main parachute system is substituted for the Navy main parachute system.

Table 3-23 shows the NASA BQM-34E and Navy BQM-34E flight phase reliability prediction comparison on a system by system basis. Table 3-24 shows the same comparison for the recovery phase.

Maintainability

A preventive-maintenance man-hour analysis for the NASA BQM-34E was performed based on the Navy BQM-34E maintenance engineering

TABLE 3-23

NASA BQM-34E AND NAVY BQM-34E FLIGHT PHASE RELIABILITY PREDICTION COMPARISON

RFB No.	System Element	NASA BQM-34E		NAVY BQM-34E	
		R	MTBF	R	MTBF
0.0	Air Vehicle (less Cooling) Air Vehicle (with Cooling)	0.97901 0.97793	51.05 48.53	0.98038 0.97933	54.65 51.85
1.0	Airframe	0.99762	454	0.99846	702
2.0	Propulsion	0.99620	285	0.99620	285
3.0	Electrical	0.99682	340	0.99685	344
4.0	Flight Control	0.99344	152	0.99490	212
5.0	Guidance, Telemetry, Tracking	0.99541	236	0.99448	196
6.0	(Not Used)				
7.0	Cooling	0.99890	984	0.99890	984
8.0	Pressurization	0.99933	1,623	0.99933	1,623
9.0	Recovery	(NOT ACTIVE DURING FLIGHT)			

TABLE 3-24

NASA BQM-34E AND NAVY BQM-34E RECOVERY PHASE RELIABILITY PREDICTION COMPARISON

RFB No.	System Element	NASA BQM-34E		NAVY BQM-34E	
		R	MTBF	R	MTBF
0.0	Air Vehicle	0.99422	-------	0.99632	-------
1.0	Airframe	0.99780	454	0.99948	702
2.0	Propulsion	0.99995	-------	0.99995	-------
3.0	Electrical	0.99926	497	0.99927	504
4.0	Flight Control	0.99951	152	0.99962	212
5.0	Guidance, Telemetry, Tracking	0.99964	236	0.99963	218
6.0	(Not Used)				
7.0	Equipment Cooling	(NOT ACTIVE DURING RECOVERY)			
8.0	Pressurization	0.99972	-------	0.99972	-------
9.0	Recovery	0.99833	-------	0.99864	-------

analysis report. The results are compared with the predicted and demonstrated preventive maintenance man-hours for the Navy BQM-34E, which does not have the MARS system, as follows:

	NASA BQM-34E (with MARS)	NAVY BQM-34E (no MARS)
Estimated	114.90 PMMH	166.19 PMMH
Demonstrated	--	178.37 PMMH

These are the direct, average, preventive-maintenance man-hours per flight. The NASA estimate is based on the following assumptions:

a. This estimate is for the second and subsequent flights. The first flight requires an additional 12 man-hours if uncrating is considered.

b. The flight control system will require 75 percent additional man-hours due to additional flight control system functions.

c. MARS recovery is used.

d. Maintenance man-hours are direct (i.e., "screwdriver-time") man-hours.

e. Maintenance hours do not include time for operational tasks such as uploading, prelaunch tests, launching, flight, or retrieval.

f. The cooling system is not used.

g. Augmentation (for target missions) is not installed.

h. Test time for the VTCS (Vega system) is equivalent to that for the AN/DRW-29 receiver and the AN/AKT-21 TLM transmitter.

i. A ground launch is assumed.

Table 3-25 shows the breakdown of the separate task estimates.

TABLE 3-25

ESTIMATE OF TASKS

No.	Task Description	Clock Hours	Man-Power	Freq/ Flt	PMMH/ Flt
1.	Systems Confidence Test (Completed Vehicle)	1.25	3	1	3.75
2.	Service Vehicle with Fuel	0.50	1	1	0.50
3.	Weigh Vehicle	0.50	2	1	1.00
4.	Assemble & Align RATO Bottle to Attach Fitting	1.50	2	1	3.00
5.	Service Battery	1.00	1	1	1.00
6.	Preflight Servicing	1.90	1	1	1.90
7.	Disassembly after Flight (Remove Equip. Comp. Doors, ADC, Gyros, etc.)	1.20	1	1	1.20
8.	Check Components	7.35	1	1	7.35
9.	Pressure Checks	2.50	1	1	2.50
10.	Prepare for Installed Engine Run	2.00	1	1	2.00
11.	Installed Engine Run	1.00	3	1	3.00
12.	Prepare for Systems Tests	4.25	2	1	8.50
13.	Install Equipment in Equipment Compartment	8.50	1	1	8.50
14.	Perform Systems Tests	18.30	2	1	36.60
15.	Complete Assembly of Vehicle	5.75	2	1	11.50
16.	Build up and Install Recovery System (Includes MARS)	8.30	2	1	16.60
17.	Weigh and Balance Vehicle	3.00	2	1	6.00
	TOTAL PMMH				114.90

Component Test Requirements

The current NASA BQM-34E configuration will require only one new major component that will not have demonstrated flightworthiness. This is the wing control surface actuator package. Assuming it is a unit comparable to the existing electrohydraulic actuator, it is recommended that each unit procured be subjected to a flight-assurance test equivalent to the reliability sampling test performed on the selected units procured for the BQM-34E. The test profile includes low and high-temperature soak, low and high-temperature operation, three-axis vibration, an acceptance test, and visual inspection. After successful completion of this test, each unit will then be refurbished for flight readiness and subjected to the acceptance test procedure prior to shipment from the supplier.

Elements to be considered in a flight-assurance determination are presented in Table 3-26.

TABLE 3-26

POSSIBLE ELEMENTS OF FLIGHT ASSURANCE DETERMINATION

1. Reliability

   - Predict inherent existing system reliability
   - Predict inherent modification reliability
   - Determine requirements/goals of modification items

2. Maintainability

   - Use existing T.O. manuals to spell out maintenance and checkout requirements
   - Use of existing AGE
   - Determine special AGE
   - Evaluate impact of NASA versus military operational differences on maintenance and operations. (Including mission planning/operational profile data.)

3. Test Requirements

   - Component qualification/performance/proof tests
   - Simulator tests components/systems (compatibility/performance)
   - Structural (proof) tests
   - Predelivery (acceptance) factory tests
   - Field/flight tests

4. Training and Training Aides

   - Simulator
   - T.O.'s and manuals

"Page missing from available version"

PAGE 182

4.0 CONCLUSIONS

As a result of this feasibility study, it is concluded that the basic BQM-34E is readily amenable to modification for conversion to a NASA research drone. Wings were sized to indicate the applicability of the BQM-34E to a wide range of subsonic and supersonic missions. Six point designs with research wings applicable to advanced transports, RPVs as well as an air-to-air fighter, were identified. Comprehensive structural and design analyses were accomplished on a representative research configuration to indicate practical modifications to provide high and low-wing structural attachment capabilities. Typical inboard and outboard ailerons and active control devices were configured with practical actuation system arrangements. Cost-effective methods of constructing wings with various degrees of bending and torsional rigidity were determined, for possible loads and flutter suppression research studies.

The required modifications to the existing command and control system, to provide capabilities of accomplishing control law functions via ground-based or airborne computers, were identified within the state of the art and available avionic systems.

"Page missing from available version"

PAGE 184

5.0 RECOMMENDATIONS

According to the results of this study, the basic BQM-34E drone system is readily adaptable into an unique NASA free-flight research system capable of accomplishing both subsonic and supersonic tasks. ROM costs, delivered to the customer (per Reference 16), indicate that this research drone can provide substantial savings in terms of time and resources in the development of man-rated systems. Free-flight validations without tunnel-wall constraints can readily be established in critical flight regimes and where wind tunnel test data are in question (such as at Mach 1.0). It is therefore recommended that such a program be pursued immediately to provide NASA with this capability within time schedules indicated in Figure 5-1.

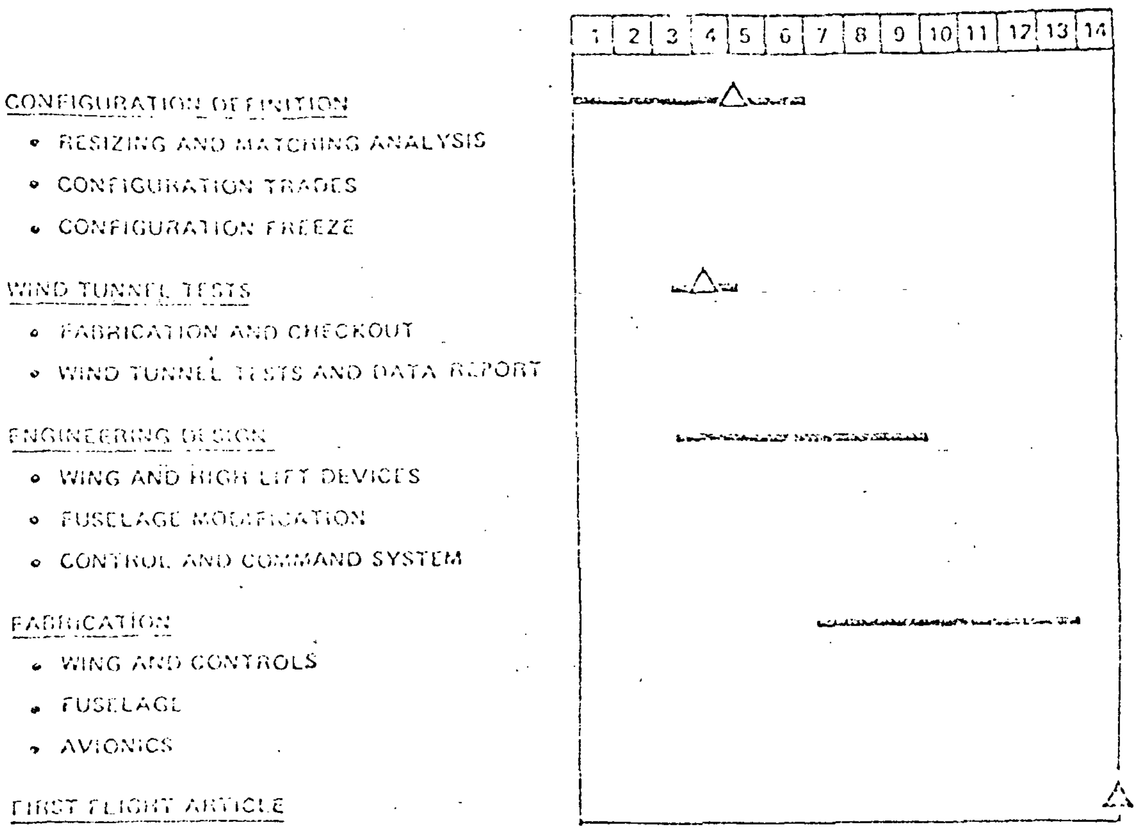

Figure 5-1. Recommendations for Phase II

6.0 NOTATIONS AND SYMBOLS

Conventional notations are used throughout this report. They are listed as follows:

A	Wing aspect ratio
AVSYN	Air vehicle synthesis program (Teledyne Ryan)
b	Wing span
$\bar{c}$	Wing mean aerodynamic chord
CFE	Equivalent flat-plate drag coefficient
C_r	Wing-root chord
C_f	Coefficient of friction
C_t	Wingtip chord
cg	Center of gravity
C_D	Drag coefficient, $\frac{\text{Drag}}{qS}$
$C_{D,\,b}$	Base drag coefficient, $\frac{\text{Base Drag}}{qS}$
C_{D_o}	Drag coefficient at zero lift
$\frac{C_D}{{C_L}^2}$	Drag-due-to-lift parameter
C_L	Lift coefficient, $\frac{\text{Lift}}{qS}$
C_{L_α}	Slope of lift curve, per degree
C_m	Pitching moment coefficient, $\frac{\text{Pitching Moment}}{qS\bar{c}}$

C_m/C_L	Longitudinal - stability parameter
C_m/S_H	Pitch control effectiveness of horizontal tail
C_{N_β}	Directional - stability parameter, per degree
g	Acceleration due to gravity
h	Altitude, feet
K_{F_N}	Relative engine size to base reference engine lift-to-drag ratio
L/D	Lift-to-drag ratio
M	Free-stream Mach number
Nz	Normal load factor
q	Free-stream dynamic pressure, pounds per square foot
R	Distance, nautical miles
RN	Reynolds number
rpm	Revolutions per minute
S	Reference wing area, square feet
TOS	Time on station, minutes
$\bar{V}_H$	Horizontal tail volume coefficient, $= \frac{\ell_H}{\bar{c}} \times \frac{Su}{Sw}$
$\bar{V}_v$	Vertical tail volume coefficient, $= \frac{\ell_v}{b} \times \frac{Sv}{Sw}$
W/S	Wing loading, psf
WT	Weight, pounds
Wb	Body width, feet
	Angle of attack, degrees
	Angle of sideslip, degrees
δ_n	Horizontal-tail, deflection, degrees
ϵ	Effective downwash angle, degrees
Γ	Dihedral angle, degrees

SUBSCRIPTS

max	Maximum
B	Body
c	Cruise
H	Horizontal tail
V	Vertical tail
W	Wing or wetted area
REF	Reference
0	Zero lift

"Page missing from available version"

PAGE 190

7.0 REFERENCES

1. NASA Memo 334/Pleasants, 20 July 1972, "Study Guidelines for Contract NAS1-11758".

2. Proposal for a Feasibility Study of Incorporating a Research Wing on a BQM-34E Drone, ASTM 72-13, 12 May 1972.

3. Task I Results. NASA Wing Feasibility Study BQM-34E, ASTM 72-22, 30 August 1972.

4. NASA Letter 126A/NAS1-11758, dated 30 October 1972.

5. Statement of Work, Feasibility Study of Incorporating Research Wing on BQM-34E Drone, 1-18-2662, dated 3 March 1972.

6. Basic Data Report for BQM-34E Supersonic Aerial Target, Report No. TRA 16620-1E, 25 May 1970.

7. Actual Weight Report for BQM-34E Supersonic Aerial Target, Serial Number BQ-16181, Report No. TRA 16644-22, dated 4 May 1972.

8. Actual Weight Report for BQM-34F Supersonic Aerial Target, Report No. TRA 16644-25, dated 4 February 1972.

9. NASTRAN Program, Office of Technology Utilization, NASA, 1970.

10. Bowers, N.M., Compendium of Computer Data from NASTRAN.

11. Stress Memo 88a, Lockheed Aircraft Corp., 15 September 1955.

12. "Buckling of Flat Plates", Handbook of Structural Stability, Part 1, NACA TN 3781.

13. Peery, D.M., Aircraft Structures, McGraw-Hill Book Co., Inc., 1950.

14. Letter of Transmittal 7/60/3826, Santos to NASA Contracting Officer, ROM Costs, dated 14 December 1972.

15. Brown, W.R., Guidance System Report for BQM-34E Supersonic Aerial Target, Report No. 16618-2C, 19 March 1970.

16. Downey, P.J., Control and Stabilization System Report for BQM-34E Supersonic Aerial Target, Report No. TRA 16654-4E, 12 June 1972.

17. Wooley, M., and Jones, J.G., System Dynamics Report for BQM-34F Supersonic Aerial Target, Report No. TRA 16654-3D, Supplement No. 1, 20 January 1971.